INSTITUTE

FOR

COSMIC RAY RESEARCH

UNIVERSITY OF TOKYO

ANNUAL REPORT
(APRIL 2011 – MARCH 2012)

5-1-5, Kashiwanoha, Kashiwa, Chiba 277-8582, Japan

Telephone: (81) 4-7136-3102
Facsimile: (81) 4-7136-3115
WWW URL: http://www.icrr.u-tokyo.ac.jp/

TABLE OF CONTENTS

PREFACE

This report summarizes the scientific activities of the Institute for Cosmic Ray Research (ICRR) of the University of Tokyo in the Japanese FY 2011.

ICRR is an inter-university research institute for studies of cosmic rays. The headquarters of ICRR is located in Kashiwa, Chiba prefecture, Japan. In order to promote various cosmic-ray-related studies efficiently, ICRR has three research divisions; Neutrino and Astroparticle division, High Energy Cosmic Ray division, and Astrophysics and Gravity division. ICRR has 3 observatories in Japan; Kamioka Observatory (Kamioka underground, Gifu prefecture), Norikura Observatory (2770 meters above sea level, Mt. Norikura, Gifu prefecture), and Akeno Observatory (Yamanashi prefecture), together with 1 research center; Research Center for Cosmic Neutrinos (Kashiwa, Chiba prefecture). In addition, there are 3 major experimental facilities outside of Japan. They are located in Utah in USA, Yangbajing in Tibet, China, and Woomera in Australia (the last one was shut down at the end of this fiscal year).

More than 300 researchers from various Japanese institutions are involved in the research programs of ICRR. It should be noted that most of the scientific outputs from this institute are the results of the collaborative efforts by many institutions. In order to produce outstanding results, it is very important to carry out an experiment by an international collaboration composed of top-level researchers all over the world. Hence, most of the experimental collaborations that ICRR is involved are international ones. For example, the number of collaborators in the Super-Kamiokande experiment is about 130; among them 60 are from abroad (USA, Korea, China, Poland and Spain).

Many exciting scientific activities of ICRR are described in this report. One of the highlights is the results from the T2K long-baseline neutrino oscillation experiment, which studies neutrino oscillations in detail including the third mixing angle θ_{13}. Another highlight is the the construction of the large-scale cryogenic gravitational wave telescope (KAGRA), which intends to detect gravitational waves for the first time and open a new field of "gravitational wave astronomy". On the other hand, the experiments that finished thier mission has little reason to continue running. At the end of this fiscal year, the Cangaroo experiment in Woomera, Australia was shut down.

We hope that this report is useful for the understanding of the current research activities of ICRR. Finally, we appreciate very much the strong support of our colleagues in this research field, the University of Tokyo and the Japanese Ministry of Education, Culture, Sports, Science and Technology. They are indispensable for the continuing, and exciting scientific outcome of ICRR.

Takaaki Kajita,
Director,
Institute for Cosmic Ray Research,
The University of Tokyo

The ICRR building at Kashiwa, Chiba, Japan.

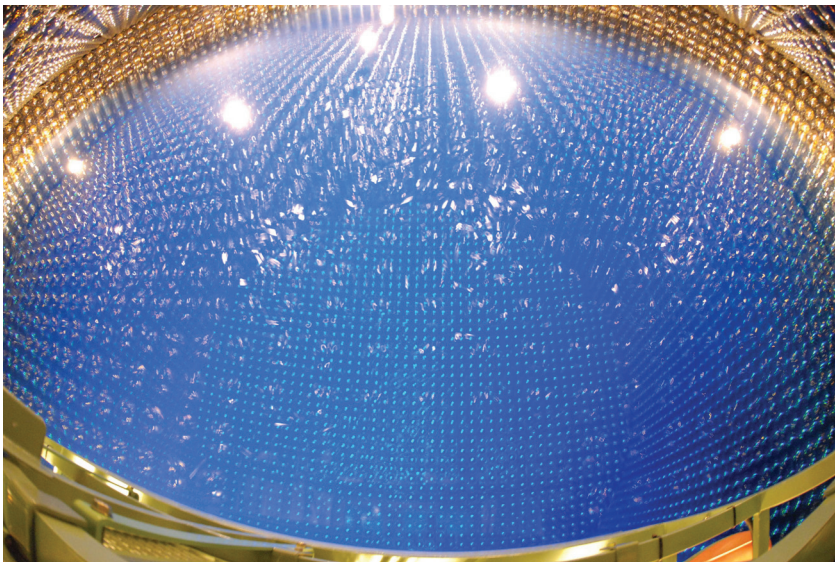

The inner detector of Super-Kamiokande-III during the full reconstruction. The purified water is under filling.

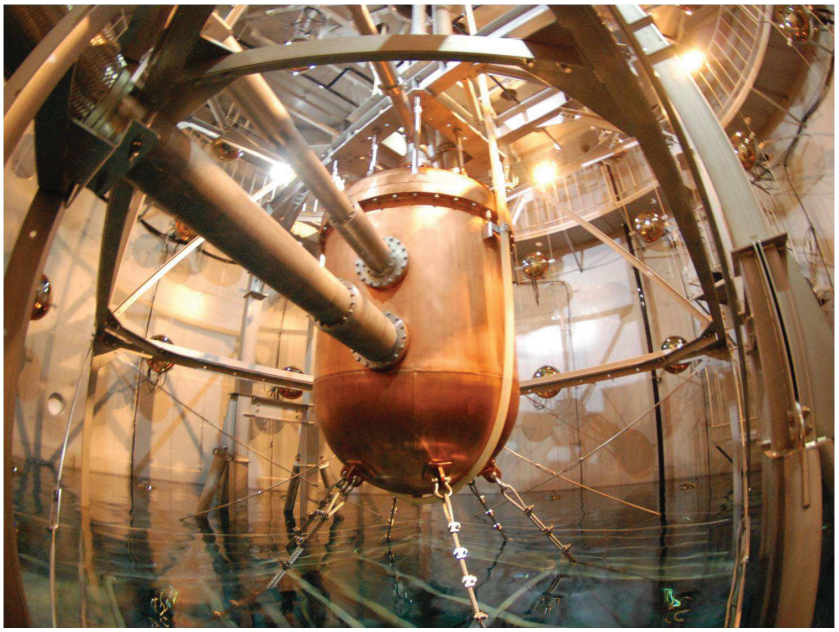

XMASS detector using 835 kg of liquid xenon. Radiations are shielded and cosmic-ray muons can be vetoed by a water-Cherenkov detector outside.

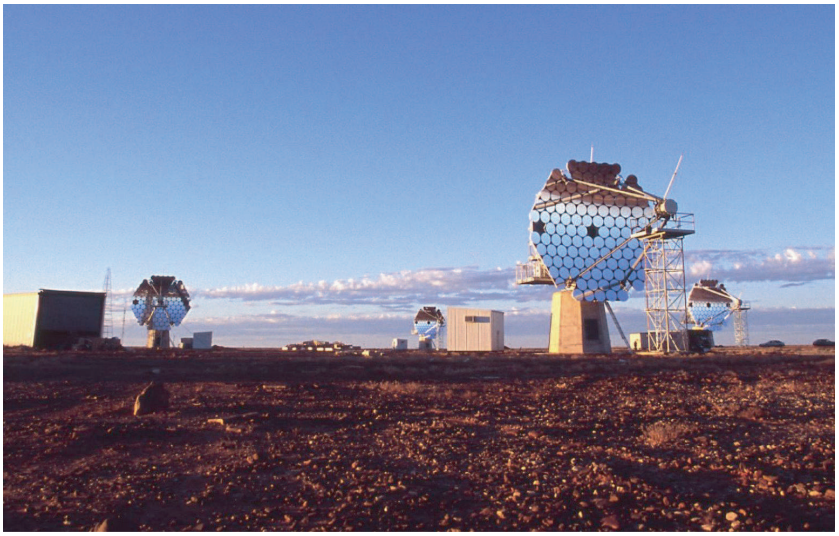

The system of four imaging atmospheric Cherenkov telescopes of 10m diameter of CANGAROO project for detection of very high energy gamma-rays The whole system is in operation since March 2004 in Woomera, South Australia.

Tibet-III air shower array (37000 m^2) at Yangbajing, Tibet (4300 m in altitude).

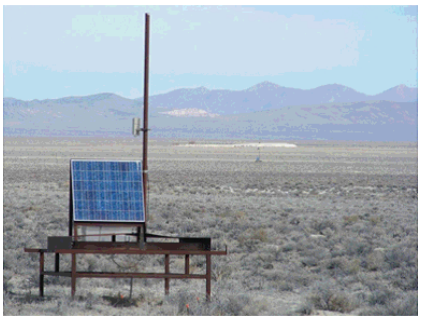

Air fluorescence telescopes (left) and a scintillator surface detector (right) of the Telescope Array experiment in Utah, USA to explore the origin of extremely high energy cosmic rays.

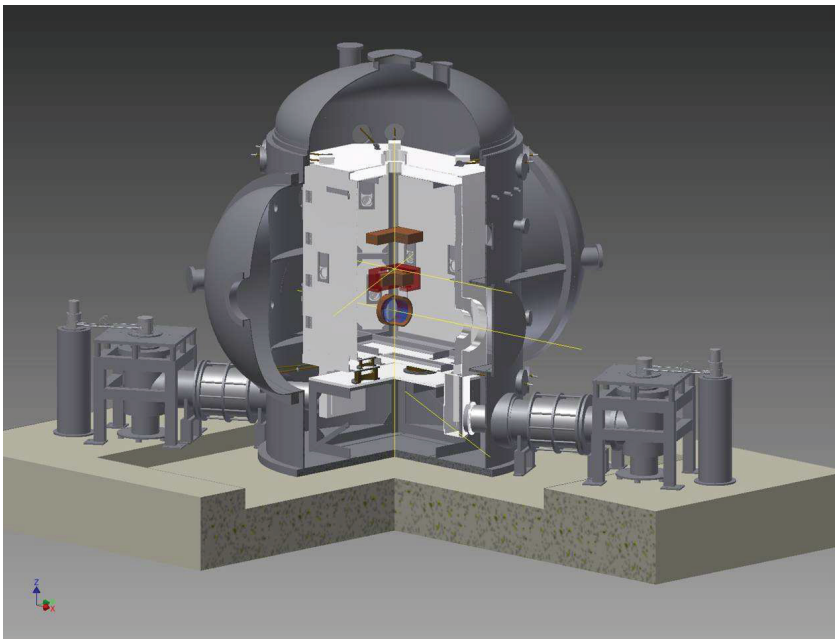

Cryogenic mirror sysytem for KAGRA with a cryostat and a cryocooler.

A public lecture held by Research Center for Cosmic Neutrinos.

Organization

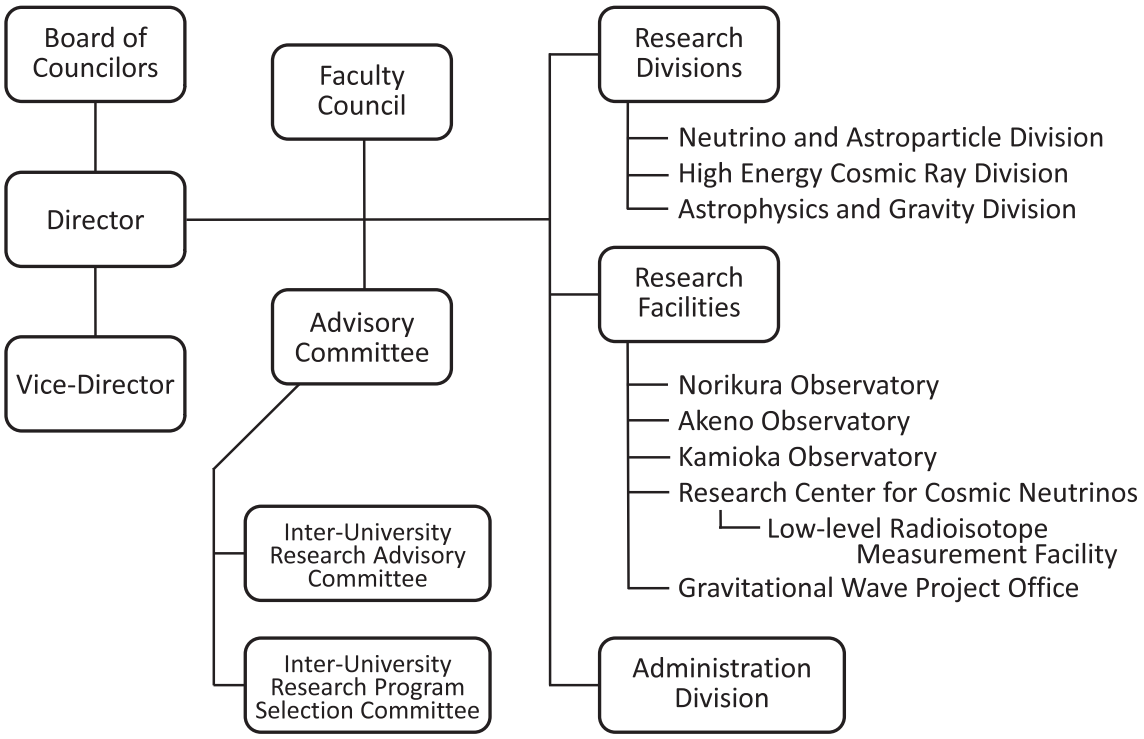

Number of Staff Members (As of May 1, 2011)

	Scientific Staff	Technical Staff	Research Fellows	Administrators and Secretaries	Total
Neutrino and Astroparticle Div.	21	4	5	17	47
High Energy Cosmic Ray Div.	14	14	4	3	35
Astrophysics and Gravity Div.	14	0	5	3	22
Administration	1	0	0	12	13
Total	50	18	14	35	117

FY 2006–2011 Budget

	2006	2007	2008	2009	2010	2011
Personnel expenses	566 000	624 000	632 000	590 000	576 000	653 000
Non-personnel expenses	812 000	1 253 000	1 121 000	1 292 000	1 048 000	1 400 000
Total	1 378 000	1 877 000	1 753 000	1 882 000	1 624 000	2 053 000

(in 1 000 yen)

RESEARCH DIVISIONS

Neutrino and Astroparticle Division

Overview
Super-Kamiokande Experiment
Hyper-Kamiokande
T2K Experiment
XMASS Experiment

High Energy Cosmic Ray Division

Overview
Cherenkov Cosmic Gamma-Ray Group
TA: Telescope Array Experiment
Tibet ASγ Project
Ashra Project
High Energy Astrophysics Group

Astrophysics and Gravity Division

Overview
Gravitational Wave Group
- KAGRA Project
- CLIO Project

Observational Cosmology Group
Primary Cosmic Ray Group
Theory Group
- Particle Phenomenology
- Astrophysics and Cosmology

NEUTRINO AND ASTROPARTICLE DIVISION

Overview

This division aims to study particle physics with prime interests in physics of neutrinos and proton decay, and astroparticle physics with the use of underground experimental facilities.

Our most important facility is the Super-Kamiokande (SK) detector. It is a 50 kton water Cherenkov detector using 11,129 50 cm-diameter photomultipliers (PMTs) for its inner detector and 1,885 20 cm-diameter PMTs for its outer detector. The data taking of SK started in April 1996. The neutrino oscillations in atmospheric neutrinos were discovered in 1998 and thereby demonstrating that neutrinos have a finite mass. In 2001, the accurate measurements of the ^{8}B solar neutrino flux by SK and SNO discovered that neutrino oscillations are the solution of the solar neutrino problem beyond doubt. Since those discoveries, various studies on neutrino oscillations have been performed at SK.

The search for nucleon decay at SK gives the current best limit which strongly constrains the grand unification scenario of particle interactions. SK also has been searching for neutrinos from supernovae. One is a search for burst neutrinos orignate from nearby supernovae, another is so-called supernova relic neutrinos, which is an accumulated supernova burst neutrinos from the biginning of the universe.

A high intensity neutrino beam experiment using the J-PARC accelerator (T2K) was started in 2009. The T2K experiment uses the SK detector as the far detector. Electron neutrino appearance (the effect of the mixing angle θ_{13}) and the high precision measurement of oscillation parameters are main physics subjects in T2K. An indication of electron neutrino appearance was announced in June 2011, and the significance of the appearance has been improved after the J-PARC recovery in early 2012.

Another activity of the Neutrino and Astroparticle division is a multi-purpose experiment using liquid xenon aiming at the detection of cold dark matter, neutrino absolute mass using neutrinoless double beta decay, and low energy solar neutrinos. The construction of a 800 kg liquid xenon detector which is dedicated for the dark matter search was finished in 2010 and the commissioning of the detector has been performed in 2011.

Recent progress of research activities in the Neutrino and Astroparticle division is presented below.

Super-Kamiokande experiment

Supernova neutrinos

Kamiokande and IMB observed the neutrino burst from supernova 1987a. This observation confirmed that the energy released by neutrinos is about several $\times 10^{53}$ergs. However, the observed number of events were only 11 by Kamiokande and 8 by IMB, respectively. Super-Kamiokande would be able to detect several thousand neutrino events if a supernova happened near the center of our galaxy. Such an observation would enable us to investigate in detail the machanics of the supernova explosion. Galactic supernovae are searched for almost in real time at SK. The online data acquisition system running in the mine sends data to the offline computer system in the surface building of Kamioka observatory. As soon as a block of data (usually a block corresponds to several minutes) is transferred to the offline system, a program called SNWATCH searches for time clustered events. Current criteria of SNWATCH are (1) more than or equal to 7 events within 0.5sec, (2) more than or equal to 8 events within 2sec, and (3) more than or equal to 13 events within 10sec. When at least one of these criteria are met, SNWATCH reconstructs vertex position and energy of the events together with neighboring cosmic ray muons. In most cases, these clusters are due to spallation products whose vertex positions are aligned with their parent cosmic ray muon. If SNWATCH finds an event cluster whose vertex spread is larger than a given criterion, an alarm signal is sent to experts by e-mail and an automatic call to their cellphones. Then, the experts check whether it is a real supernova signal or not by looking at various plots which are uploaded to a secured site accessible from the Internet. These alarms are usually due to the accidental coincidence of two cosmic ray induced clusters. We have a supernova drill at least once per year. So far, no real supernova neutrino burst signal has been observed at Super-Kamiokande.

We also search for neutrinos from old supernovae, which are called Supernova Relic Neutrinos (SRNs). The SRN signal is the diffuse supernova neutrino background from all the supernovae in the past. This signal has never been detected, but it is expected to be detectable in the 16-30 MeV energy region, which is the gap between the energy ranges of solar neutrinos and atmospheric neutrinos. We have applied carefully tuned data selection to enhance the SRN candidates, improving the efficiency of our search by over 20% compared to the 2003 SK-I study, which currently provides the world's best limit on SRN flux. Our improved data selection also allows us to now search the 16-18 MeV positron energy region, which was previously unusable due to spallation background. Our updated search utilizes SK-II and SK-III data as well as SK-I, considers two new background channels, and performs a sophisticated maximum likelihood search in multiple regions of the Cherenkov angle distribution to extract the most accurate flux limit possible(Fig.1). Multiple systematic errors are considered. A flux limit of between 2.7 and 3.0 $\bar{\nu}cm^{-2}s^{-1}$ (positron energy $>$ 16 MeV) is our new result, with the exact value depending on the shape of the neutrino spectrum assumed. This new result will replace the 2003 study to be the most accurate measure of the SRN signal ever performed. Furthermore, a new method of presenting the SRN flux limit is also ready which is of great use to theorists and does no depend on any particular model (Fig.2).

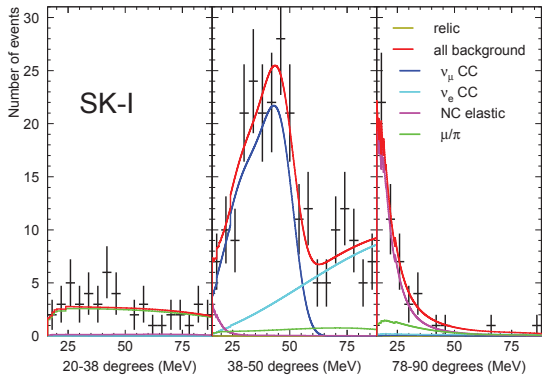

Fig. 1. SK-I best fit result, assuming Ando et al's LMA model. The relic best fit is negative, so a relic fit of 0 is shown. SK-II and SK-III have small but positive relic best fits.

Fig. 3. In the new cavern the Gd pre-mixing and pre-treatment 15 ton tank (front left), the selective filtration system (front right) and the 200 ton tank (rear of the hall) have been installed.

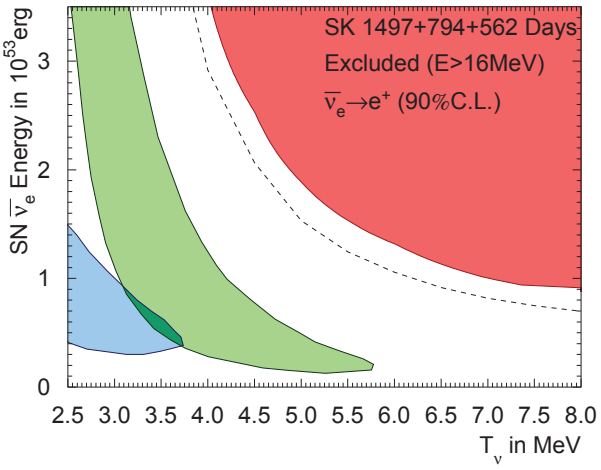

Fig. 2. Results plotted as an exclusion contour in SN neutrino luminosity vs. neutrino temperature parameter space. The green and blue contours show IMB and Kamiokande allowed areas for 1987a data, respectively. The red shows our new 90% c.l. result. The dashed line shows the individual 90% c.l. results of each temperature considered separately, which is not a true 2-D exclusion contour.

Super-Kamiokande R&D gadolinium project

As mentioned above, although at SK a few SRN events a year are expected, SRNs have not been detected yet because the large backgrounds constrain our search. The main goal of our research is to reduce these backgrounds and be able to detect SRNs. The observation of SRNs in general or neutrinos from distant supernovae in particular, would give us some information about the universe, for example the core collapse rate from SRNs, and the neutrino itself too, for example about its lifetime. Since most of the neutrinos that can be detected at SK undergo inverse beta decay, electron anti-neutrinos are the most copiously detected neutrinos:

$$\bar{\nu}_e + p \rightarrow e^+ + n \qquad (1)$$

Presently, the SK detector can only detect the positrons efficiently but if we could detect the neutrons, we could greatly reduce the backgrounds that constrain our SRN search. This could be attained by the coincidence detection of positron and neutron (in space, vertices within tens of cm and in time, with the neutron capture delayed about 20 μsec). By adding 0.2% of gadolinium (Gd) sulfate into the water tank we could achieve this goal. Gadolinium has a neutron capture cross section of 49.000 barns (about 5 orders of magnitude larger than of protons) and emits a gamma cascade of 8 MeV that can be easily detected at SK.

We want to show that adding Gd into the SK water, SK will become an electron anti-neutrino detector, able to tag inverse beta decays, while keeping all its previous capabilities in the other analyses like solar and atmospheric neutrinos. The EGADS (Evaluation Gadolinium's Action on Detector Systems) project was funded in 2009 and since then a new hall near the SK detector has been excavated and a 200 ton tank with its ancillary equipment has been installed, see Fig.3. The idea is to mimic the conditions at SK inside the 200 ton tank. It has been equipped with a selective water filtration system, that will filter out water impurities while keeping Gd in the water, a Gd pre-mixing and pre-treatment 15 ton tank and a device to measure the water attenuation length (UDEAL). Since the middle of January, the 200 ton tank has been filled with pure water. The water system, which has been running stably since the beginning of February has proven to keep a high water quality, see Fig.4. Soon we will test adding gadolinium sulfate to the pre-mixing 15 ton tank and circulate the water through the water system. The next step will be to add gadolinium sulfate to the 200 ton tank and by the end of 2011 we expect to mount 240 50-cm photomultipliers, thus entering in the last phase of this exciting project.

Solar Neutrinos

Over the past decade, a solar neutrino oscillation scenario had been established by the solar neutrino experiments (SK, SNO, and radio chemical experiments) and the KamLAND re-

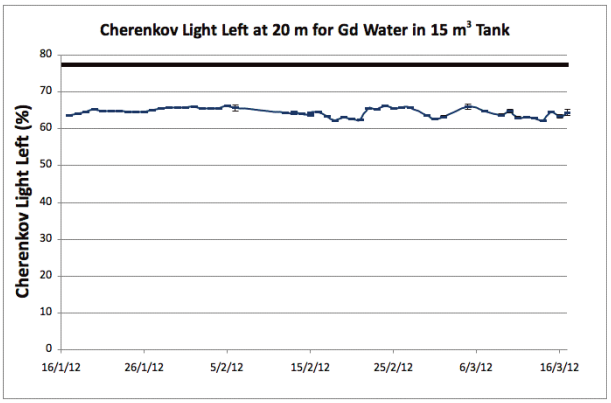

Fig. 4. Water attenuation length for pure water from the 200 ton tank for three wave lenghts: 337nm, 375nm and 405nm. The water attenuation length decreases first and then increases as soon as the water filtration system ran continuously.

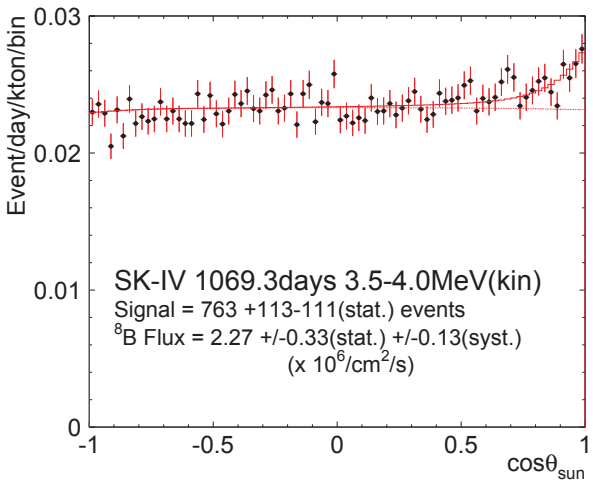

Fig. 5. Solar angle distributions of 1069.3 days SK-IV data sample with energy between 3.5-4.0 MeV.

actor experiment. The next step then for solar neutrino measurements is the precise determination of the oscillation parameters and the role of matter therein. SK makes an important role by collecting high statistics solar neutrino data to attempt measurements of a day-night flux difference and a distortion of the energy spectrum.

SK detects solar neutrinos through neutrino-electron elastic scattering, $\nu + e \rightarrow \nu + e$, where the energy, direction, and time of the recoil electron are measured. Due to its large (22.5 kiloton) fiducial mass SK makes precise measurements of ^{8}B solar neutrinos, including precision information on their energy spectrum and its time variation. To achieve these measurements, precise calibrations using both an electron LINAC [1] and ^{16}N radioisotopes generated by a deuterium-tritium neutron generator[2] are employed to determine the Super-K energy scale, energy and angular resolution, and the vertex position resolution with high precision.

As written in the last paragraph in the annual report in the last year, the background rate in the lower energy region (below 6 MeV) in SK-IV has been reduced by a factor of more than three compared to the SK-I period. It comes from many efforts we have been made to reduce backgrounds and to increase the precision of the detector calibrations since SK-III started. Both are crucial for solar neutrino measurements. The most serious background comes from the beta decay of ^{214}Bi, which is produced in the decays of radon in the air and detector materials (PMT glass and FRP(fiber reinforced plastic) cases) as well as from radium in the water. In order to reduce the ^{214}Bi background, the SK water system was upgraded. First, a new reverse osmosis unit was added to further reduce the radium content of the water. Second, a new heat exchanger was added to supply water without inducing convection in the tank, which transports radon near the PMTs into the fiducial volume. Third, new membrane degasifier units were added to increase the efficiency of radon removal from the supply water. Additionally, the water flow in the detector was precisely investigated and optimized to reduce the the background contamination in the fiducial volume as much as possible. During the SK-IV period we have introduced a precise temperature control system for the inlet water to further reduce convection in the water. As a result of these improvements, the background rate in the lower energy region (below 6 MeV) in SK-IV has been reduced by a factor of more than three compared to the SK-I period. Further, it has allowed a lower analysis energy threshold: down to 3.5 MeV from 4.5 MeV of kinetic energy.

In this year, we first reported solar neutrino results in SK-IV. By the end of March 2012, 1069.3 days of SK-IV solar neutrino data for analysis was taken. One of the most important improvements has been the reduction of the energy threshold, which now triggers at 100% efficiency at 4.0 MeV electron kinetic energy. A clear solar neutrino signal in the 3.5-4.0 MeV energy region can also be seen at more than 7 σ as shown in Fig.5. This success was achieved as a result of the background reduction efforts described above. The total flux systematic error during SK-IV becomes $\pm 1.7\%$, which is nearly half that of the SK-I period, $^{+3.5}_{-3.2}\%$ [3]. This reduction comes from improvements in the uncertainty of the fiducial volume size ($\pm 1.3\%$ in SK-I, $\pm 0.17\%$ in SK-IV), better understanding of the absolute energy scale ($\pm 0.64\%$ in SK-I, $\pm 0.54\%$ in SK-IV), and careful studies of the data reduction. During SK-IV the measured ^{8}B flux is $2.34 \pm 0.03(stat.) \pm 0.04(sys.) \times 10^6 cm^{-2} s^{-1}$, which is consistent with previous measurements from SK-I, II, and III and is shown in Fig.6.

The energy spectrum of the recoil electron is shown in Fig.7(upper). The vertical axis shows the ratio of the observed energy spectrum to the expectation from the unoscillated MC simulation assuming a ^{8}B flux of 5.25×10^6 /cm^2/sec. Fig.7(lower) shows SK-I to SK-IV combined energy spectrum with expectations from the solar global and solar+KamLAND as well as flat reduction of the neutrino spectrum. The combined energy spectrum is consistent with the flat prediction, but the level of favoring flat over the upturn is $1.1 \sim 1.9\sigma$ level.

Concerning differences in the day and night fluxes the expected flux asymmetry, defined as $A_{DN} = (day - night)/\frac{1}{2}(day + night)$, is about 2% based on current understanding of neutrino oscillation parameters. Although this is

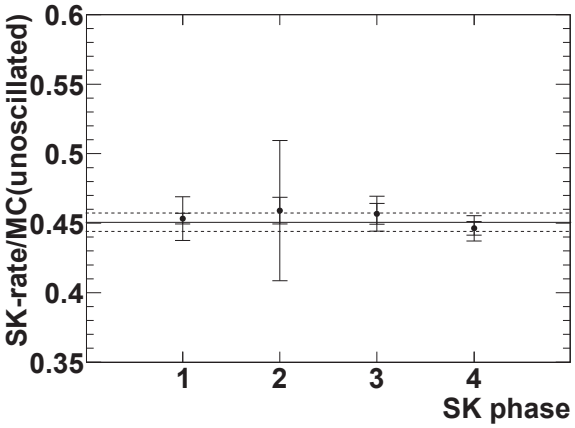

Fig. 6. Solar neutrino flux measurements from SK-I to SK-IV with statistic and systematic errors and normalized to the unoscillated MC prediction using a ^{8}B flux of 5.25×10^6 /cm^2/sec. The dashed lines show the averaged over all phases.

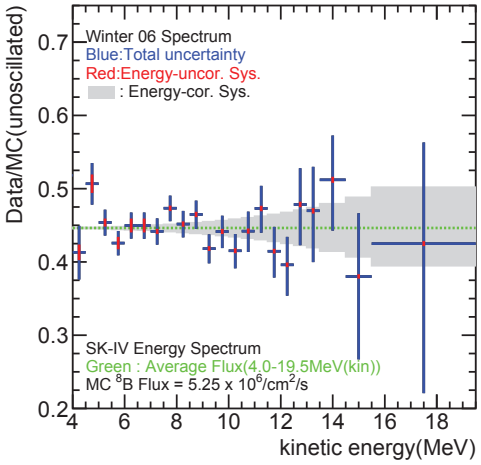

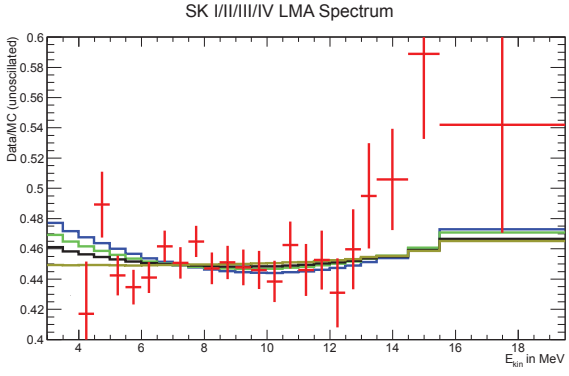

Fig. 7. The upper figure shows solar neutrino energy spectrum in SK-IV. Each point shows the ratio of the data to the expected flux using an unoscillated ^{8}B solar neutrino spectrum. The lower shows the spectrum combined SK-I to SK-IV with predictions for (1) $sin^2\theta_{12} = 0.304$ and $\Delta m^2_{21} = 7.4\times10^{-5}$eV^2(blue), (2) $sin^2\theta_{12} = 0.314$ and $\Delta m^2_{21} = 4.8\times10^{-5}$eV^2(light blue), (3) flat probability (black), and (4) flat probability and $d\sigma/dE$ shape for pure $\nu_e + e$ scattering (blond)

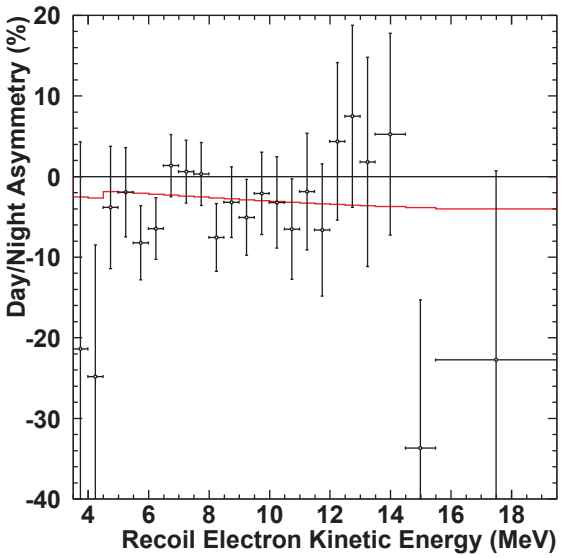

Fig. 8. The day-night asymmetry as a function of energy in the combined SK-I,II,III and IV data. The red line shows the predicted amplitude assuming neutrino oscillations with $sin^2\theta_{12} = 0.314$ and $\Delta m^2_{21} = 4.8\times10^{-5}$eV^2.

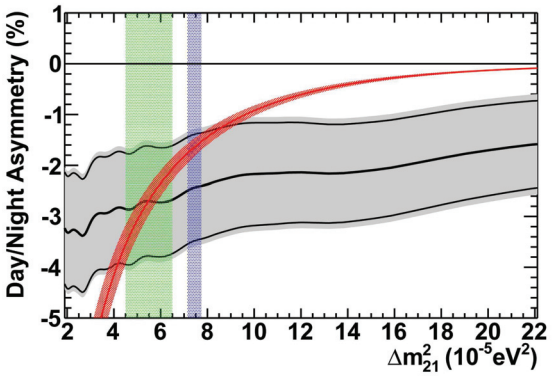

Fig. 9. The day-night asymmetry as a function of Δm^2. A thick black line shows the result of the SK fit and the surrounding gray band indicates statistical and systematic uncertainty (thin black lines for statistical error only). The red curve shows the expectation assuming $\sin^2(\theta_{12}) = 0.314$. The light blue and light green vertical bands show the allowed range of Δm^2 from the KamLAND reactor and solar global, respectively.

not a large effect, long term observations by SK enable discussion of a finite value of the day-night asymmetry. The A_{DN} value using the combined SK-I to SK-IV data is $-2.8\pm1.1\pm0.5$%, which is a 2.3σ difference from zero. Fig.8 shows the A_{DN} distribution as a function of energy. The day-night asymmetry is obtained by fitting the observed time variation during the night with its expected variation, meaning that A_{DN} depends on the assumed value of Δm^2. Fig.9 shows A_{DN} as a function of Δm^2 together with the expectation. The observed A_{DN} is consistent with the expectation using the best fit Δm^2 from both KamLAND and the global solar analysis.

A global solar neutrino oscillation analysis has been per-

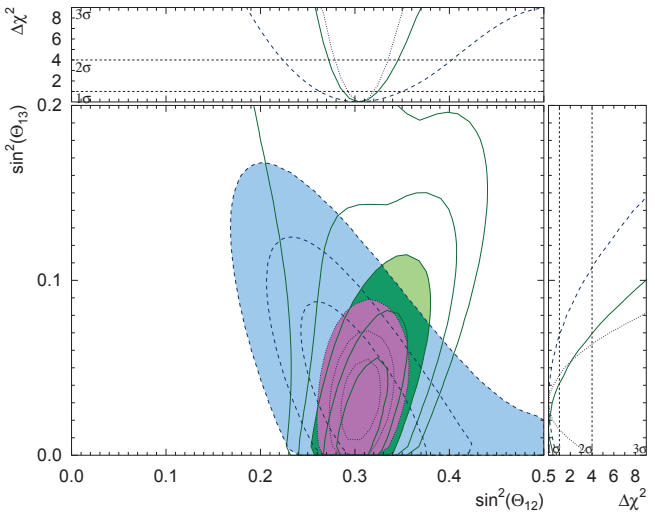

Fig. 10. Allowed regions of the neutrino oscillation parameters $\sin^2\theta_{12}$ and $\sin^2\theta_{13}$ from the global solar neutrino analysis (green) and the KamLAND reactor neutrino data (light blue). The purple region shows the contour from the combined global solar and KamLAND reactor analysis. Curves are drawn for each 1-σ step between 1 and 5 σ for the global solar analysis, and 1-3σ for the KamLAND and solar+KamLAND regions. Contours at 3 σ are filled with their colors.

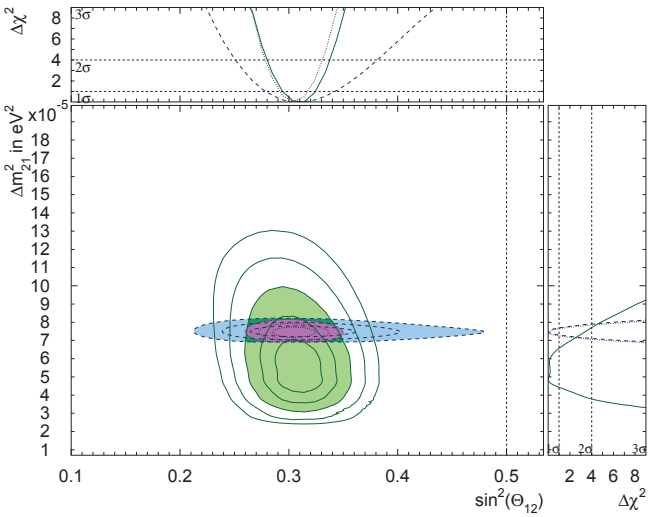

Fig. 11. Allowed regions of neutrino oscillation parameters in the Δm^2_{21} and $\sin^2\theta_{12}$ plane with $\sin^2\theta_{13}$ fixed at 0.025 from the global solar neutrino analysis (green) and the KamLAND reactor neutrino data (light blue). The purple area shows the combined contour of the global solar and the KamLAND reactor analysis. The curves are drawn for each 1-σ step from 1-5 σ for the global solar, and from 1-3 σ for the KamLAND and solar+KamLAND results. Contours at 3 σ are filled with their colors.

formed including all SK data (SK-I[3],SK-II[4], SK-III[5], and SK-IV) as well as the most recent results from SNO[1], the radiochemical experiments [2], [3] and the latest ^{7}Be flux measurement from Borexino[4]. This analysis was then compared and combined with the reactor neutrino results from KamLAND[5]. The green contours in Fig.10 show the allowed region of the neutrino oscillation parameters $\sin^2\theta_{12}$ and $\sin^2\theta_{13}$ in 1-σ steps from 1 to 5 σ. The obtained range of $\sin^2\theta_{13}$ from the solar global analysis is $0.014^{+0.027}_{-0.021}$, while the value of the KamLAND reactor analysis is $0.031^{+0.038}_{-0.036}$. The dependence of neutrino oscillations on θ_{12} and θ_{13} are different for solar neutrinos and reactor neutrinos because of the existence of matter effects in the higher energy part of the solar neutrino spectrum. For this reason their combination could give more sensitivity to θ_{13}. In the combined fit $\sin^2\theta_{13}$ was found to be $0.030^{+0.017}_{-0.015}$, which is a roughly 2 σ hint that θ_{13} is different from zero. This hint has been discussed prior to 2010[6][5]. After 2011, the T2K, Double Chooz, Daya Bay, and Reno experiments presented indications and later evidence for a finite θ_{13}. The combination of their measurements yields $\sin^2\theta_{13} = 0.025^{+0.003}_{-0.004}$ and the result of the combined analysis of the global solar and KamLAND reactor data is consistent with this value. Figure 11 shows the allowed region of neutrino oscillation parameters in the Δm^2_{21} and $\sin^2\theta_{12}$ plane assuming $\sin^2\theta_{13}$ is fixed at 0.025. The obtained parameters from the global solar analysis are $\Delta m^2_{21} = (4.86^{+1.44}_{-0.52}) \times 10^{-5}\mathrm{eV}^2$ and $\sin^2\theta_{12} = 0.310^{+0.014}_{-0.015}$. Comparing these values with those from KamLAND, ($\Delta m^2_{21} = (7.49^{+0.20}_{-0.19}) \times 10^{-5}\mathrm{eV}^2$ and $\sin^2\theta_{12} = 0.309^{+0.039}_{-0.029}$), there is a 1.8 σ level tension in the Δm^2_{21} results, which is evident in the figure. Combining the global solar data with KamLAND, the oscillation parameters become $\Delta m^2_{21} = (7.44^{+0.20}_{-0.19}) \times 10^{-5}\mathrm{eV}^2$ and $\sin^2\theta_{12} = 0.304 \pm 0.013$. Obtained values of those oscillation parameters are summarized in Table 1.

	Δm^2_{21} ($10^{-5}\mathrm{eV}^2$)	$\sin^2\theta_{12}$
Super-K with ^{8}B flux from SNO NC	$4.69^{+1.80}_{-0.83}$	$0.339^{+0.028}_{-0.024}$
Solar global	$4.86^{+1.44}_{-0.52}$	$0.310^{+0.014}_{-0.015}$
KamLAND reactor	$7.49^{+0.20}_{-0.19}$	$0.309^{+0.039}_{-0.029}$
Solar + KamLAND	$7.44^{+0.20}_{-0.19}$	0.304 ± 0.013

Table 1. Neutrino oscillation parameters of Δm^2_{21} and $\sin^2\theta_{12}$ obtained by Super-K, solar global analysis, KamLAND reactor, and solar+KamLAND. $\sin^2\theta_{13}$ is fixed at 0.025.

Bibliography

[1] Super-Kamiokande Collaboration, M.Nakahata et al., "Calibration of Super-Kamiokande using an electron LINAC", Nucl. Instr. and Meth. A421 (1999) 113

[2] Super-Kamiokande Collaboration, E.Blaufuss, G.Guillian et al., "^{16}N as a calibration source for

*1 B. Aharmim et al., arXiv:1109.0763 [nucl-ex]
*2 Bruce T. Cleveland et al., Astrophys. J. 496 (1998) 505
*3 J. N. Abdurashitov et al.,Phys. Rev. C80 (2009) 015807
*4 G. Bellini et al., Phys. Rev. Lett. 107 (2011) 141302
*5 A. Gando et al., Phys. Rev. D83 (2011) 052002
*6 G. L. Fogli, E. Lisi, A. Marrone, A. Palazzo, and A. M. Rotunno, Phys. Rev. Lett. 101(2008) 141801

Super-Kamiokande", Nucl. Instr. and Meth. A458 (2001) 638

[3] Super-Kamiokande Collaboration, "Solar neutrino measurements in Super-Kamiokande-I", Phys. Rev. D 73 (2006) 112001.

[4] Super-Kamiokande Collaboration, "Solar neutrino measurements in Super-Kamiokande-II", Phys. Rev. D 78 (2008) 032002

[5] Super-Kamiokande Collaboration, "Solar neutrino results in Super-Kamiokande-III", Phys. Rev. D 83 (2011) 052010.

[6] The SNO collaboration(B. Aharmim et al.), "Combined Analysis of all Three Phases of Solar Neutrino Data from the Sudbury Neutrino Observatory", arXiv:1109.0763 [nucl-ex].

[7] The Borexino collaboration(G. Bellini et al.), "Precision measurement of the ^{7}Be solar neutrino interaction rate in Borexino", Phys. Rev. Lett. 107 (2011) 141302.

[8] B.T.Cleveland et al., "Measurement of the Solar Electron Neutrino Flux with the Homestake Chlorine Detector Bruce T. Cleveland", Astrophys. J. 496 (1998) 505.

[9] J. N. Abdurashitov et al., "Measurement of the solar neutrino capture rate with gallium metal. III. Results for the 2002.2007 data-taking period", Phys. Rev. C80 (2009) 015807.

[10] KamLAND collaboration(A. Gando et al.), "Enhanced Constraints on θ_{13} from A Three-Flavor Oscillation Analysis of Reactor Antineutrinos at KamLAND", Phys. Rev. D83 (2011) 052002.

[11] G. L. Fogli, E. Lisi, A. Marrone, A. Palazzo, and A. M. Rotunno, "Hints of theta(13) $>$ 0 from global neutrino data analysis.", Phys. Rev. Lett. 101(2008) 141801.

Atmospheric neutrinos

Cosmic ray interactions in the atmosphere produce neutrinos. The prediction of the absolute flux has an uncertainty of at least $\pm 20\,\%$. However, the flavor ratio of the atmospheric neutrino flux, $(\nu_\mu + \bar{\nu}_\mu)/(\nu_e + \bar{\nu}_e)$, has been calculated to an accuracy of better than $5\,\%$. Another important feature of atmospheric neutrinos is that the fluxes of upward and downward going neutrinos are expected to be nearly equal for $E_\nu >$(a few GeV) where the effect of the geomagnetic field on primary cosmic rays is negligible.

Neutrino oscillation was discovered in the study of atmospheric neutrinos in SK in 1998 [14]. Two flavor $\nu_\mu \rightarrow \nu_\tau$ oscillation hypothesis successfully describe the SK atmospheric neutrino data with maximum mixing angle (θ_{23}=π/4). We have continued observing atmospheric neutrino events in Super-Kamiokande. The livetime and observed number of atmospheric neutrino events during the four SK run periods are summarized in Table 2.

Fully contained (FC) events deposit all of their Cherenkov light in the inner detector, while partially contained (PC) events have exiting tracks which deposit some Cherenkov light in the outer detector. The neutrino interaction vertex is required to be reconstructed within a 22.5 kiloton fiducial volume, defined to be $>$ 2 m from the PMT wall. The FC events are classified into "sub-GeV" ($E_{vis} < 1330$ MeV) and "multi-GeV" ($E_{vis} > 1330$ MeV). These events are further separated into sub-samples based on the number of observed Cherenkov rings. Single- and multi-ring are then divided into electron-like (e-like) or muon-like (μ-like) samples depending on pattern identification of the most energetic Cherenkov ring. The sub-GeV samples are additionally divided based on their number of decay-electrons and their likelihood of being a π^0. The PC events are separated into "OD stopping" and "OD through-going" categories based on the amount of light deposit by the exiting particle in the OD.

Energetic atmospheric ν_μ's passing through the Earth interact with rock surrounding the detector and produce muons via charged current interactions. These neutrino events are observed as upward going muons. Upward going muons are classified into two types. One is "upward through-going muons" which have passed through the detector, and the other is "upward stopping muons" which come into and stop inside the detector. The upward through-going muons are subdivided into "showering" and "non-showering" based on whether their Cherenkov pattern is consistent with light emitted from an electro-magnetic shower produced by a very high energy muon. The livetime and number of observed events for each SK periods are summarized in Table 3.

Table 2. Atmospheric neutrino livetimes and the number of observed FC and PC events for each SK run period. (*)Numbers for SK-IV are those observed until Sep. 24th in 2011, and preliminary since data taking is still ongoing.

	Livetime(days)	FC	PC
SK-I	1,489	12,232	896
SK-II	799	6,584	429
SK-III	518	4,356	343
SK-IV*	961	7,814	634

Table 3. Atmospheric neutrino induced upward-going muon livetime and the number of observed events for each SK run periods. (*)Numbers for SK-IV are those observed until Sep. 24th in 2011, and preliminary since data taking is still ongoing.

	Livetime(days)	through-going	stopping
SK-I	1,646	1,856	458
SK-II	828	889	228
SK-III	636	735	210
SK-IV*	961	1,163	275

The zenith angle and lepton momentum distributions for SK-I+II+III samples compared with the atmospheric neutrino Monte Carlo predictions are shown in Fig. 12. The prediction is based on the recent precise measurements of primary cosmic rays by BESS, AMS and a three dimensional calculation of the neutrino flux by Honda *et al*. The μ-like data from SK exhibit a strong up-down asymmetry in their zenith angle (Θ) distribution while no significant asymmetry was observed in the e-like data. The data were compared with the Monte

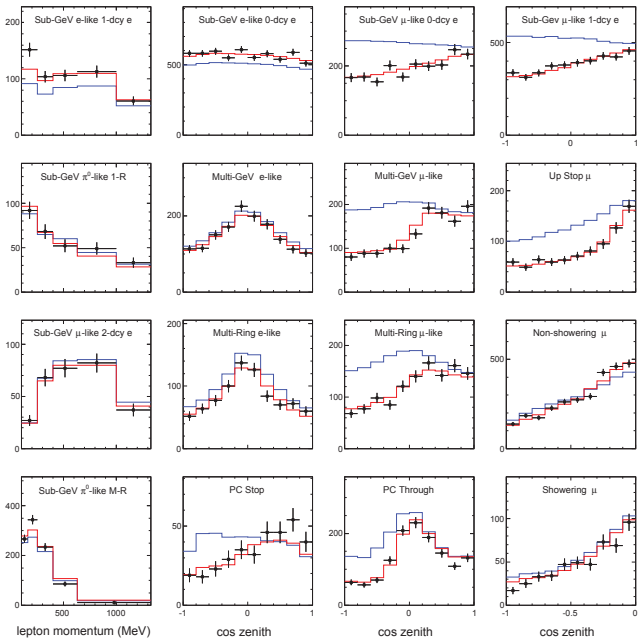

Fig. 12. The zenith angle and lepton momentum distributions for each data sample observed in SK-I+II+III. $\cos\Theta$ =1 indicates downward-going particles. The blue histograms show the MC prediction without neutrino oscillation and the red histograms show the MC prediction for $\nu_\mu \leftrightarrow \nu_\tau$ oscillations with $\sin^2 2\theta = 1.0$ and $\Delta m^2 = 2.1 \times 10^{-3}\mathrm{eV}^2$.

Carlo expectation without neutrino oscillations and the best-fit expectation for $\nu_\mu \leftrightarrow \nu_\tau$ oscillations. The oscillated Monte Carlo reproduces the zenith angle distributions of the data well. According to the $\nu_\mu \rightarrow \nu_\tau$ 2-flavor oscillation analysis, the best fit oscillation parameters are fitted to $\sin^2 2\theta = 1.0$ and $\Delta m^2 = 2.2 \times 10^{-3}\mathrm{eV}^2$.

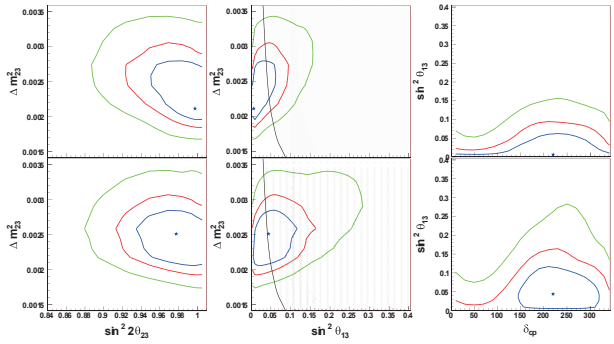

Fig. 13. The allowed regions for (Δm^2, $\sin^2 2\theta_{23}$); left, (Δm^2, $\sin^2\theta_{13}$); middle, and ($\sin^2\theta_{13}$, δ_{cp}); right for the normal (upper figure) and inverted (lower figure) hierarchy. The blue, red, and green contours correspond to 68, 90 and 99% C.L. allowed regions obtained by this analysis, respectively. The shaded regions corresponds to the area excluded at 90% C.L. by the CHOOZ experiment.

Two flavor neutrino oscillations which assume that θ_{13}=0 and $\Delta m^2_{12} \ll \Delta m^2_{23}$ successfully describe the SK atmospheric neutrino data with maximum mixing angle (θ_{23}=π/4). However, nonzero θ_{13} may be observable in the excess of multi-GeV electron neutrino events, and to a lesser extent in the

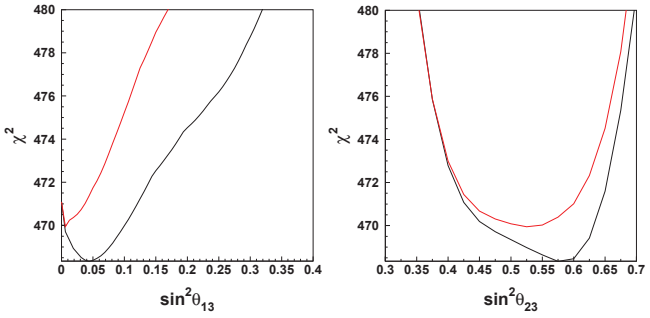

Fig. 14. χ^2 distribution as a function of (left:)$\sin^2\theta_{13}$ and (right:)$\sin^2\theta_{23}$. The normal hierarchy and inverted hierarchy cases are plotted with red and black lines, respectively.

oscillations of multi-GeV muon neutrinos. Additionally, the effects of the solar oscillation parameters and non-maximal mixing are observable as a sub-leading oscillation effect on the event rate of the Sub-GeV electron-like samples. If the CP violating term δ_{cp} is also considered, there are additional sub-dominant oscillation effects predicted across many of the SK atmospheric neutrino samples.

We have performed an extended oscillation analysis including all the mixing parameters and the CP violating term. The matter effect in the Earth is also considered in this calculation and both the normal and inverted mass hierarchies are tested. Figure 13 shows the allowed regions for (Δm^2, $\sin^2 2\theta_{23}$), (Δm^2, $\sin^2\theta_{13}$), and ($\sin^2\theta_{13}$, δ_{cp}) for the normal and inverted mass hierarchies. A comparison of χ^2 between normal and inverted hierarchy case is shown in Figure 14. The best fit parameter sets are (Δm^2_{23}, $\sin^2\theta_{23}$, $\sin^2\theta_{13}$, δ_{CP})= ($2.11{\cdot}10^{-3}eV^2$, 0.525, 0.006, 220°) for the normal hierarchy and ($2.51{\cdot}10^{-3}eV^2$, 0.575, 0.044, 220°) for the inverted hierarchy case. All fits are consistent with the two flavor oscillation results and CHOOZ experiment's upper limit on θ_{13}. No indication for either mass hierarchy is seen in the data. [15].

It becomes possible to search for *CPT* violation effects in the neutrino system via differences in the oscillation probabilities of neutrinos and antineutrinos. By inspiring oscillation result by MINOS [7], we also performed a *CPT* violation test of the atmospheric neutrino data using separated two-neutrino disappearance model, which allows neutrino and antineutrino to oscillate with different parameter sets of (Δm^2, θ) and ($\Delta\bar{m}^2$, $\bar{\theta}$), respectively. According to the fitting result, the allowed region for antineutrino mixing parameters is shown in Figure 15. The atmospheric mixing parameters for antineutrino oscillations are consistent with those for neutrinos and therefore no evidence for *CPT* violation is found.

Tau events, which are produced via ν_τ charge current (CC) interactions oscillated from ν_μ, are expected to be observed in SK. It would bring the direct evidence of $\nu_\mu \rightarrow \nu_\tau$ oscillation, however, the detection of ν_τ CC events in SK is challenging; the interaction rate of ν_τ charged current events is low since the neutrino energy threshold is 3.5 GeV and the atmospheric neutrino flux above this energy is relatively low. Also tau events are difficult to be identified individually because they tend to produce multiple particles. Tau analysis is

*[7] P. Adamson *et al.* (MINOS), Phys. Rev. Lett. 107, 021801 (2011)

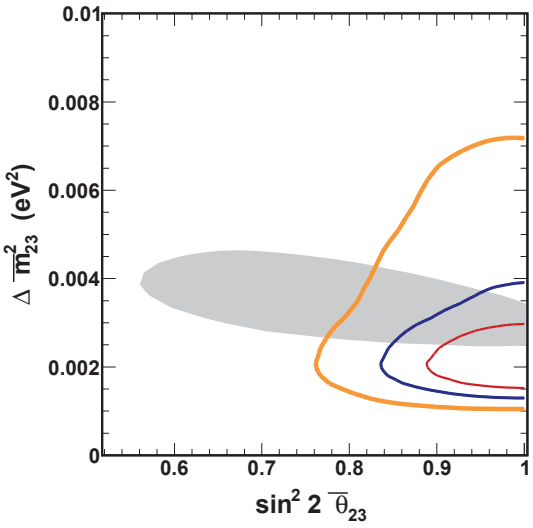

Fig. 15. Allowed regions for the antineutrino mixing parameters for SK-I+II+III data set. The 68%, 90%, and 99% allowed region appear in red thin, blue medium, and orange thick lines, respectively. The shaded region shows the 90% C.L. allowed region for antinuetrino disappearance in an antineutrino beam from MINOS.

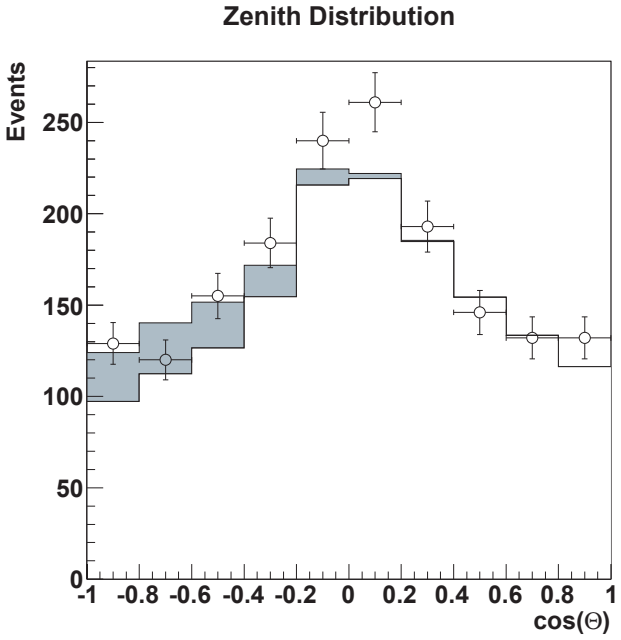

Fig. 16. Zenith angle distribution of tau-selected events by neural network method. SK-I, II, III dataset is used. Zenith angle $\cos(\theta)$=-1 (1) indicates upward-going (downward-going) direction. The data (dot with error bar) and the best-fit MC including tau signal (shaded region) and background from atmospheric neutrinos (ν_e and ν_μ) are shown.

performed employing neural network technique to discriminate tau events of hadronic decay from backgrounds of atmospheric ν_e and ν_μ events. Figure 16 shows the zenith angle distribution of tau-selected events. Tau events are expected to appear in the upword-going events because they originates $\nu_\mu \rightarrow \nu_\tau$ oscillation. The zenith angle shape of data is fitted with the MC expectation including tau signal and background with their normalizations free. According to the fitting result, the signal excess is estimated to 180.1 $\pm$ 4.3 (stat) $^{+17.8}_{-15.2}$ (syst) events compared to an expectation of 120.2 $^{+34.2}_{-34.8}$ (syst) and the detection significance correspond to 3.8 σ.

From recent observations, Weakly Interacting Massive Particles (WIMPs) are considered a favorite candidate for cold dark matter. From the viewpoint of minimum supersymmetric extensions of the Standard Model, the most well-motivated candidate for WIMPs in the universe is the lightest supersymmetric neutral particle (LSP). One method of searching for a WIMP dark matter signal is an indirect search where decay or annihilation products from WIMPs are observed as originating from the center of a gravitational potential well such as a celestial body. WIMP annihilation products in the form of muon-neutrinos are an excellent instrument for indirect searches since they can pass thorough the matter of the Sun, and interact in the Earth. Here we investigate upward-going muons(upmus) which are generated from high energy neutrinos come from the WIMP annihilations using Super-Kamiokande [17]. We search in the direction of the Sun, and an excess of neutrino flux above the atmospheric neutrino background is sought in the upmu events. Although volume array detectors such as IceCube have larger acceptances for higher mass WIMPs, SK is better equipped for the search of lower mass WIMPs (<100 GeV) due to its lower energy threshold for neutrino signals. The calculated upper limit is shown in Fig. 17 with the results from direct detection experiments.

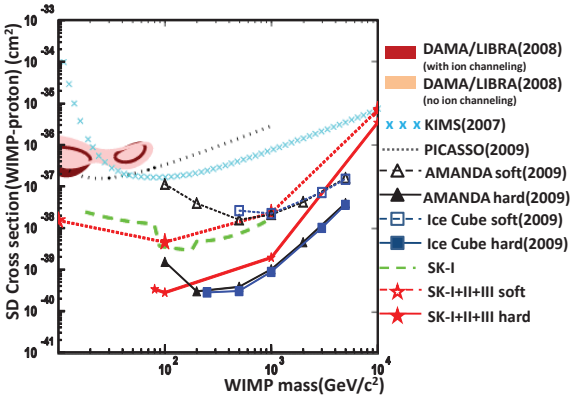

Fig. 17. Limit on the WIMP-proton spin-dependent cross section as a function of WIMP mass. Limits from direct detection experiments: DAMA/LIBRA allowed region (dark red and light red filled, for with and without ion channeling, respectively), KIMS (light blue crosses), and PICASSO (grey dotted line) are shown. Also we show here the results of indirect detection (neutrino telescopes): AMANDA (black line with triangles), IceCube (blue line with squares), and this analysis (red line with stars). Two annihilation senarios, soft channel ($b\bar{b}$) and hard channel (W^+W^-), are considered. Also the previous limit from Super-K (green dashed line) is shown.

We have preliminary analyzed 763 days of SK-IV atmospheric neutrinos data. The quality of the observed data are consistent with the previous SK-I, II, III results. The

zenith angle distributions for single-ring events of sub-GeV and multi-GeV FC and PC are shown in Figure 18. Due to the electronics upgrade, several performance are expected to be improved, such as the performance of Michel electrons tagging, the energy resolution in multi-GeV electron sample, etc. The further analysis including SK-IV data are going on.

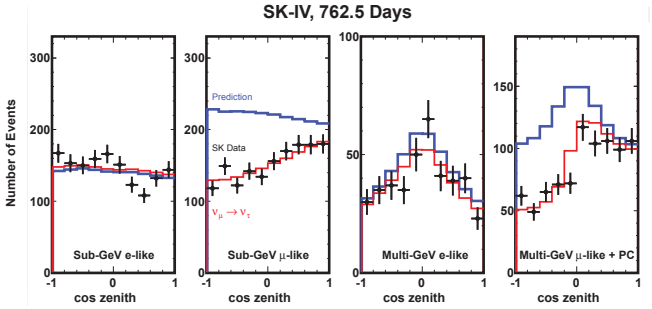

Fig. 18. Zenith angle distributions of SK-IV FC and PC events. From left, sub-GeV single-ring electron-like, sub-GeV single-ring muon-like, multi-GeV single-ring electron-like, sub-GeV single-ring muon-like plus PC events are shown. The horizontal axis shows the zenith angle, and -1 (1) indicates upward-going (downward–going) direction. The data (dot with error bar) and the prediction (blue) and best-fit MC (red) are shown.

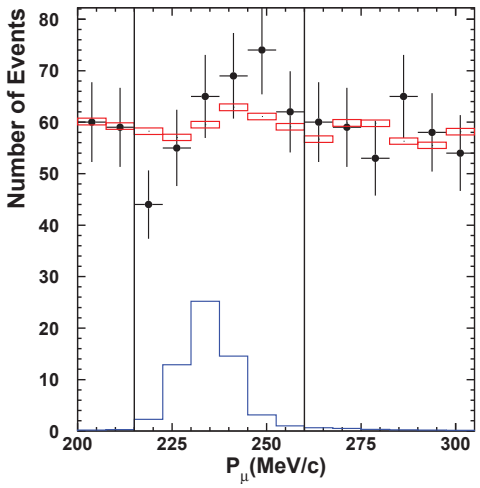

Fig. 19. The comparison between data and fitting results of the muon momentum distribution for single-ring μ-like events. The filled circles show data with statistical errors. The solid line shows $p \to \bar{\nu}K^+$ MC. The dashed line shows the best fitted atmospheric neutrino MC with free normalization.

Search for nucleon decay

Proton decays and bound neutron decays (nucleon decays in general) is the most dramatic prediction of Grand Unified Theories in which three fundamental forces of elementary particles are unified into a single force. Super-Kamiokande (SK) is the world's largest detector to search for nucleon decays and it has accumulated data of 91.7 kt·yrs (SK-I), 49.2 kt·yrs (SK-II), 31.9 kt·yrs (SK-III), and 46.5 kt·yrs (SK-IV), resulting in 220 kt·yrs data in total. Various nucleon decay modes have been looked for in the period from SK-I to SK-IV data but we have found no significant signal excess so far.

A proton decay into one positron and one neutral pion ($p \to e^+\pi^0$) is one of the most popular decay modes. This decay mode is mediated by super-heavy gauge bosons and discovery of the signal would give us the information of the mass of the gauge mesons. To discriminate the signal from the atmospheric neutrino background, we reconstruct the number of particles (Cherenkov rings) and reconstruct the total visible energy corresponding to parent proton mass and total momentum corresponding to the proton's Fermi momentum. The signal efficiency of SK-IV is estimated to be 45.0 % and the background induced by the atmospheric neutrino interactions is estimated to be 0.05. The BG rate was confirmed by an artificial neutrino beam by using 1-kton water Cherenkov detector [18]. There are no candidate events in data from SK-I to SK-IV, on the other hand, expected background in total (from SK-I to SK-IV) is 0.45. Then we obtained a lower limit on the partial lifetime of the proton; $\tau/B_{p\to e^+\pi^0} > 1.3 \times 10^{34}$ years at 90% confidence level.

In addition, we looked for SUSY favored decay modes which include K mesons in the final state, $p \to \bar{\nu}K^+$, $n \to \bar{\nu}K^0$, $p \to \mu^+K^0$, and $p \to e^+K^0$. In $p \to \bar{\nu}K^+$ search, we have analyzed data until SK-IV. In this mode, we tag the signal by decay products from K^+. The momentum of K^+ is below the Cherenkov threshold, and is stopped in the water and decay into $\mu^+\nu$ or $\pi^+\pi^0$ with monochromatic momenta. On the other hand, the residual nucleus after proton decay emits γ ray (40% probability) and it is also useful to tag the proton decay signal. In SK-IV, electronics has been replaced and all of hits information are recorded by DAQ. As a result, the decay electron tagging effieciency is improved and the selection efficiencies of $p \to \bar{\nu}K^+$ are improved. The efficiency of the prompt γ tagging method is increased from 7.2 % (SK-I) to 8.2 % (SK-IV), and the efficiency of the $\pi^+\pi^0$ method is increased from 6.5 % to 7.9 %.

Figure 19 shows one analysis method in which we search for muon with the monochromatic momentum 236 MeV/c. It shows the comparison of the muon momentum distributions for single-ring μ-like events between data, atmospheric ν MC, and proton decay MC, and there are no significant excess in data. We have analyzed the data from SK-I to SK-IV, there are no candidates in the prompt γ method and the $\pi^+\pi^0$ method. Therefore we conclude that there is no evidence of nucleon decays and we calculated partial lifetime limits taking into account systematic uncertainties. Obtained limit is 4.0×10^{33} years at 90% confidence level for $p \to \bar{\nu}K^+$.

Figure 20 shows a summary of nucleon decay searches by the Super-Kamiokande detector. In each decay mode, we have not observed significant excesses from the atmospheric neutrino back ground and we got lower limits of nucleon lifetime. In $p \to e^+\pi^0$ and $p \to \mu^+\pi^0$ mode, the lower limits of proton life time have been exceeded 10^{34}, that is the entrance of the interested region because many GUT models are predicting proton lifetime in 10^{34}?10^{35}.

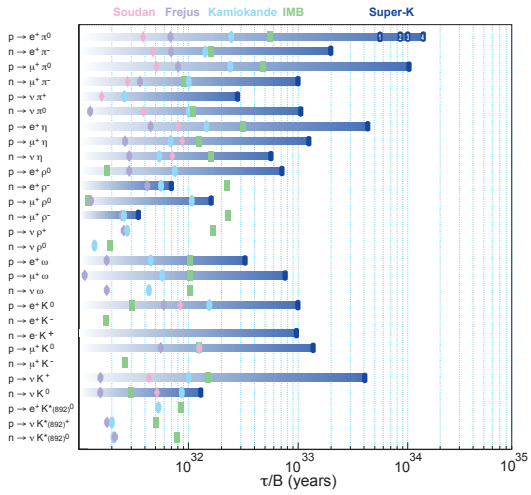

Fig. 20. A summary of nucleon life time limits studied by the Super-Kamiokande detector. Most of them are the most stringent limits in the world.

Bibliography

[1] Super-Kamiokande Collaboration, "Solar neutrino results in Super-Kamiokande-III", *Phys. Rev.* D 83 (2011) 052010.

[2] Super-Kamiokande Collaboration, "Solar neutrino measurements in Super-Kamiokande-I", *Phys. Rev.* D 73 (2006) 112001.

[3] W. T. Winter *et al.*, "The ^{8}B neutrino spectrum", *Phys. Rev.* C 73 (2006) 025503.

[4] J.N.Bahcall and M.H.Pinsonneault, "What Do We (Not) Know Theoretically about Solar Neutrino Fluxes?", *Phys. Rev. Lett.* 92 (2004) 121301.

[5] B. Aharmim *et al.*, "Independent Measurement of the Total Active ^{8}B Solar Neutrino Flux Using an Array of ^{3}He Proportional Counters at the Sudbury Neutrino Observatory", *Phys. Rev. Lett.* 101 (2008) 011301.

[6] B. Aharmim *et al.*, "Low Energy Threshold Analysis of the Phase I and Phase II Data Sets of the Sudbury Neutrino Observatory" *Phys. Rev.* C 81 (2010) 055504.

[7] B. Aharmim *et al.*, "Determination of the ν_e and Total ^{8}B Solar Neutrino Fluxes with the Sudbury Neutrino Observatory Phase I Data Set", *Phys. Rev.* C 75 (2007) 045502.

[8] S.N.Ahmed *et al.*, "Electron Energy Spectra, Fluxes, and Day-Night Asymmetries of ^{8}B Solar Neutrinos from the 391-Day Salt Phase SNO Data Set", *Phys. Rev.* C 72 (2005) 055502.

[9] C.Arpesella *et al.*, "Direct Measurement of the ^{7}Be Solar Neutrino Flux with 192 Days of Borexino Data", *Phys. Rev. Lett.* 101 (2008) 091302.

[10] B.T.Cleveland *et al.*, "Measurement of the Solar Electron Neutrino Flux with the Homestake Chlorine Detector Bruce T. Cleveland", *Astrophys. J.* 496 (1998) 505.

[11] J.N.Abdurashitov *et al.*, "Measurement of the solar neutrino capture rate with gallium metal", *Phys. Rev.* C 60 (1999) 055801.

[12] M.Altmann *et al.*, "GNO solar neutrino observations: results for GNO I", *Phys. Lett.* B 490 (2000) 16.

[13] S. Abe *et al.*, "Precise Measurement of Neutrino Oscillation Parameters with KamLAND", *Phys. Rev. Lett.* 100 (2008) 221803.

[14] Y. Fukuda *et al.*, "Evidence for Oscillation of Atmospheric Neutrinos", Phys. Rev. Lett. **81** 1562 (1998).

[15] R. Wendell, C. Ishihara *et al.* [Super-Kamiokande Collaboration], "Atmospheric neutrino oscillation analysis with subleading effects in Super-Kamiokande I, II, and III", Phys. Rev. D 81 (2010) 092004.

[16] P. Adamson *et al.* [MINOS collaboration], "First direct observation of muon antineutrino disappearance," arXiv:1104.0344 [hep-ex].

[17] T. Tanaka *et al.*, "An Indirect Search for WIMPs in the Sun using 3109.6 days of upward-going muons in Super-Kamiokande", Astrophys. J. **742**, 78 (2011)

[18] S. Mine *et al.* [K2K Collaboration], "Experimental study of the atmospheric neutrino backgrounds for proton decay to positron and neutral pion searches in water Cherenkov detectors," Phys. Rev. D **77**, 032003 (2008) [arXiv:0801.0182 [hep-ex]].

[19] H. Nishino *et al.* [Super-Kamiokande Collaboration], "Search for Proton Decay via $p \to e^+\pi^0$ and $p \to \mu^+\pi^0$ in a Large Water Cherenkov Detector," Phys. Rev. Lett. **102**, 141801 (2009) [arXiv:0903.0676 [hep-ex]].

Hyper-Kamiokande

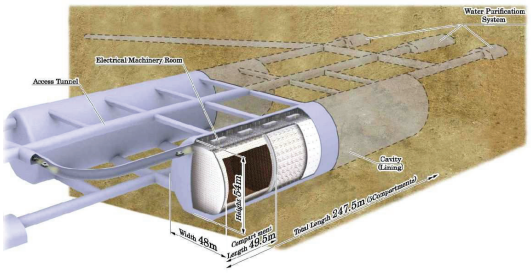

Fig. 1. Schematic view of the Hyper-Kamiokande. The detector consists of two cylindrical tanks holding 500 kton ultrapure water (1 Mton in total). The each tank is divided by segmentation walls every 50 m.

The Hyper-Kamiokande is the third generation nucleon decay and neutrino detector at Kamioka that aims to explore unification of elementary particles and full picture of neutrino masses and mixings. The schematic view of the Hyper-K detector is illustrated in Fig. 1 and 2. We released a letter of intent [3] in which the detectors baseline design and physics

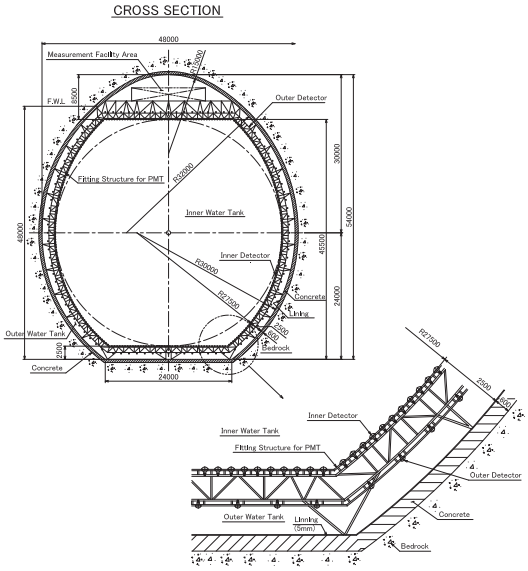

Fig. 2. The cross section view of the Hyper-Kamiokande water tank.

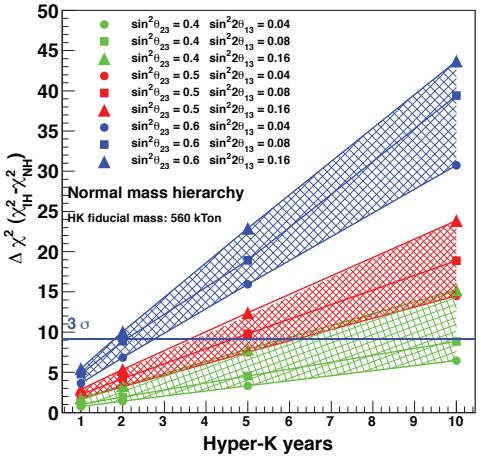

Fig. 4. Expected discrimination power for neutrino mass hierarchy as a function of observation years. Blue horizontal line shows $\Delta\chi^2$ of nine which corresponds to hierarchy determination with 3σ significance. Typical observation years to reach the 3σ level is 5 years.

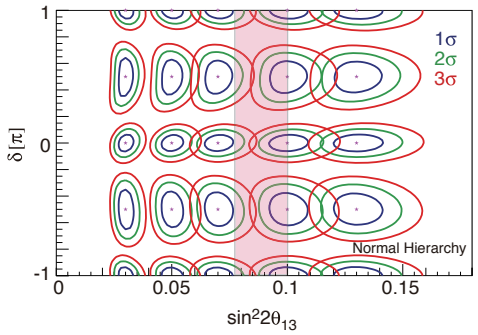

Fig. 3. Expected sensitivity for $\sin^2 2\theta_{13}$ and *CP* phase δ assuming the 2.25 Mton·years of ν and 5.25 Mton·years of $\bar{\nu}$ runs. The pink band represents the measurement by Daya Bay reactor experiment.

potential of Hyper-K are described. The water Cherenkov detector with the dimension of 1 million tones has capability of exploring nucleon lifetimes about 10 times as long as the limits set by the Super-Kamiokande. For example, the sensitivity for the decay mode $p \to e^+\pi^0$ is expected to be beyond 1×10^{35} years [1]. The detector also aims to study neutrino properties such as Dirac *CP* phase, mass hierarchy, octant of θ_{23}, and so on by using a high power accelerator based neutrino beam and atmospheric neutrinos. Figure 3 shows the expected size of allowed regions for the parameter space of θ_{13} and δ_{CP} by using upgraded J-PARC neutrino beam with the power of 0.75 MW $\times$10 years and the Hyper-Kamiokande detector with the fiducial volume of 0.56 Megaton [1]. The high statistics data sample of atmospheric neutrinos obtained by Hyper-K will also allow us to extract information on the mass hierarchy and the octant of θ_{23}. With a full 10 year period of data taking, the significance for the mass hierarchy determination is expected to reach 3σ or greater as is shown in Fig. 4.

T2K presented an evidence for $\nu_\mu \to \nu_e$ oscillations in 2012. Furthermore the Reactor Neutrino Experiments announced that they have observed $\bar{\nu}_e$ disappearance and the measured θ_{13} value is consistent with the ν_e appearance observed in T2K [2]. The observed nonzero θ_{13} opened the possibility of exploring remaining neutrino parameters, *i.e. CP* phase and mass hierarchy. The large size of θ_{13} is really encouraging and it boosted the activities toward realization of the future detector.

Extensive development works by the Hyper-Kamiokande working group have been performed on geological surveys in the candidate sites, design of cavern and tank, water purification and circulation system design, new photon sensor and DAQ system, detector calibration system, analysis software, and physics sensitivities. The 20-inch PMTs which have been used in the Super-K satisfy necessary requirement of Hyper-K. However, lower-cost higher-sensitivity photo-sensors are preferred because one of main cost drivers is the PMT. A hybrid photo-detector (HPD) using a photocathode and an avalanche photo-diode with 10 kV high voltage is being developed. Proof-test will be conducted in 2013 by long term operation of several prototypical HPDs installed in a 100 ton scale water Cherenkov detector. Photo-sensors using other techniques are also being developed. In parallel, many development works are going on or starting mainly to enhance the physics potential of the detector and optimize its construction cost. DAQ electronics and computer system design was made based upon the Super-K. R&D of the front-end electronics under water is being started. The design of water purification system is going on with companies in Japan and US. The water flow control in the big tank is under investigation. Moreover, sophisticated detector calibration system and dedicated software development are also under discussions.

Furthermore, we held the first international Hyper-K meeting in August to review the project and formed international organization (Hyper-Kamiokande working group).

There are about 100 participants in the meeting. We plan to hold the second meeting in 2013 to further discuss the physics potential and design of the detector.

Bibliography

[1] M. Shiozawa, "Large Underground Water Cherenkov Detectors", Proceeding of the XXIV International Conference on Neutrino Physics and Astrophysics (Neutrino2010), June, 2010. to be published in Nuclear Physics B Proceedings Supplement.

[2] K. Abe *et al.* [T2K Collaboration], "Indication of Electron Neutrino Appearance from an Accelerator-produced Off-axis Muon Neutrino Beam," arXiv:1106.2822 [hep-ex].

[3] K. Abe, T. Abe, H. Aihara, Y. Fukuda, Y. Hayato, K. Huang, A. K. Ichikawa and M. Ikeda *et al.*, arXiv:1109.3262 [hep-ex].

T2K Experiment

The T2K (Tokai-to-Kamioka) experiment [1] is a long baseline neutrino oscillation experiment. Its main goal is to establish the existence of $\nu_\mu \to \nu_e$ neutrino oscillations and measure the mixing angle θ_{13} by observing ν_e appearance in a ν_μ beam. It also aims to make a precision measurement of the known neutrino oscillation parameters with precision of $\delta(\Delta m^2_{23}) \sim 10^{-4}\,\mathrm{eV}^2$ and $\delta(\sin^2 2\theta_{23}) \sim 0.01$ via ν_μ disappearance studies. In addition to neutrino oscillation studies, the T2K neutrino beam (with $E_\nu \sim 1$GeV) will enable a rich fixed-target physics program of neutrino interaction studies at energies covering the transition between the resonance production and deep inelastic scattering regimes.

T2K adopts the off-axis method [2] to generate the narrow-band neutrino beam using the new MW-class proton synchrotron at J-PARC. In this method the neutrino beam is purposely directed at an angle with respect to the baseline connecting the proton target and the far detector, Super-Kamiokande. The off-axis angle is set at 2.5° so that the narrow-band muon neutrino beam generated toward the far detector has a peak energy at ~ 0.6 GeV, which maximizes the effect of the neutrino oscillation driven by $\Delta m^2_{32} \simeq \Delta m^2_{13}$ at 295 km and minimizes the background to electron-neutrino appearance detection.

Details of the T2K experimental setup are described elsewhere [3]. The J-PARC Main Ring (MR) accelerator [4] provides 30 GeV protons with a cycle of 0.3 Hz. Beam bunches are single-turn extracted in 5 μs and transported an extraction line arc defined by superconducting combined-function magnets to the production target. The target is a graphite rod with a diameter of 2.6 cm and a length of 90 cm (corresponding to 1.9 interaction length). Charged particles exiting the target are sign selected and focused into the 96 m long decay tunnel by three magnetic horns pulsed at 250 kA.

The near detector complex [5] is located 280 m downstream from the target and hosts two detectors. The on-axis Interactive Neutrino GRID (INGRID) [6] records neutrino interactions with high statistics to monitor the beam intensity,

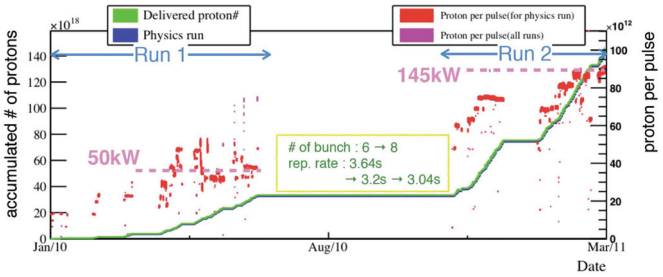

Fig. 1. Accumulated number of protons on target (green/blue lines) and protons per pulse (red/purple dots) during the T2K's first two physics runs.

direction and profile. It consists of 14 identical 7-ton modules composed of iron-absorber/scintillator-tracker sandwich arranged in 10 m by 10 m crossed horizontal and vertical arrays centered on the beam. The off-axis detector (ND280) reconstructs exclusive final states to study neutrino interactions and beam properties corresponding to those expected at the far detector. Embedded in the refurbished UA1/NOMAD magnet (field strength 0.2 T), it consists of three large volume time projection chambers (TPCs) [7] interleaved with two fine-grained tracking detectors (FGDs, each 1 ton), a π^0-optimized detector and a surrounding electromagnetic calorimeter. The magnet yoke is instrumented as a side muon range detector.

The SK water-Cherenkov far detector [8] has a fiducial volume (FV) of 22.5 kt within its cylindrical inner detector (ID). Enclosing the ID is the 2 m-wide outer detector (OD). The front-end readout electronics allow for a dead-time-free trigger. Spill timing information, synchronized by the Global Positioning System (GPS) with < 150 ns precision, is transferred to SK and triggers the recording of photomultiplier hits within ± 500 μs of the expected neutrino arrival time.

The T2K experiment began accumulating neutrino beam data for physics analsis in January 2010. Figure 1 shows accumulated number of protons on target (p.o.t.), along with number of protons per pulse. The first two physics runs are defined as Run 1 (January–June 2010) and Run 2 (November 2010–March 2011). During this time period, the MR proton beam power was continuously increased and reached 145 kW with 9×10^{13} protons per pulse. The number of bunches was six during Run 1 and eight during Run 2. By the end of Run 2, a total of 2,474,419 spills were retained for analysis after beam and Super-Kamiokande quality cuts, yielding 1.43×10^{20} p.o.t.. The proportion of Super-Kamiokande good spills to the total number of spills selected by beam conditions was 99 %. In FY2011, two physics results had been published by using the whole Run 1+2 data: electron neutrino appearance search from $\nu_\mu \to \nu_e$ neutrino oscillation [**?**], and muon neutrino disappearance analysis [**?**].

The neutrino flux is predicted by a Monte Carlo (MC) simulation based on experimental data. Pion production is based on the data by the NA61/SHINE experiment [11], which measured hadron production by 30 GeV protons on a graphite target. Other hadronic interactions inside the target are simulated by FLUKA. GEANT3/GCALOR handles particle propagation through the magnetic horns, target hall, decay volume and

beam dump. The predicted neutrino flux is predominantly ν_μ with $< 1\%\nu_e$ contamination. Pion and kaon production uncertainties dominate the neutrino flux prediction uncertainty.

The NEUT MC event generator [12], which has been tuned with recent neutrino interaction data in an energy region compatible with T2K, is used to simulate neutrino interactions in the near and far detectors. An energy-dependent error on charged-current quasi-elastic interactions (CCQE) is assigned to account for the uncertainty in the low energy cross-section, especially for the different target materials between the near and far detectors.

An inclusive ν_μ charged-current (CC) measurement in the off-axis near detector is used to constrain the expected event rate at the far detector. Neutrino interactions in the FGDs with tracks entering the downstream TPC are selected. A dE/dx of the most energetic negative track in the TPC is require to be compatible with a muon. To reduce background from interactions outside the FGDs, there must be no track in the upstream TPC. The analysis selects 1529 events. The measured data/MC ratio is 1.036 ± 0.028(stat.) $^{+0.044}_{-0.038}$(det.syst.)$\pm$0.038(phys.syst.). The detector systematic errors mainly come from tracking and particle identification efficiencies, and physics uncertainties are related to the interaction modeling.

At Super-Kamiokande, a fully-contained fiducial volume (FCFV) sample is extracted by requiring no event activity in either the OD or in the 100 μs before the event trigger time, at least 30 MeV electron-equivalent energy deposited in the ID (defined as visible energy E_{vis}), and the reconstructed vertex in the 22.5 kton fiducial region. The Run 1+2 data have 88 such FCFV events. All of them are within the time range from -2 to 10 μs around the beam trigger time. The accidental contamination from non-beam related events (predominantly from atmospheric neutrino interactions) is estimated to be 0.003 events.

A sample enhanced in ν_e CCQE interacions from $\nu_\mu \rightarrow \nu_e$ neutrino oscillation is prepared for ν_e appearance analysis. The main background are intrinsic ν_e contamination in the beam and neutral-current (NC) interactions with a misidentified π^0. The selection criteria for this analysis were fixed from MC studies before the data were collected, optimized for the initial running conditions. To select the sample, we require conditions below:(a) FCFV selection (b) single Cherenkov rings (c) identified as electron-like ring (d) visible energy is greater than 100 MeV (e) no delayed-electron signal (e) an invariant mass forcibly reconstructed with assumption of two e-like rings is less than 105 MeV/c, and (f) reconstructed neutrino energy is less than 1250 MeV, which is calculated by assuming a ν_e CCQE interaction kinematics with fixed neutron target. Finally we obsered 6 events in this data period. Fig. 2 shows the reconstructed neutrino energy distribution for ν_e appearance analysis sample.

The expected number of events at Super-Kamiokande (N_{SK}^{exp}) is calculated by using the near detector ν_μ CC interaction rate measurement as normalization, and the ratio of expected events in the near and far detectors, where common systematic errors cancel. The oscillation parameters other than $\sin^2 2\theta_{13}$ are fixed at $\Delta m^2_{12} = 7.6 \times 10^{-5}\mathrm{eV}^2$, $\Delta m^2_{32} = 2.4 \times 10^{-3}\mathrm{eV}^2$, $\sin^2 2\theta_{12} = 0.8704$, $\sin^2 2\theta_{23} = 1.0$, and $\delta_{\mathrm{CP}} =$ 0 unless otherwise noted.

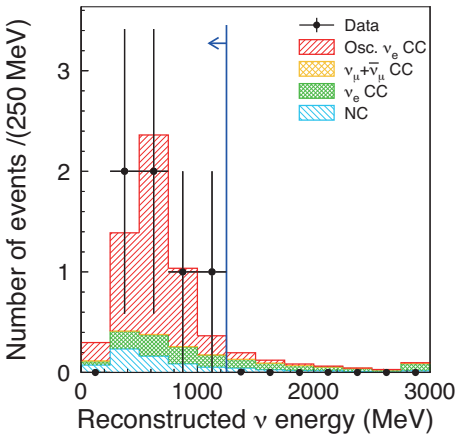

Fig. 2. Reconstructed neutrino energy spectrum of the events which pass all ν_e appearance signal selection criteria with the exception of the energy cut. The vertical line shows the applied cut at 1250 MeV. The data are shown using points with error bars (statistical only) and the MC predictions are in shaded histograms, corresponding to oscillated ν_e CC signal and various background sources for $\sin^2 2\theta_{13} = 0.1$.

Table 1. Systematic error for ν_e appearance analysis sample. Contributions from various sources and the total relative uncertainty for $\sin^2 2\theta_{13} = 0$ and 0.1 are shown.

Source	$\sin^2 2\theta_{13} = 0$	$\sin^2 2\theta_{13} = 0.1$
neutrino flux	$\pm$ 8.5 %	$\pm$ 8.5 %
near detector	$^{+5.6}_{-5.2}$ %	$^{+5.6}_{-5.2}$ %
near det. statistics	$\pm$ 2.7 %	$\pm$ 2.7 %
cross section	$\pm$ 14.0 %	$\pm$ 10.5 %
far detector	$\pm$ 14.7 %	$\pm$ 9.4 %
Total $\delta N_{SK}^{exp}/N_{SK}^{exp}$	$^{+22.8}_{-22.7}$ %	$^{+17.6}_{-17.5}$ %

The computed N_{SK}^{exp} are $1.5\pm0.3(5.5\pm1.0)$ events for $\sin^2 2\theta_{13} = 0(0.1)$. Table 1 shows the estimated systematic errors of N_{SK}.

The errors from cross-section modeling are dominated by uncertainties in intranuclear final state interactions (FSI) and by the knowledge of the $\sigma(\nu_e)/\sigma(\nu_\mu)$ ratio. estimated to $\pm$6 %. The systematic uncertainties due to event selection in Super-Kamiokande were studied with cosmic-ray muons, electrons from muon decays, and atmospheric neutrino events. Main contribution to $\delta N_{SK}^{exp}/N_{SK}^{exp}$ for e.g. $\sin^2 2\theta_{13} = 0.1$ is 5.0 % from ring counting, 4.9 % from particle identification, and 6.0 % from the M_{inv} cut.

Our oscillation result is based entirely on comparing the number of ν_e candidate events with predictions, varying $\sin^2 2\theta_{13}$ for each δ_{CP} value. At each oscillation parameter point, a probability distribution for the expected number of events is constructed, incorporating systematic errors [18], which is used to make the confidence interval (Fig. 3), following the unified ordering prescription of Feldman and Cousins [19].

In conclusion, the observation of six single ring e-like events exceeds the expectation of a three-flavor neutrino os-

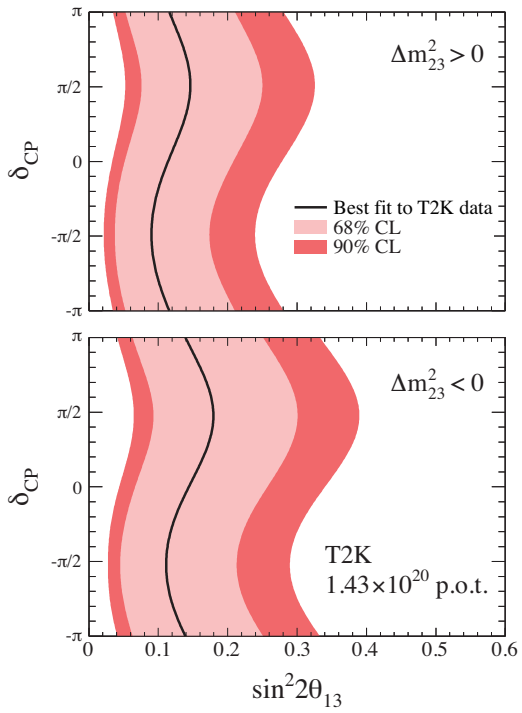

Fig. 3. (color). The 68% and 90% C.L. regions for $\sin^2 2\theta_{13}$ as a function of δ_{CP}, consistent with the observed number of events in the three-flavor oscillation case for normal (top) and inverted (bottom) mass hierarchy. The other oscillation parameters are fixed (see text). The best fit values are shown with solid lines.

cillation scenario with $\sin^2 2\theta_{13} = 0$. The null θ_{13} hypothesis is excluded at 99.3% level (2.5σ). This result converted into a confidence interval yields $0.03(0.04) < \sin^2 2\theta_{13} < 0.28(0.34)$ at 90% C.L. for $\sin^2 2\theta_{23} = 1.0$, $|\Delta m^2_{32}| = 2.4\times10^{-3}$ eV^2, $\delta_{CP} = 0$ and for normal (inverted) neutrino mass hierarchy. Under the same assumptions, the best fit points are 0.11(0.14), respectively.

For ν_μ disappearance analysis, we select a ν_μ CCQE enhanced sample. To select the sample, we require conditions below:(a) FCFV selection (b) single Cherenkov rings (c) identified as muon-like ring (d) zero or one delayed-electron signal, and (e) moun momentum is greater than 200 MeV/c. Finally, we observed 31 events. The reconstructed energy spectrum of the 31 data events is shown in Fig. 4 along with the expected far-detector spectra without disappearance and with best-fit oscillations. Calculation of the expected number of events and energy spectrum is calculated in same manner as in ν_e appearance analysis. Systematic uncertainty are shown in Table 2. The computed N^{exp}_{SK} for null oscillation case is $103.6^{+13.8}_{-13.4}$ events.

An energy-depending deficit of ν_μ are quantitatively studied and extract neutrino oscillation parameters, $\sin^2\theta_{23}$ and Δm^2_{32}. We had tested the observed energy spectrum with tow method: one is based on a likelihood ratio with binned energy spectrum, and another is based maximum likelihood method with unbinned energy spectrum. We assume a $\nu_\mu \to \nu_\tau$ 2-flavor neutrino oscillation and survey

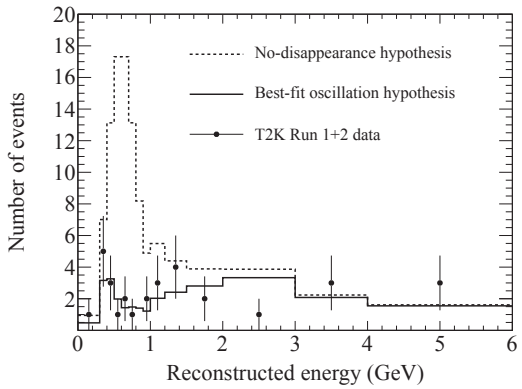

Fig. 4. Reconstructed energy spectrum of the 31 data events compared with the expected spectra in the far detector without disappearance and with best-fit $\nu_\mu \to \nu_\tau$ oscillations.

Table 2. Systematic error for ν_μ disappearance analysis sample. Contributions from various sources and the total relative uncertainty for $\sin^2 2\theta_{23} = 0$ and 1.0 are shown.

Source	$\sin^2 2\theta_{23} = 0$	$\sin^2 2\theta_{23} = 1.0$
neutrino flux	$\pm$ 7.3 %	$\pm$ 4.8 %
near detector	$^{+5.5}_{-5.3}$ %	$^{+5.5}_{-5.3}$ %
near det. statistics	$\pm$ 2.6 %	$\pm$ 2.6 %
cross section	$^{+7.8}_{-7.3}$ %	$^{+10.5}_{-9.4}$ %
far detector	$\pm$ 5.1 %	$\pm$ 10.3 %
Total $\delta N^{exp}_{SK}/N^{exp}_{SK}$	$^{+13.3}_{-13.0}$ %	$^{+15.0}_{-14.8}$ %

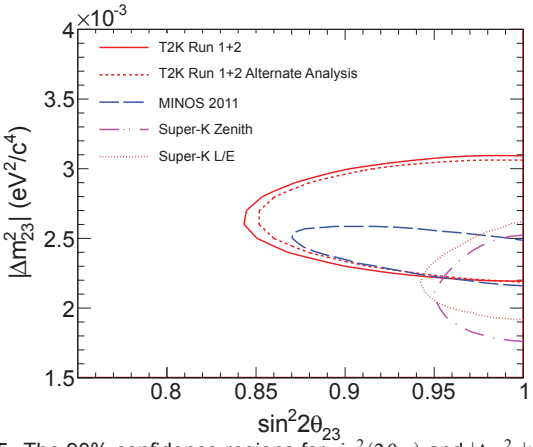

Fig. 5. The 90% confidence regions for $\sin^2(2\theta_{23})$ and $|\Delta m^2_{32}|$; results from the two analyses reported here are compared with those from MINOS [21] and Super-Kamiokande [22, 23].

$(\sin^2\theta_{23}, |\Delta^2 m_{32}|)$ space. The best-fit point by first method is obtained at $(\sin^2\theta_{23}, |\Delta^2 m_{32}|) = (0.98, 2.65\times10^{-3}\text{eV}^2)$ and at $(\sin^2\theta_{23}, |\Delta^2 m_{32}|) = (0.99, 2.63\times10^{-3}\text{eV}^2)$ by second method.

We construct confidence regions in the oscillation parameters using the method of Feldman and Cousins [19]. Statistical variations are taken into account by Poisson fluctuations of toy MC datasets, and systematic uncertainties are incorporated using the method of Cousins and Highland [20, 18]. The 90% confidence region for $\sin^2(2\theta_{23})$ and $|\Delta m^2_{32}|$ is shown in Fig. 5 for combined statistical and systematic uncertainties.

The T2K beam production has been suspended since the

Tohoku Earthquake occured on March 11, 2011. Recovery works on the dameged accelerator and beamline components were successfully done and the neutrino beam was resumed from December, 2011. About double of neutrino data was accumulated by June 2012, and physics analyes are on-going and will be shown in FY2012.

Bibliography

[1] Letter of intent: Neutrino oscillation experiment at JHF, 2003. http://neutrino.kek.jp/jhfnu/loi/loi_JHFcor.pdf.

[2] D. Beavis, A. Carroll, I. Chiang, *et al.*, Long Baseline Neutrino Oscillation Experiment at the AGS (Proposal E889), 1995. Physics Design Report, BNL 52459.

[3] K. Abe *et al.* (T2K Collaboration), accepted for publication in Nucl. Instrum. Methods, article in press (2011), doi: 10.1016/j.nima.2011.06.067, arXiv:1106.1238 [physics.ins-det].

[4] Y. Yamazaki *et al.*, KEK Report 2002-13 and JAERI-Tech 2003-44 and J-PARC-03-01 (2003).

[5] K. Abe *et al.* (T2K Collaboration), Nucl. Instrum. Meth. A659, 106 (2011), arXiv:1106.1238 [hep-ex].

[6] K. Abe *et al.* (T2K Collaboration), Nucl. Instrum. Meth. A694, 211 n(2012), arXiv:1111.3119 [hep-ex].

[7] N. Abgrall *et al.*, Nucl. Instrum. Meth. A637, 25 (2011), arXiv:1012.0865 [physics.ins-det].

[8] Y. Fukuda *et al.* (Super-Kamiokande Collaboration), Nucl. Instrum. Meth. A501, 418 (2003).

[9] K. Abe *et al.* (T2K Collaboration), Phys. Rev. Lett. 107, 041801 (2011)

[10] K. Abe *et al.* (T2K Collaboration), Phys. Rev. D85, 031103(R) (2011)

[11] N. Abgrall *et al.* (NA61/SHINE Collaboration), submitted to Phys. Rev. C (2011), arXiv:1102.0983 [hep-ex].

[12] Y. Hayato, Nucl. Phys. (Proc. Suppl.) B112, 171 (2002).

[13] Y. Ashie *et al.* (Super-Kamiokande Collaboration), Phys. Rev. D71, 112005 (2005), hep-ex/0501064.

[14] T. Barszczak, (2005), Ph.D. Thesis (University of California, Irvine), UMI-31-71221.

[15] G. J. Feldman and R. D. Cousins, Phys. Rev. D57, 3873 (1998).

[16] M. Apollonio *et al.* (Chooz Collaboration), Eur. Phys. J. C27, 331 (2003), hep-ex/0301017.

[17] P. Adamson *et al.* (MINOS Collaboration), Phys. Rev. D82, 051102 (2010), arXiv:1006.0996 [hep-ex].

[18] J. Conrad *et al.* Phys.Rev. D67, 012002 (2003)

[19] G.J.Feldman *et al.* Phys. Rev. D57, 3873 (1998)

[20] Nucl. Instrum. Meth. A320, 331 (1992)

[21] P. Adamson *et al.* (MINOS Collaboration) Phys. Rev. Lett. 106, 181801 (2011)

[22] K. Abe *et al.* (Super-Kamiokande Collaboration), Phys. Rev. Lett. 107, 241801 (2011)

[23] Y. Ashie *et al.* (Super-Kamiokande Collaboration), Phys. Rev. Lett. 93, 101801 (2004)

XMASS experiment

XMASS is a multi-purpose (detection of dark matter, neutrino-less double beta decay, and ^{7}Be/pp solar neutrinos) experiment using ultra-pure liquid xenon. The first stage of XMASS experiment is concentrated on dark matter searches using 800 kg liquid xenon detector (100 kg fiducial-mass detector). The detector construction in the Kamioka mine was funded and started in April 2007. Construction work was completed in September 2010 and commissioning run has been started since October 2010.

Several astronomical observations indicate that the universe contains a large amount of nonbaryonic dark matter. One of the most plausible candidates for the nonbaryonic dark matter is a weakly interacting massive particle (WIMP) provided by the supersymmetry in the form of the lightest supersymmetric particle. WIMPs can be directly detected through their elastic scattering off target nuclei in a detector. XMASS searches for the WIMP-xenon nucleus interaction in liquid xenon. Liquid xenon has the several advantages for dark matter searches. Large amount of scintillation light (42,000 photons/MeV), which is as good as NaI(Tl) scintillator enables us to detect small energy signals such as dark matter recoil. Owing to the high atomic number of xenon ($Z = 54$) and the high density of liquid xenon ($\sim 2.9\,\mathrm{g/cm^3}$), target volume can be small and external background gamma-rays can be absorbed within a short distance from the detector wall. WIMPs, however, interact throughout the detector. Therefore, if the vertices of the events can be reconstructed, WIMPs can be observed in a low background environment by extracting only events which were observed deep inside the detector. The expected sensitivity of the XMASS experiment is 10^{-45} cm^2 for 100 GeV mass of WIMPs.

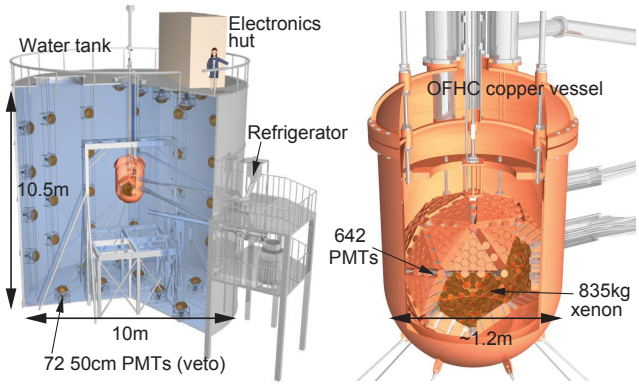

Fig. 1. Schematic view of the water tank and the liquid xenon vessel.

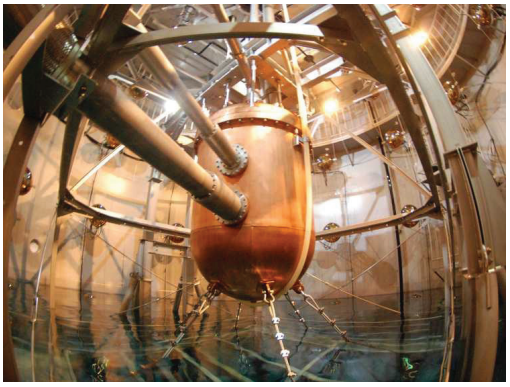

Fig. 2. Photo of liquid xenon vessel inside the water tank.

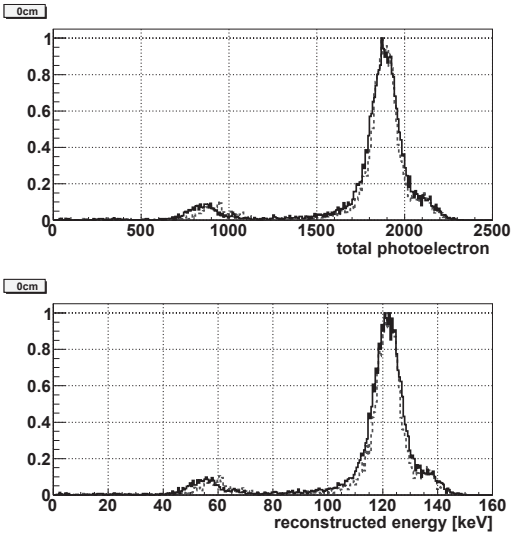

Fig. 3. Calibration data with ^{57}Co source at the center of the detector. The top figure shows a distribution for observed total photo electron and the bottom figure shows the reconstructed energy. The solid histograms and dotted histograms depict real data and Monte Carlo simulation, respectively.

The XMASS detector consists of the cylindrical water tank with 72 50cm PMTs and spherical liquid xenon detector with 642 2inch PMTs as shown in Fig. 1. This is the first case to adopt a pure-water tank as an active and passive shield for dark matter experiments. The spherical array of PMTs is contained in a double wall vessel. The vessel consisting of inner and outer vacuum chamber is made from oxygen free high conductivity copper. The gap between IVC and OVC is kept vacuum for thermal isolation. All the detector assembling work was completed in 2010 as shown in Fig. 2.

Commissioning data with a 100 kg fiducial-mass detector

Commissioning data were taken from the end of 2010. Figure 3 shows a calibration data taken with a radioactive source, ^{57}Co, at the center of the detector. The two peaks observed correspond to 122-keV full absorption peak of ^{57}Co and 60-keV fluorescence X-ray peak from tungsten wire inside. The dashed line is showing simulated data which gives a reasonable agreement with real data. Similar calibration data in various points along an axis of the sphere were taken. From

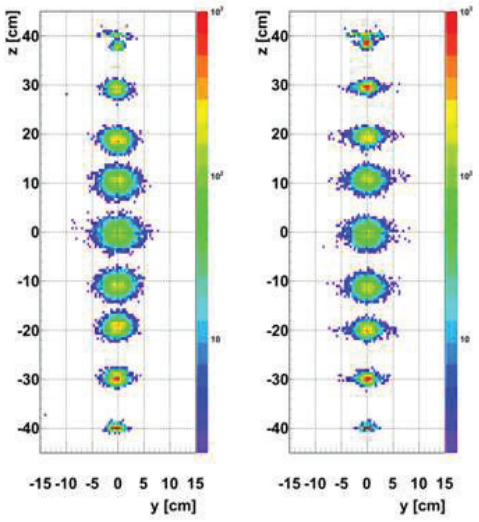

Fig. 4. Distribution of reconstructed vertices for the calibration data with ^{57}Co source at various positions along the detector axis. The left figure shows the real data and the right figure shows the Monte Carlo simulations. They agree well each other

this data, the photoelectron yield was found to be higher than expected (14.7 photoelectrons for one keV deposit by 122 keV gamma rays) which is the best light yield among existing detectors for dark matter search. This is a great advantage for a dark matter search, especially for light WIMPs. Figure 4 shows distributions of reconstructed vertices for the calibration data at various positions of the source along the detector axis. Those for real data are well reproduced by the Monte Carlo simulations.

As for the internal sources of background, we evaluated the contamination in liquid xenon. The radioactive contamination, ^{85}Kr, in xenon is a potential source of background and reduced using a distillation system last year. According to a measurement using a gas analysis system (APIMS), it was found that a contamination of Krypton was less than 2.3 parts per trillion (ppt) which was the world best purity achieved for the dark matter experiments. Other origins of background, such as radon gas in liquid xenon, is also important but found to be small at this stage. To evaluate ^{222}Rn contamination as well as its daughter nuclei, we measured it through ^{214}Bi-^{214}Po consecutive decay and found to be 8.2 ± 0.5 mBq inside the detector. With a similar method, ^{220}Rn was measured to be less than 280 μBq (90% C.L.). They are satisfactorily low at this moment.

The observed energy spectrum is being studied. In particular, event selection using a fiducial volume cut based on the event reconstruction is being optimized and developed. After finalizing the tool, a sensitive search for dark matter will be done.

Bibliography

[1] Y. Suzuki et al., "Low energy solar neutrino detection by using liquid xenon", Aug. 2000, hep-ph/0008296.

[2] Y. Kishimoto, "Status of XMASS", in the proceedings of the 7th Patras Workshop on Axions, WIMPs and WISPs,

Mykonos, Greece, 26 June - 1 July, 2011.

[3] K. Ueshima *et al*, “Scintillation-only based pulse shape discrimination for nuclear and electron recoils in liquid xenon”, Nucl. Instr. Meth. A, 659, 161 (2011)

HIGH ENERGY COSMIC RAY DIVISION

Overview

There are three major experimental research activities in the High Energy Cosmic Ray Division, the study of high energy gamma rays and the design study of the next generation telescopes by the Cherenkov Cosmic Gamma Ray group, the study of extremely high energy cosmic rays by the Telescope Array (TA) group, and the study of very high energy cosmic rays and gamma rays by the Tibet AS gamma group. Other activities, such as experiments utilizing the Akeno observatory, the Norikura observatory, the Mt. Chacaltaya observatory (jointly operated with Bolivia), and the emulsion-pouring facilities are closely related to inter-university joint research programs. Also an all-sky high resolution air-shower detector (Ashra) has been installed on the Hawaii island. The High Energy Astrophysics Group created in the fiscal year 2009 aims to explore various high energy astrophysical phenomena, through theoretical and observational approaches.

The CANGAROO telescopes have been in operation in South Australia since 1992, with a 3.8 m small telescope and then with four 10 m telescopes. The major scientific objective was the study of Very High Energy (VHE) gamma-ray sources in our galaxy in the southern hemisphere. The mission of these telescopes was completed and the CANGAROO observation site was closed in 2011. For further development of VHE gamma-ray astronomy, the Cherenkov Cosmic Gamma Ray Group is working on the design study and development of the next generation international ground-based gamma ray observatory CTA.

At the Akeno observatory, a series of air shower arrays of increasing geometrical sizes were constructed and operated to observe extremely high energy cosmic rays (EHECRs). The Akeno Giant Air Shower Array (AGASA) was operated from 1991 to January 2004 and covered the ground area of 100 km^2 as the world largest air shower array. In 13 years of operation, AGASA observed a handful of cosmic rays exceeding the theoretical energy end point of the extra-galactic cosmic rays (GZK cutoff) at 10^{20} eV. The Telescope Array (TA), a large plastic scintillator array with air fluorescence telescopes, has been constructed in Utah, USA, which succeeds AGASA and measures the EHECRs with an order of magnitude larger aperture than that of AGASA to unveil the origin of super-GZK cosmic rays discovered by AGASA. The full-scale TA is accumulating data as the largest array viewing the northern sky.

An air shower experiment aiming to search for celestial gamma-ray point sources started in 1990 with Chinese physicists at Yangbajing (Tibet, 4,300 m a.s.l.) and has been successful. This international collaboration is called the Tibet ASγ Collaboration. An extension of the air shower array was completed in 1995 and an emulsion chamber has been combined with this air shower array since 1996 to study the primary cosmic rays around the knee energy region. After successive extensions carried out in 1999, 2002 and 2003, the total area of the air shower array amounts to 37,000 m^2. The sun's shadow in cosmic rays affected by the solar magnetic field was observed for the first time in 1992, utilizing its good angular resolution at multi-TeV energy region. From this experiment with better statistics, we expect new information to be obtained on the large-scale structure of the solar and interplanetary magnetic field and its time variation due to the 11-year-period solar activities.

A new type of detector, called Ashra (all-sky survey high resolution air-shower detector), was developed. The first-phase stations were installed near the Mauna Loa summit in the Hawaii Island and high-efficiency observation is continuing. It monitors optical and particle radiation from high-energy transient objects with a wide field-of-view.

The High Energy Astrophysics group is conducting theoretical researches on fundamental processes responsible for nonthermal particle acceleration in various astrophysical environments, including first-order diffusive shock acceleration, second order stochastic acceleration in shock downstream regions, modification of shock structure by pick-up interstellar neutrals, as well as injection processes of suprathermal particles. In addition to these theoretical works, R/D studies for radio observations of pulsars and cosmic ray air showers are also being made.

Cherenkov Cosmic Gamma-Ray Group

CANGAROO-III

[Spokespersons: R.W. Clay, T. Tanimori, and T. Yoshikoshi]

Collaboration list:

Institute for Cosmic Ray Research, University of Tokyo, Chiba, Japan; School of Chemistry and Physics, University of Adelaide, Australia; Mt Stromlo and Siding Spring Observatories, Australian National University, Australia; Australia Telescope National Facility, CSIRO, Australia; Faculty of Science, Ibaraki University, Ibaraki, Japan; Department of Physics, Konan University, Hyogo, Japan; Department of Physics, Kyoto University, Kyoto, Japan; Solar-Terrestrial Environment Laboratory, Nagoya University, Aichi, Japan; National Astronomical Observatory of Japan, National Institutes of Natural Sciences, Tokyo, Japan; Department of Physics, Tokai University, Kanagawa, Japan; Department of Radiation Oncology, Tokai University, Kanagawa, Japan; Department of Physics, Yamagata University, Yamagata, Japan; Faculty of Management Information, Yamanashi Gakuin University, Yamanashi, Japan; Faculty of Medical Engineering and Technology, Kitasato University, Kanagawa, Japan; Department of Physics, Ritsumeikan University, Shiga, Japan; Institute of Particle and Nuclear Studies, High Energy Accelerator Research Organization (KEK), Ibaraki, Japan; Department of Applied Physics, Waseda University, Tokyo, Japan [1].

Status of the Project

CANGAROO is the acronym for the Collaboration of Australia and Nippon (Japan) for a GAmma-Ray Observatory in the Outback. The collaboration started in 1992 with a single Imaging Atmospheric Cherenkov Telescope (IACT) of 3.8 m diameter called CANGAROO-I in the desert area near Woomera, South Australia (136°47′E, 31°06′S, 160 m a.s.l.). As its third-generation experimental setup, the CANGAROO-III stereoscopic IACT system has been in operation since March 2004 with four IACTs of 10 m diameter. Stereoscopic observations of atmospheric Cherenkov light images produced by air showers caused by high-energy particles bombarding the earth allow effective discrimination of gamma rays from charged cosmic rays which are the overwhelming backgrounds. Two of the four telescopes (called T3 and T4 in the order of construction) have been used in observations since May 2008, as the first and second telescopes have degraded. A stereoscopic triggering system was installed at the beginning of 2005 and has been working properly, rejecting most single muon events, which are the major background component at low energies. Observations of various candidates of celestial gamma-ray emitters have been carried out on moonless, clear nights.

Since the CANGAROO-III telescopes, which, due to financial considerations, were not sheltered from the harsh desert environment, have seriously deteriorated over time from their original performance, we have stopped observations in 2011 and the telescopes will be demolished in 2012.

CANGAROO-III Observations

Observations of CANGAROO-III have been carried out since 2010 selecting relatively bright TeV gamma-ray sources as targets, considering deteriorated performance of the system. In the fiscal year 2011, we observed the bright TeV supernova remnant (SNR) RX J1713.7−3946 for about 26 hr and this data can be used to check the final performance of the system. Optical performance or system throughput of each telescope has also been monitored utilizing muon ring events and background air-shower events. Single cosmic-ray secondary muons falling near an IACT make ring Cherenkov images on the imaging camera, which can be used for absolute throughput calibration as the Cherenkov light yield is well known [2]. However, the accuracy of this calibration rapidly becomes worse as the optical performance is deteriorated. The throughput calibration using background air-shower events compensates this but can estimate only relative values [3]. Throughput values of T3 and T4 calibrated using the both methods are plotted as a function of time since their installations in 2003–2004 in Figure 1, in which the relative throughput values obtained using air-shower events are normalized to the absolute throughput values calculated from muon ring events. The two calibration methods have given almost consistent results with each other. The throughput values have degraded over the eight year period down to about 50 % and 20 % of their initial values for T3 and T4, respectively. This was one of the reasons why we decided to stop observations of CANGAROO-III.

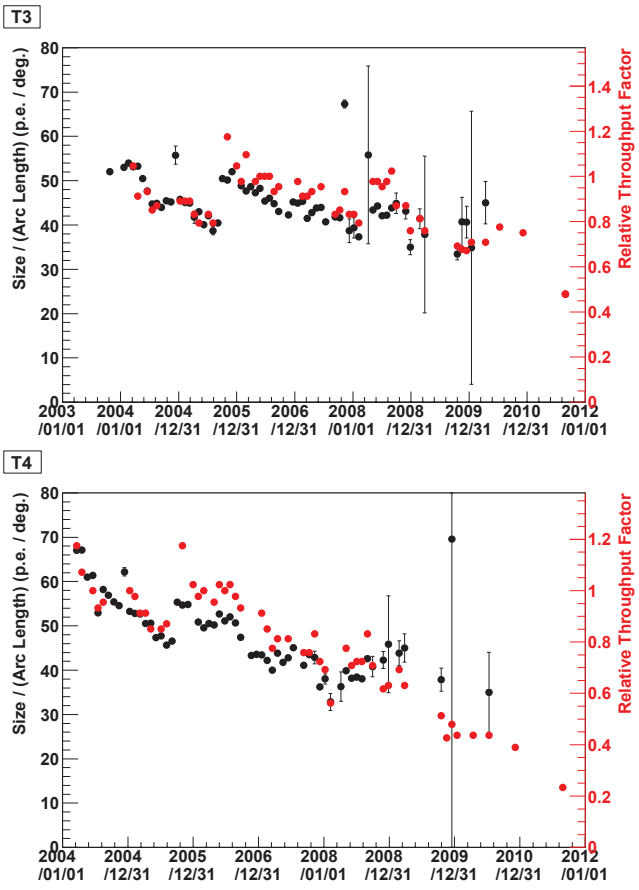

Fig. 1. Results of throughput calibrations for T3 (top) and T4 (bottom) obtained using muon ring events (black) and background air-shower events (red). The relative throughput values estimated using air-shower events are normalized to the absolute throughput values calculated from muon ring events.

Results from CANGAROO-III

Unidentified HESS Source HESS J1614−518

HESS J1614−518 is one of the unidentified TeV sources discovered in the H.E.S.S. Galactic plane survey. This source has a relatively high flux level among the unidentified H.E.S.S. sources (25 % of the Crab flux above 200 GeV), and is possibly associated with the young open star cluster Pismis 22 [4].

CANGAROO-III has observed HESS J1614−518 from May to August 2008 and diffuse gamma-ray emission was detected above 760 GeV at the 8.9σ level during an effective exposure of 54 hr (Figure 2) [5]. The spectrum is represented with a power-law: $(8.2 \pm 2.2_{\mathrm{stat}} \pm 2.5_{\mathrm{sys}}) \times 10^{-12} \times (E/1\,\mathrm{TeV})^{-\gamma}\,\mathrm{cm}^{-2}\,\mathrm{s}^{-1}\,\mathrm{TeV}^{-1}$ with a photon index γ of $2.4 \pm 0.3_{\mathrm{stat}} \pm 0.2_{\mathrm{sys}}$, which is compatible with that of the H.E.S.S. observations. By combining our result with multi-wavelength data, we discussed the possible counterparts for HESS J1614−518 and consider radiation mechanisms based on hadronic and leptonic processes for a SNR, stellar winds from massive stars, and a pulsar wind nebula (PWN). Although a leptonic origin from a PWN driven by an unknown pulsar remains possible (the nearby known pulsars are not responsible since the spin-down powers are insufficient to produce the observed TeV gamma-ray luminosity), hadronic-

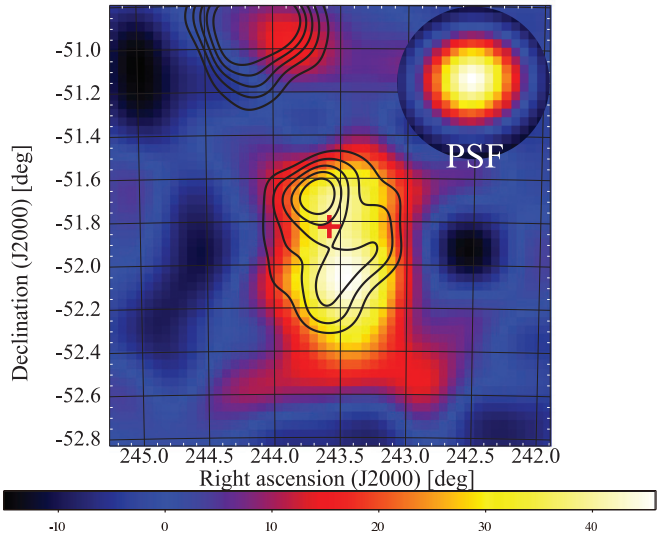

Fig. 2. Morphology of gamma-ray–like events observed from HESS J1614−518. The number of excess events per $0.^{\circ}2 \times 0.^{\circ}2$ cell is smoothed and plotted in the equatorial coordinate. The black solid contours show the very high energy (VHE) gamma-ray emission seen by H.E.S.S. The red cross shows the center position of HESS J1614−518.

origin emission from an unknown SNR is preferred.

Blazars H 2356−309, PKS 2155−304, PKS 0537−441, and 3C 279

We have observed four selected blazars, H 2356−309, PKS 2155−304, PKS 0537−441, and 3C 279, with the CANGAROO-III IACTs from 2005 to 2009. No statistically significant excess of events above 510–720 GeV from the direction of any of these objects was found, and we derived flux upper limits for very high energy (VHE) gamma-ray emissions [6]. In addition, we analyzed GeV gamma-ray data between 0.2 and 300 GeV taken with Fermi/LAT from August 2008 to May 2011.

To derive some important physical parameters of these blazars, we consider a simple leptonic jet model to explain the multiwavelength spectral energy distributions (SEDs) including GeV and TeV spectra, even though non-simultaneous. The observed SED of H 2356-309 (HBL) could be explained by a simple synchrotron-self-Compton (SSC) model with a single power-law electron spectrum, and to keep a consistency with GeV spectrum, we need to assume a large beaming factor $\delta = 59$ and weak magnetic field strength of 0.012 G. Radiation from PKS 2155−304, a nearby HBL, was well modeled by the SSC scenario, and obtained parameters are consistent with earlier works. PKS 0537−441, a luminous LBL, was studied and we found SSC + EC (external Compton) model could explain the observed multiwavelength spectrum where the EC component is dominant in the gamma-ray photons. The SED of one of the distant FSRQ, 3C 279, were also well explained by the SSC + EC model.

Additionally, from our parameter fit results as the HBL to the FSRQ of blazar sub-classes, it is seen that the beaming factor becomes smaller, and in contrast the strength of the magnetic field becomes stronger and the size of blob becomes larger. Although we could not take into account of the uncertainties such as simultaneity of the data and the differences of models, these latter two tendencies are in agreement with the proposed blazar sequence.

Bibliography

[1] Collaboration website: `http://vesper.icrr.u-tokyo.ac.jp/`.

[2] R. Enomoto et al., Astrophys. J. **638**, 397–408 (2006).

[3] S. LeBohec & J. Holder, Astropart. Phys. **19**, 221–233 (2003).

[4] G. Rowell et al., Proc. of 4th Internat. Meeting on High Energy Gamma-Ray Astronomy, AIP **1085**, 241–244 (2008).

[5] T. Mizukami et al., Astrophys. J. **740**, 78 (2011).

[6] Y. Mizumura et al., Astropart. Phys. **35**, 563–572 (2012).

CTA Project (Cherenkov Telescope Array)

[Spokespersons : M.Teshima and H.Kubo]

Collaboration list:

Institute for Cosmic Ray Research, University of Tokyo, Chiba, Japan; Department of Physics, Yamagata University, Yamagata, Japan; Faculty of Science, Ibaraki University, Ibaraki, Japan; Institute of Particle and Nuclear Studies, High Energy Accelerator Research Organization (KEK), Ibaraki, Japan; Department of Physics, The University of Tokyo, Tokyo, Japan; Interactive Research Center of Science, Tokyo Institute of Technology, Tokyo, Japan; Department of Physics, Aoyama Gakuin University, Tokyo, Japan; Faculty of Science and Engineering, Waseda University, Tokyo, Japan; Department of Physics, Saitama University, Saitama, Japan; Institute of Space and Astronautical Science, JAXA, Kanagawa, Japan; Department of Physics, Tokai University, Kanagawa, Japan; Department of Radiation Oncology, Tokai University, Kanagawa, Japan; Faculty of Medical Engineering and Technology, Kitasato University, Kanagawa, Japan; Faculty of Management Information, Yamanashi Gakuin University, Yamanashi, Japan; Department of Physics, Nagoya University, Aichi, Japan; Solar-Terrestrial Environment Laboratory, Nagoya University, Aichi, Japan; Kobayashi-Maskawa Institute, Nagoya University, Aichi, Japan; Department of Astronomy, Kyoto University, Kyoto, Japan; Department of Physics, Kyoto University, Kyoto, Japan; Yukawa Institute for Theoretical Physics, Kyoto University, Kyoto, Japan; Department of Earth and Space Science, Osaka University, Japan; Department of Physics, Kinki University, Osaka, Japan; Department of Physics, Konan University, Hyogo, Japan; Department of Physics, Hiroshima University, Hiroshima, Japan; Hiroshima Astrophysical Science Center, Hiroshima University, Hiroshima, Japan; Faculty of Integrated Arts and Sciences, The University of Tokushima; Department of Applied Physics, University of Miyazaki, Miyazaki, Japan; Graduate School of Science and Technology, Kumamoto University, Kumamoto, Japan; Center for Cosmology and AstroPar-

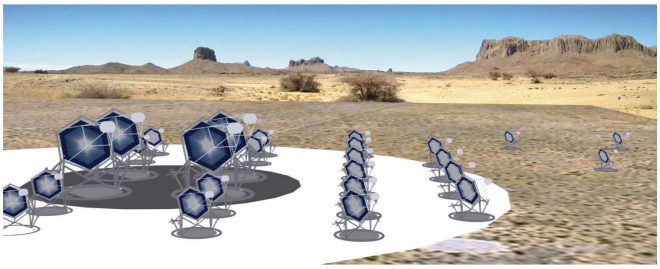

Fig. 3. Artist view of the CTA observatory. CTA consists of three types of telescopes, Large Size Telescopes (23m diameter), Mid Size Telescopes (12m) and Small Size Telescopes (6m), and covers the broad energy band from 20GeV to 100TeV.

ticle Physics, Ohio State University, Ohio, USA; Max-Planck-Institute for Physics, Munich, Germany [1].

CTA Project

During the past few years, Very High Energy (VHE) gamma ray astronomy has made spectacular progress and has established itself as a vital branch of astrophysics. To advance this field even further, we propose the Cherenkov Telescope Array (CTA) [2], the next generation VHE gamma ray observatory, in the framework of a worldwide, international collaboration. CTA is the ultimate VHE gamma ray observatory, whose sensitivity and broad energy coverage will attain an order of magnitude improvement above those of current Imaging Atmospheric Cherenkov Telescopes (IACTs). By observing the highest energy photons known, CTA will clarify many aspects of the extreme Universe, including the origin of the highest energy cosmic rays in our Galaxy and beyond, the physics of energetic particle generation in neutron stars and black holes, as well as the star formation history of the Universe. CTA will also address critical issues in fundamental physics, such as the identity of dark matter particles and the nature of quantum gravity.

VHE gamma rays from 100GeV to 10TeV can be observed with ground-based IACTs. The history of VHE gamma ray astronomy began with the discovery of VHE gamma rays from the Crab Nebula by the Whipple Observatory in 1989. To date, the current generation IACTs featuring new technologies, such as H.E.S.S., MAGIC, VERITAS, and CANGAROO, have discovered more than 100 Galactic and extragalactic sources of various types.

CTA is designed to achieve superior sensitivity and performance, utilizing established technologies and experience gained from the current IACTs. The project is presently in its preparatory phase, with international efforts from Japan, the US and EU. It will consist of several 10s of IACTs of three different sizes (Large Size Telescopes, Mid Size Telescopes, and Small Size Telescopes). With a factor of 10 increase in sensitivity (1m Crab $\sim 10^{-14} erg\ s^{-1}\ cm^{-2}$), together with a much broader energy coverage from 20GeV up to 100TeV, CTA will bring forth further dramatic advances for VHE gamma ray astronomy. The discovery of more than 1000 Galactic and extragalactic sources is anticipated with CTA.

CTA will allow us to explore numerous diverse topics in physics and astrophysics. The century-old question of the origin of cosmic rays is expected to be finally settled through detailed observations of supernova remnants and other Galactic objects along with the diffuse Galactic gamma ray emission, which will also shed light on the physics of the interstellar medium. Observing pulsars and associated pulsar wind nebulae will clarify physical processes in the vicinity of neutron stars and extreme magnetic fields. The physics of accretion onto supermassive black holes, the long-standing puzzle of the origin of ultrarelativistic jets emanating from them, as well as their cosmological evolution, will be addressed by extensive studies of active galactic nuclei (AGN). Through dedicated observing strategies, CTA will also elucidate many aspects of the mysterious nature of gamma ray bursts (GRBs), the most energetic explosions in the Universe. Detailed studies of both AGNs and GRBs can also reveal the origin of the highest energy cosmic rays in the Universe, probe the cosmic history of star formation including the very first stars, as well as provide high precision tests of theories of quantum gravity. Finally, CTA will search for signatures from elementary particles constituting dark matter with the highest sensitivity yet. Realization of the rich scientific potential of CTA is very much feasible, thanks to the positive experience gained from the current IACTs.

The CTA-Japan consortium [1] is aiming at contributing in particularly to the construction of the Large Size Telescopes (LSTs) and is involved in their development. The LST covers the low energy domain from 20GeV to 1000GeV and is especially important for studies of high redshift AGNs and GRBs. The diameter and area of the mirror are 23m and $400m^2$, respectively, in order to achieve the lowest possible energy threshold of 20GeV. All optical elements/detectors require high specifications, for example, high reflectivity, high collection efficiency, high quantum efficiency and ultra fast digitization of signal, etc. For this purpose, CTA-Japan is developing high quantum efficiency photomultipliers, ultrafast readout electronics and high precision segmented mirrors. On the strength of their experience gained from construction of the MAGIC telescope, the Max-Planck-Institute for Physics in Munich is responsible for the design of the 23m diameter telescope structure, based on a carbon fiber tube space frame. The LSTs require very fast rotation (180 degrees/20seconds) for promptly observing GRBs.

The Cherenkov Cosmic Gamma Ray group is also operating the MAGIC Telescopes [5] on La Palma, Canary Islands. This facility is used not only for scientific observations but also for technological development toward the future observatory CTA.

Bibliography

[1] CTA Consortium website: `http://www.cta-observatory.jp/` and `http://www.cta-observatory.org/`.

[2] **Design Concepts for The Cherenkov Telescope Array,** The CTA Consortium, Exper. Astron. 32 (2011) 193-316.

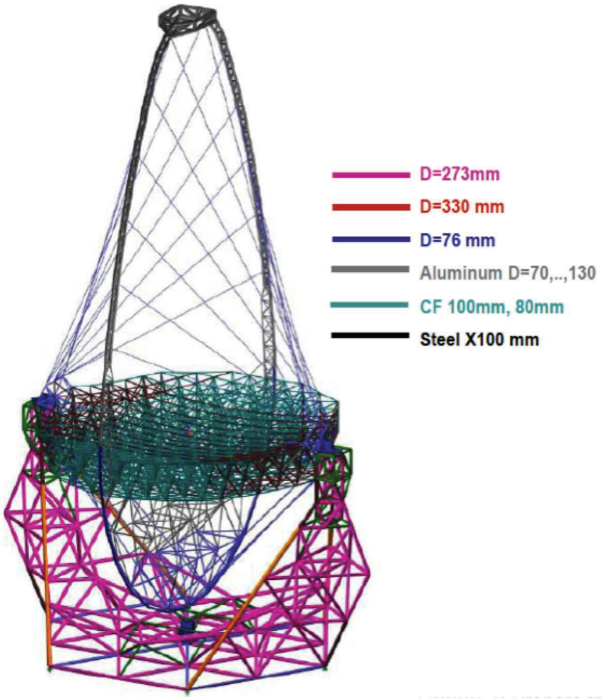

Fig. 4. Large Size Telescope (23m diameter) designed by Max–Planck-Institute for Physics. CTA Japan is contributing to the design and prototyping of the imaging camera at the focal plane, ultrafast readout electronics, and high precision segmented mirrors.

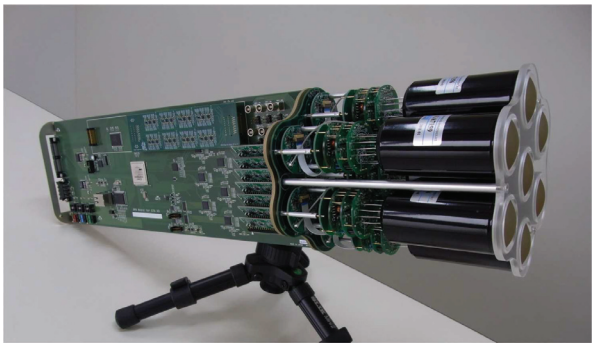

Fig. 5. Camera cluster for the Large Size Telescope (LST) developed by CTA-Japan. This cluster consists of seven high quantum efficiency photomultipliers (R11920-100), CW High Voltages, pre-amplifier, Slow Control Board, DRS4 Ultra fast waveform recording system and Trigger. The LST camera can be assembled with 400 of these clusters, cooling plates and camera housing.

[3] **Status of Very High Energy Gamma Ray Astronomy and Future Prospects,** M. Teshima, The Astronomical Herald, 104 (2011) 333-342.

[4] **Design Study of a CTA Large Size Telescope, Prof. of ICRC2012 at Beijing China,** M. Teshima, arXiv:1111.2183.

[5] MAGIC Collaboration website: `http://magic.mppmu.mpg.de/`.

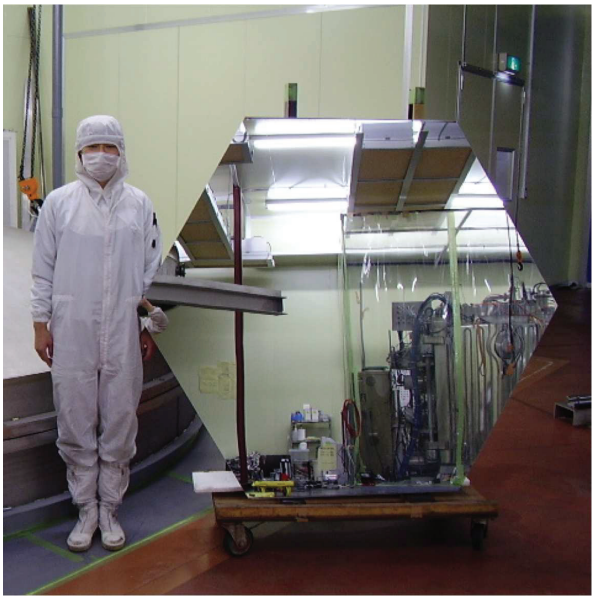

Fig. 6. Prototype of the high precision segmented mirror for the Large Size Telescope (LST) developed by CTA-Japan in cooperation with Sanko Co.LTD. The mirror is made of a 60mm thick aluminum honeycomb sandwiched by 3mm thin glass on both sides. A surface protection coat consisting of the materials SiO2 and HfO2 will be applied to enhance the reflectivity and to elongate the lifetime.

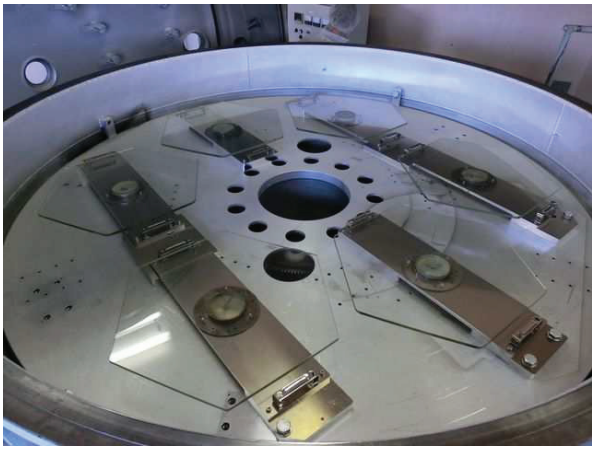

Fig. 7. Six segment mirrors of the Akeno atmospheric Cherenkov telescope placed in a chamber of the Okayama Astrophysical Observatory (OAO), the National Astronomical Observatory of Japan (NAOJ), waiting for a following vapor-deposition process.

Other Activities

As a test bench of domestic R & D activities for future ground-based gamma-ray observatory projects, a used atmospheric Cherenkov telescope of a 3 m diameter was obtained and placed at the Akeno Observatory in November 2010. In the fiscal year 2011, six of the 18 deteriorated segment mirrors of the telescope were recoated at the Okayama Astrophysical Observatory (OAO), the National Astronomical Observatory of Japan (NAOJ) (Figure 7). Their reflectivity has successfully recovered up to more than 90 % at the wavelengths utilized by atmospheric Cherenkov telescopes. Some prototype imaging cameras and electronics systems are planned to be installed to this telescope (e.g. [1]), and test observations will be carried out in the near future.

Bibliography

[1] T. Yoshikoshi et al., Proc. of 32nd Internat. Cosmic Ray Conf. (Beijing), **9**, 226–229 (2011).

TA: Telescope Array Experiment

Spokespersons:

H. Sagawa / ICRR, University of Tokyo
G. B.Thomson / Dept. of Physics, University of Utah

Collaborating Institutions:

Chiba Univ., Chiba, Japan; Chungnam Nat. Univ., Daejeon, Korea; Earthquake Research Institute, Univ. of Tokyo, Tokyo, Japan; Ehime Univ., Matsuyama, Japan; Ewha W. Univ., Seoul, Korea; Hiroshima City Univ., Hiroshima, Japan; Hanyang Univ., Seoul, Korea; ICRR, Univ. of Tokyo, Kashiwa, Japan; INR, Moscow, Russia; IPMU, Univ. of Tokyo, Kashiwa, Japan; Kanagawa Univ., Yokohama, Japan; KEK/IPNS, Tsukuba, Japan; Kinki Univ., Higashi-Osaka, Japan; Kochi Univ., Kochi, Japan; Kyoto Univ., Kyoto, Japan; Nat. Inst. of Rad. Sci., Chiba, Japan; Osaka City Univ., Osaka, Japan; RIKEN, Wako, Japan; Ritsumeikan Univ., Kusatsu, Japan; Rutgers Univ., Piscataway, NJ, USA; Saitama Univ., Saitama, Japan; Tokyo City Univ., Tokyo, Japan; Tokyo Inst. of Tech., Tokyo, Japan; Tokyo Univ. of Science, Noda, Japan; ULB, Brussels, Belgium; Univ. of Utah, Salt Lake City, UT, USA; Univ. of Yamanashi, Kofu, Japan; Waseda Univ., Tokyo, Japan; Yonsei Univ., Seoul, Korea

Overview and Status of TA

The Telescope Array (TA) is the largest Ultra-High Energy Cosmic Ray (UHECR) observatory in the northern hemisphere. The aim of the TA experiment is to explore the origin, propagation and interaction of extremely-high energy (EHE) cosmic rays by measuring energy, arrival direction and mass composition. The TA consists of a surface array of 507 plastic scintillator detectors (SD) and three stations of fluorescence detectors (FD). It is located in the desert of Utah in USA (lat. 39.3°N, long. 112.9°W, alt.∼1400 m). The TA was constructed mainly by the Grants-in-Aid for Scientific Research (Kakenhi) of Priority Areas "The Origin of Highest Energy Cosmic Rays" (JFY2003-2008) and the US National Science Foundation (NSF). All three FD stations started the observation in November 2007. Major construction of the SD array was completed in February 2007, and started the full operation in March 2008. The TA is operated by the international collaboration of researchers from US, Russia, Korea, Belgium and Japan. The main fund for the TA operation is the Grants-in-Aid for Scientific Research (Kakenhi) of Specially Promoted Research "Extreme Phenomena in the Universe Explored by Highest Energy Cosmic Rays" (JFY2009-2013).

Surface Detector Array

Each SD has two layers of 1.2 cm thick scintillator. The light is gathered by wavelength shifting fibers in the grooves of a scintillator layer and brought out to a PMT for each layer. We use 12-bit FADCs with 50 MHz sampling. Solar power system supplies power for the PMTs and electronics. The SDs are divided into three sub-arrays which communicate via wireless LAN each with an SD host electronics at a communication tower in their sub-array. In addition to shower trigger data, we collect a variety of monitor information for SD calibration and maintenance. The fraction of running time is greater than 96% . The performance of the SD is described in [1].

Fluorescence Telescope

The Middle Drum (MD) FD site is located to the north of the TA site, and is instrumented with 14 refurbished telescopes from the HiRes-I site. The cameras each contain 256 hexagonal Photonics PMTs in a 16×16 array. Each PMT views $\sim1^\circ$ of sky. The telescopes view from 3-31° above horizon and 114° in azimuth.

The Black Rock Mesa (BRM) and Long Ridge (LR) FD sites are located to the southeast and southwest of the TA site, respectively. They are each instrumented with 12 new telescopes [2]. The cameras use a Hamamatsu PMT with the 1° field of view. The PMTs are calibrated with a laser [3]. The relative calibration is described in [4]. The sites view 3-33° above horizon and 108° in azimuth. The trigger system is described in [5, 6]. The BRM and LR FD sites have duty cycles of 12 and 10%, respectively.

A monostatic LIDAR (LIght Detection And Ranging) system, in which the laser and receiver are collocated, is located in the BRM site to measure atmospheric transparency [7]. The BRM site has an IR camera to monitor clouds.

A laser facility (CLF) sits at the center of the three FD sites. This allows one to measure the atmospheric transmission parameters [8] as well as to directly compare the reconstruction of the three FD sites.

No absolute energy calibration source existed on the sites of previous UHECR experiments. At KEK in Japan, we built an electron linear accelerator (ELS, Electron Light Source) for an end-to-end energy calibration of the FD [9]. The maximum beam energy is 40 MeV and the charge of one pulse is 10^9 e^-. The ELS was installed 100 m forward from the BRM FD in March 2009. With the FD, we observed pseudo air shower induced by an electron beam that was shot in the air from ELS in September, 2010.

Results

Energy Spectrum

The HiRes [10] and PAO [11] published the results of energy spectrum. The HiRes observed the GZK cutoff and the PAO confirmed it. We present energy spectra using three different methods: the MD monocular FD, hybrid, and SD analyses.

MD FD Monocular Energy Spectrum

The analysis of the MD monocular FD data provides a direct comparison between the TA and HiRes energy spectra. The MD spectrum uses the data collected between December 16, 2007 and December 16, 2010 [12]. The spectrum is measured using the reconstruction technique developed by the HiRes-I. The MD monocular energy spectrum is shown in

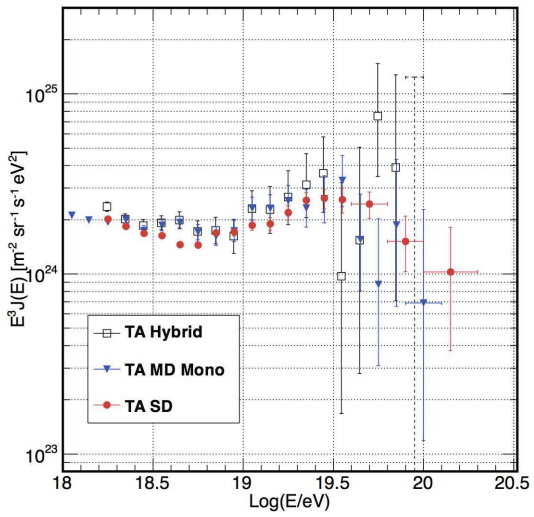

Fig. 1. The TA energy spectra measured by hybrid analysis (black open squares), MD monocular FD analysis (blue filled triangles), and SD analysis (red filled circles).

Fig. 1. The spectrum is in good agreement with the other TA results.

Hybrid Energy Spectrum

The hybrid events detected both by FD and SD are useful to compare the reconstructed results from FD and SD. We can improve the reconstruction of FD events by adding information of SD. Here we use timing of one SD. The 1978 hybrid events were selected from May 27, 2008 through September 7, 2010. The total systematic uncertainty is 21% in energy measurement. Figure 1 shows the preliminary hybrid energy spectrum, which is consistent with the other TA results.

SD Energy Spectrum

We measured the energy spectrum by using the SD data from May 11, 2008 through April 25, 2011. The exposure is $\sim$2640 km^2 sr yr. The Monte Carlo (MC) data were generated by CORSIKA air shower simulation with QGSJET-II proton model. GEANT4 simulation is used for the detector simulation. The correlation of S_{800} and zenith angle with primary energy from MC study is used for the first estimation of the CR energy. Here S_{800} is the charge density at a distance of 800 m from shower core.

We compare the FD and SD energies using hybrid events. The SD energy is 27% larger than that of FD. The SD energy is rescaled by 27%. The plot of the energies is shown in Fig. 2.

We obtain 10997 reconstructed events with zenith angles below 45°. The energy spectrum is shown together with other experiments in Fig. 3 [13]. The SD spectrum is consistent with HiRes spectra. Using a power-law fit, we found the two breaks at $(4.9 \pm 0.3)\times10^{18}$ eV and at $(4.8 \pm 0.1)\times10^{19}$ eV, which correspond to the ankle and the GZK suppression, respectively. We observed 28 events above the break at 4.8×10^{19} eV while a linear extrapolation of the power law below the break predicts 54.9 events above the break. This result provides evidence for the flux suppression with the significance

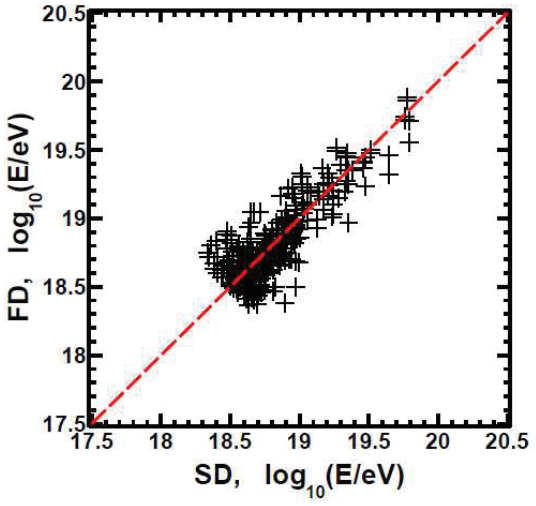

Fig. 2. The SD and FD energy comparison after applying 27% normalization to the SD. The dashed line corresponds to $E_{SD} = E_{FD}$.

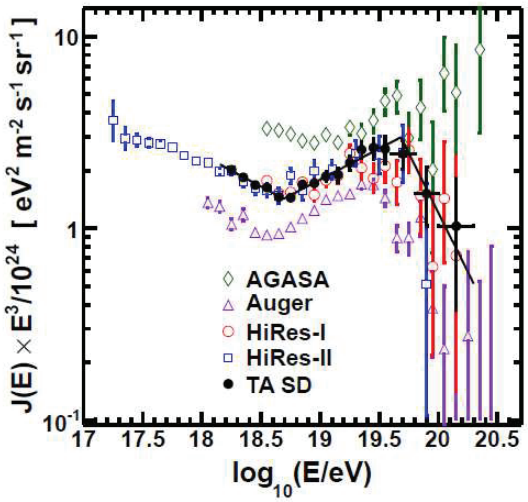

Fig. 3. The TA SD spectrum together with the spectra from other experiments: the TA SD (black filled circles), AGASA (green open diamonds), PAO (purple open triangles), HiRes-1 (red open circles), and HiRes-2 (blue open squares). Solid line shows the broken power line fit to the TA SD data.

of 3.9σ. The difference of the TA and Auger fluxes corresponds to the difference of the TA and Auger energy scales of approximately 20%,. which is consistent with systematic energy uncertainties.

Mass Composition

The dependence of $X_{\rm max}$ on the primary energy is used to determine the mass composition. The Auger data suggests a change to a heavier composition for E $> 10^{18.5}$ eV [14] while the HiRes data is consistent with constant elongation rate which stays with proton [15].

The events simultaneously observed at two new FD stations (stereo events) from November 2007 through September 2010 are used. The distribution of reconstructed $X_{\rm max}$ for the TA data with QGSJET-01 MC data is shown in Fig. 4 and is in good agreement with the proton distribution.

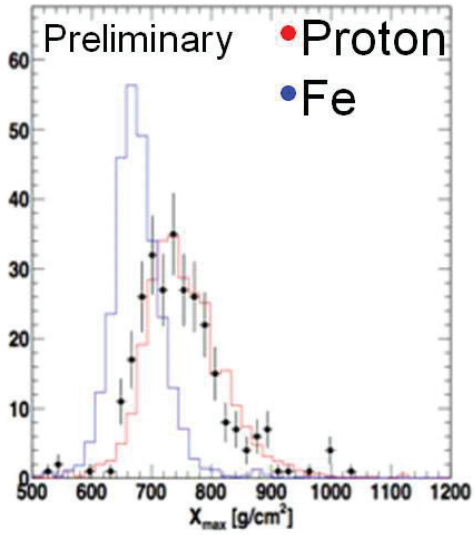

Fig. 4. The preliminary reconstructed $X_{\rm max}$ distribution for the data (points) with QGSJET-01 MC data above $10^{18.0}$ eV. The red and blue histograms are the proton and iron predictions, respectively.

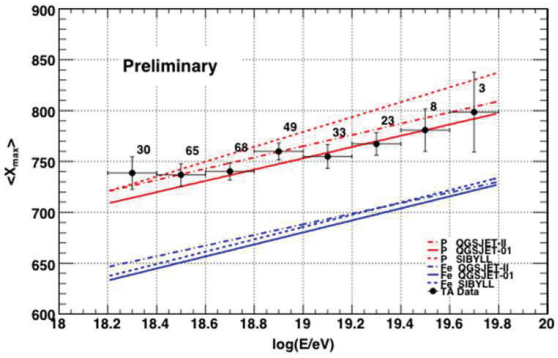

Fig. 5. The preliminary TA average reconstructed $X_{\rm max}$ (black points) as a function of energy. The upper set of red lines are predictions for pure protons with the interaction models of QGSJET-01 (solid line), QGSJET-II (dot-dash line) and SIBYLL (dashed line). The lower set of blue lines are under the assumption of iron.

The evolution of the average $X_{\rm max}$ with energy was shown with the MC data in the energy range from $10^{18.2}$ to $10^{19.8}$ eV in Fig. 5. The observed TA data are in good agreement with the QGSJET-01 pure proton prediction. The details of the mass composition study are described in [16].

Arrival Directions of UHECRs

We report the analysis of UHECRs for correlations with AGNs, autocorrelations and correlations with the LSS [17]. The SD data set from May 11, 2008 through September 15, 2011 contains 988 events above 10 EeV, 57 events above 40 EeV, and 25 events above 57 EeV.

Correlations with AGNs

The PAO reported correlations between the arrival directions of UHECRs with E $>$ 57 EeV and positions of nearby AGN from Véron 2006 catalog with $0<z\leq0.018$ in 2007 [18]. The probability that the correlations for angular separations less than 3.1° occurred by chance is 1.7×10^{-3}. The number of correlating events was 9 out of 13, which corresponds to about 69% of events. The PAO has updated the analysis and found that the number of correlating events was 21 out of 55, which corresponds to about 38% of events [19]. The HiRes reported that no correlations had been found [20]. There are 11 correlating events (44%) out of 25 total events while the expected number of random coincidences for this total number of events is 5.9. As is seen in Fig. 6, the TA result is compatible both with isotropic distribution and the AGN hypothesis. By using binomial distribution with the probability of a single event to correlate p_{iso} = 0.24, such an excess has probability of ∼2% to occur by chance with isotropic distribution.

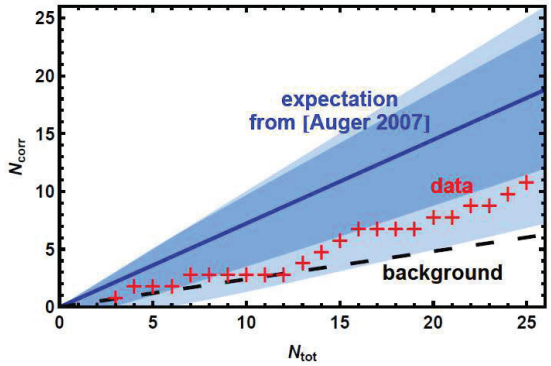

Fig. 6. The TA result of the correlations with AGN. The horizontal axis is the number of observed events and the vertical axis is the number of correlated events with AGN. The red crosses are the TA data. The black dashed line is the prediction from isotropic distribution. The expectation from the original PAO claim is represented by the blue line together with the 1- and 2-σ bands.

Autocorrelations

The small-scale clusters of UHECR arrival directions were observed by the AGASA at the angular scale of 2.5° above 40 EeV [21, 22]. On the other hand, the result by the HiRes is consistent with an isotropic distribution [23]. Figure 7 shows the distribution of separation angles for any two cosmic rays above 40 EeV for the TA data set. We find 0 pair separated by less than 2.5° while 1.5 are expected for the isotropic model. There is no excess of small-scale clusters in the TA data, and no significant excess is found for angles from 0 to 40° and three energy thresholds of 10 EeV, 40 EeV, and 57 EeV. There is a hint of grouping of events at angular scales between 20 and 30° at the highest energies. However, the statistical significance of this feature is not sufficient.

Correlations with LSS

Next we check the compatibility of the TA event sets with the isotropic distribution at large angular scales. The flux sampling test gives the values of statistical probability (p-values) 0.5, 0.9 and 0.6 for the three energy thresholds (10 EeV, 40 EeV, 57 EeV), respectively. The data are compatible with an isotropic distribution.

At large angular scales, the anisotropy in the PAO data was claimed [24] , and that in the HiRes data was not confirmed [25]. We use the galaxies at distances from 5 to 250 Mpc and with Ks magnitudes less than 12.5 in the 2MASS Galaxy Redshift Catalog (XSCz) [26]. This catalog provides

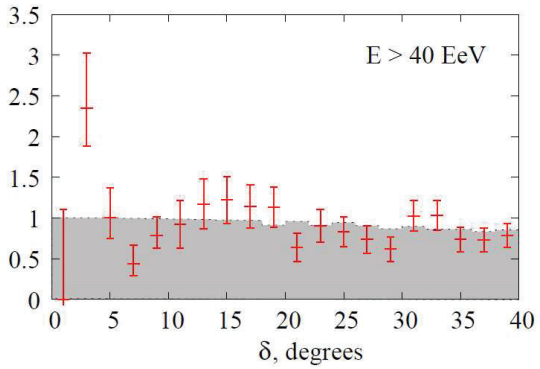

Fig. 7. The distribution of separation angles for any two cosmic rays above 40 EeV normalized by solid angle. The points are the observed data and the shaded region represents the average number of pairs expected for the uniform distribution. The expectation in the first bin is set to be one as the overall normalization.

the most accurate information about three-dimensional galaxy distribution. We assume that UHECRs are protons and the effects of the Galactic and extragalactic magnetic fields on each arrival direction are approximated by a Gaussian probability density function with an angular resolution called a smearing angle θ, which is treated as a free parameter. The sky maps of the expected flux at the smearing angle of 6° are shown in Fig. 8 together with the TA events. Figure 9 shows the p-values as a function of the smearing angle. The data both above 40 EeV and 57 EeV are compatible with LSS model even without regular GMF. For E $>$ 10 EeV, the data set is compatible with LSS hypothesis that includes the regular GMF with strong and thick halo component. Here we adopt the recent GMF model with the magnitude of 4 μG and the thickness of 1.5 kpc for the halo [27].

Prospects

We describe the TA Low-energy Extension (TALE), the possible processes to solve the discrepancies between the TA and Auger results such as energy spectrum and mass composition, and the plan of the next-generation huge aperture experiment including JEM-EUSO.

TA Low Energy Extension (TALE)

The TALE will give us the detailed studies of energy spectrum and composition from $10^{16.5}$ eV to the highest energies. The second knee has been observed at about 4×10^{17} eV in the cosmic-ray spectrum by previous experiments. The energy scales of these detectors differed by about a factor of two, so the energy at which this spectral break occurs is quite uncertain. There is a possibility that the transition from galactic cosmic rays to extragalactic cosmic rays occurs around this energy region. Then it is expected to observe the transition of heavier to lighter composition. The laboratory equivalent proton energy is 10^{17} eV in the center of mass energy of 14 TeV at the LHC. The cosmic-ray data to be observed by the TALE and the air shower MC simulation to be tuned by the result of the LHC forward (LHCf) experiment could be compared at about 10^{17} eV.

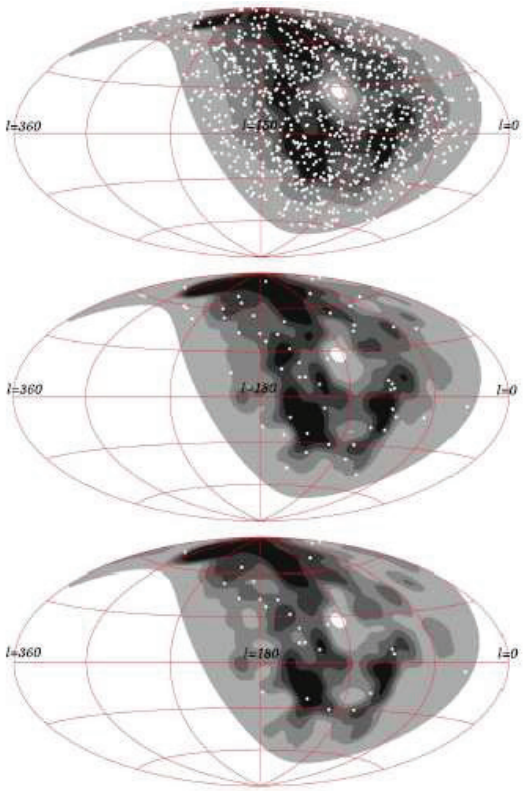

Fig. 8. The sky map of expected flux from LSS model together with the TA events (white dots) at energy thresholds of 10 EeV, 40 EeV, and 57 EeV (from top to bottom) in Galactic coordinates. The smearing angle is 6°. Darker gray region indicates larger flux and each band contains 1/5 of the total flux.

We will add new telescopes viewing higher elevation (31°-59°) and an infill array which the new telescopes overlook. The mirror building of the TALE FD was constructed right next to the MD FD building in the spring o 2012. The 10 telescopes from the HiRes-II are coming. The FDs will be completed in the spring of 2013.

The TALE SD array consists of scintillation counters identical to the TA SD. The infill array will consist of 103 counters, of which 76 will form the infill array (40 for 400-m spacing and 36 for 600-m spacing), and 27 will be used at the 1200 m spacing to extend the TA SD out to the infill array.

UHECR2012 symposium

The International Symposium on Future Directions in UHECR Physics (UHECR2012) was held in CERN in February 2012 [28]. We discussed the highlights and future UHECR experiments. Towards the symposium, we formed five working groups: energy spectrum, composition, anisotropy, multi-messenger, and modeling and description of air showers, which discussed the issues in advance and reported the summaries at the symposium. The energy scale difference of approximately 20% between the TA and PAO was partially understood by the energy spectrum working group, for example.

The ground array 60 times of the TA consisting of 10,000 SDs with 2 km spacing was proposed as a next-generation air-shower ground array experiment [29] in the UHECR2010 symposium. There were talks about a multi-

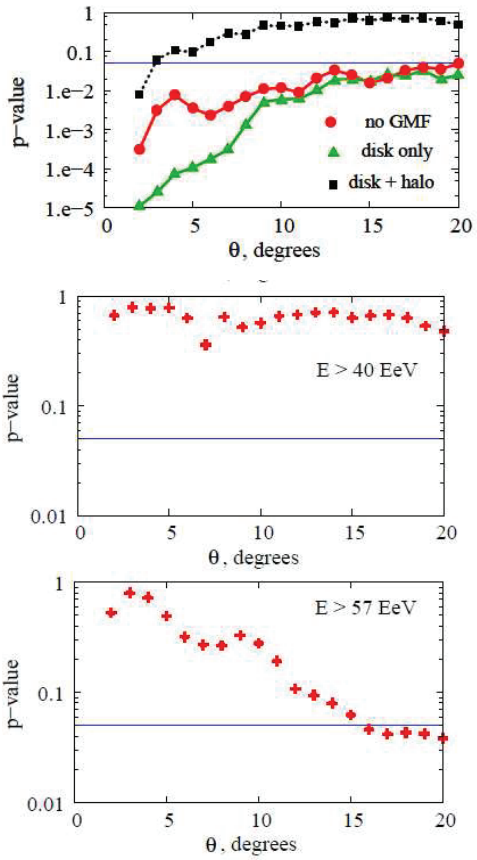

Fig. 9. The results of the statistical test for the compatibility between the data and the LSS hypothesis. The p-values are shown as a function of the smearing angle θ. The horizontal blue line shows a confidence level of 95%. The three panels correspond to energy thresholds of 10 EeV, 40 EeV, and 57 EeV from top to bottom. Red circles represent that with no regular GMF, In the upper panel with E $>$ 10 EeV, black squares represent the result of the TA events with the LSS hypothesis with disk and halo components, and green triangles represent that with disk component only.

component UHECR observatory consisting of water tanks and electromagnetic detectors such as GHz radio detectors [30], and a large ground array of fluorescence detectors with low cost [31]. The merit of the huge ground array experiment is its guaranteed ability of the conventional technique and/or possible ability of new method or new technique to be well calibrated with the existing observatories. We have already started the R&D experiments in the TA site with the group outside the TA. The R&D of the radio echo detection from air showers is being performed in the TA site [32]. An R&D of GHz radio detection in the TA site started in 2012 together with the Auger members from the Karlsruhe Institute of Technology (KIT) and University of Chicago.

The JEM-EUSO is the first space project to investigate EHE cosmic rays by a super-wide view (60°) telescope on the International Space Station (ISS). The advantage is its rather uniform and huge aperture (1.5×10^6 km^2 sr) in the whole sky. The prototype of the JEM-EUSO will be installed late in JFY 2012 and will be tested with ELS, CLF and air shower events simultaneously observed by TA.

After the symposium, the TA and Auger spokespersons agreed to have telephone conferences to discuss about the folowng items:continuation of the activities of the workindiscussed a few times and confirmed the following items to solve the discrepancies between the TA and PAO results:

- Understanding the discrepancies between the TA and PAO results,
- Continuation of the activities of the working groups,
- Exchange optical calibrations between the TA and PAO to understand more for the energy scale difference between the TA and PAO,
- Joint analysis such as the whole sky anisotropy analysis,
- The working group of the next-generation experiment, which discusses ground array experiments including JEM-EUSO.

Summary

The TA group confirmed GZK suppression with a significance of 3.9σ and the ankle. The $X_{\rm max}$ measurement above $10^{18.2}$ eV is consistent with proton composition. The analyses of arrival directions of UHECRs for the correlations with AGNs, correlations with LSS proton model and autocorrelations show some hints of anisotropy while they are consistent with isotropic model with the current statistics.

We are constructing the TALE, of which main aim is to investigate the transition from galactic and extragalactic cosmic rays. Based on the UHECR2012 symposium and continuation of the working groups, we would solve the discrepancies between TA and Auger by the joint studies. The TA results are consistent with proton GZK model, which leads to UHECR astronomy with the next generation cosmic ray observatory.

Bibliography

[1] T. Abu-Zayyad *et al.*, "The surface detector array of the Telescope Array experiment", *Nucl. Instrum. Methods* **A 689** (2012) 87-97.

[2] H. Tokuno *et al.*, "New air fluorescence detectors employed in the telescope Array experiment", *Nucl. Instrum. Methods* **A 676** (2012) 54-65.

[3] S. Kawana *et al.*, "Calibration of photomultiplier tubes for the fluorescence detector of telescope array experiment using a Rayleigh scattered laser beam", *Nucl. Instrum. Methods* **A 681** (2012) 68-77.

[4] H. Tokuno *et al.*, "On site calibration for new fluorescence detectors of the telescope array experiment", *Nucl. Instrum. Methods* **A 601** (2009) 364-371.

[5] Y. Tameda *et al.*, "Trigger system for the TA fluorescence detector", Proc. of nano PHYS'07, *Physica* **E 40** (2007) 430-433.

[6] Y. Tameda *et al.*, "Trigger electronics of the new Fluorescence Detectors of the Telescope Array Experiment", *Nucl. Instrum. Methods* **A 609** (2009) 227-234.

[7] T. Tomida *et al.*, "The atmospheric transparency measured with a LIDAR system at the Telescope Array experiment", *Nucl. Instrum. Methods* **A 654** (2011) 653-660.

[8] T. Tomida *et al.*, "Development of atmospheric transparency measurement system", *International Journal of Nanomanufacturing*, 2012, 047031.

[9] T. Shibata *et al.*, "End-to-end absolute energy calibration of atmospheric fluorescence telescopes by an electron linear accelerator", *Nucl. Instrum. Methods* **A 597** (2008) 61-66.

[10] R.U. Abbasi *et al.*, *Phys. Rev. Lett.* **100** (2008) 101101.

[11] J. Abraham *et al.*, *Phys. Rev. Lett.* **101** (2008) 061101.

[12] T. Abu-Zayyad *et al.*, "The Energy Spectrum of Telescope Array's Middle Drum Detector and the Direct Comparison to the High Resolution Fly's Eye Experiment", arXiv:1202.5141 [astro-ph.IM], accepted to *Astroparticle Phys.*

[13] T. Abu-Zayyad *et al.*, "The Cosmic Ray Energy Spectrum Observed with the Surface Detector of the Telescope Array Experiment", arXiv:1205.5067 [astro-ph.HE], submitted for publication.

[14] J. Abraham *et al.*, *Phys. Rev. Lett.* **104** (2010) 09110.

[15] R.U. Abbasi *et al.*, *Phys. Rev. Lett.* **104** (2010) 161101.

[16] Y. Tameda et al., "HiRes and TA Composition Measurements", Proc. of UHECR2012 Symposium, CERN, Geneva, Switzerland, 2012.

[17] T. Abu-Zayyad et al., "Search for anisotropy of ultrahigh energy cosmic rays with the Telescope Array experiment", arXiv:1205.5984 [astro-ph.HE], accepted for *Ap. J.*

[18] J. Abraham *et al.*, *Science* **318** (2007) 939; J. Abraham *et al.*, *Astropart. Phys.* **29** (2008) 188-204.

[19] P. Abreu *et al.*, *Astroparticle Phys.* **34** (2010) 315-326.

[20] R.U. Abbasi *et al.*, *Astroparticle Phys.* **30** (2008) 175-179.

[21] N. Hayashida *et al.*, *Phys. Rev. Lett.* **77** (1996) 1000-1003.

[22] M. Takeda *et al.*, *J. Phys. Soc. Jpn (Suppl.)* **B 70** (2001) 15-21.

[23] R.U. Abbasi *et al.*, *Ap. J. Lett.*, **610** (2004) 73-76.

[24] T. Kashti and E. Waxman, *JCAP* **05** (2008) 006.

[25] R.U. Abbasi *et al.*, *Ap. J. Lett.* **71B** (2010) 64-68.

[26] T. Jarrett, arXiv:astro-ph/0405069.

[27] M. Pshirkov, P. Tinyakov, P. Kronberg, K. Newton-McGee, *Ap. J.* **738** (2011) 192.

[28] http://indico.cern.ch/conferenceDisplay.py?confId=152124.

[29] S. Ogio, "Future Plans of the Telescope Array Experiment", Proc. of UHECR2012 Symposium, CERN, Geneva, Switzerland, 2012.

[30] A. Letessier-Selvon, Proc. of UHECR2012 Symposium, CERN, Geneva, Switzerland, 2012.

[31] P. Privitera, Proc. of UHECR2012 Symposium, CERN, Geneva, Switzerland, 2012.

[32] J. Belz et al., "TARA: Forward-Scattered Radar Detection of UHECR at the Telescope Array", Proc. of UHECR2012 Symposium, CERN, Geneva, Switzerland, 2012.

Tibet ASγ Project

Experiment

The Tibet air shower experiment has been successfully operated at Yangbajing (90°31' E, 30°06' N; 4300 m above sea level) in Tibet, China since 1990. It has continuously made a wide field-of-view (approximately 2 steradian) observation of cosmic rays and gamma rays in the northern sky.

The Tibet I array was constructed in 1990 and it was gradually upgraded to the Tibet II by 1994 which consisted of 185 fast-timing (FT) scintillation counters placed on a 15 m square grid covering 36,900 m^2, and 36 density (D) counters around the FT-counter array. Each counter has a plastic scintillator plate of 0.5 m^2 in area and 3 cm in thickness. All the FT counters are equipped with a fast-timing 2-inch-indiameter photomultiplier tube (FT-PMT), and 52 out of 185 FT counters are also equipped with a wide dynamic range 1.5-inch-indiameter PMT (D-PMT) by which we measure up to 500 particles which saturates FT-PMT output, and all the D-counters have a D-PMT. A 0.5 cm thick lead plate is put on the top of each counter in order to increase the counter sensitivity by converting gamma rays into electron-positron pairs in an electromagnetic shower. The mode energy of the triggered events in Tibet II is 10 TeV.

In 1996, we added 77 FT counters with a 7.5 m lattice interval to a 5,200 m^2 area inside the northern part of the Tibet II array. We called this high-density array Tibet HD. The mode energy of the triggered events in Tibet HD is a few TeV.

In the late fall of 1999, the array was further upgraded by adding 235 FT-counters so as to enlarge the high-density area from 5,200 m^2 to 22,050 m^2, and we call this array and further upgraded one Tibet III. In 2002, all of the 36,900 m^2 area was covered by the high-density array by adding 200 FT-counters more. Finally we set up 56 FT-counters around the 36,900 m^2 high density array and equipped 8 D-counters with FT-PMT in 2003. At present, the Tibet air shower array consists of 761 FT-counters (249 of which have a D-PMT) and 28 D-counters as in Fig. 1.

The performance of the Tibet air shower array has been well examined by observing the Moon's shadow (approximately 0.5 degrees in diameter) in cosmic rays. The deficit

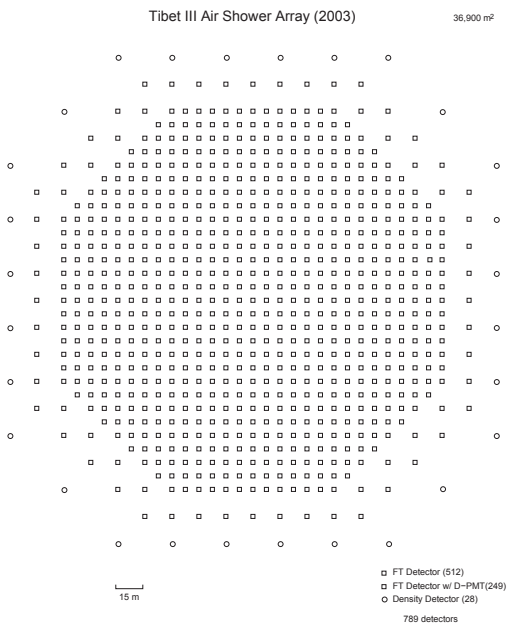

Fig. 1. Schematic view of Tibet III.

map of cosmic rays around the Moon demonstrates the angular resolution to be around 0.9° at a few TeV for the Tibet III array. The pointing error is estimated to be better than ∼0.01°, as shown in Fig. 2, by displacement of the shadow's center from the apparent center in the north-south direction, as the east-west component of the geomagnetic field is very small at the experimental site. On the other hand, the shadow center displacement in the east-west direction due to the geomagnetic field enables us to spectroscopically estimate the energy scale uncertainty at ±12 % level, as shown in Fig. 3. Thus, the Tibet air shower experiment introduces a new method for energy scale calibration other than the conventional estimation by the difference between the measured cosmic-ray flux by an air shower experiment and the higher-energy extrapolation of cosmic-ray flux measured by direct measurements by balloon-borne or satellite experiments.

Physics Results

Our current research theme is classified into 4 categories:

(1) TeV celestial gamma-ray point/diffuse sources[2],

(2) Chemical composition and energy spectrum of primary cosmic rays in the knee energy region[1, 3],

(3) Cosmic-ray anisotropy in the multi-TeV region with high precision,

(4) Global 3-dimensional structure of the solar and interplanetary magnetic fields by observing the Sun's shadow in

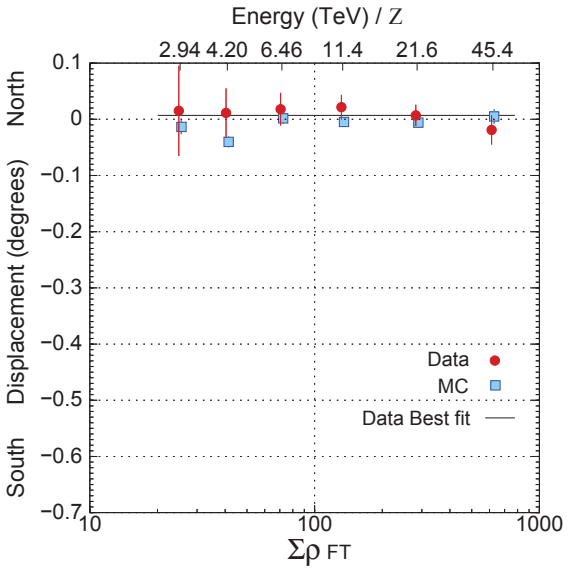

Fig. 2. From [?]. The Moon's shadow center displacement from the apparent position in the north-south direction as a function of energy, observed by Tibet III.

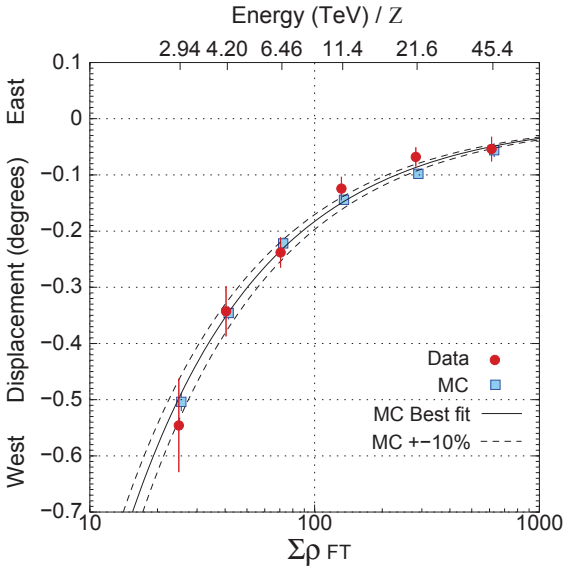

Fig. 3. From [?]. The Moon's shadow center displacement from the apparent positionin the east-west direction as a function of energy, observed by Tibet III.

cosmic rays.

We will introduce a part of the results obtained in this fiscal year.

The Tibet air shower array is very powerful to get new information on the relation between time variation of the large-scale structure of the solar and interplanetary magnetic fields and the solar activities by the sun's shadow in cosmic rays, since high-statistics data taken by the Tibet air shower array can follow up the movement of the Sun's shadow at every one-two months. The depth and displacement of the center position in the Sun's shadow are expected to have an anti-correlation with the 11-year-period solar activities which affect the solar and interplanetary magnetic fields, as the

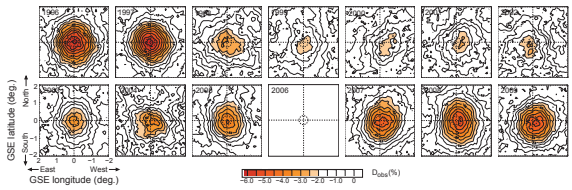

Fig. 4. Year-to-year variation of the observed Sun's shadow between 1996 and 2009. Each panel displays a 2 dimensional contour map of the observed flux deficit ($D_{\rm obs}$) due to the Sun's shadow as a function of GSE longitude and latitude (horizontal and vertical axes, respectively). The map in 2006 is omitted because of insufficient statistics for drawing a map.

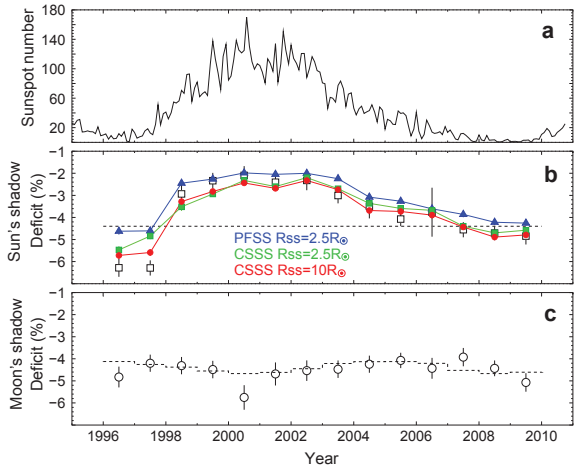

Fig. 5. Yearly variation of (a) sunspot numbers, (b) the deficit intensity in the Sun's shadow and (c) the deficit intensity in the Moon's shadow. The open squares in the panel (b) are the observed central deficit ($D_{\rm obs}$) by the Tibet air shower array. The blue triangles, green squares and red circles indicate the central deficits ($D_{\rm MC}$) by the MC simulations assuming the PFSS ($R_{\rm ss}$ = 2.5$R_{\odot}$), the CSSS ($R_{\rm ss}$ = 2.5$R_{\odot}$) and the CSSS ($R_{\rm ss}$ = 10.0$R_{\odot}$) models, respectively. The dashed lines in the panels (b) and (c) are the deficits expected from the apparent angular size of the Sun and the Moon.

charged cosmic rays are bent by them.

A clear solar-cycle variation of the Sun's shadow in 10 TeV cosmic rays are observed by the Tibet air shower array covering a full solar cycle from 1996 to 2009, as is shown in Fig. 4

Numerical simulations of the Sun's shadow are developed, employing the Potential Field Source Surface (PFSS) model and the Current Sheet Source Surface (CSSS) model for the coronal magnetic field, to interpret the physical implications of the observed solar cycle variation. It is found that the intensity deficit in the simulated Sun's shadow is very sensitive to the coronal magnetic field structure, and the observed variation of the Sun's shadow is better reproduced by the CSSS model than the PFSS model, as is shown in Fig. 5. This is the first successful attempt to evaluate the coronal magnetic field models by means of the Sun's shadow observed in 10 TeV cosmic rays .

Other Activities

The emulsion-pouring facilities can meet the demands for making any kind of nuclear emulsion plates which are used for cosmic ray or accelerator experiments. The thermostatic emulsion-processing facilities are operated in order to develop nuclear emulsion plates or X-ray films. Using these facilities, it is also possible to make and develop emulsion pellicles in 600-micron thickness each. In this way, these facilities have been open to all the qualified scientists who want to carry out joint research programs successfully. Of recent, however, the shrinking demand for the facilities let us decide that we should suspend calls for joint research programs to utilize the emulsion-pouring facilities, starting from 2012.

Fig. 6. YAC2 set up at Yangbajing.

Future Plans

(1)Chemical composition of primary cosmic rays making the knee in the all-particle energy spectrum

We have measured the energy spectra of primary cosmic-ray protons, heliums, all particles around the knee energy region. The main component responsible for making the knee structure in the all particle energy spectrum is heavier nuclei than helium. The next step is to identify the chemical component making the knee in the all particle energy spectrum. We have a plan to install an Yangbajing Air shower Core detector array (YAC) around the center of Tibet III to distinguish the chemical component making the knee. We set up YAC2 ($\sim$100 detectors over $\sim$160m^2 in area) in 2011, as is shown in Fig. 6 to mainly study the energy spectra of proton and helium components in the knee energy region.

Currently, we are planning to set up YAC3 ($\sim$400 detectors over $\sim$5000m^2 in area) to measure the iron flux in the knee energy region.

(2) Gamma-ray astronomy in the 100 TeV region

We have a plan[**?**] to construct a large ($\sim 10,000$ m$^2 \times$1.5m deep) underground ($\sim$ 2.5 m soil+concrete overburden) water Cherenkov muon detector array (Tibet MD) around an extended version (Tibet AS, $\sim$83,000 m^2) of Tibet III. By Tibet AS + MD, we aim at background-free

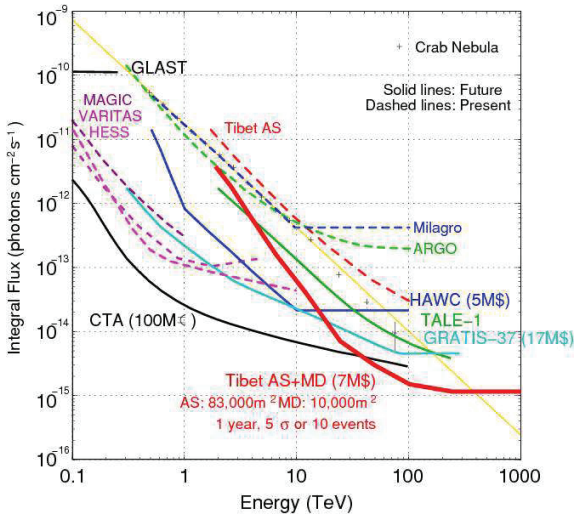

Fig. 7. Tibet AS + MD (red curve) integral flux sensitivity (5σ or 10 events/1yr) for a point source.

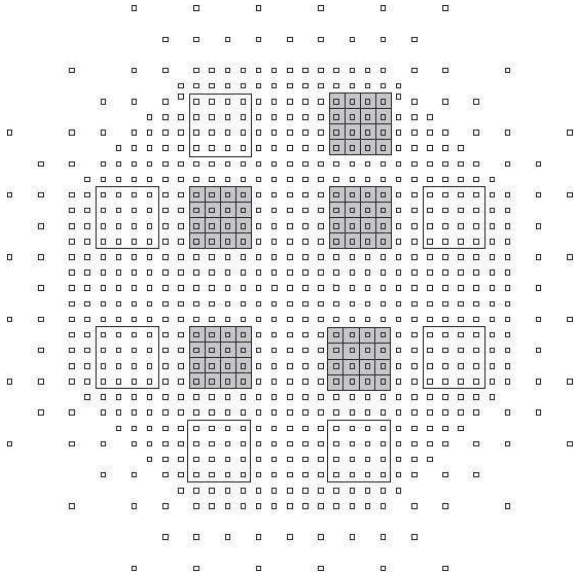

Fig. 8. The 5 shaded squares represent the constructed 5 MD pools.

detection of celestial point-source gamma rays in the 100 TeV region (10 TeV – 1000 TeV) with world-best sensitivity and at locating the origins of cosmic rays accelerated up to the knee energy region in the northern sky. The measurement of cut off energies in the energy spectra of such gamma rays in the 100 TeV region may contribute significantly to understanding of the cosmic- ray acceleration limit at SNRs. Search for extremely diffuse gamma-ray sources by Tibet AS + MD, for example, from the galactic plane or from the Cygnus region may be very intriguing as well. Above 100 TeV, the angular resolution of Tibet AS with 2-steradian wide field of view is 0.2° and the hadron rejection power of Tibet MD is 1/10000. The proposed Tibet AS + MD, demonstrated in Fig. 7, has the world-best sensitivity in the 100 TeV region, superior to HESS above 10-20 TeV and to CTA above 30-40 TeV.

In addition to unknown point-like sources, we expect to detect established sources in the 100 TeV region: TeV J2032+4130, HESS J1837-069, Crab, MGRO J2019+37, MGRO J1908+06, Milagro candidate sources, Mrk421, Mrk501 are sufficiently detectable and Cas A, HESS J1834-087,LS I+63 303, IC443 and M87 are marginal.

Furthermore, our integral flux sensitivity to diffuse gamma rays will be the world-best as well. The diffuse gamma rays from the Cygnus region reported by the Milagro group and also diffuse gamma-rays from the galactic plane will be clearly detected. Diffuse gamma-rays of extragalactic origin may be an interesting target as well.

In fall, 2007, a prototype underground muon detector, composed of two $52m^2$ water pools, was successfully constructed in Tibet to demonstrate the technical feasibility, cost estimate, validity of our Monte Carlo simulation. Data analyses demonstrate that our MC simulation reproduces real data quite reasonably.

In 2010, construction of 5/12 of the full-scale MD, as is shown in Fig. 8, started and the concrete-based water pools were successfully completed. The remaining works are under way.

Bibliography

Papers in refereed journals

[1] "Cosmic-ray energy spectrum around the knee observed with the Tibet air-shower experiment", M. Amenomori *et al.*, Astrophysics and Space Sciences Transactions, **7** , 15-20 (2011).

[2] "Observation of the Fermi pulsar catalog at TeV energies with the Tibet air shower experiment", M. Amenomori *et al.*, Astrophysics and Space Sciences Transactions, **7** , 211-215 (2011).

[3] "Cosmic-ray energy spectrum around the knee obtained by the Tibet experiment and future prospects", M. Amenomori *et al.*, Advances in Space Research, **47** , 629-639 (2011).

Papers in conference proceedings

[4] "The TIBET AS+MD Project; progress report 2011", M. Amenomori *et al.*, Proceedings in the 32nd International Cosmic Ray Conference, (11-18 August 2011, Beijing, China), ID=351, (2011).

[5] "Correlation between Solar Activity and the Sun's Shadow Observed by the Tibet Air Shower Array", M. Amenomori *et al.*, Proceedings in the 32nd International Cosmic Ray Conference, (11-18 August 2011, Beijing, China), ID=352, (2011).

[6] "Air-shower core detector array to study the mass composition of cosmic rays beyond 100 TeV by Tibet hybrid experiment", M. Amenomori *et al.*, Proceedings in the 32nd International Cosmic Ray Conference, (11-18 August 2011, Beijing, China), ID=356, (2011).

[7] "Modeling of the galactic cosmic-ray anisotropy at TeV energies", M. Amenomori *et al.*, Proceedings in the 32nd

International Cosmic Ray Conference, (11-18 August 2011, Beijing, China), ID=361, (2011).

[8] "Time Dependence of Loss Cone Amplitude measured with the Tibet Air-shower Array", M. Amenomori *et al.*, Proceedings in the 32nd International Cosmic Ray Conference, (11-18 August 2011, Beijing, China), ID=379, (2011).

[9] "Observation of atmospheric charged particles associated with thunderstorms at Tibet", M. Amenomori *et al.*, Proceedings in the 32nd International Cosmic Ray Conference, (11-18 August 2011, Beijing, China), ID=497, (2011).

[10] "Observation of Sub-PeV Gamma Rays from the Galactic Plane Using the Tibet Air Shower Array", M. Amenomori *et al.*, Proceedings in the 32nd International Cosmic Ray Conference, (11-18 August 2011, Beijing, China), ID=748, (2011).

[11] "Variability of TeV Gamma-ray Flux from the Crab Nebula with the Tibet Air Shower Array", M. Amenomori *et al.*, Proceedings in the 32nd International Cosmic Ray Conference, (11-18 August 2011, Beijing, China), ID=786, (2011).

[12] "Tibet AS+MD detector simulation using GEANT4", M. Amenomori *et al.*, Proceedings in the 32nd International Cosmic Ray Conference, (11-18 August 2011, Beijing, China), ID=1058, (2011).

[13] "On temporal variations of the multi-TeV cosmic ray anisotropy using the Tibet III Air Shower Array", M. Amenomori *et al.*, Proceedings in the 32nd International Cosmic Ray Conference, (11-18 August 2011, Beijing, China), ID=1167, (2011).

[14] "Study of the large Tyvek bag technique for the water Cherenkov detector in TIBET AS+MD", M. Amenomori *et al.*, Proceedings in the 32nd International Cosmic Ray Conference, (11-18 August 2011, Beijing, China), ID=1168, (2011).

[15] "Calibration of the Yangbajing air-shower core detector (YAC) using the beam of BEPC", M. Amenomori *et al.*, Proceedings in the 32nd International Cosmic Ray Conference, (11-18 August 2011, Beijing, China), ID=1217, (2011).

[16] "Test of the hadronic interaction models at around *10 TeV with Tibet EAS core data", M. Amenomori *et al.*, Proceedings in the 32nd International Cosmic Ray Conference, (11-18 August 2011, Beijing, China), ID=1238, (2011).

[17] "A Monte Carlo study to measure the energy spectra of the primary proton and helium components at the knee using a new Tibet AS core detector array", M. Amenomori *et al.*, Proceedings in the 32nd International Cosmic Ray Conference, (11-18 August 2011, Beijing, China), ID=1239, (2011).

[18] "Measurement of some properties of EAS-cores using new air-shower core detectors array developed for the Tibet hybrid experiment", M. Amenomori *et al.*, Proceedings in the 32nd International Cosmic Ray Conference, (11-18 August 2011, Beijing, China), ID=1241, (2011).

[19] "The forward particle production in the energy range of 10^{15} eV as seen with the Tibet hybrid experiment", M. Amenomori *et al.*, Proceedings in the 32nd International Cosmic Ray Conference, (11-18 August 2011, Beijing, China), ID=1251, (2011).

[20] "TeV Gamma Ray Survey on the Direction of Fermi-LAT Pulsars with the Tibet Air Shower Array", M. Amenomori *et al.*, Proceedings of the First Session of the Sant Cugat Forum on Astrophysics, (12-16 April 2010, Sant Cugat, Spain), Springer, ed. by Nanda Rea and Diego F. Torres, pp491-495 (2011).

The Tibet ASγ Collaboration

M. Amenomori,[1] X. J. Bi,[2] D. Chen,[3] S. W. Cui,[4] Danzengluobu,[5] L. K. Ding,[2] X. H. Ding,[5] C. F. Feng,[6] Zhaoyang Feng,[2] Z. Y. Feng,[7] Q. B. Gou,[2] H. W. Guo,[5] Y. Q. Guo,[2] K. Hakamada,[8] H. H. He,[2] Z. T. He,[4,2] K. Hibino,[9] N. Hotta,[10] Haibing Hu,[5] H. B. Hu,[2] J. Huang,[2] W. J. Li,[2,7] H. Y. Jia,[7] L. Jiang,[2] F. Kajino,[11] K. Kasahara,[12] Y. Katayose,[13] C. Kato,[14] K. Kawata,[15] Labaciren,[5] G. M. Le,[2] A. F. Li,[16,6,2] C. Liu,[2] J. S. Liu,[2] H. Lu,[2] X. R. Meng,[5] K. Mizutani,[12,17] K. Munakata,[14] H. Nanjo,[1] M. Nishizawa,[18] M. Ohnishi,[15] I. Ohta,[19] H. Onuma,[17] S. Ozawa,[12] X. L. Qian,[6,2] X. B. Qu,[2] T. Saito,[20] T. Y. Saito,[21] M. Sakata,[11] T. K. Sako,[13] J. Shao,[2,6] M. Shibata,[13] A. Shiomi,[22] T. Shirai,[9] H. Sugimoto,[23] M. Takita,[15] Y. H. Tan,[2] N. Tateyama,[9] S. Torii,[12] H. Tsuchiya,[24] S. Udo,[9] H. Wang,[2] H. R. Wu,[2] L. Xue,[6] Y. Yamamoto,[11] Z. Yang,[2] S. Yasue,[25] A. F. Yuan,[5] T. Yuda,[15] L. M. Zhai,[2] H. M. Zhang,[2] J. L. Zhang,[2] X. Y. Zhang,[6] Y. Zhang,[2] Yi Zhang,[2] Ying Zhang,[2] Zhaxisangzhu,[5] X. X. Zhou[7]

[1]*Department of Physics, Hirosaki University, Hirosaki 036-8561, Japan*

[2]*Key Laboratory of Particle Astrophysics, Institute of High Energy Physics, Chinese Academy of Sciences, Beijing 100049, China*

[3]*National Astronomical Observatories, Chinese Academy of Sciences, Beijing 100012, China*

[4]*Department of Physics, Hebei Normal University, Shijiazhuang 050016, China*

[5]*Department of Mathematics and Physics, Tibet University, Lhasa 850000, China*

[6]*Department of Physics, Shandong University, Jinan 250100, China*

[7]*Institute of Modern Physics, SouthWest Jiaotong University, Chengdu 610031, China*

[8]*Department of Natural Science and Mathematics, Chubu University, Kasugai 487-8501, Japan*

[9]*Faculty of Engineering, Kanagawa University, Yokohama 221-8686, Japan*

[10]*Faculty of Education, Utsunomiya University, Utsunomiya*

321-8505, Japan
[11]*Department of Physics, Konan University, Kobe 658-8501, Japan*
[12]*Research Institute for Science and Engineering, Waseda University, Tokyo 169-8555, Japan*
[13]*Faculty of Engineering, Yokohama National University, Yokohama 240-8501, Japan*
[14]*Department of Physics, Shinshu University, Matsumoto 390-8621, Japan*
[15]*Institute for Cosmic Ray Research, University of Tokyo, Kashiwa 277-8582, Japan*
[16]*School of Information Science and Engineering, Shandong Agriculture University, Taian 271018, China*
[17]*Saitama University, Saitama 338-8570, Japan*
[18]*National Institute of Informatics, Tokyo 101-8430, Japan*
[19]*Sakushin Gakuin University, Utsunomiya 321-3295, Japan*
[20]*Tokyo Metropolitan College of Industrial Technology, Tokyo 116-8523, Japan*
[21]*Max-Planck-Institut für Physik, München D-80805, Deutschland*
[22]*College of Industrial Technology, Nihon University, Narashino 275-8576, Japan*
[23]*Shonan Institute of Technology, Fujisawa 251-8511, Japan*
[24]*Japan Atomic Energy Agency, Tokai-mura 319-1195, Japan*
[25]*School of General Education, Shinshu University, Matsumoto 390-8621, Japan*

The Ashra Project

[Spokesperson: Makoto Sasaki]
ICRR, Univ. of Tokyo, Kashiwa, Chiba 277-8582
In collaboration with the members of:
ICRR, University of Tokyo, Kashiwa, Japan; Toho University, Funabashi, Japan; University of Hawaii at Manoa, Honolulu, USA; University of Hawaii at Hilo, Hilo, USA; Nagoya University, Nagoya, Japan; Kanagawa University, Yokohama, Japan

Overview

Ashra (*All-sky Survey High Resolution Air-shower detector*) [1, 2, 3, 4] is a project to build an unconventional optical telescope complex that images very wide field of view, covering 77% of the sky, yet with the angle resolution of a few arcmin, sensitive to the blue to UV light with the use of image intensifier and CMOS technology. The project primarily aims to observe Cherenkov and fluorescence lights from the lateral and longitudinal developments of very-high energy cosmic rays in the atmosphere. It can also be used to monitor optical transients in the wide field of sky. The observatory will firstly consist of one main station having 12 detector units and two sub-stations having 8 and 4 detector units. One detector unit has a few light collecting systems with segmented mirrors. The main station and one of the sub stations were constructed on Mauna Loa (3,300 m) on Hawaii Island in 2007 as shown in Fig.1.

Since January 2012, we have highly efficiently made physics observation runs (Observation03) with triple types of triggers for Cherenkov tau showers induced by earth-skimming tau neutrinos, Cherenkov cosmic ray showers, and optical flashes from transient objects like GRBs.

Project

Main Technical Features

The key technical feature of the Ashra detector rests on the use of electrostatic lenses to generate convergent beams rather than optical lens systems. This enables us to realise a high resolution over a wide field of view. This electron optics requires:

- *photoelectric lens imaging-tube*[5]; the world's largest imaging-tube uses electrostatic lens in addition to an optical system to generate convergent beams from photocathode of 20-in. diameter to output phospher window of 1-in. diameter, enabling a very low cost and high performance image sensor providing a high resolution over a wide FOV, and
- *image pipeline*[6]; the image transportation from imaging-tube (image intensifier) to a trigger device and image sensors of fine pixels (CCD+CMOS), with high gain and resolution, enabling very fine images with parallel self-trigger systems that trigger separately for optical flash, atmospheric Cherenkov and fluorescence lights.

Observational Objectives

optical transients; Ashra will acquire optical images every 1 s with 1-s exposure without deadtime. An example of a

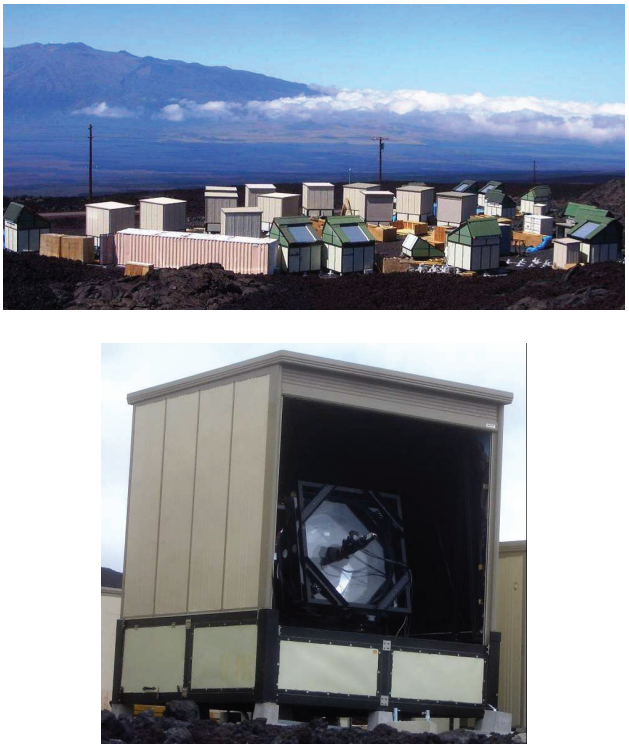

Fig. 1. The Ashra main and sub stations at the Mauna Loa site (top), and a light collector towards Mauna Kea (bottom).

42° FOV image taken by the Ashra light collector is shown in Figure 2. This enables us to explore optical transients, possibly associated with gamma ray bursts (GRBs), flares of soft gamma-ray repeaters (SGRs), supernovae explosion, and so on, in so far as they are brighter than $B \simeq 13$ mag, for which we expect 3-σ signals. The unique advantage is the on-time detection of the events without resorting to usual satellite alerts. In each detector unit FOV, 1∼2 events per year are expected in coincodence with the Swift gamma-ray events. The total Ashra field of view that is wider than satellite instruments allows to detect more optical transients, including an interesting possibility for an optical flash, not visble with gamma-rays.

TeV gamma rays; Atmospheric Cherenkov radiation is imaged by Ashra. Requiring the signal-to-noise ratio (SNR) >5, the system will allow to explore VHE gamma-ray sources with the energy threshold of several TeV at the limiting flux sensitivity of 5% Crab for 1-year observation.

EeV cosmic rays; For fluorescence lights from VHE cosmic rays the effective light gathering efficiency is comparable with that of the High Resolution Fly's Eye detector (HiRes). The arcmin pixel resolution of Ashra provides finer images of longitudinal development profiles of EeV cosmic ray (EeV-CR) air-showers. The resolution of arrival direction with the stereo reconstruction is thus significantly improved and it is better than one arcmin for the primary energy of EeV and higher [7]. This is useful to investigate events clustered around the galactic and/or extragalactic sources. This in turn would give us information as to the strength and coherence properties of the magnetic field [8]. The great advantage of the fine image of Ashra can be applied to the detection of Cherenkov light emitted from the primary particle in the energy range around PeV prior to its first insteraction in the atmosphere. The charge of the primary particle (Z) is estimated from the intensity of this light which is propotional to Z^2. A typical emission angle for the direct Cherenkov light is 0.15° to 0.3°, whereas most of the air-shower light is emitted at angle greater 0.4° from the shower axis [9, 10] The Ashra image resolution of a few arcmin is useful for the discrimination between the direct Cherenkov and the air-shower lights.

PeV-EeV neutrinos; Ashra may detect Cherenkov and/or fluorescence signals generated from tau-particle induced air-showers that is generated from interactions of tau neutrinos with the mountain and/or the earth. This is identified by peculiar geometry of the air-shower axis. The 1-year detection sensitivity with the full configuration of Ashra is 5 and 2 times larger than the Waxman-Bahcall limit for mountain-produced event (Cherenkov) and earth-skimming event (fluorescence), respectively [11, 12]. The most sensitive energy of around 100 PeV is suitable for the detection of neutrinos originating from hadrons accelerated to EeV at astronomical objects.

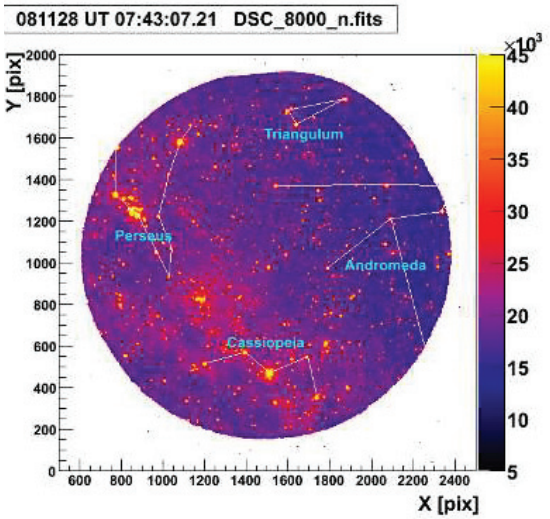

Fig. 2. An example of a 42° FOV image taken by the Ashra light collector (4-s exposure). The solid lines are drawn to indicate constellations.

Brief History

- *October, 2000;* M.Sasaki presented the conceptual idea of fluorescence telescope modifying Baker-Nunn optics and a large diameter image intensifier at ICRR2000 Satellite Symposium (Comprehensive Study of High Energy Universe) [13].
- *March, 2002;* M.Sasaki presented the conceptual design of cosmic ray telescope (NTA) with 50° field of view and 1 arcmin resolution at Workshop on Comprehensive Study of High Energy Universe (Pioneering Cosmic Ray Physics with New Technology).
- *July, 2002;* The Ashra collaboration distributed copies of a proposal for All-sky High Resolution Air-shower telescope (ASHRA).
- *November, 2002;* Ashra failed in the ICRR assessment for the nomination on the project lists in Mid-term Plan of University of Tokyo for 6 years since 2004.
- *June, 2003;* Ashra succeeded to obtain a grant ($5M for 3 years since FY2003) for the proposed program of Pioneering Very High Energy Particle Astronomy, supported by the Coordination Fund for Promoting Science and Technology (157-20004100) from the Ministry of Education, Science, Sports and Culture of Japan. We started systematic design and R&D works to realize the main part of the Ashra phase-1 project (Ashra-1).
- *January, 2004;* University of Hawaii joined in the Ashra collaboration as a local host institute. Agreement on Academic Exchange between the University of Hawaii and the University of Tokyo was ratified. MOU between the Institute for Astronomy of the University of Hawaii and the Ashra Experiment Collaboration was

ratified. The use of Haleakala Observatory for a test observation by the Ashra group was agreed.

- *August, 2004;* The test observation with Ashra prototype detectors at Haleakala Observatory in Hawaii was started. We observed for 10 months.
- *August, 2004;* The Department of Physics and Astronomy of the University of Hawaii at Hilo joined the Ashra collaboration and assumed responsibility for site aquisition and management.
- *December, 2004;* We submitted a report to the GCN circular on the null result on the optical flash associated with GRB041211 [14]. This was the first astronomical report from Ashra. After this measurement, we circulated two more prompt follow-up observations [15, 16].
- *July, 2005;* The state of Hawaii granted to the Department of Physics and Astronomy of the University of Hawaii at Hilo the use of the proposed land on Mauna Loa at 3,300m a.s.l. for the Ashra experiment. Immediately after the permission, we started earthworks, preparation for infrastructure.
- *August, 2007;* The civil engineering construction of light collectors in shelters at the Mauna Loa site was completed.
- *June, 2008;* We started observation of optical transients and commissioning observation of VHE tau neutrinos (see the left panel of Fig.3) with some of the light collectors (Obs01). In this observation period, we submitted an optical observation report of GRB081203A [17] as shown in the right panel of Fig. 3.
- *October, 2009;* We restarted observation of optical transients after three-month shut down (Obs02). In this observation period, we submitted a report of GRB100906A observation [18].
- *June, 2011;* We published the paper about PeV–EeV tau neutrino search from GRB081203A [19] in Astrophysical Journal Letters.
- *June, 2011;* The permit for the 10 year extension of the Ashra Mauna Loa site was granted.
- *January, 2012;* We started observation of optical transients VHE CRs, and VHE tau neutrinos after upgrading our detectors for both targets (Obs03).

Observation

As a first step, we have started the observation of optical transients. During observation, Optical images were constantly collected every 6 s after 4-s exposure. Figure 4 summarizes our observation statistics until the end of Obs02. Maximum observable time is defined by the following condition:

- *Sun condition;* the sun altitude must be lower than -18°.
- *Moon condition;* the moon altitude is lower than 0° or the moon fraction is less than 0.2.

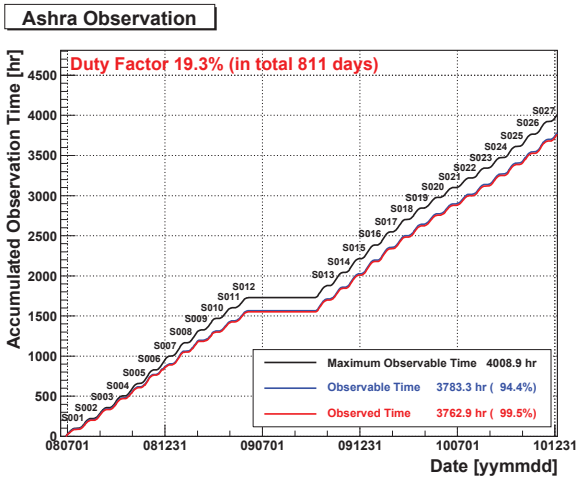

Fig. 4. Summary of Ashra optical transient observation time.

We have accumulated more than 3500 hours of observation time in two years of observation. Good weather rate of 94% shows the superiority of our site and operation efficiency of 99% demonstrates the stability of our operation, where good weather rate is defined by observable time divided by maximum observation time and operation efficiency is defined by observed time divided by observable time.

Ashra-1 observation of early optical emissions: GRB081203A and GRB100906A [17, 18]

Our wide field observation covered the Swift-BAT error circle at the time of GRB081203A [17]. We have searched for optical emission in the field of GRB081203A around the BAT-triggered GRB time (T0) with one of the light collector units in the Ashra-1 detector. The Ashra-1 light collector unit used in this analysis has the achieved resolution of a few arcmin, viewing 42° circle region of which center is located at Alt = 11.7°, Azi = 22.1°. The sensitive region of wavelength is similar with the B-band. We quickly analyzed 83 images covering the field of GRB081203A every 7.2s with 6s exposure time respectively during the observation between T0-300s and T0+300s. We detected no new optical object within the PSF resolution around the GRB081203A determined by Swift-UVOT. As a result of our preliminary analysis, the 3-sigma limiting magnitudes were estimated in comparison with stars in Tycho-2 Catalog to be distributed between 11.7 and 12.0. The summarized light curve is shown in the right panel of Fig. 3.

Our observation also covered the Swift-BAT error circle at the time of GRB100906A [18]. We searched for optical emission in the field of GRB100906A around T0 with an Ashra-1 light collector, viewing 42° circle region of which center is located at Alt = 60°, Azi = 0°. We analyzed 200 images covering the field of GRB100906A every 6s with 4s exposure time respectively during the observation between T0-600s and T0+600s. We detected no new optical object within the PSF resolution around the GRB100906A determined by Swift-UVOT. In the same manner as GRB081203A, the 3-sigma limiting magnitudes were estimated and they were dis-

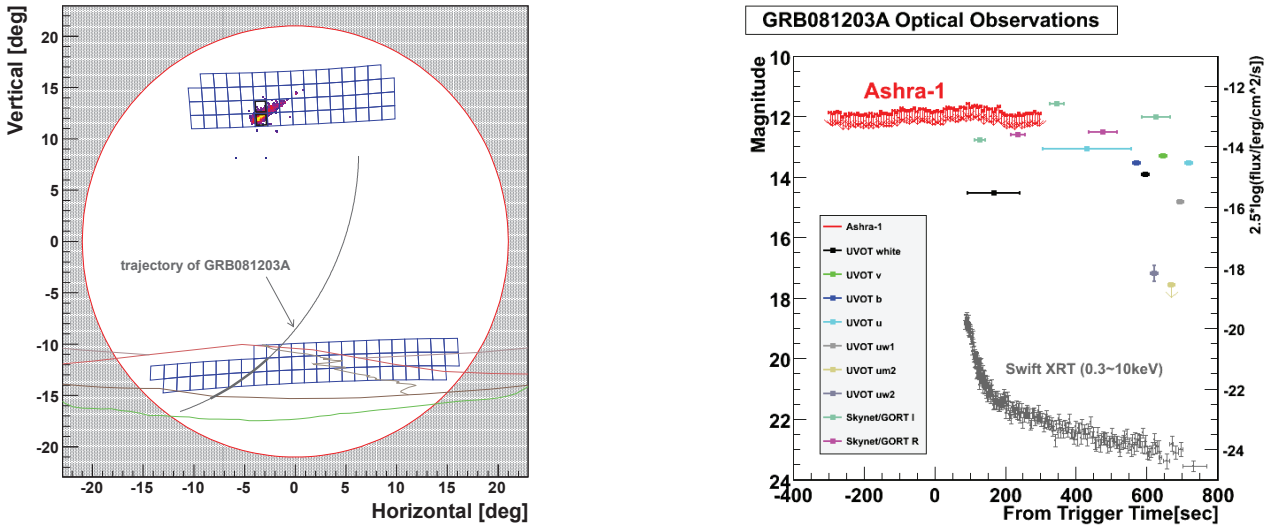

Fig. 3. (*Left*) Boundary (large red circle) between the inside (open circle) and outside (hatched area) of the FOV of the Ashra-1 light collector, which faces Mauna Kea, and the layout of trigger pixel FOVs (blue boxes) for Cherenkov τ shower observation [19]. Repositioned array of the trigger pixel FOVs (upper blue boxes) to check the detection sensitivity with ordinary cosmic-ray air showers at a higher elevation. Firing trigger pixels (thick blue boxes) of an observed image of a cosmic-ray air shower readout along the trigger (points). An extended portion of the trajectory of GRB081203A counterpart (circular arc), the segment of this trajectory used in the ν_τ search (thick circular arc), the ridge lines of Mauna Kea (red) and Mauna Loa (green) mountains, the horizon, and Mauna Kea access road are shown. (*Right*) Summarized lightcurve for GRB081203A [17] around the trigger time. 3-sigma limiting magnitudes of our observation (labeled as Ashra-1) and other observations are compared as a function of time after GRB. The horizontal axis is in linear scale. The vertical axis in the right is only for the data by Swift XRT (gray data), where the scale is arbitrary.

tributed between 12.0 and 12.2.

Observational search for PeV–EeV tau neutrino from GRB081203A [19]

The GRB standard model [20], which is based on internal/external shock acceleration, has been used to describe the general features of a GRB and the observed multi-wavelength afterglow. However, the standard model cannot well reproduce the complicated time evolution of GRBs and the high energy components in the prompt emission [21, 22, 23]. Although many authors have proposed theoretical models to reproduce these features, none of them are conclusive [24]. To better understand the ambiguous mechanisms of GRBs, observational probes of the optically thick region of the electromagnetic components, as well as hadron acceleration processes throughout the precursor, prompt, and afterglow phases are required. VHE νs can be used as direct observational probes, which are effective even in optically thick regions. A monitor search with sufficient time and spatial resolution and survey capability for VHEνs associated with GRBs is plausible.

The earth-skimming tau neutrino (ν_τ) technique [25], which detects extensive air showers, has the advantage of a large target mass, since it uses air showers produced by decay particles of tau leptons (τs) in the atmosphere as the observed signals. τs emerge out of the side of the mountain or the ground facing the detector; they are the product of interactions between VHE ν_τ and the earth matter they traverse. No air Cherenkov observation was made to date based on the earth-skimming ν_τ technique with air showers induced by τ decays (hereafter referred to as the Cherenkov τ shower method). However, it can achieve sufficient detection sensitivity in the PeV–EeV region to be useful in the search for νs originating from hadrons accelerated to EeV at astronomical objects. Additional advantages of the Cherenkov τ shower method are its perfect shielding of cosmic-ray secondary particles, highly precise arrival direction determination for primary ν_τ and negligible background contamination by atmospheric νs in the PeV–EeV energy range.

As shown in Fig. 5, one of the Ashra light collectors built on Mauna Loa has two geometrical advantages: (1) it faces Mauna Kea, allowing it to encompass the large target mass of Mauna Kea in the observational FOV, (2) it has an appropriate distance of $\sim$30 km from Mauna Kea, yielding good observational efficiency when imaging air-shower Cherenkov lights which are directional with respect to the air-shower axis. Using the advanced features, we performed commissioning search for Cherenkov τ showers for 197.1 hr between October and December of 2008. We served limited 62 channels of photomultiplier tubes (PMTs) as trigger sensors prepared for the commissioning runs to cover the view of the surface area of Mauna Kea, maximizing the trigger efficiency for Cherenkov

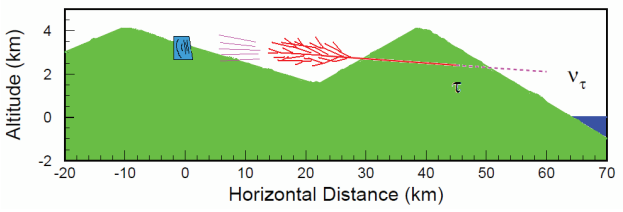

Fig. 5. Conceptual drawing of Cherenkov τ shower method. The right mountain is Mauna Kea and the left is Mauna Loa.

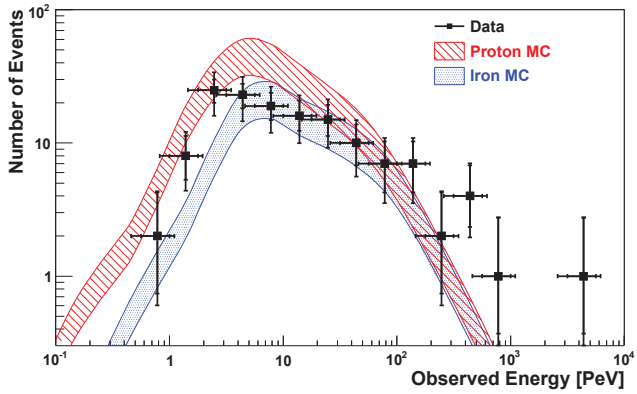

Fig. 6. Observed cosmic-ray flux spectrum (filled box) with bars indicating statistical and systematic errors and the MC predictions for proton primary (hatched band) and iron primary (shaded band) assumptions [19]. The width of the bands shows the evaluated systematic error of 30% of the MC prediction.

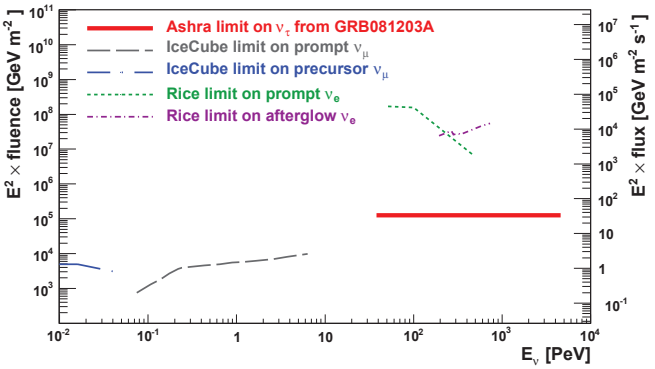

Fig. 7. Ashra 90% CL limit (thick continuous line (red)) on ν_τ fluence of precursor and afterglow emissions from the GRB081203A counterpart in the PeV–EeV region [19]. For comparison, IceCube limits in the prompt (long dashed dotted (gray)) and precursor (long dashed dotted (blue)) phases and RICE limits in the prompt (dashed (green)) and afterglow (dashed dotted (magenta)) phases are shown. The energy ranges were defined as containing 90%, 90%, and 80% of the expected signals from assumed spectrum for Ashra, IceCube, and RICE, respectively.

τ showers from Monte Carlo (MC) study, as shown in Fig.3 (*left*). Adjacent-two logic was adopted to trigger the fine imaging, by judging discriminated waveform signals from each pixel of the multi-PMT trigger sensor. During the search period, ∼2 hr before the trigger of GRB081203A. GRB counterpart (R.A. 15:32:07.58, decl. +63:31:14.9) passed behind Mauna Kea, as viewed from the Ashra-1 observatory.

To investigate the features, selection criteria, detection efficiency, and background rate for the observation of Cherenkov τ shower images, intensive Monte Carlo (MC) studies were performed by utilizing CORSIKA, TAUOLA, and other relevant MC packages. The photometric and trigger sensitivity calibration of the Ashra light collector was based on a very stable YAP-light pulser. Non-uniformity in the detector gain due to the input light position was relatively corrected by mounting a spherical plate uniformly covered with luminous paint on the input window. To correct for the time variation of the photometric and trigger sensitivity because of variations in atmospheric optical thickness, we performed careful cross-calibration to compare the instrumental photoelectric response with the photometry of standard stars such as BD+75D325 of B-magnitude 9.2, for which the detected images passed through the same optical and photoelectric instruments except for the final trigger-controlled readout device.

To confirm the detection sensitivity and gain calibration for the Cherenkov τ shower, we detected and analyzed 140 events of normal cosmic-ray air-shower Cherenkov images for a total of 44.4 hr in 2008 December using the same instruments used in neutrino observation, but after rearranging the trigger pixel layout to view the sky field above Mauna Kea (Fig.3 (*left*)). In the cosmic-ray observation, the trigger pixel layout is centered at zenith angle of ∼65°. The observed and MC cosmic-ray flux spectra are shown in Fig. 6, in which the MC prediction used the typically observed cosmic-ray flux in the knee region [26, 27]. Since the primary cosmic-ray components are observationally undefined, we present the MC prediction of cosmic-ray flux spectra, assuming either only protons or irons as the primary cosmic rays in Fig. 6. Note that the same reconstruction procedure was applied to both of the observed and MC data to extract the observed energy. In both cases, the observed data and the MC prediction agreed well on the normalization and the shape of the distribution within the expected errors. The estimation of the detection sensitivity of the Ashra light collector and the validity of the reconstruction procedure were well demonstrated.

For the ν_τ search, we used image data acquired using the trigger for 197.1 hr in only case of the data status defined as good out of the total observation time of 215.8 hr. Detailed data analysis yielded a null ν_τ candidate [19]. Effective areas for Cherenkov τ showers induced by ν_τs from the GRB081203A counterpart with changing ν_τ energy (E_{ν_τ}) were obtained from an MC study that assumed seven original positions on the GRB counterpart trajectory. On the basis of the above null result and the estimated effective areas, we placed 90% confidence level (CL) upper limits on the ν_τ fluence of precursor and afterglow emissions in the PeV–EeV region, for two 3780 s periods, the first between 2.83 and 1.78 hr before GRB081203A and the second between 21.2 and 22.2 hr after it, as shown in Fig. 7. As sources of systematic uncertainty in the MC estimates of the effective detection areas, we considered the ν_τ charged current interaction cross section, the energy loss by τ in the earth and the mountain, the geological model around the observation site, and the gain calibration of the light collector, which were evaluated to be 50%, 50%, 10%, and 30%, respectively. The conservatively combined systematic sensitivity error was obtained from the square sum of the above uncertainties as 77%, which affects the result of the 90% CL upper limit shown in Fig. 7, where we assumed a typical E_ν^{-2} flux to ensure unbiased constraints on observationally undefined physical mechanisms of a GRB.

For comparison, Fig. 7 shows other observational limits on the ν fluence from point sources [28, 29]. Our results are the most stringent in the PeV–EeV region and complementary to the IceCube results for the sub-PeV energy region, and indicate the advanced instantaneous sensitivity of

the system even during this commissioning phase. Full-scale Ashra observations are expected to have 100 times better sensitivity, since the trigger pixel size is halved (1/4 the pixel area) and the trigger sensor will cover the entire FOV of the light collector. With this higher sensitivity, contamination of 0.55 clusters of air-shower secondary particles is expected in one year of observation data. The advanced angular determination of Ashra for Cherenkov τ showers to within 0.1° will allow perfect rejection against contamination from air-shower secondary particles, and will provide a viable search method for earth-skimming ν_τ events, fully utilizing the zero background conditions. Our first search for PeV–EeV ν_τ reported in Ref. [19] complements other experiments in energy range and detection method, and implies the prologue of "multi-particle astronomy" [13] with a precise determination of time and location.

Prospects

In this Ashra-1 experiment, we were performing device installation and specific observation in a step-by-step way to enhance the scientific impacts as shown in the previous sections. We have already made a referee journal publication of PeV-EeV tau neutrino search [19] as important physics results with the Ashra-1 detector unit adding to publications on the detector or methodorogical developments and circulations [5, 17, 18]. We are now preparing for a few physics publications from the optical observation data of the 2.5 years from the Obs01 to Obs02 as well as keeping highly efficient observation runs in Obs03 for optical transients, VHE CRs and tau neutrinos. Adding that, the R&D for the direct Cherenkov method applied to Ashra-1 has been granted and under development.

The full Ashra observatory (Ashra-2) will consist of three experimental sites separated by about 30 km at Mauna Loa (3,300 m), Camp Kilohana (2,014 m) on the side of Mauna Kea, and Hualalai (2,320 m) on the island of Hawaii. The full configuration emphasizes the stereoscopic observation Cherenkov and fluorescence lights from air-showers with two or three stations at separated sites as well as the effective detection area for air-showers. The parallax observation for optical transients with two or more stations is also useful for rejecting local background events.

Bibliography

[1] http://www.icrr.u-tokyo.ac.jp/∼ashra

[2] Sasaki, M., Progress of Theoretical Physics Supplement, **151**, 192 (2003).

[3] Sasaki, M., et al., Proc. 29th Int. Cosmic Ray Conf. (Pune, India), Vol. 8, 197-200, 2005.

[4] M. Sasaki, 30th Intl. Cosmic Ray Conf. (Merida), ID1232, 2007.

[5] Y. Asaoka and M. Sasaki, Nucl. Instrum. Methods Phys. Res. A **647**, 34 (2011).

[6] M. Sasaki, Y. Asaoka and M. Jobashi, Nucl. Instrum. Methods Phys. Res. A **501**, 359 (2003).

[7] M. Sasaki, A. Kusaka and Y. Asaoka, Nucl. Instrum. Methods Phys. Res. A **492**, 49 (2002).

[8] D. Harari, S. Mollerach and E. Roulet, JHEP 0207 (2002) 006.

[9] D. Kieda, S. P.Swordy, and S.P. Wakely, Astropart.Phys. 15 (2001) 287.

[10] F. Aharonian et al., Physical Rev. D75 (2007) 042004.

[11] G.W.S. Hou and M.A. Huang, astro-ph/0204145.

[12] E. Waxman and J.N. BahCall, Phys. Rev. D59 (1998) 023002.

[13] M. Sasaki, in *Proc. ICRR2000 Satellite Symposium: Workshop of Comprehensive Study of the High Energy Universe*, p. 110 (2000).

[14] Sasaki, M., et al., GCN Circ. 2846, 2004.

[15] Sasaki, M., et al., GCN Circ. 3499, 2005.

[16] Sasaki, M., Manago, N., Noda, K., Asaoka, Y., GCN Circ. 3421, 2005.

[17] Y. Aita *et al.*, GCN Circ., 8632 (2008).

[18] Y. Asaoka *et al.*, GCN Circ., 11291 (2010).

[19] Y. Aita *et al.*, ApJL **736**, L12 (2011).

[20] P. Mészaros, Rep. Prog. Phys. **69**, 2259 (2006), and references therein.

[21] J. A. Nousek *et al.*, ApJ **642**, 389 (2006).

[22] A. A. Abdo *et al.*, ApJ **706**, L138 (2009).

[23] M. De Pasquale *et al.*, ApJL **709**, L146 (2010).

[24] M. Ackermann *et al.*, ApJ **716**, 1178 (2010).

[25] D. Fargion, ApJ **570**, 909 (2002).

[26] T. Antoni *et al.*, Astropart. Phys. **24**, 1 (2005).

[27] M. Amenomori *et al.*, ApJ **678**, 1165 (2008).

[28] R. Abbasi *et al.*, ApJ **710**, 346 (2010).

[29] D. Besson, S. Razzaque, J. Adams, and P. Harris, Astropart. Phys. **26**, 367 (2007).

High Energy Astrophysics Group

[Spokesperson: T. Terasawa]
ICRR, Univ. of Tokyo, Kashiawa, Chiba 277-8582

Overview

The high energy astrophysics group has been making theoretical and observational studies of violent astrophysical phenomena in which nonthermal cosmic ray particles are being accelerated. Targets of the group's study include high energy astrophysical objects such as supernova explosions/pulsar

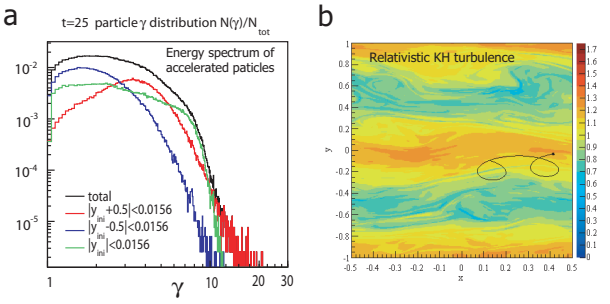

Fig. 1. Particle acceleration in a simulated turbulence in relativistic Kelvin-Helmholtz instability for the plasma layer with an initial velocity shear of $\pm 0.6c$. **(a)** Energy spectra of accelerated particles depend on their initial positions (blue, green, and red) with respect to the velocity shear layer, where the maximum acceleration efficiency (red) was seen for those from the layer with a maximum negative vorticity ($|y+0.5|<0.0156$). **(b)** An example of the orbits of accelerated particles, superposed onto the color map of the magnetic field component B_z, shows the gradient-B drift motion within the magnetic inhomogeneity generated in the turbulence.

magnetospheres [7], giant flares and repeating bursts of magnetars [2], jets from active galactic nuclei (AGN), and mysterious gamma ray bursts (GRB) [4]. Research works on the origin of ultra high energy cosmic rays (UHECRs) are also within the coverage of the group [8].

In addition, studies have been made also for nonthermal phenomena within the heliosphere [1, 6], such as interplanetary shocks and the earth's bow shock, magnetic reconnection, the interaction processes between the solar wind and the moon. While these heliospheric phenomena are limited in their energy coverage, their studies have proved to give a theoretical basis to interpret distant astrophysical high energy phenomena.

Research topics: 1. Reevaluation of acceleration processes

While the diffusive shock acceleration process has been accepted as the standard model of astrophysical particle acceleration, interests are being renewed on other processes such as second-order stochastic acceleration in relativistic turbulences created in regions where relativistic jets, such as those from AGNs and GRBs, collide with surrounding circum-galactic plasmas. We have obtained new results on the stochastic acceleration in a simulated relativistic Kelvin-Helmholtz turbulence (Figure 1, Obi et al., in preparation).

Both in diffusive shock acceleration and second-order acceleration processes, cyclotron resonant interaction between particles and turbulence plays the dominant role, whose condition is given by,

$$\omega - k_{\parallel} v_{\parallel} = n \frac{\Omega_c}{\gamma} \qquad (2)$$

where $(\omega, k_{\parallel})$ define the properties of turbulence, namely the frequency and wavenumber parallel to the background magnetic field $\vec{B}_0$. $v_{\parallel}$ is the particle velocity component parallel to $\vec{B}_0$, γ the Lorentz factor, and Ω_c the nonrelativistic cyclotron frequency. In eq.(2) the choice of n is named as follows: $n = +1$ the fundamental cyclotron resonance, $n = -1$ the anomalous cyclotron resonance, $n = 0$ the transit-time resonance (or Landau resonance), and $n = \pm 2, \pm 3, \ldots$ the cyclotron higher harmonic resonance. Since the middle 60's when the above definitions were made, there seem to have been some confusion and misunderstanding about their interpretation. By presenting a unified review of the cyclotron resonant interaction process [5], we have contributed to clarify the interpretation.

Research topics: 2. Magnetars and pulsars

The magnetosphere around neutron stars are candidate sites for efficient particle acceleration. Magnetars, slowly-rotating neutron stars with strong magnetic field of 10^{13-15} G, occasionally show giant-flare (GF) activities with peak gamma-ray luminosities reaching to 10^{47} erg s^{-1}, which are as strong as the luminosities of AGNs. We have reported on the first clear detection of transient Extremely-Low-Frequency (ELF) radio signal caused by the largest-ever-known GF from the magnetar, SGR 1806-20, on 27 December 2004 [2] (Figure 2).

Crab pulsar, the remnant of the supernova explosion in 1054 A.D., is one of the well-known neutron stars. While its physical properties have been studied for more than 40 years since its discovery, there remains an enigma about the origin of giant radio pulses (GRPs). While for a long time the GRPs had been regarded as a phenomenon limited to the radio frequency pulsar emission, a 3% enhancement of the optical emission at the GRP timing was discovered recently (Shearer et al., *Science*, 2003). Since only a very loose upper limit (<250%) was obtained for the enhancement, if any, of the hard X-ray emission at the GRP timing (Lundgren et al., 1995), we have started a correlational study between the radio and hard X-ray observations collaborating with radio and X-ray astronomers at National Institute of Information and Communications Technology, Tokyo Institute of Technology, and Institute of Space and Astronautical Science in Japan Aerospace Exploration Agency. Figure 3 shows the preliminary result of our analysis based on the simultaneous observations of radio and X-ray signals from the Crab pulsar in three opportunities, on 6 April 2010, 22 March 2011, and 1-2 September 2011. The superposed photon count rates (red dots with error bars) at the main-pulse GRP phase (180^{o}) were marginally enhanced (by 2.9 sigma level) above the average photon count rates obtained with normal (namely, non-giant) radio pulses (a black curve). To obtain statistically significant results, we are waiting for further opportunities of the simultaneous radio and X-ray observations to improve the photon statistics.

Research topics: 3. R/D study for radar detection of UHECRs and extraterrestrial grains

Wide attention has been attracted to the detection of ultra high energy cosmic rays (UHECRs) with radio techniques, either passive and active, towards future large-scale UHECR observatory on the ground. Collaborating with the TA group of ICRR, we have made a R/D study of the active method, namely, the detection of radar echoes from extensive air showers of UHECRs (UHECR echoes, hereafter) [8]. Parallel to the above R/D study, we have also joined a radar research project for extraterrestrial grains (meteors) collaborating with

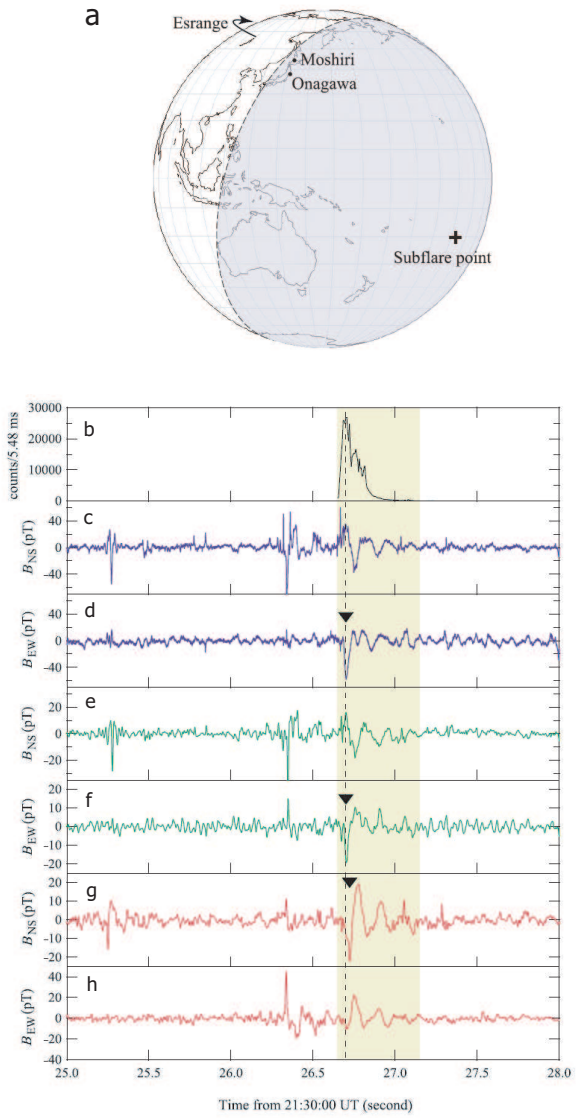

Fig. 2. (a) The shaded hemisphere indicates the part of the earth illuminated by the giant gamma-ray flare of SGR 1806-20 on 27 December 2004. The positions of the three relevant ELF observing stations (Moshiri, Onagawa, and Esrange) are depicted by filled circles. (b) GEOTAIL gamma-ray light curve ($E > 50$ keV) during the most intense period of this flare (a yellow bar). (c), (e), and (g) are the North-South components of the ELF magnetic field recorded at the stations, Moshiri, Onagawa, and Esrange. (d), (f), and (h) are similar to (c), (e),and (g) but for the East-West components detected at these stations. Triangles in the panels (d), (f), and (g) indicate the onsets of the ELF signals at these stations, just corresponding to the peak time of the giant flare at 21:30:26.70 UT, which is shown by a vertical dashed line.

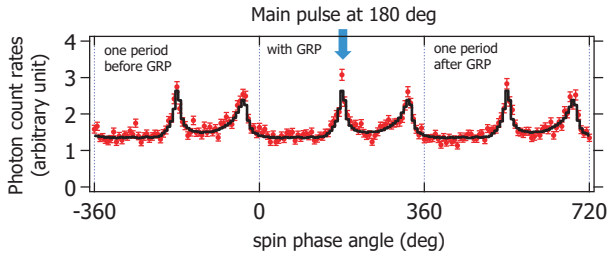

Fig. 3. A black curve shows the averaged X-ray intensity profile (SUZAKU/HXD, 15-75 keV) superposed over the periods of normal pulses from the Crab pulsar. Red dots show the X-ray intensity profile superposed over three adjacent periods (from -360^o to $+720^o$) around main-pulse GRPs (at 180^o). The error bars are drawn according to the photon count statistics with 6-degrees binning boxes.

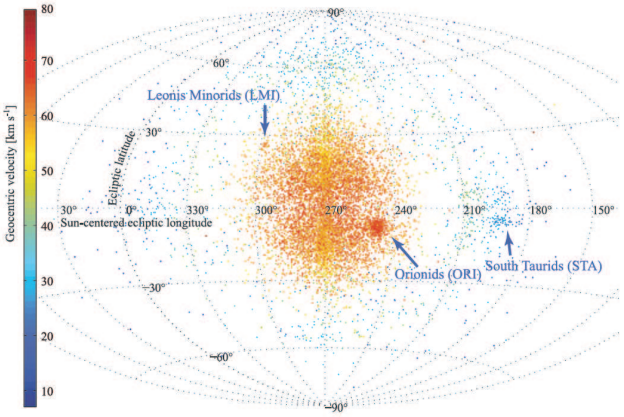

Fig. 4. The radiant distribution of the ∼10000 meteors detected during the 33-h MU radar experiment plotted in Sun-centered ecliptic coordinates. In addition to the known sporadic meteor radiants scattered around the longitude $\sim 270^o$, there is a significant enhancement in the Orionids radiant region (ORI) as well as less significant enhancements around Leonis Minorids (LMI) and South Taurids (STA).

radar physicists and planetary physicists at National Institute for Polar Research, Research Institute for Sustainable Humanosphere in Kyoto University, and Department of Earth Planetary Sciences in the University of Tokyo. Despite more than three orders of magnitude difference in the echo duration between UHECR echoes ($<\sim \mu$s, expected but not yet identified) and meteor echoes (several - several tens of ms, observed), the know-how developed in the latter project (e.g., [3], Figure 4) provides a technical basis for the former. It is further noted that the radar meteor project involves a search for the grains of the interstellar origin, and that there is a suggestion that a general enhancement of refractory elements to volatile elements in low energy galactic cosmic rays (GCR) is due to the injection of interstellar grains to the acceleration process (Meyer et al., 1997). Therefore, the radar observation of the interstellar grain flux, if realized, can contribute to the quantitative modeling of GCR refractory elements.

Research topics: 4. Interaction process between supersonic flow and solid objects

It is expected that the interactions between supersonic plasma flows and surfaces of solid bodies play important roles in many astrophysical environments. The nearest example is from the solar-wind-moon interaction, where detailed studies of plasma and electromagnetic behaviors can be made [1].

Figure 5 (a) and (b) shows the geometrical configurations of two spacecraft, SELENE and CE-1, Japanese and Chinese lunar orbiters, in (a) $X-Y$ (equatorial) plane and (b) $X-Z$ (meridian) plane. Figure 5 (c) shows the variation of the magnetic field across the boundary region of the lunar wake obtained by the SELENE magnetometer. The gradual nature of

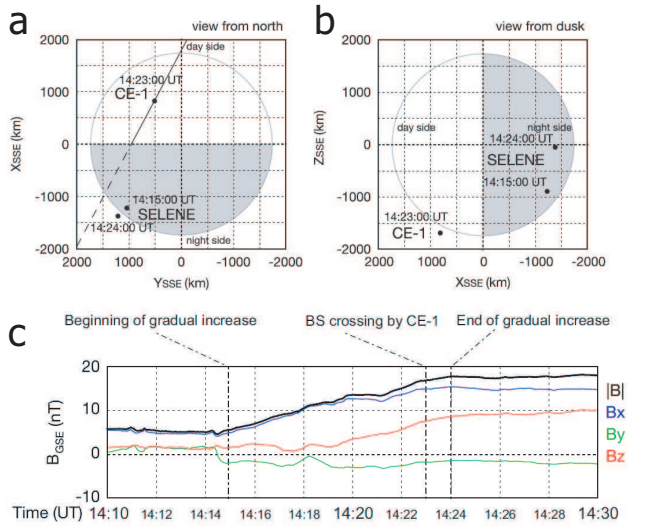

Fig. 5. Panels (a) and (b) show the spacecraft locations projected to the equatorial plane (a) and to the meridian plane (b) at the epochs of 14:15:00 and 14:24:00 UT for SELENE, and 14:23:00 UT for CE-1. The bow shock location at 14:23:00 UT in the dayside region is shown as a oblique line, while its linear extension to the night-side region is illustrated as a broken line. Panel (c) shows the gradual transition of the magnetic field in the wake region observed by SELENE/MAP-LMAG, where the black, blue, green and red curves show the magnetic field data, magnitude $|B|$, and B_x, B_y, and B_z components, respectively.

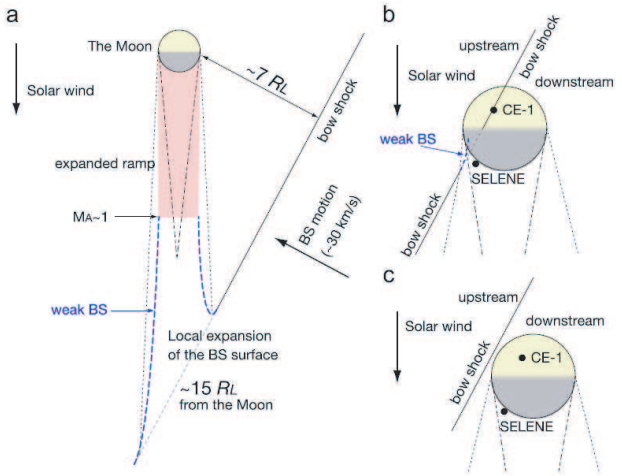

Fig. 6. A schematic view of the bow shock configuration at three epochs, **a** 14:15:00 UT, **b** 14:23:00 UT, and **c** 14:24:00 UT. The dotted (dash-dotted) lines illustrate the outer (inner) edge of the wave boundary region.

the magnetic variation makes a marked contrast with the sharp change of the plasma properties at 14:23:00 UT observed in the dayside region of the bow shock by CE-1.

Figure 6 shows the interpretation of this wake-crossing observation, where the local deformation of the bow shock surface due to the moon-solar wind interaction is illustrated. It is noted that the size of the moon ($R_M = 1738$km) is several times of the characteristic kinetic scale of the plasma (the ion gyroradius ~ 250km). The above observations of the lunar perturbation on the bow shock shape teaches us that down to this spatial scale the magnetohydrodynamics description is applicable to the plasma-solid body interaction process.

Bibliography

Papers in refereed journals

1. Nishino, M. N., X. D. Wang, M. Fujimoto, H. Tsunakawa, Y. Saito, S. Yokota, W. Bian, C. L. Li, M. Matsushima, H. Shibuya, H. Shimizu, F. Takahashi, and T. Terasawa, "Anomalous deformation of the Earth's bow shock in the lunar wake: Joint measurement by Chang'E-1 and SELENE", Planet. Space Sci., 59, 378-386, Apr. 2011.

2. Tanaka, Y. T., M, Hayakawa, Y. Hobara, A. P. Nickolaenko, K. Yamashita, M. Sato, Y. Takahashi, T. Terasawa, and T. Takahashi, "Detection of transient ELF emission caused by the extremely intense cosmic gamma-ray flare of 27 December 2004", Geophys. Res. Lett., 38, L08805.1-4, Apr. 2011.

3. Kero,, J., C. Szasz, T. Nakamura, D. D. Meisel, M. Ueda, Y. Fujiwara, T. Terasawa, H. Miyamoto, and K. Nishimura, "First results from the 2009-2010 MU radar head echo observation programme for sporadic and shower meteors: the Orionids 2009", Mon. Not. R. Astron. Soc., 416, 2550-2559, Oct. 2011.

4. Murase, K., K. Asano, T. Terasawa, and P. Meszaros, "The Role of Stochastic Acceleration in the Prompt Emission of Gamma-Ray Bursts: Application to Hadronic Injection", Astrophys. J., 746, 164-175, Feb. 2012.

5. Terasawa, T., and S. Matsukiyo, "Cyclotron resonant interactions in cosmic particle accelerators", Space Sci. Rev., in press, 2012.

Books

6. Terasawa, T., "Collisionless shocks and particle acceleration: Lessons from studies of heliospheric shocks", IAU Symposium, Volume 274, p. 214-219, June 2011.

Thesis

7. Yamakoshi, Y., "Propagation of Giant Radio Pulses from the Crab Pulsar through Interstellar Plasmas" (in Japanese), Master thesis, Department of Physics, Tokyo Institute of Technology, March 2012.

Conference papers

8. Othman, M. A., C. Allen, J. Belz, D. Besson, B. Farhang-Boroujeny, D. Ikeda, S. Kunwar, J. P. Lundquist, I. Kravchenko, I. Myers, T. Nakamura, H. Sagawa, P. Sokolsky, H. Takai, T. Terasawa, and G. B. Thomson, "Air Shower Detection by Bistatic Radar, International Symposium on the recent progress of ultra-high energy cosmic ray observation", AIP Conference Proceedings, 1367, 143-146, Sept. 2011.

ASTROPHYSICS AND GRAVITY DIVISION

Overview

Astrophysics and Gravity Division consists of Gravitational Wave Group, The Observational Cosmology Group, Primary Cosmic Ray Group and Theory Group. The Gravitational Wave Group conducts experimental research of gravitational wave with researchers of gravitational wave experiment and theory in Japan. The main items are the construction of the large scale cryogenic interferometer(KAGRA) at Kamioka underground and the operation of CLIO. The Observational Cosmology Group has completed the planned imaging and spectroscopy observations, and it continues publishing papers in collaboration with worldwide researchers. This group has started a new optical deep survey project with the wide-field imager of Hyper Suprime-Cam mounted on the Subaru telescope. Primary Cosmic Ray Group reconstructs past cosmic ray changes and studies their impacts on climate change. Theory Group conducts both theoretical study of the Universe and astroparticle physics.

Gravitational Wave Group

KAGRA project

[Spokesperson: Takaaki Kajita] ICRR, Univ. of Tokyo, Kashiwa, Chiba 277-8582

In collaboration with the members of:
National Astronomical Observatory (NAOJ), High Energy Accelerator Research Organization (KEK), Department of Physics (University of Tokyo, abbreviated as UT hereafter), Research Center for the Early Universe (UT), Institute for Laser Science (University of Electro-Communications), Graduate School of Engineering (UT), Graduate School of Frontier Sciences (UT), Earthquake Research Institute (UT), Department of Astronomy (UT), Department of Physics (Osaka City University), Faculty of Engineering (Hosei University), Metrology and Measurement Science (National Institute of AIST), Space-Time Standards Group (National Institute of Information and Communication Technology), Department of Earth and Space Science (Osaka University), Department of Physics (Kyoto University), Yukawa Institute for Theoretical Physics (Kyoto University), Department of Humanities (Yamanashi Eiwa College), Sokendai, School of Science and Engineering (Teikyo University), Graduate School of Humanities and Sciences (Ocahnomizu University), Advanced Research Institute for the Sciences and Humanities (Nihon University), Department of Advanced Physics (Hirosaki University), Astronomical Institute (Tohoku University), Department of Physics (Niigata University), Department of Physics (Rikkyo University), College of Industrial Technology (Nihon University), Department of Physical Science (Hiroshima University), Faculty of Science (University of the Ryukyu), Max Planck Institute for Gravitational physics (AEI), California Institute of Technology, Department of Physics (University of Western Australia), Department of Physics (Louisiana State University), Center for Computational Relativity and Gravitation (Rochester Institute of Technology), Department of Physics (Glasgow University), Columbia Astrophysics Laboratory (Columbia University in the city of New York), Department of Astronomy (Beijing Normal University), Information Science and Technology (Tsinghua University), Inter University Center for Astronomy & Astrophysics (Pune University), Sternberg State Astronomical Institute (Moscow University), LATMOS (CNRS), Center for Astrophysics (University of Science and Technology of China), Shanghai United Center for Astrophysics (Shanghai Normal University), Center for Astrophysics (Tsinghua University), Center for Measurement Standards (Industrial Technology Research Institute), ARTEMIS (CNRS), Department of Astronomy (Maryland University), Department of Engineering (University of Sannio at Benevento), Department of Physics (Korea University), College of Natural Science (Inje University), Department of Physics and Astronomy (Seoul University), Department of Physics (Myongi National University), Quantum Optics Center (Korea Atomic Energy Research Institute), Department of Physics (Hanyang University), Department of Physics (Pusan National University), Korea Institute of Science and Technology of Information, National Institute of Mathematical Sciences (Korea), Department of Astronomy and Atmospheric Sciences (Kyungpook National University), Department of Physics (Gunsan National University), Korean Insitute for Advanced Study, Shanghai Institute of Ceramics (Chinese Academy of Sciences)

Overview of KAGRA[8]

KAGRA (The new nickname has been given for LCGT : Large-scale Cryogenic Gravitational wave Telescope), as one of the world network of gravitational wave detectors, aims at the detection of gravitational waves by a 3 km baseline laser interferometer with cryogenic mirror system placed underground at Kamioka.

The development of KAGRA started as a 6.5 year project in October 2010, but later it was rescheduled as a 7.5 year project due to the suspension of the budget for the start of tunnel excavation as a result of the Great East Japan Earthquake which occurred on March 11, 2011. The KAGRA development is divided into two stages: initial KAGRA (iKAGRA) and baseline KAGRA (bKAGRA). In the 5 year iKAGRA stage the mirror system will be kept at room temperature with SAS (Seismic Attenuation System) and RSE (Resonant Sideband Extraction) not in operation while the bKAGRA is the latter 2.5 year development stage where the final goal is to be pursued with full equipment in operation including SAS, cryogenic system and RSE.

The host organization to conduct the KAGRA project is the Institute for Cosmic Ray Research, the University of

*8 Seiji Kawamura, ICRR, University of Tokyo

Tokyo with a number of organizations both domestic and international involved. Up to now 31 Japanese and 32 overseas universities and research institutes have joined the KAGRA collaboration and still counting. The official agreements to establish international collaborations have been concluded between ICRR and 7 foreign institutes.

KAGRA, in the final configuration of bKAGRA, is designed to achieve the aim to detect gravitational-wave signals. Among several expected gravitational-wave sources, the primary observation target is selected to be an inspiral and merger of neutron-star binary. This is because it is the most certain source: its existence has been proved by radio-pulsar surveys, and its event rate has been theoretically estimated from astronomical observation results.

It is required that the KAGRA sensitivity be high enough to realize more than one detection of gravitational waves from neutron-star binaries in a one-year observation run with probability 90% or higher. For the requirement, the KAGRA duty factor must be higher than 80% and the observation range must be higher than 180Mpc. Here the signal-to-noise ratio is 8 and the normal incidence of gravitational waves on to the detector is assumed.

Figure 1 shows the estimated ultimate sensitivity limits of KAGRA where incoherent sum of the fundamental noise sources is assumed. The observation range with the ultimate sensitivity limit of KAGRA is 280Mpc.

With the currently-practical design parameter set for bKAGRA, the sensitivity limited by fundamental noise sources gives the observation range of 240Mpc. The requirement allocation to each subsystem is determined in such a way as not to deteriorate the sensitivity more than 10% in total.

The observation range of bKAGRA with the 10% deterioration is 210Mpc. It is also required to each subsystem that the duty factor of KAGRA during the observation run be 80% or higher in total. More detailed requirement allocation is shown in the Interface Control Document (ICD).

The requirement for KAGRA is to be flowed down into that for each of the subsystems. Required values for the subsystem components are determined in such a way that the KAGRA target sensitivity be achieved with all the noise curves summed up in the spectrum. Some of the setup parameters are shared by multiple subsystems and those interface parameters shall be controlled by the System Engineer Office (SEO).

Major components of each subsystem are listed below.

- **Tunnel (TUN):** 3km tunnels, center room, end rooms, entrance tunnels, water drainage system
- **Facility Support (FCL):** buildings, power supply system, clean rooms, air conditioning, temperature control, humidity control
- **Vacuum (VAC):** vacuum ducts, vacuum chambers, baffles, flanges, vacuum pumps
- **Cryogenic System (CRY):** cryostats, heat link, Sapphire fibers, radiation shields, refrigerators
- **Vibration Isolation System (VIS):** Type-A/B/C SAS, suspension fibers (excl. Sapphire fibers), local controls
- **Mirror (MIR):** core optics, MC mirrors, MMT mirrors
- **Laser (LAS):** laser (1064nm, 532nm)
- **Main Interferometer (MIF):** optical layout of the main interferometer
- **Input Output Optics (IOO):** MC, OMC, Faraday isolator, EOM, MZ, BRT
- **Auxiliary Optics (AOS):** light control components (including suspended baffles), beam reducing telescopes, optical levers, moniors (CCD/CMOS cameras), viewports, automatic targets, beam shutters
- **Analog Electronics (AEL):** PD, QPD, actuators, CCD, monitors
- **Digital System (DGS):** CDS, signal transferring cables, ADC, DAC
- **Data Analysis (DAS):** DAQ system, data analysis pipelines
- **Geophysics Interferometer (GIF):** 1.5km interferometers, seismometers, environmental sensors

The rapidly changing status of KAGAR is presented in several international conferences.[1] There are also special articles presented in journals of academic societies.[2] We also present activitiy in our web-page.[3]

Bibliography

[1] S. Miyoki and LCGT collaboration, ”Curent Status of LCGT project”, TAUP 2011 in Minich, Munchen.

[2] K. Kuroda, ”Large-scale Cryogenic Gravitational wave Telscope (LCGT) -Construction Status of LCGT project-”, J. Cryo. Super. Soc. Jpn **46** (2011) 385 (in Japanese).

[3] http://gwcenter.icrr.u-tokyo.ac.jp/en/

Tunnel Subsystem[9]

Definition and scope of the subsystem The KAGRA interferometer will be constructed in a large experiment room placed under Ikenoyama mountain in Gifu prefecture in Japan. The experiment room needs access tunnel from the outside. The

*9 Takashi Uchiyama, ICRR, University of Tokyo

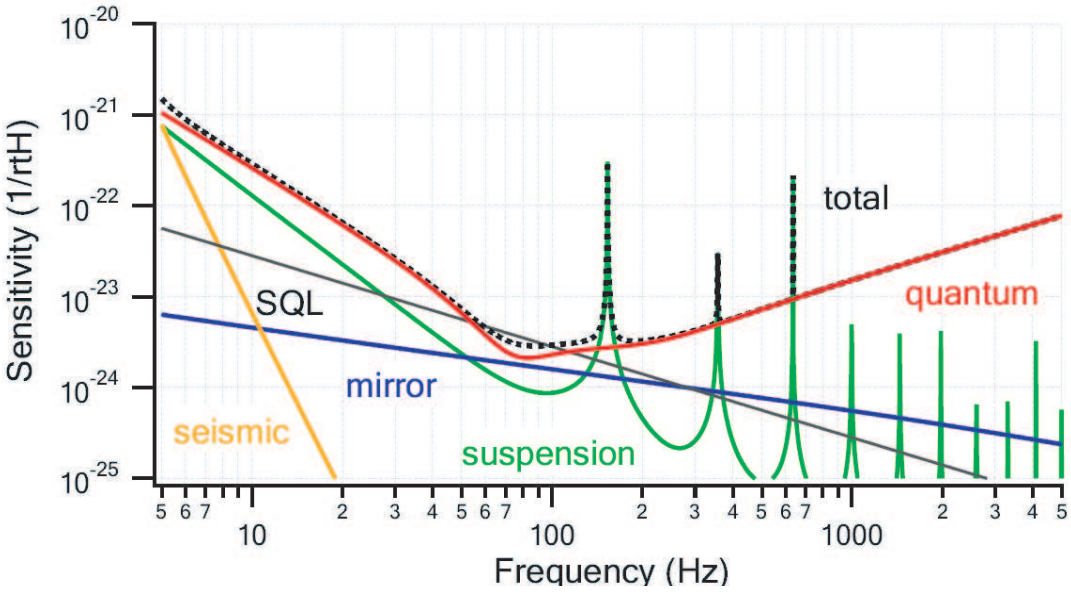

Fig. 1. Ultimate sensitivity limit of KAGRA.

experiment room and the access tunnel consists of a lot of tunnels which will be newly excavated for KAGRA. The tunnel subsystem is responsible to make the tunnel design which must satisfy requirements described in the interface section. We made the design document with Suncoh consultant for the bid of tunnel construction. Kajima corporation won the bid and is responsible for the tunnel construction. After the excavation, construction of a drainage system, splaying concrete on the tunnel surface, and making floors will be done as the finish of the tunnel construction. The facility subsystem is responsible for construction of the experiment rooms which realize environment satisfying with requirements of the experiments and construction of infrastructure.

bKAGRA

Requirements Following is a conceptual requirements list for the tunnel design.

- The tunnels must be designed to have enough safety.
- The tunnels must be designed to achieve the target sensitivity of bKAGRA.
- The tunnels must be designed to be enough large area for the interferometer and facilities.

For the enough safety, all the experiment room must have multiple escape routes.

Table 1 shows required dimensions of the experiment room. The arm tunnel is length of 3km, width of 4m, and height of 4m. The arm tunnels are tilted with 1/300 for natural water drainage. The experiment rooms were designed to be fit for the arrangement and height of vacuum chambers. The width of arm tunnels is 4m and it was taken into account of the diameter of the beam duct tube for KAGRA and the geophysical interferometer and width of a transporter car which will be used in the arm tunnels.

Design Fig. 2 shows location map of KAGRA. KAGRA has two 3km arms (X arm and Y arm). Those arms cross perpendicularly at the center of BS chamber in center area. The location of the center of the BS chamber is latitude of 36.41°N and longitude of 137.31°. Altitude of the floor of the BS chamber from the sea level is 372m. Y arm is rotated by 28.31° from the North to the West. KAGRA has three important areas, center, Xend (end side of the X arm) and Yend (end side of the Y arm), where the test mass vacuum chambers will be placed. Those areas are located to be inside more than 200m from the surface of the mountain for the small seismic motion.

KAGRA has two access tunnels; New Atotsu and Mozumi. New Atotsu tunnel provides access to the center area of KAGRA. Mozumi tunnel provides access to the Yend. New Australian Tunneling Method (NATM) will be used for excavating the tunnels and the experiments rooms. Fig. 3 shows that cross-sectional figures of the arm tunnels and the access tunnels. The arm tunnels are tilted with 1/300 for natural water drainage. Since height of the sea level of the end room is approximately 10m higher or lower from the BS, Yend is the lowest and height of the sea level is 362m. Xend is the highest and height of the sea level is 382m. Therefore, the direction of water flow is from the X end to the Y end through the center. The amount of water leakage is expected more than $2m^3$/min in the X arm. The less water leakage is expected in the Y arm, even though there is a fault. There are water drain points in both arms. A water drain pipe in an arm tunnel is divided into two pipes at the water drain point. One pipe goes down to the other old tunnel that is located at the lower height of the sea level. It prevents the massive water from passing through the side of the mirror vacuum chambers.

Fig. 4 shows the experiment room map of KAGRA. All the rooms are named and numbered. The centre area, the X end area and the Y end area consist of the rooms numbered 1 to 13, 18 to 25 and 28 to 36, respectively. The experiment room for the test mass suspension designed as two layers tun-

Table 1. Dimensions of the experiment room. Room Numbers are represented in Fig. 4.

Room No.	Room name	Length [m]	Width [m]	Height [m]
1	Center parking	15	15	7.5
2	Center front room	15	15	7.5
3	Center exp. room A	40	15	7.5 to 9.5
4	Center exp. room B	32	15	7.5 to 9.5
5	Center exp. room C	27	10	6
7	X-front cryostat room	30.5	12	8
8	X-front VI room	12	8	7
11	Y-front cryostat room	26.5	12	8
12	Y-front VI room	12	8	7
19	X-end cryostat room	20	12	8
20	X-end VI room	12	8	7
24	X-end exp. room	20	8	4
25	X-end staff room	15	8	4
28	Y-end cryostat room	20	12	8
29	Y-end VI room	12	8	7
33	Y-end exp. room	20	8	4
35	Y-end staff room	10	8	4
36	Y-end parking	10	8	4

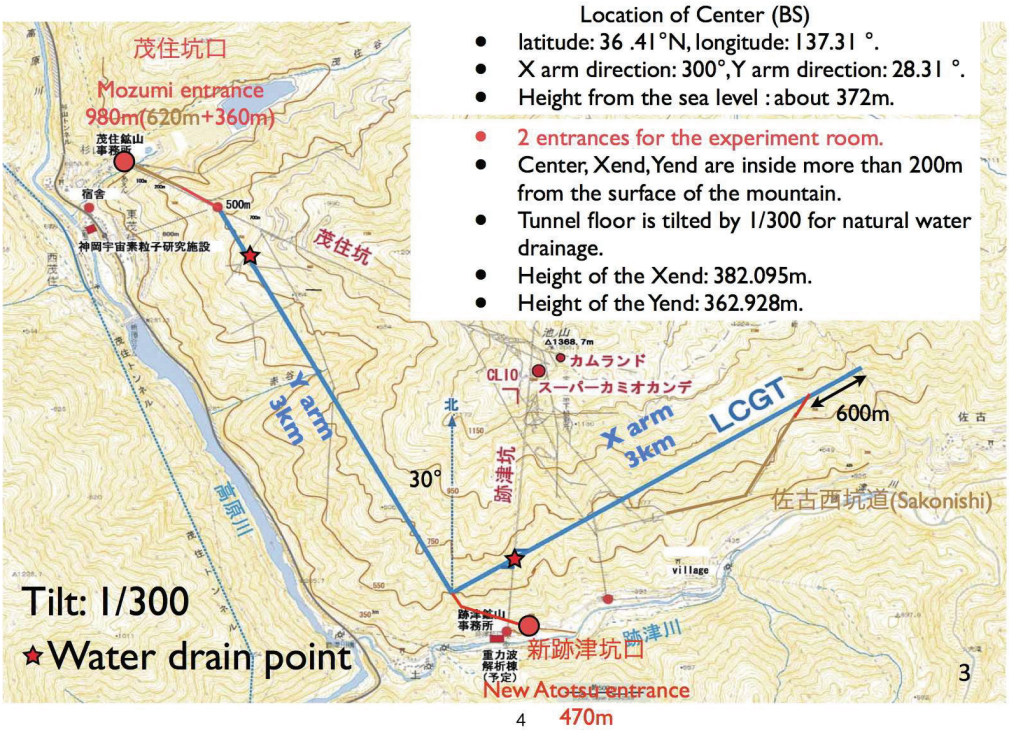

Fig. 2. Location map of KAGRA

nel. For example, the 1st floor is the X-end cryostat room (No. 19) and the 2nd floor is the X-end VI room (No. 20). A vertical hole with diameter of 1150 mm to be made for a vacuum tube connecting a cryostat at the 1st floor and a vacuum chamber for the vibration isolation system. Thickness between the 1st and the 2nd floor is larger than 5m. It provides enough stiffness for the base of the vibration isolation system. The approach tunnel for the 2nd floor (No. 23) is tilted by 18% and 73m in length. The geophysical interferometer that has 1.5km length will be installed in both the X arm and the Y arm.

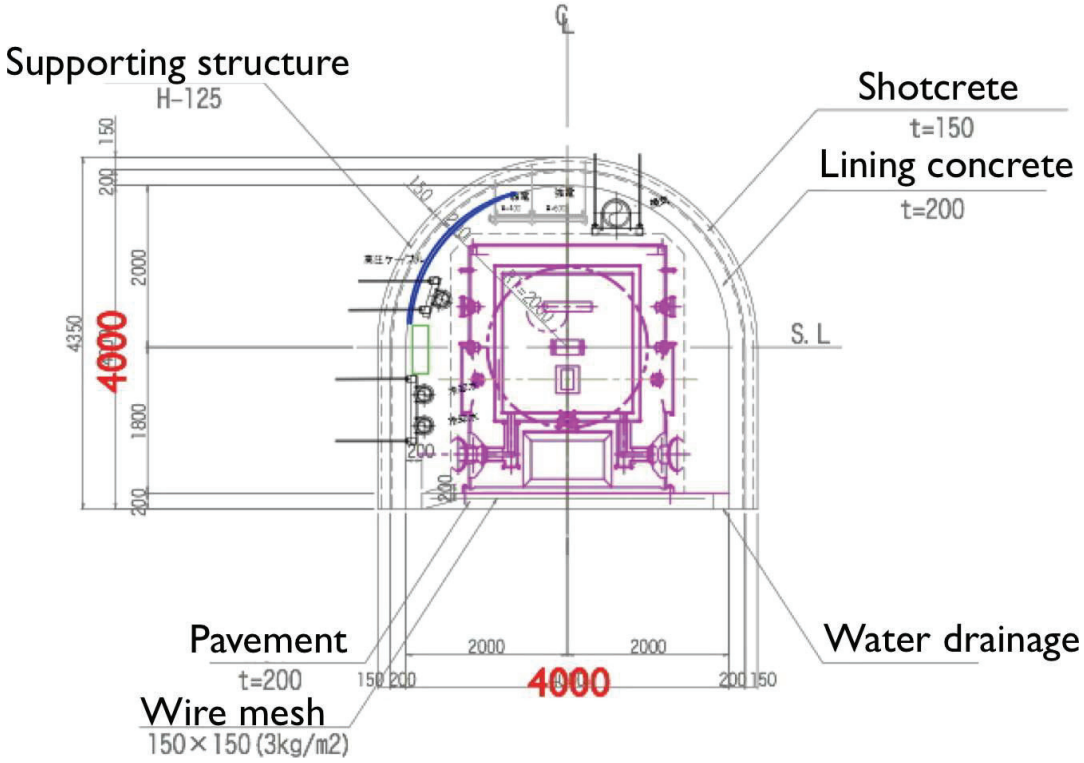

Fig. 3. Cross-sectional figures of the arm tunnels and the access tunnels. Purple line idicates the cryostat for KAGRA, which is the largest item to be transported to Xend through the Xarm tunnel.

Vacuum Subsystem[10]

Scope The substantial items of the KAGRA Vacuum Subsystem are manufacturing and installing the two beam tubes of 3-km long and 800 mm in diameter, as well as 21 of chambers for the mirrors with suspension and vibration isolation devices. Optical baffles installed at every 12 m in the beam tube for suppressing small angle scattering from the main mirrors are also to be designed so that the structure and surface-finish are optimized for optical and vacuum performance. Further, overall layout of the vacuum chambers and interconnecting tubes and Gate Valves are to be managed by the vacuum group (layout is shown in Fig. reffig:vacuumsystem). [1].

Target specification The aimed sensitivity of KAGRA is $h = 3 \times 10^{-24}$ /$\sqrt{}$ Hz at 100 Hz, corresponding to a horizontal displacement of $dx = 1 \times 10^{-20}$ m/$\sqrt{}$ Hz. The predicted noise due to the residual gas (water) is $dx = 1 \times 10^{-21}$m/$\sqrt{}$ Hz when the pressure in the KAGRA beam tubes is kept at 2×10^{-7} Pa. Then, we can obtain a safety margin of 10.

The displacement noise for multiple reflections from the tube wall was estimated to be $dx = 3 \times 10^{-21}$ m/ Hz, using the value of tube vibration amplitude of 1×10^{-11} m/$\sqrt{}$ Hz in Kamioka.We can expect to reduce the noise to $dx = 5 \times 10^{-22}$ m/$\sqrt{}$ Hz by installing baffles with a projected height of 40 mm at every 12 m along the beam tube.

Manufacturing process of the beam tube In order to realize the ultra-high vacuum, the outgassing rate of the materials for component use is to be reduced to the order of 10^{-8} Pa m^3 s^{-1} m^{-2}, or lower, for 50 hours pumping. The stainless-steel material SS314L and 316 are chosen for beam tube and bellows, respectively. The inner surface of the unit tube (12-m long and 800 mm in diameter) after welding flanges and bellows is processed by electropolishing so as to remove 30 μm of the surface degraded layer (Fig. 6). A pre-baking process at 200°C for 20 hours is finally performed to the unit tube in order to passivate the surface layer. The result of outgassing rate measured for a tube shows a value of the order of 10^{-9}Pa m^3 s^{-1} m^{-2} for 100 hours of pumping. For fiscal years of 2010 and 2011, 320 of 500 beam tubes are manufactured (Fig. 7).

*[10] Yoshio Saito, Visiting professor of ICRR, Accelerator Laboratory, KEK

Bibliography

[1] R. Takahashi, Y. Saito, "Vacuum-system Design for the Large-scale Cryogenic Gravitational wave Telescope", Vacuum **84** (2010) 709-712.

Cryogenics - Cooling System[11]

Definition and scope of the subsystem Subject of the subsystem is to carry out designing, prototype test, manufacture inspection, storage, transportation, installation and adjustment for those equipments of cryochambers, cryocooler units, shield ducts, monitoring instruments and cryogenic payloads.

*[11] Toshikazu Suzuki, ICRR visiting professor, Cryogenic Science Center, KEK

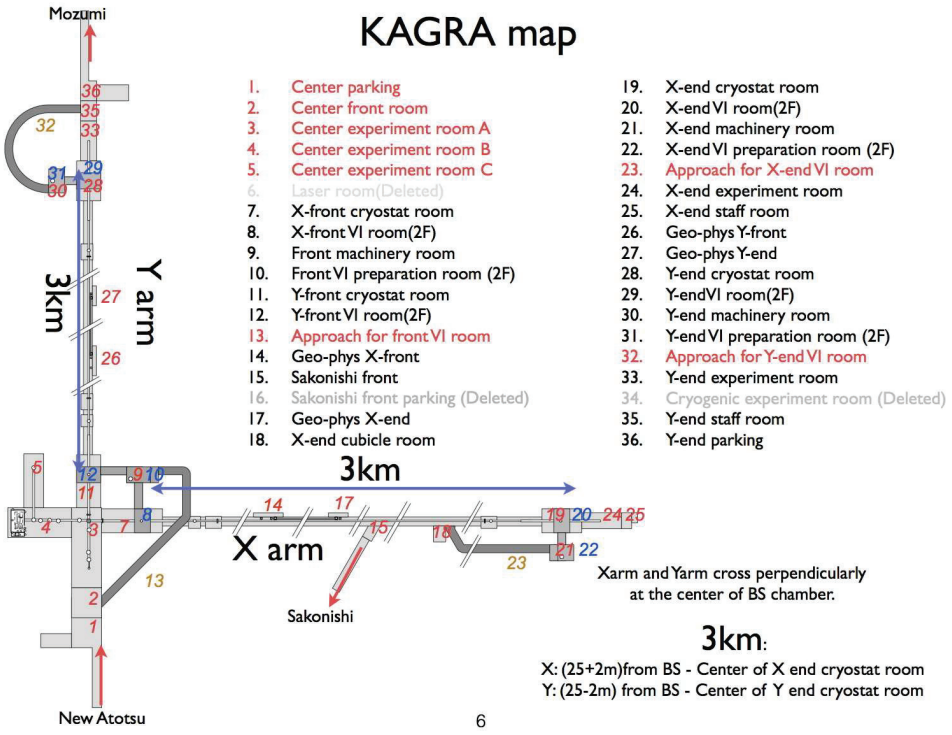

Fig. 4. Experiment room map of KAGRA. All rooms are named and numbered for convenience. The BS tank is represented by a gray circle in the center experiment room B (No. 3). The laser room (No. 6) is deleted from the original design. The clean booth for the laser source will be placed the edge of Center experiment room B.

iKAGRA

Target specifications Specifications of chambers accord with the instruction of vacuum system. Decision to use a new material was made after passing the measurement of outgassing rate. For example, measurements were made for a new type of thermal insulation film and bulk of polyimide.[1] Tolerances of machining accord with JIS B0405 standard.

Final design The schemtic design of cryogenic system is shown in Fig. 8, which is compatible with vibration isolation system in a vacuum.

Design of cryochambers and 4K cryocooler units were finished.[2] Those equipments are in manufacturing (Fig.9, Fig. 10).

bKAGRA

Requirements Cool test masses down to 20 K and keep the temperature during operation.

Preliminary design Basic design of cryochambers and 4 K cryocoolers are finished. Design of shield ducts and 80 K cryocooler units are in progress.

Estimation of incoming heat radiation

The heat radiation coming from the vacuum duct maintained at room temperature was shown to be suppressed by infrared optical baffles placed in front of the cooled mirror. We measured the surface emmissivity of the material used for radiation shield.[3]

Fig. 9. A large cryochambers are waiting for assembling.

Bibliography

[1] T. Ohmori *et al.*, "Vacuum and Insulation Technology for Large-scale Cryogenic Gravitational wave Telescope (LCGT)",J. Cryo. Super. Soc. Jpn **46** (2011) 408 (in Japanese).

[2] N. Kimura *et al.*, "Refrigerator and Cryostat Design for LCGT",GWADW 2011, 22-28 May, 2011, La Biodola, Isola d'Elba, Italy.

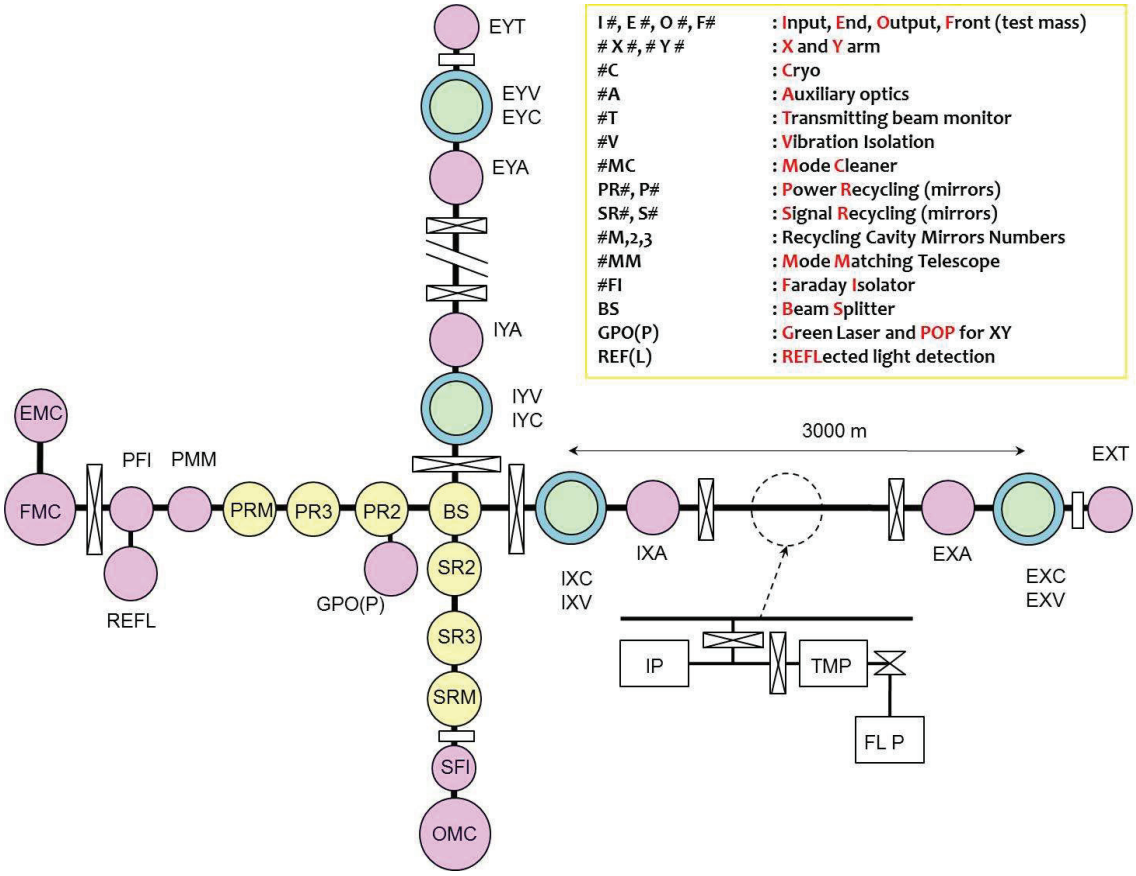

Fig. 5. Schematic drawing of the KAGRA vacuum system.

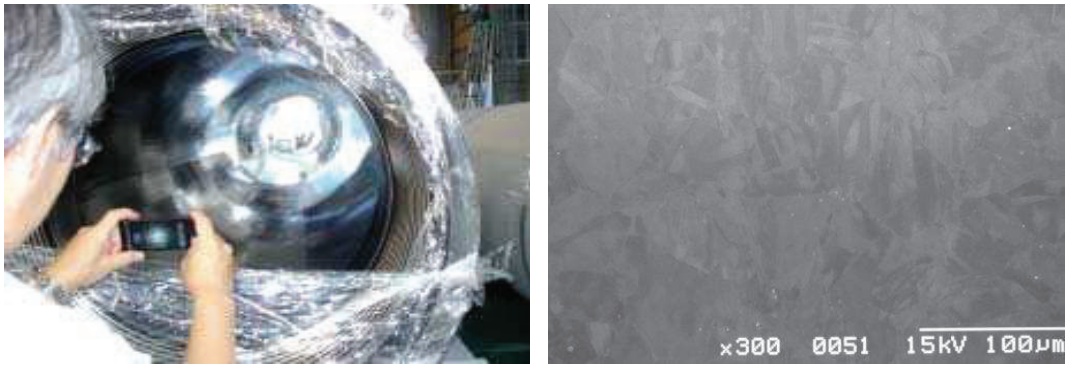

Fig. 6. Electropolished tube and surface.

[3] Y.Sakakibara *et al.*, "Emmissivity of radiation shield metal in cryogenic temperature at wavelength 10μm for Large scale Cryogenic Gravitational wave Telescope", J. Cryo. Super. Soc. Jpn **46** (2011) 434 (in Japanese).

Cryogenics - Cryogenic Payload[12]

Definition and scope of the subsystem The cryogenic payload means the suspension systems for the cooled mirrors of the main Fabry-Perot cavity. They are suspended from the vibration isolation system called Type-A and surrounded by the radiation shield. The heat links between the masses of the payloads and the shield (or heat path near the radiation shield) belong to the cryogenic payload. Therefore, the cryogenic payload is on the border between the vibration isolation and cryogenics.

iKAGRA

Since the room temperature interferometer will be constructed in iKAGRA phase, nothing is mentioned here. However, it must be noted that the cryogenic payload will be made

*[12] Kazuhiro Yamamoto, ICRR, University of Tokyo

Fig. 7. Tube delivery to the storage tunnel.

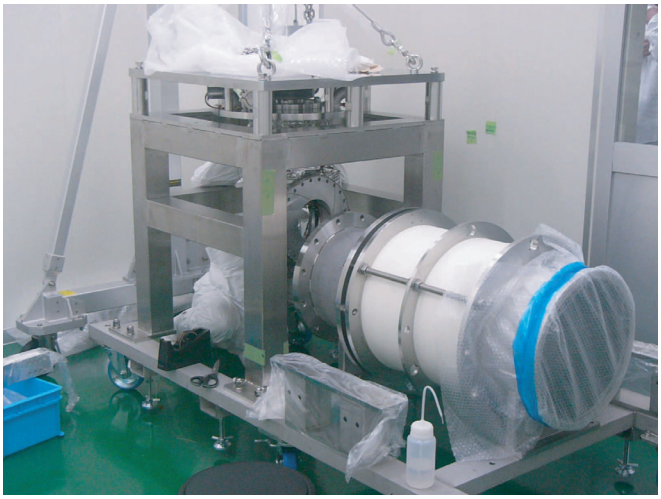

Fig. 10. A cryocooler unit is assembling in the clean room.

and some of them will be installed in iKAGRA phase.

bKAGRA

Requirement The cryogenic payload should be installed in safe and clean environment within the short period. The sapphire mirrors should be enough cooled (below 20 K). The initial cooling time must be as short as one month. The control (and damping) for the angle and position of the mirrors and the other masses are necessary and they must work well at cryogenic temperature. The thermal noise, the external vibration via heat links, and control noise should be smaller than the sensitivity of bKAGRA.

Preliminary design The cryogenic payload is the triple pendulum and is suspended from the Type-A SAS. Figure 11 is a preliminary schematic view. It is enclosed by the double radiation shields. The mirror (23 kg) and recoil mass (about 30 kg) are suspended from the intermediate mass (about 60 kg). The distance between the centers of mirror and the intermediate mass is 30 cm. The intermediate mass and its recoil mass (about 60 kg) are suspended from the platform (about 120 kg). The distance between the centers of the intermediate mass and platform is 40 cm. The heat links are between the inner radiation shield and payload. The radiation shield is cooled by pulse tube cryocoolers. For one sapphire mirror, 4 cryocoolers are necessary.[1]

How to assemble and install, control and damping system will be considered. The thermal noise should be evaluated. The initial cooling time and mirror temperature with absorption of laser are evaluated by Y. Sakakibara and seismic motion is calculated by T. Sekiguchi. Noise of control and damping system should be estimated.

Bibliography

[1] N. Kimura *et al.*, "Present design of LCGT cryogenic payload -Status of cryogenic design-", GWADW 2011, 22-28 May, 2011, La Biodola, Isola d'Elba, Italy.

Vibration Isolation Subsystem[13]

This subsystem makes vibration isolation for all optics used in KAGRA. There are two purposes required for this subsystem. One is attenuation of seismic noise in the observation band (less than 4×10^{-20} m/$\sqrt{}$ Hz at 10 Hz). The other is reduction of RMS displacement or RMS velocity of mirrors (less than 0.1μm or 0.1μm/s). Three kinds of system are disposed to 21 vacuum chambers to accomplish their purposes. Main mirrors are isolated by Type-A system, which consists of an inverted pendulum (IP), five stage geometric anti-spring

*[13] Ryutaro Takahashi, ICRR, University of Tokyo

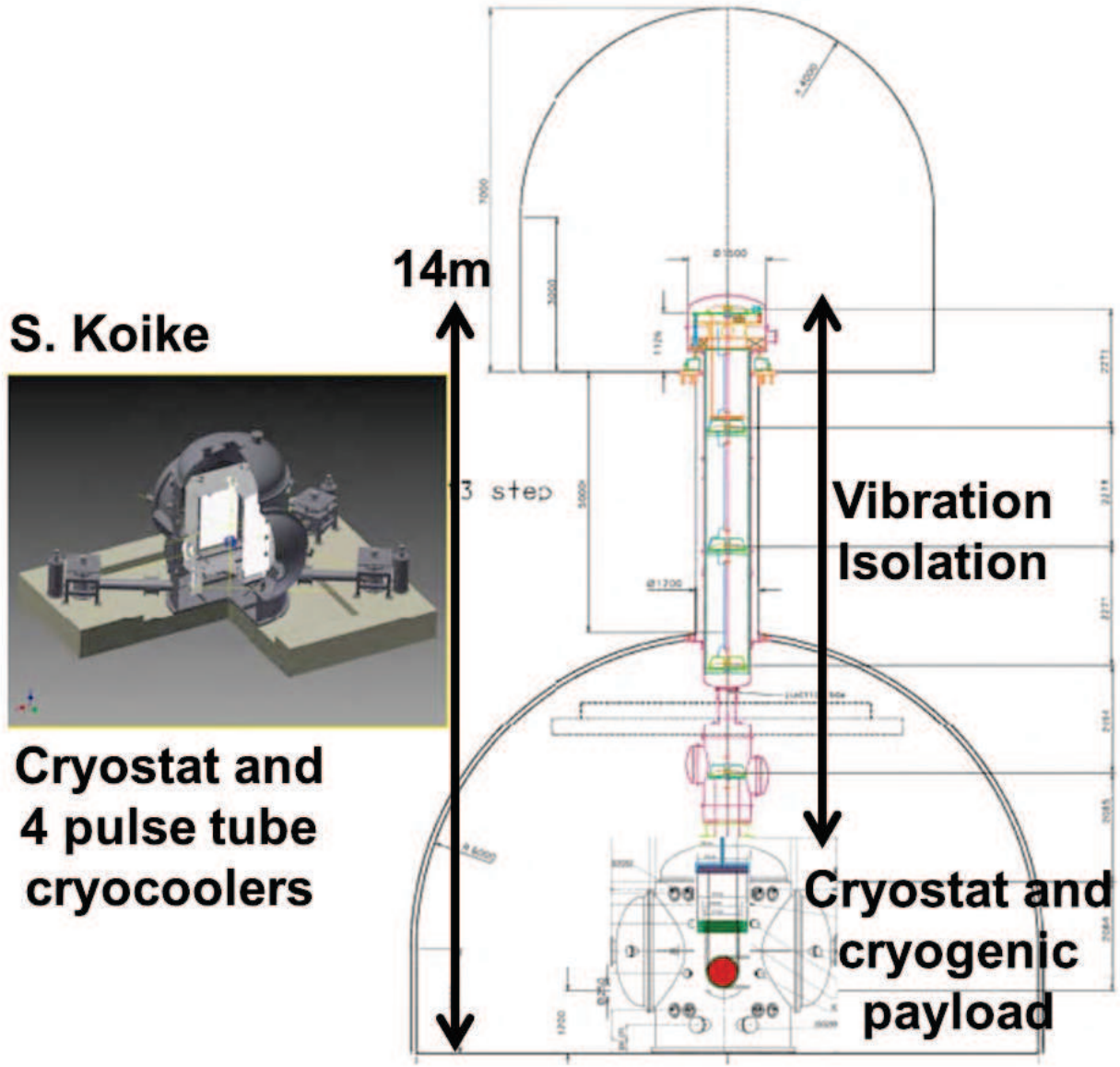

Fig. 8. Cryogenic system consists of a large cryostat with 4 cryocoolers and a cryogenic suspension system.

(GAS) filters and a cryogenic mirror suspension. Other core optics is isolated by Type-B system, which consists of an IP, three stage GAS filters and a mirror suspension. Small opticsis isolated by Type-C system, which consists of three stage stack and a mirror suspension. Schematic view of Type-A/B system is shown in figure 12. The mirror suspensionis called "payload". Type-A test mass is a sapphire mirror of 22 cm in diameter, 15 cm in thickness and 23 kg in weight. Type-B test mass is a silica mirror of 25 cm in diameter, 10 cm in thickness and 10 kg in weight. GAS filters are linked by connection wires each other. The GAS blades and the connection wires are made of maraging steel. The top part is called "pre-isolator" which consists of IP and top filter. The diameter of the top filter is larger than that of standard filter's to reach lower resonant frequencies and to suspend a larger total mass.[1]

Bibliography

[1] R. Takahashi, "Vibration Isolation System for Mirrors", J. Vac. Jpn **54** (2011) 24-27.

Mirror Subsystem[14]

Overview

Definition and scope of the subsystem Mirrors for the main cavities are initially made of silica for iKAGRA and will be changed to sapphire for bKAGRA. The beam splitter and mirrors that will be used in room temperature are all made of silica. The diameter of the mirrors is set to 25 cm in order to suppress the diffraction loss; the size is the same as that of initial LIGO mirrors. As for sapphire mirrors, the diameter is limited to 22 cm because of the size of the sapphire

*[14] Norikatsu Mio, Photon Science Center, University of Tokyo

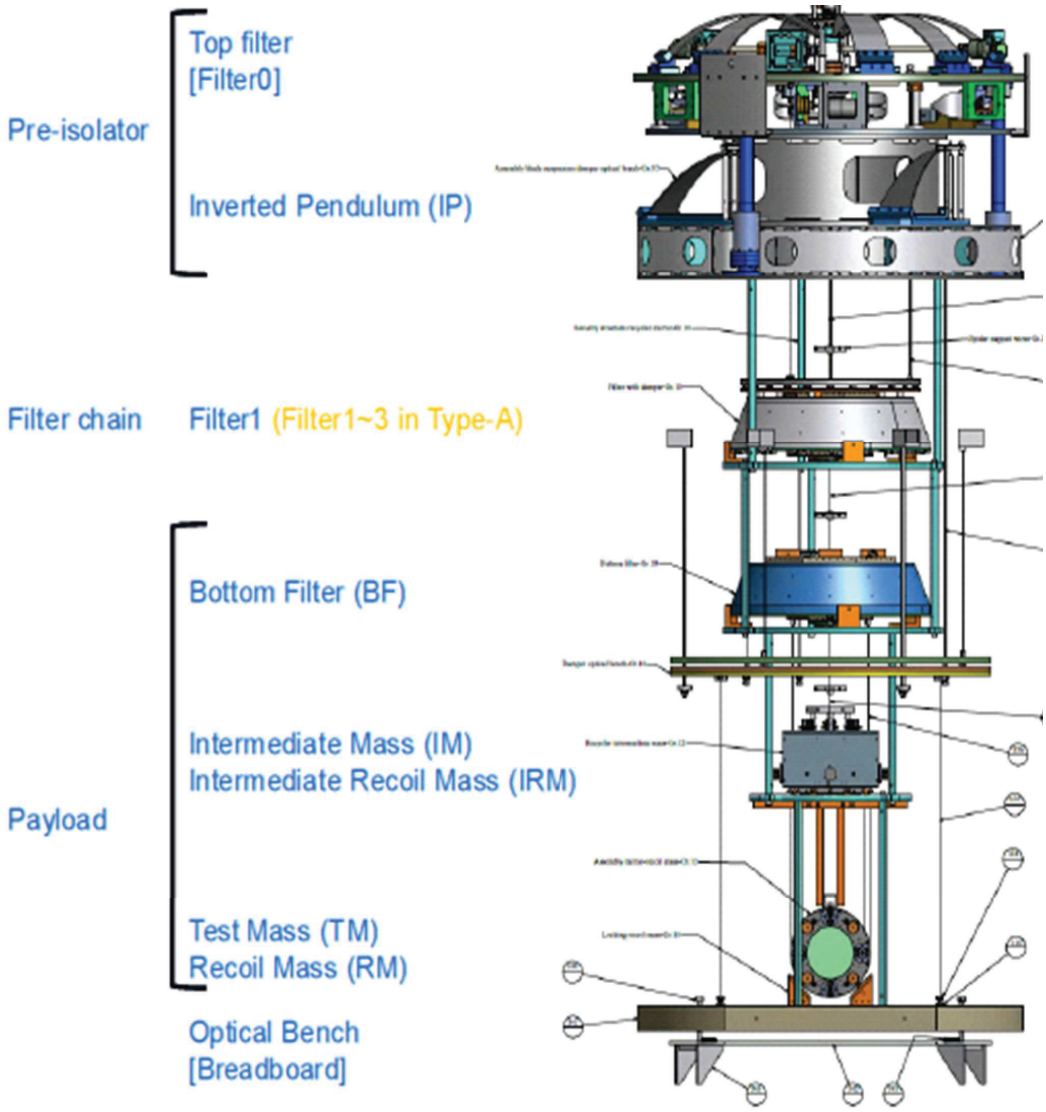

Fig. 12. Schematic view of Type-A/B system. Type-A system has additional two filters (Filter2 and 3). The payload for Type-A system is cryogenic (see Fig. 11).

mono-crystal. The diameter of BS is also the same as that of aLIGO in order to reduce the cost for fabrication. For small mirrors such as mirrors for the mode-matching telescope and the mode cleaner, the diameter is 10 cm.

iKAGRA

Target specification The mirrors for iKAGRA are made of silica with ultra-fine polish and IBS coating in order to realize a small loss of 30 ppm by scattering and 1 ppm absorption. In order to obtain high-interference fringe contrast, the surface figure should be polished with the tolerance of less than 1 nm.

Final design Most of the parameters of each mirror are determined.

bKAGRA

Requirements

Table 2. Requirement on main mirror of bKAGRA

Material for ETMs and ITMs	Sapphire
Coating absorption loss	< 1 ppm
Material absorption loss of Sapphire	< 20 ppm/cm

Preliminary design The basic design of the optics for bKAGRA is the same as that of iKAGRA. The most significant difference is that sapphire is used for the test masses. The absorption of sapphireis 30 ppm/cm. It is not enough for the initial requirements of KAGRA. However, these issues might be solved within a few years. We will be making efforts to realize the requirements.

Laser Subsystem[15]

*15 Norikatsu Mio, Photon Science Center, University of Tokyo

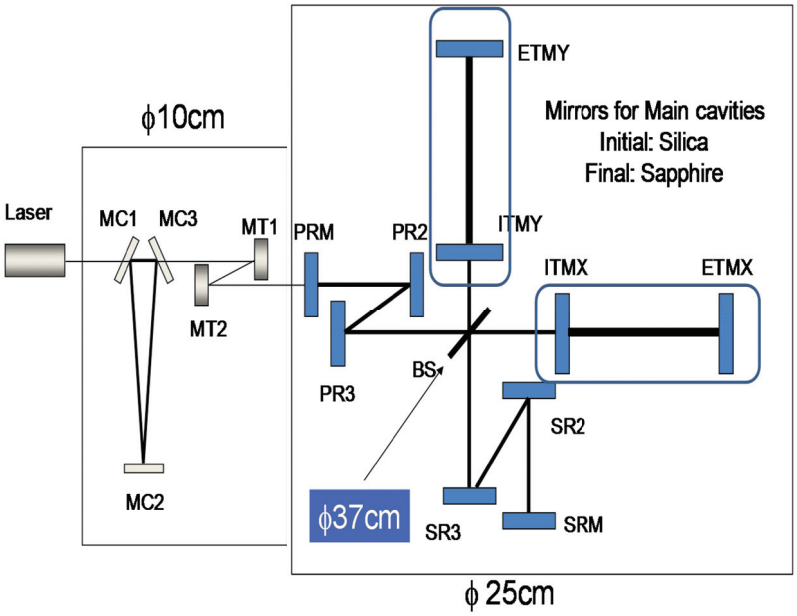

Fig. 13. Mirrors for Main cavities with input & output recyling cavities

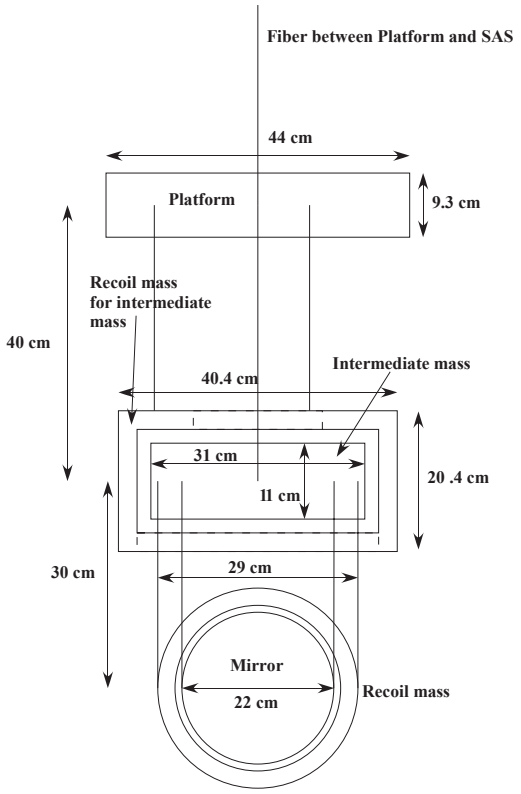

Fig. 11. PRELIMINARY schematic view of cryogenic payload (from optical axis)

Definition and scope of the subsystem The laser subsystem includes laser light sources, power supplies, tillers and peripheral systems such as monitor systems and an interlock system. An optical table on which the laser system will be installed should be prepared as a part of the laser sub system.

iKAGRA

Target specifications The laser system for iKAGRA is almost the same as the laser used in TAMA300 (1064 nm, 10 W) with the stability limited by the NPRO.

Final design A commercially available solid-state laser of 10-W output will be used; its performance is quite satisfactory for the use in iKAGRA.

bKAGRA

Requirements The most sever requirement for the bKAGRA laser is the output power of 180 W with a single-frequency, single-mode, linear polarization.[1] Other requirements are almost the same as those for iKAGRA.

Preliminary design In a preliminary design, a power amplifier is adopted, as shown in Fig. 14. The output of the NPRO is lead to two fiber amplifiers. Two outputs of the amplifiers are coherently added to obtain 80 W output power.[2] The laser light is introduced into three-stage solid-state amplifiers in order to obtain 180 W output power.

Bibliography

[1] K. Takeno, N. Ohmae, N. Mio, T. Shirai, ”Determination of wavefront aberrations using a Fabry-Perot cavity”, OPTICS COMMUNICATIONS **284** (13) (2011) 3197-3201.

[2] N. Ohmae, S. Moriwaki and N. Mio, ”High-efficiency electro-optic amplitude modulation with delayed coherent addition”, Opt. Lett. **36** (2) (2011) 238-240.

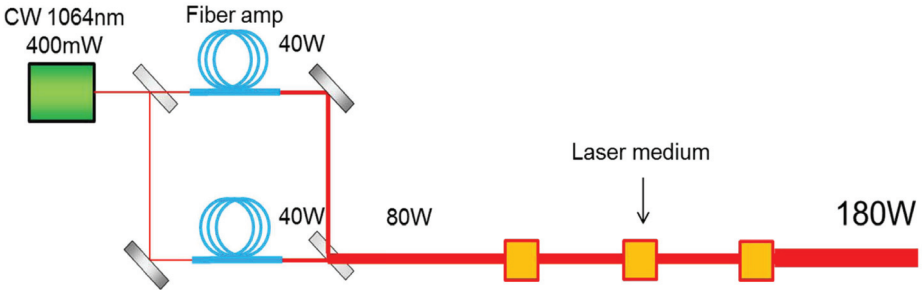

Fig. 14. Laser for KAGRA

Main Interferometer Subsystem[16]

Definition and scope of the subsystem The main interferometer (MIF) is a subsystem which is responsible for converting gravitational waves into electronic signals on a photodetector. It includes two arm cavities, the power recycling cavity and the signal recycling cavity. The MIF subsystem also provides specifications for output mode cleaner, which will be manufactured by the input/output optics subsystem. The MIF team is also responsible for the development of the robust interferometer sensing and control schemes, both for length and alignment. The team will design the necessary electronic circuits, such as PDs, demodulation boards etc. The fabrication of the circuits is supposed to be out of scope of this subsystem, although we may end up doing it. After the mirrors are installed in the vacuum system, the MIF team will be mostly responsible for the commissioning of the interferometer to achieve the target sensitivity as soon as possible.

iKAGRA The minimum goal of iKAGRA is to lock a Fabry-Perot Michelson interferometer. The duty factor and the sensitivity are irrelevant. The design of iKAGRA is set to be a natural pass point to bKAGRA. Details of the design are explained in **JGW-T1200913**, which is found at http://gwdoc.icrr.u-tokyo.ac.jp/cgi-bin/DocDB/DocumentDatabase.

bKAGRA The main goal of the bKAGRA interferometer is to achieve the target sensitivity while keeping the duty factor of the interferometer above 90%.

The optical configuration, parameters and the control scheme for the bKAGRA interferometer have been almost fully determined by Spring, 2012. The design is documented in detail in the KAGRA document **JGW-T1200913**, which is found at http://gwdoc.icrr.u-tokyo.ac.jp/cgi-bin/DocDB/DocumentDatabase.

Figure 15 shows the design of the main interferometer on sideband resonant conditions and signal ports.

Input Output Optics subsystem[17]

Definition and scope of the subsystem Input Output Optics (IOO) subsystem provides the input optics system, located between the laser and the power recycling mirror, and the output optics system. Some parts of the output optics systems are assigned to the Auxiliary Optics Subsystem (AOS). IOO prepares various optical components excluding the core optics and is also in charge of the facility for the laser. Target specification of IOO items for iKAGRA and bKAGRA are shown in following Table 3.

An optical design of input optics system is shown in following Fig. 16. Optics components in front of the mode cleaner are placed on an optical table in the laser room. The mode cleaner, the Faraday isolator and mirrors for the mode matching telescope are placed in vacuum. Frequency stabilization and intensity stabilization of laser beam is performed by the reference cavity, the pre-mode cleaner and the mode cleaner.

Digital Subsystem[18]

Digital Subsystem is in charge of development of a whole real time control system for a km scale interferometer with flexible human interfaces. Digital system is a key system to operate interferometer and all subsystems for control/monitor/diagnostic/tuning (see Fig. 17). This subsystem has following items;

1. Development of real-time (RT) control computer with signal input/output using ADC/DAC modules under RT core software. Each RT computer has real-time communication network interfaces for control, synchronization, and data transfer.

2. Development of client workstations including monitor/diagnosis software.

3. Network design and development for a reflective memory based real time control network, timing network for synchronization all RT computers, 10 GigaByte Ethernet (GE) data acquisition (DAQ) network, and 1GE general network including EPICS control.

4. Producing frame data for data storage/analysis.

We started a prototype test for single RT PC at CLIO from 2009. The channel numbers was not so many, but we tested important basic functions for IFO operation like lock acquisition, calibration, noise performance check. Then we decided

*16 Yoichi Aso, Department of Physics, University of Tokyo
*17 Souichi Telada, Metrology, AIST
*18 Osamu Miyakawa, ICRR, University of Tokyo

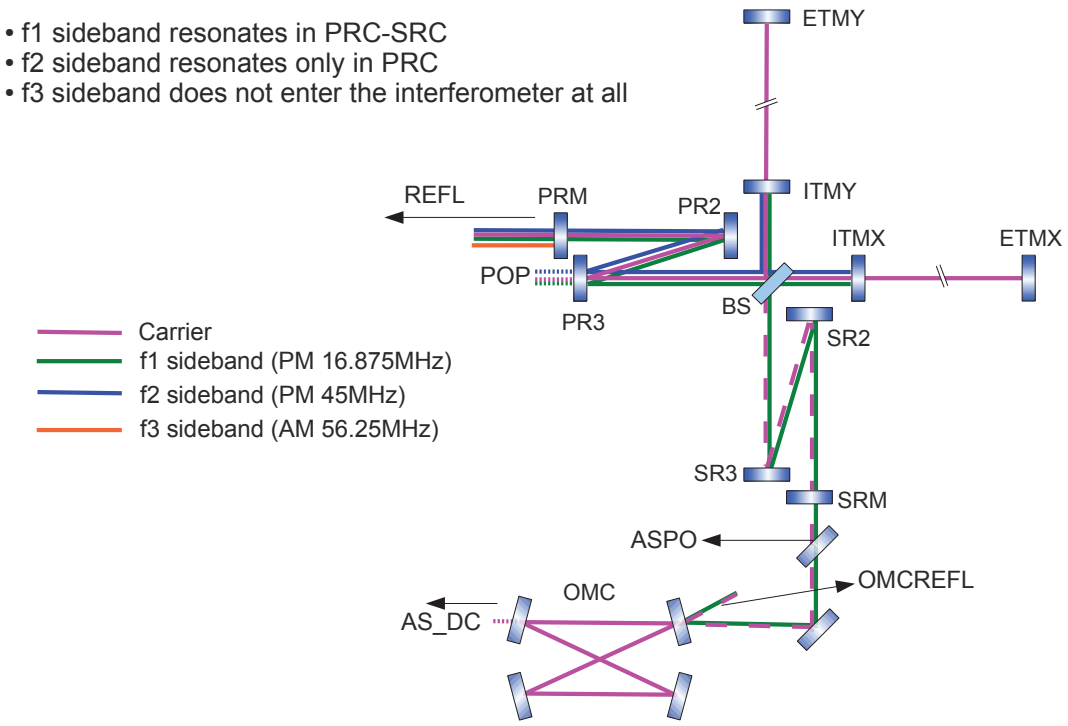

Fig. 15. Sideband resonant conditions and signal ports in bKAGRA interferometer design.

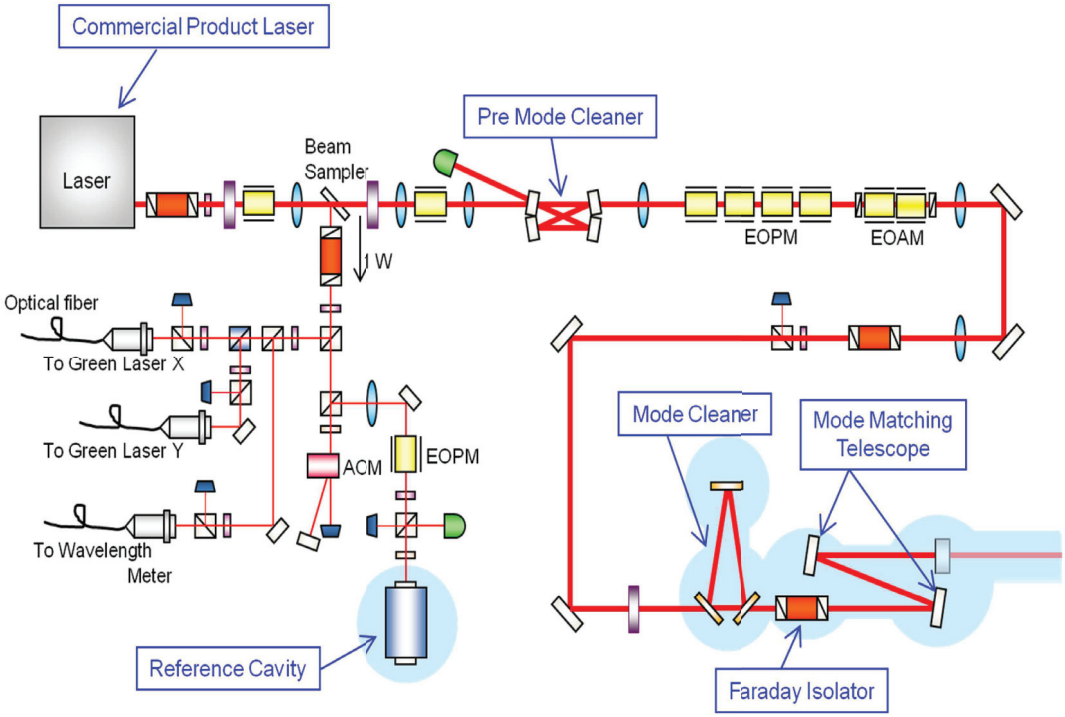

Fig. 16. Optical design of input optics system.

Table 3. Specifications of parts supplied by IOO.

Item	Specification
Total throughput to Interferometer	throughput ¡ 50 %
Pre Mode Cleaner	FSR = 154 MHz Cutoff frequency = 495 kHz FSR = 1.5 GHz
Reference Cavity	Finesse = 30000 Input laser power = 100 mW
Mode Cleaner	FSR = 5.625 MHz Finesse = 500 Throughput> 80 %
Isolator in Vacuum	Isolation ratio *LT* 30 dB Throughput> 95 % (only Faraday rotator) Aperture > 20 mm
Mode Matching Telescope	ROC (MMT1) = -17.628 m ROC (MMT2) = 23.924 m Distance b/w MC waist and MMT1 = 7.625 m Distance b/w MMT1 and MMT2 = 3.820 m Distance b/w MMT2 and recycling mirror = 4.243 m
Green Laser	Frequency Stability = 56 mHz (RMS) Finesse of arm cavity = 19 Input points = behind of PR2 and of SR2
Output Mode Cleaner (for bKAGRA)	FSR = 27.4 MHz Finesse = 785.4 Loss < 2 %
Output Mode Matching Telescope (for bKAGRA)	Distance b/w SRM and OMMT1 = 6.5 m Distance b/w OMMT1 and OMMT2 = 6.2 m Distance b/w OMMT2 and input mirror of OMC = 6.266 m
Output Faraday Isolator (for bKAGRA)	Isolation ratio > 30 dB Throughput > 98 % Aperture > 20 mm

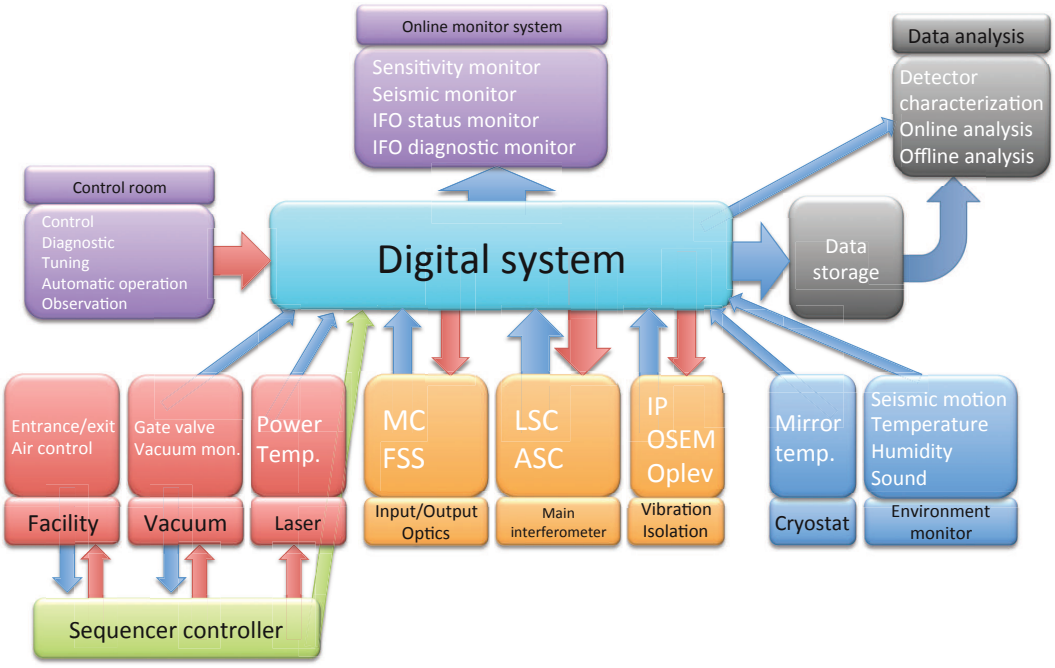

Fig. 17. Interferometer is controlled by digital system.

to deliver standalone(STDA) systems for development subsystem with a digital control. This STDA system is based on experiences at CLIO prototype test. By the end of FY2011 we distributed two STDA systems. One is to data analysis group for testing frame data and data analysis software, and another one is to vibration isolation subsystem for controlling a Pre-Isolator (see Fig. 18). We are preparing another STDA system for monitoring temperatures in a cryostat.

In parallel with delivering STDA system, we tested a network connection using 2 or 3 RT control computers in FY2011. Real time control using a single computer is not so difficult, but when two or more computers are connected, real time control will be much more difficult due to network bandwidth, latency, synchronization etc. This setup will be extended to a large scale network system in FY2012 with 7-10 server PCs and 5 RT PCs for an important test as a full network operation with enough network bandwidth, latency and redundancy. This large scale test will be performed on the new floor of Hokubu-Kaikan at Kamioka (currently remodeling). This Large network system will be moved and installed into mine directly and it will be an actual full system for commissioning.

Data Analysis Subsystem[19]

Definition and scope of the subsystem Coordination of "Data Analysis Subsystem (DAS)" covers the acquisition, the storage and the management of observational data. The outline of this subsystem is illustrated in Fig. 19. The architecture, tasks and services of the subsystem consist of following:

1. Data transfer and storage
2. Calibration
3. Pipeline for analyzing the data
4. Software/hardware environment for data analysis
5. Physics, astrophysics and astronomical outcomes
6. Cooperation with other experiments (GW and non-GW)

iKAGRA

Target specifications The target specifications of DAS at iKAGRA stage are as follows.

- Generation of the pre-processed data which include
  - the transfer function necessary for the calibration
  - the information of the detector characterization (e.g. quality flag of data)
- Pre-process servers, data transfer system and the data storage system (about 500 TByte)
- Off-line data analysis of the event search.

*19 Nobuyuki Kanda, Department of Physics, Osaka City University

Table 5. Specification of geophysics interferometer.

Item	Specification
Strain sensitivity	3×10^{-13}
Baseline length	1500 m
Vacuum pressure	1×10^{-4} Pa
The number of GIF	2

Final design DAS sub-system introduce two preprocess servers at Kamioka facility. One is for the data acquisition and the data transfer, and the other is for the detector characterization and backup of the 1st system. The rate of data produced by KAGRA is about 70 GB/hour. For the one month science mode observation of iKAGRA, 50 TB of data are produced. Beside those science mode data, data are produced during the commissioning phase. For the detector characterization and the commissioning, we want to store the several months of data at the detector's site and the main storage system. For this purpose, three data storage systems will be introduced. Two systems are introduced to the above pre-process servers and each has 200 TB. The 3rd system is the master data storage system with storage size of 500 TB and is introduced at ICRR-Kashiwa. The 3rd system is used for the off-line data analysis and the data archive.

bKAGRA

Requirements For iKAGRA observation, DAS sub-system will have to provide the continuous and stable data acquisition, storage and pipelines for gravitational wave event searches. Raw data rate is estimated about 70 GB/hour. Network transfer and the pre-process server throughput must be faster than this. Main data storage will be placed at ICRR-Kashiwa. Roughly 1PByte/year is need for the storage of KAGRA experimental data only (more than 600TByte raw data + simulation data * effective duty time of the operation * mirroring). International data sharing (5sites = KAGRA + LIGO*2 +Virgo + "fifth-site") will reach to 5PB/year.

Preliminary design The requirement specifications are shown in Table—4 below.

Geophysics Interferometer (GIF)[20]

GIF subgroup is in charge of constructing two fixed-mirror interferometers (1.5km$\times$2) along KAGRA. These interferometers monitor deformation of the ground for the purpose of geophysical observations as well as baseline correction data for KAGRA. This subgroup is also responsible for arrangement of sensors and benchmarks for monitoring environment parameters of the tunnel, rooms, and instruments. An overall view is shown in Fig. 20. Red lines indicate baselines of GIF. Target specifications of GIF are shown below.

Optical design of GIF is shown in Fig. 21. The interferometer is an asymmetric Michelson interferometer with two retroreflectors. An iodine-stabilized 532-nm Nd:YAG laser is used as a light source. A 5-m input baseline and ϕ400 mm

*20 Akito Araya, Earthquake Research Institute, University of Tokyo

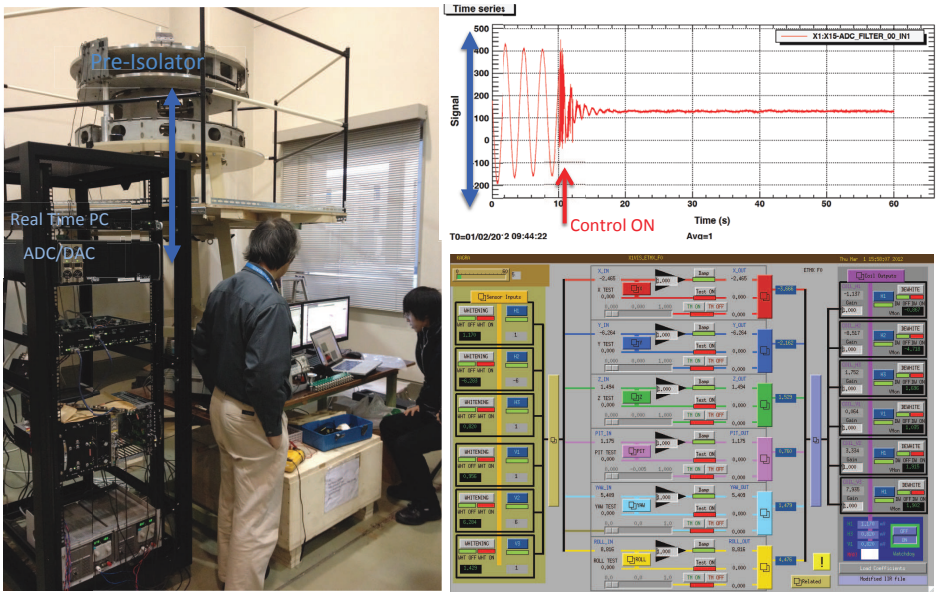

Fig. 18. STDA system distributed to Vibration Isolation subsystem

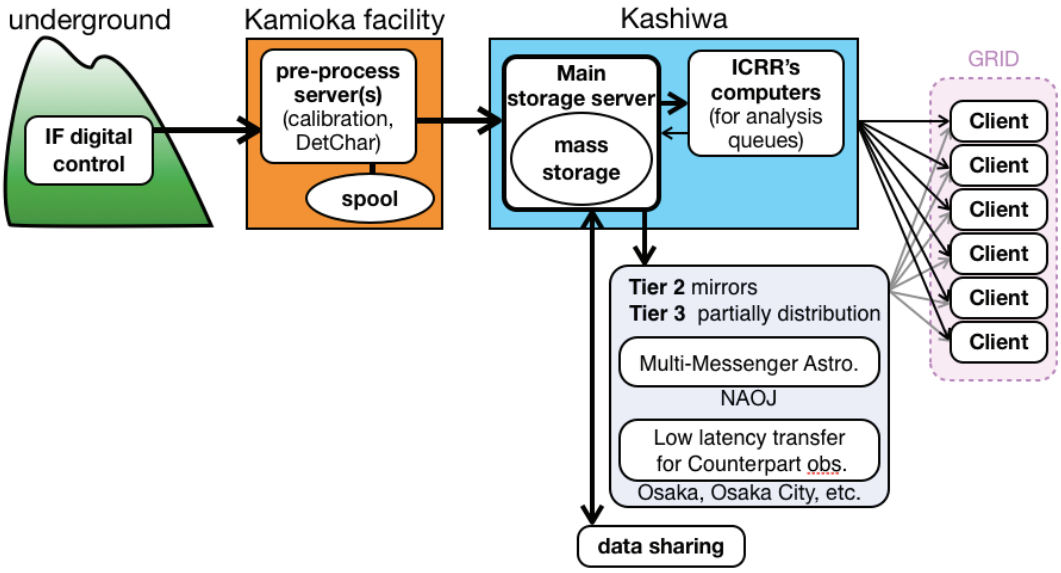

Fig. 19. Schematic outline of the Data Analysis Subsystem

Table 4. Specsifications in Preliminary Design. Items in parentheses are for iKAGRA.

	item	requrements
	Network and Pre-process throughput	70 GB/hour
Storage	two weeks safety spool	25 TB
	on site study	(500 TB)
	KAGRA own	5 PB for 5 years
	Data Sharing	30 PB for 5 years
Calculation costs for GW searches	Compact Binary	a few several Tflops
	Burst	1 Tflops
	Continuous	1 Tflops
	Stochastic	$<$ 1 Tflops
Software	Search pipeline	(need development, migration from LV, GRID system)
	Environment	

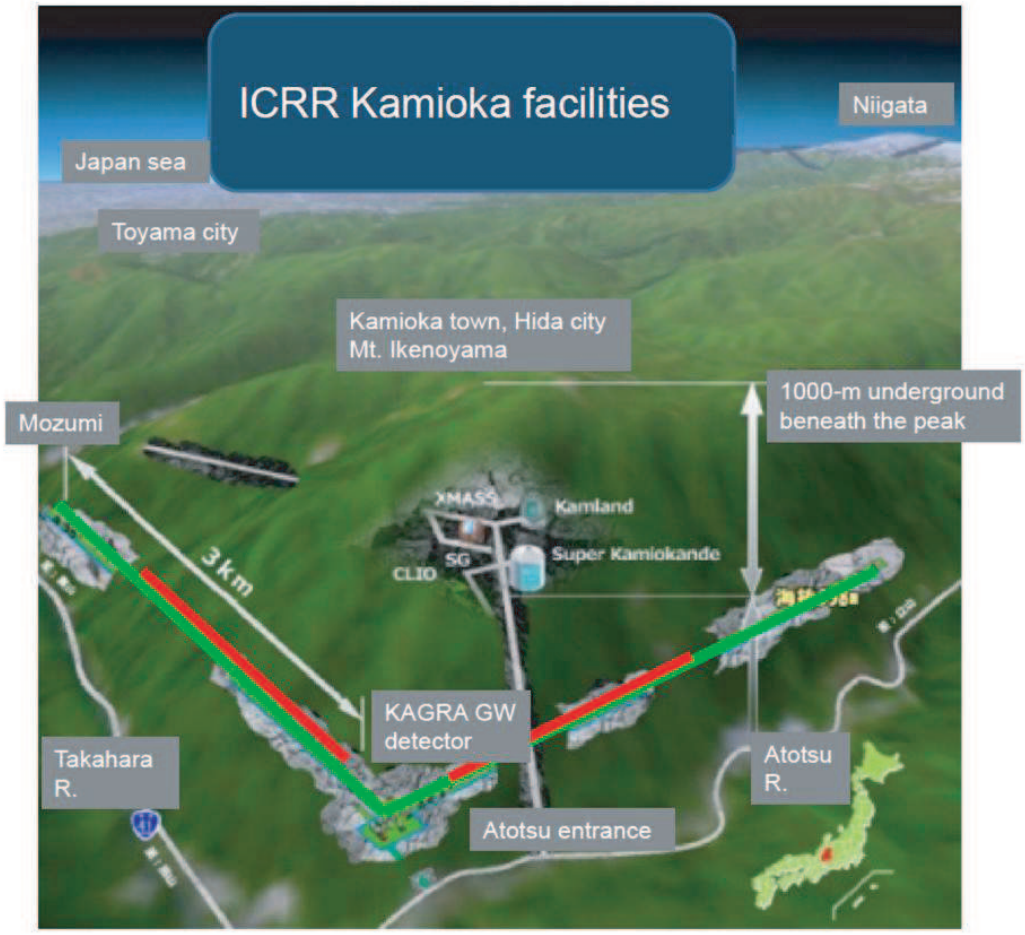

Fig. 20. An overall view of KAGRA. Red lines indicate baselines of GIF.

vacuum tubes are required. The principle and the optical design are based on the current 100-m IFO system, operating at the CLIO site (Kamioka).

Environment condition of the tunnel, rooms, and instruments need to be monitored for ensuring stable operation of detectors, correction of data analyses, and detection of anomalous operation. Figure 22 shows arrangement of some of EM sensors.

CLIO Project

[Spokesperson : Masatake Ohashi]
ICRR, Univ. of Tokyo, Kashiwa, Chiba 277-8582
In collaboration with members of: KEK, Tsukuba; Kyoto-U, Kyoto; ERI of UT, Tokyo

Overview of CLIO

CLIO (Cryogenic Laser Interferometer Observatory) is a 100 m-baseline underground cryogenic interferometer at the Kamioka Mine. CLIO forms a bridge connecting the CLIK (7 m prototype cryogenic interferometer at Kashiwa campus) and the KAGRA (3 km cryogenic interferometer at Kamioka). The site of CLIO, near the Super-Kamiokande neutrino detector, is shown in Fig. 23. The tunnel was dug in 2002, and a strain meter for geophysics was installed in 2003 [1]. The construction of CLIO began in late 2003, and installation of the mode cleaner vacuum system was reported in the annual report (2003–2004). Four sets of cryostats and whole vacuum system were installed (annual report 2004–2005). We started the operation of CLIO in 2006 (annual report 2006).

Fig. 24. Overview of the CLIO interferometer.

The prime purpose of CLIO is to demonstrate mirror thermal noise reduction with cryogenic mirrors. We achieved the

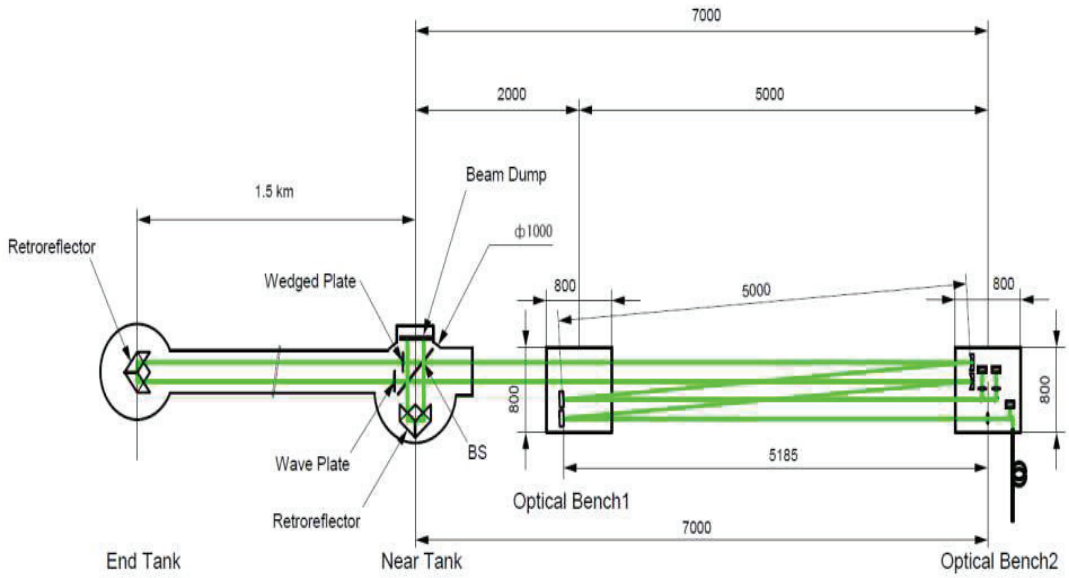

Fig. 21. Optical design of GIF.

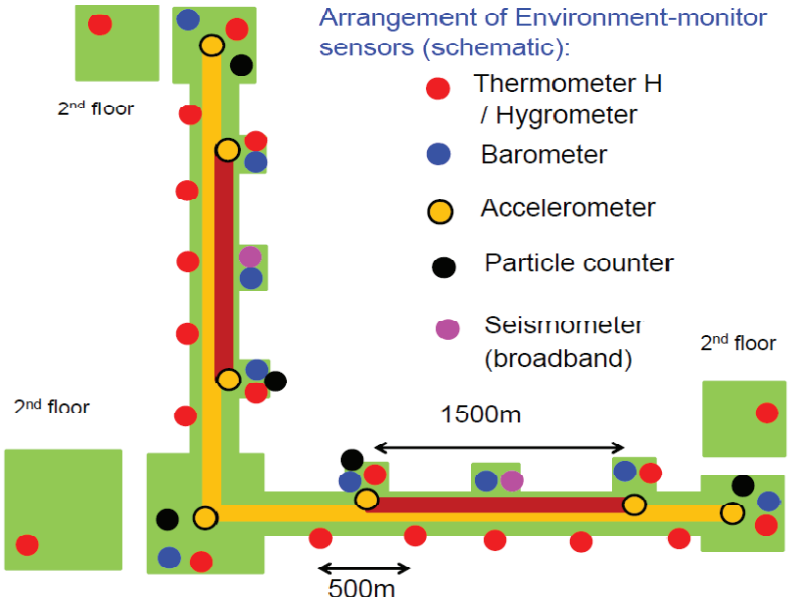

Fig. 22. Arrangement of some of EM sensors.

design sensitivity at the room temperature after noise hunting taken in 2008 (Annual report 2008) [2, 3]. After then, we started out cooling the mirrors and noise hunting with the mirrors under 20K had been done. We firstly observed the sensitivity improvement due to the mirror thermal noise reduction.

CLIO sensitivity curve with cooled mirrors (cryogenic sensitivity) and without cooling (300K sensitivity) are shown in Fig. 26 with estimation curves of the mirror thermal noise. The 300K sensitivity and the cryogenic sensitivity were measured at 2008/11/5 and at 2010/03/20, respectively. When the cryogenic sensitivity was measured, two front mirrors were cooled and the rest of two end mirrors were at the room temperature. Temperature of the front mirrors were 17K and 18K. Modifications possibly affecting the sensitivity at the cryogenic sensitivity measurement are exchange of final suspension wires and addition of heat link wires to the suspension systems. Cooling the mirror took about 250 hours and vacuum pressure was better than 10^{-4}Pa for both sensitivity measurements.

The noise floor level of the cryogenic sensitivity from 90Hz to 240Hz is below the 300K sensitivity. Observation range for GWs from neutron star binary coalescence was also improved to 159kpc from 148kpc for the optimum direction. This is the first observation of sensitivity improvement by the cryogenic mirrors. The noise floor at 165Hz was reduced to $2.2 \times 10^{-19}\,\mathrm{m}/\sqrt{\mathrm{Hz}}$ from $3.1 \times 10^{-19}\,\mathrm{m}/\sqrt{\mathrm{Hz}}$ after cooling

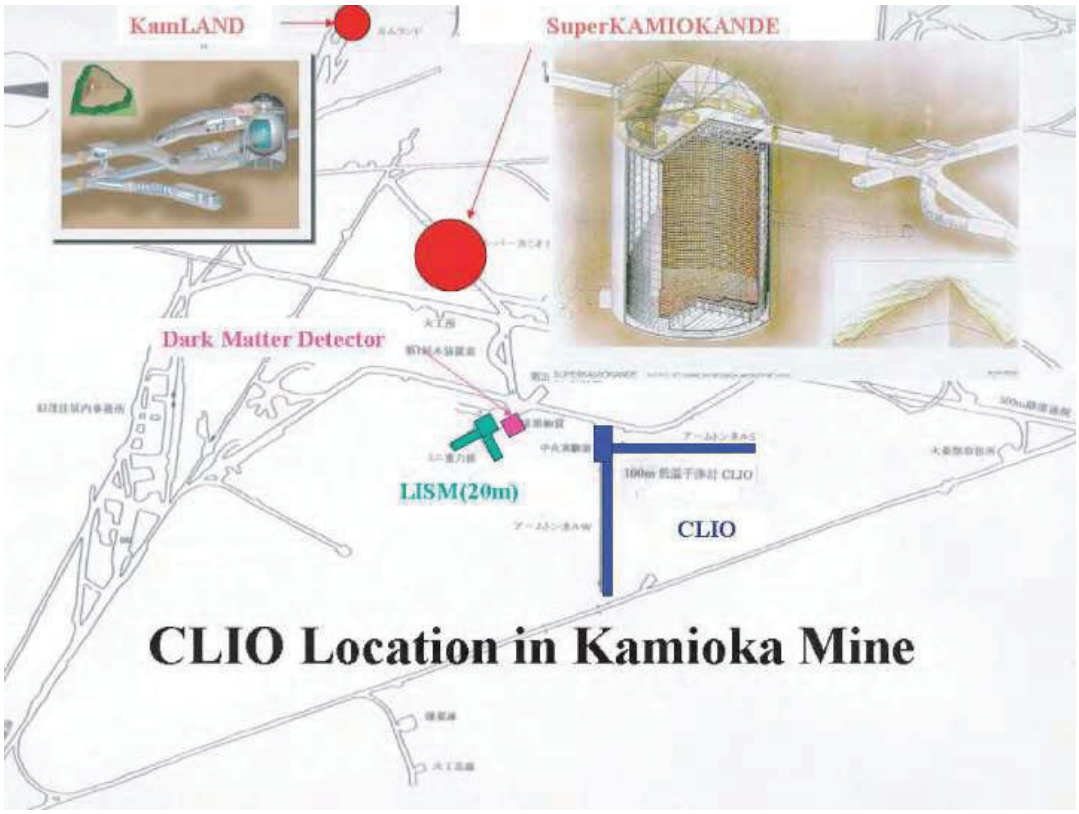

Fig. 23. Location of the CLIO interferometer.

the front mirrors. Amount of this noise floor reduction is consistent with the estimation of mirror thermal noise reduction due to cooling. This achievement has been published in 2012 [4].

Fig. 25. A sapphire mirror and cryogenic suspension system

MC Locking Demonstration Using NQD method

We tried to demonstrate the Mode Cleaner lock acquisition using NQD method [5]. CLIO has two RF sidebands, one is 11.97 MHz for the Mode Cleaner (MC) control and 15.804MHz(f_1) for 100m-FP arm cavity control. To obtain the NQD signal for MC whose FSR was same with f_1, we shifted the RF sideband frequency f_1 to 15.844MHz(f_2) by 40kHz (in other words, $f_2 = FSR + 40\text{kHz}$), and we used f_2 as a demodulation frequency. In this manner, we could obtain the beat signal of 40kHz between the f_2 sideband and the laser frequency.

We verified that the expected NQD signals could be obtained and also succeeded to lock the MC using the NQD signal. Because of small offset in the error signals, the offset locking was sometimes observed. In addition to this, we also compared the lock acquisition under the condition that the PDH signal [6]had beating wave forms because of the MC end mirror swing motion that was driven by additional force. We obtained preliminary results that lock acquisition success rate by NQD signals was much higher that that by the normal PDH signals. However, we should note that this time MC control loop that had 300kHz UGF helped a lot for the successful lock acquisition rate.

Bibliography

[1] S. Takemoto, *et al.*, Journal of Geodynamics **41** (2006) 23.

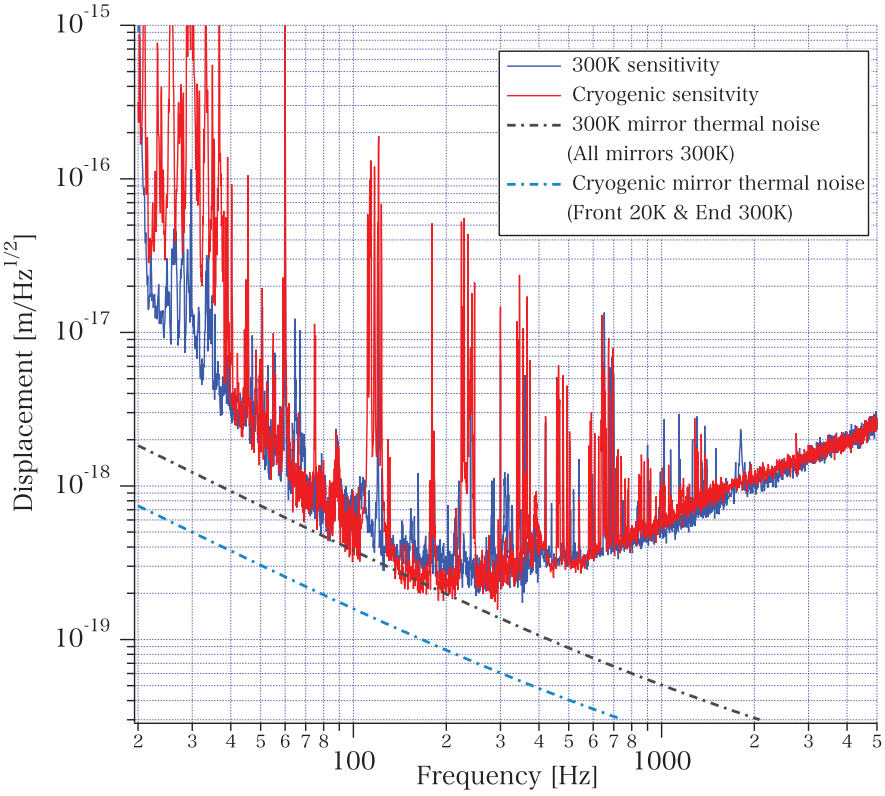

Fig. 26. Comparison of CLIO sensitivity curves. 300K sensitivity (solid blue line) and Cryogenic sensitivity (solid red line) show CLIO sensitivity curves without cooling mirrors measured at 2008/11/05 and with front mirrors under 20K measured at 2010/03/20, respectively. 300K mirror thermal noise (dot dash gray line) and Cryogenic mirror thermal noise (dot dash blue line) show estimation curve of mirror thermal noise corresponding to the each sensitivity measurements.

[2] S. Miyoki, *et al.*, Journal of Physics: Conference Series **203** (2010) 012075.

[3] T. Uchiyama and S. Miyoki, "Experimental Demonstration of Cryogenic Mirror Technique - Achievements of CLIO-", J. Cryo. Super. Soc. Jpn., **46** (2011) 392-399.

[4] Takashi Uchiyama, Shinji Miyoki, Souichi Telada, Kazuhiro Yamamoto, Masatake Ohashi, Kazuhiro Agatsuma, Koji Arai, Masa-Katsu Fujimoto, Tomiyoshi Haruyama, Seiji Kawamura, Osamu Miyakawa, Naoko Ohishi, Takanori Saito, Takakazu Shintomi, Toshikazu Suzuki, Ryutaro Takahashi, Daisuke Tatsumi, "Reduction of thermal fluctuations in a cryogenic laser interferometric gravitational wave detector", Phys. Rev. Lett. **108**, 141101 (2012) [5 pages].

[5] S. Miyoki, S.Telada and T.Uchiyama, "Expansion of linear range of Pound-Drever-Hall signal", Applied Optics, Vol. 49, Issue 28, pp.5217-5225 (2010) .

[6] R. W. P. Drever, *et al.*, Appl. Phys. B **31** (1983) 97-105.

R&D of Gravity Gradiometer[21]

Overview

We have been conducting R&Ds for detection of gravitational waves for long time. During the course of these R&Ds, many useful techniques have been developed and if these techniques were applied to industry or daily life, their usefullness is widely recognized, which might lead to successful funding to assist the large project. One year before when LCGT (KAGRA, now) was partially funded in 2010, R&D research of developing a gravity gradiometer (GG-meter) had been funded in Grants-in-Aid for Scientific Research under the JSPS program. The objective of this research is to develop GG-meter that can be applied in airborne survey for underground resources or potentially dangerous faults. Although the proposal of GG-meter itself is not new using laser interferometry, any practical apparatus does not exist. We raised an objective of achieving one order improvement or more in the sensitivity attained by the GG-meter like La-Coste Romberg type one, which is roughly 50 μGal (5×10^{-7} 1/s^2 by 1 m vertical displacement. If this objective is achieved, more efficient gravity survey of resources accumulated underground or under deep sea can be available and also utilized to clarify hidden faults that may cause serious disaster at huge earthquake that may hit Kanto or Tokai area, quite soon.[1]

Principle and Apparatus of GG-meter

The limit of the present GG-meter arose from the difficulty of measuring the accelerometer of a carrier with high sensitivity. Because the output of the GG-meter is not correct,without precise value of the carrier acceleration. In order to escape from the error of measuring acceleration of the carrier, we

*21 Kazuaki Kuroda, ICRR, University of Tokyo

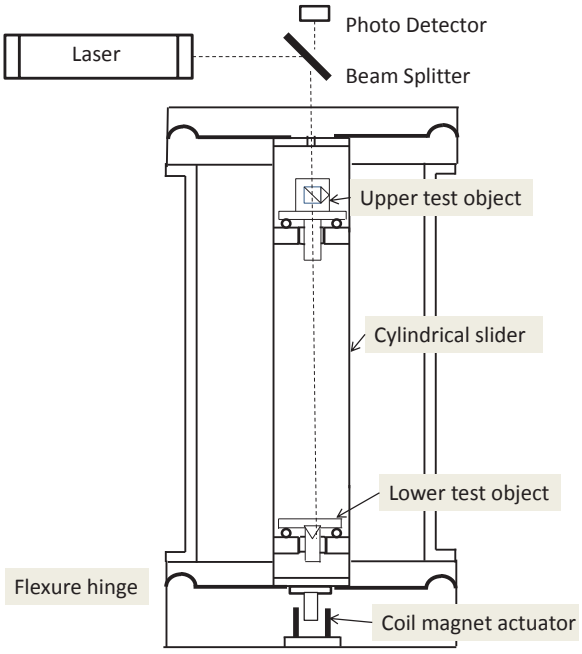

Fig. 27. Freely falling test objects of a Michelson interferometer are set on bases. One part (upper test object) houses the beam-splitter (BS) and a corner cube prism (CCP) and the other part (lower test object) has another CCP. During the course of drop, the magnitude difference of gravity causes the difference between both speeds, which creates a beat frequency of the interference signal at the BS output port.

Fig. 28. Photo view of the GG-meter prototype, developed in ICRR.

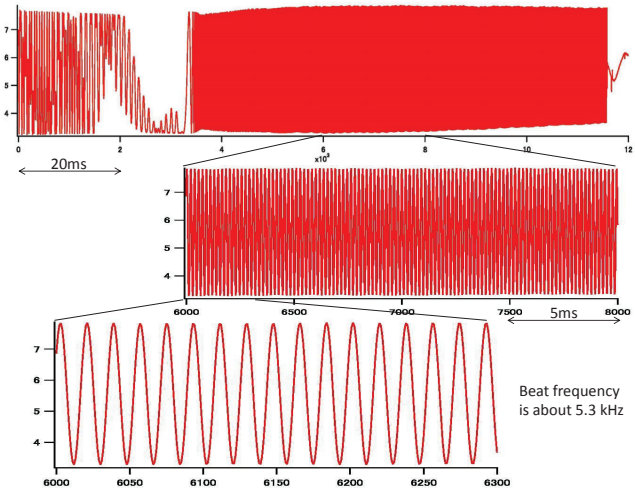

Fig. 29. Output optical fringes in time from the falling interferometer. Sampling rate is 10 μs and the number represents the sampled number. Upper most figure shows the whole optical fringes and the middle one expands the region from 60 ms to 80 ms. The bottom one shows the data of 3 ms beginning at 60 ms. The effect of throwing machine appears in the beginning of the whole data by higher frequency vibrations. Release occurs at around 35 ms. The beat frequency is roughly 5.3 kHz.

contrived a new scheme of measuring the gravity gradient using a free fall interferometer partially shown in Fig. 27. This is a part of a simple Michelson interferometer, test objects of which freely fall due to gravity. One part (upper test object) houses the beam-splitter (BS) and a corner cube prism (CCP) and the other part (lower test objects) has another CCP. During the course of drop, the magnitude difference of gravity causes the difference between both speeds, which creates a beat frequency of the interference signal at the BS output port. Since the arm lengths of the interferometer are different, the laser source should be a frequency stabilized laser. Two parts are mounted on similar bases of kinematic support displaced vertically and the cylinder connecting those bases is vertically driven by the magnet coil actuator attached underneath the cylinder, which forms a throwing mechanism.

This mechanism is housed in a vacuum chamber in Fig. 28. A turbo molecular pump evacuates the chamber and a laser optical system is mounted on a table at the top of the chamber. The vacuum pressure is about 2×10^{-5} Pa, which is enough to attain the objective.

Result and Scope

We have succeeded to throw two parts in vacuum with negligible angular rotations, which made acquiring interference signal possible as shown in Fig. 29. The total time of the flight is about 110 ms, and the maximum vertical displacement is about 15 mm. Comparing with existing freefall-type absolute gravity meter, this height might be regarded too small to be compatible with the desired resolution. This is not correct. Since computer ability collecting fast and extensive data has improved, longer height is not be needed any more in our GG-meter. We have confirmed to attain μGal level sensitivity using this rather short optical fringes by numerical simulation (in preparation for publication). Here, we show its real spectrum analyzed by "Octave" software (Fig. 30. Since the resolution of this acceleration is not high, this spectrum is used only to check the working soundness of GG-meter.

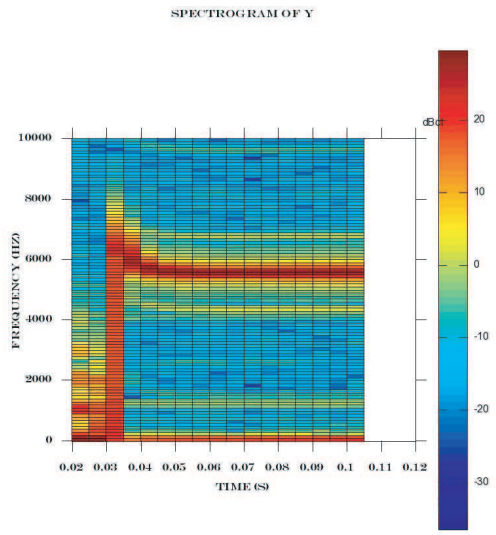

Fig. 30. Time series of data in Fig. 29 is processed by FFT. The frequency resolution of this FFT is not quite enough to discuss about the sensitivity. Initial stage of release might be affected by some force arising from electric charge. Because there is a non-linear change even after the release point (35 ms). After many trials of release, non-linear curve of the spectrum was observed in the whole region in another trial of data taking.

Test objects are made of machinable ceramic for preventing the magnetically induced current. The kinematic support is realized by symmetrical three grooves made on the attaching surface of the parts. By using this prototype machine, we have found the following problems to be solved for practical usage of this type GG-meter.

1. scratched break of grooves for kinematical support due to mechanical impact at touching
2. electrical charge produced by repeated measurements that produces false acceleration
3. lack of real-time data analysis software

All these problems are not fatal but need to be solved for practical application. Solutions against above problems are now being investigated and will be published, soon.

The prototype system developed in ICRR will be moved to Aso Volcanological Laboratory, Institute for Geothermal Sciences, Graduate School of Science, Kyoto University for monitoring the movement of volcano magma. Including above problems, problems arising from measurements of magma in practice will be surveyed and studied in near future.

Bibliography

[1] S. Shiomi, ”Development of a carrier-based gravity gradiometer”, Jpn. Geoscience Union Meeting, 23rd, May, 2011. Makuhari Messe.

[2] S. Shiomi, ”Development of a free-fall gravity gradiometer (III)”, Jpn. Phys. Soc. Meeting, 17th, September (2011), Hirosaki University.

Gravitational wave project office[22]

Gravitational wave project office was established at the beginning of the financial year of 2011 to assist the construction of KAGRA[23] project. The organization of this office is illustrated in Fig. 31. Main office is set in Kashiwa campus and its Kamioka branch is in Kamioka. It is an internal organization placed in Astrophysics and Gravity Division of ICRR.

KAGRA project is hosted by ICRR, which means the funding comes through University of Tokyo and all procurements are controlled by ICRR. However, the number of researchers working for KAGRA construction belonging to other organizations is larger than staffs belong to ICRR. Therefore, three collaboration members of KEK are recruited as guest researchers and two research staffs are temporarily shifted to ICRR. Besides these staffs, there are many other collaboration members who belong to other organizations.

The role of this office is to support execution of KAGRA project by ICRR staffs with these collaboration members. Main works are

- finance planning
- management of collaboration
- support for execution of KAGRA
- coordination of collaboration meetings
- support for research
- support for education of graduate students
- bridge collaboration members and ICRR administration office
- others

*22 Kazuaki Kuroda, ICRR, University of Tokyo
*23 nicknamed in January, 2012 by public contribution for LCGT

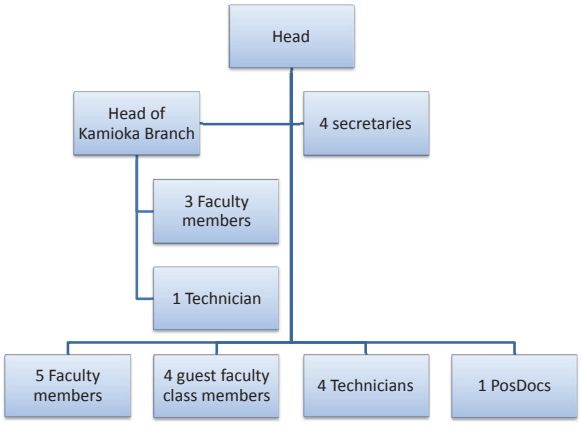

Fig. 31. Gravitational wave project office is an internal organization created in Astrophysics and Gravity Division of ICRR. The main objective of this office is to help the execution of KAGRA project

Observational Cosmology Group

[Spokesperson : Masami Ouchi]

ICRR, The University of Tokyo, Kashiwa, Chiba 277-8582

Demographics of Lyman-Alpha Emission in $z \sim 7$ Galaxies

In collaboration with the members of The University of Tokyo, IPMU, University of California Riverside, National Optical Astronomical Observatories, University of Arizona, California Institute of Technology, National Astronomical Observatory of Japan, and University of California Berkeley.

We have carried out ultra-deep Keck/DEIMOS spectroscopy for z-dropout galaxies in the SDF and GOODS-N. For 3 out of 11 objects, we detect an emission line at $\sim 1\mu$m with a signal-to-noise ratio of ~ 10. The lines show asymmetric profiles with high weighted skewness values, consistent with being Lyα, yielding redshifts of $z = 7.213$, 6.965, and 6.844 (Figs. 1-2). Specifically, we confirm the $z = 7.213$ object in two independent DEIMOS runs with different spectroscopic configurations. The $z = 6.965$ object is a known Lyα emitter, IOK-1, for which our improved spectrum at a higher resolution yields a robust skewness measurement. The three z-dropouts have Lyα fluxes of 3×10^{-17} erg s^{-1} cm^{-2} and rest-frame equivalent widths $\mathrm{EW}_0^{\mathrm{Ly}\alpha} = 33 - 43$Å. Based on the largest spectroscopic sample of 43 z-dropouts that is the combination of our and previous data, we find that the fraction of Lyα-emitting galaxies ($\mathrm{EW}_0^{\mathrm{Ly}\alpha} > 25$Å) is low at $z \sim 7$; 17 ± 10% and 24 ± 12% for bright ($M_{\mathrm{UV}} \simeq -21$) and faint ($M_{\mathrm{UV}} \simeq -19.5$) galaxies, respectively. The fractions of Lyα-emitting galaxies drop from $z \sim 6$ to 7 and the amplitude of the drop is larger for faint galaxies than for bright galaxies (Fig. 3). These two pieces of evidence would indicate that the neutral hydrogen fraction of the IGM increases from $z \sim 6$ to 7, and that the reionization proceeds from high- to low-density environments, as suggested by an inside-out reionization model.

Bibliography

[1] Ono, Y., et al. 2012, Astrophys. J., 744, 83

Average Metallicity and SFR of LAEs probed by a Triple NB Survey

In collaboration with the members of The University of Tokyo, IPMU, Observatories of the Carnegie Institution of Washington, National Taiwan Normal University, University of California Los Angeles, Space Telescope Science Institute, University of Wyoming, Indiana University, Siena College, and University of Nottingham.

We have obtained the average metallicity and star-formation rate of Lyα emitters (LAEs) measured from our large-area survey with three narrow-band (NB) filters covering the Lyα, [O II]λ3727, and Hα+[N II] lines of LAEs at $z = 2.2$. We select 919 $z = 2.2$ LAEs from Subaru/Suprime-Cam NB data in conjunction with Magellan/IMACS spectroscopy. Of these LAEs, 561 and 105 are observed with KPNO/NEWFIRM near-infrared NB filters whose central wavelengths are matched to redshifted [O II] and Hα nebular lines, respectively. By stacking the near-infrared images of the LAEs, we successfully obtain average nebular-line fluxes of LAEs, the majority of which are too faint to

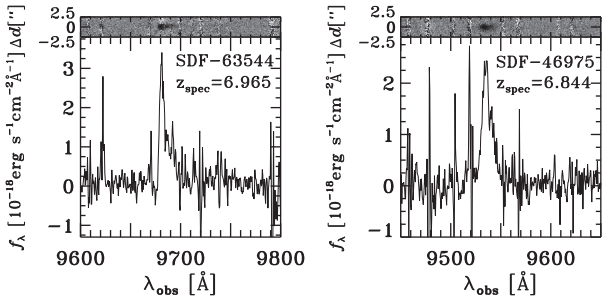

Fig. 1. Spectra of the $z = 6.965$ (SDF-63544; left) and $z = 6.844$ (SDF-46975; right) z-dropout galaxies. The top panels show the composite two-dimensional spectra, from which the one-dimensional spectra shown in the bottom panels are derived. A prominent emission line is seen at 9683 Å for SDF-63544 ($S/N \simeq 13$), and at 9536 Å for SDF-46975 ($S/N \simeq 14$). This figure is reproduced by permission of the AAS.

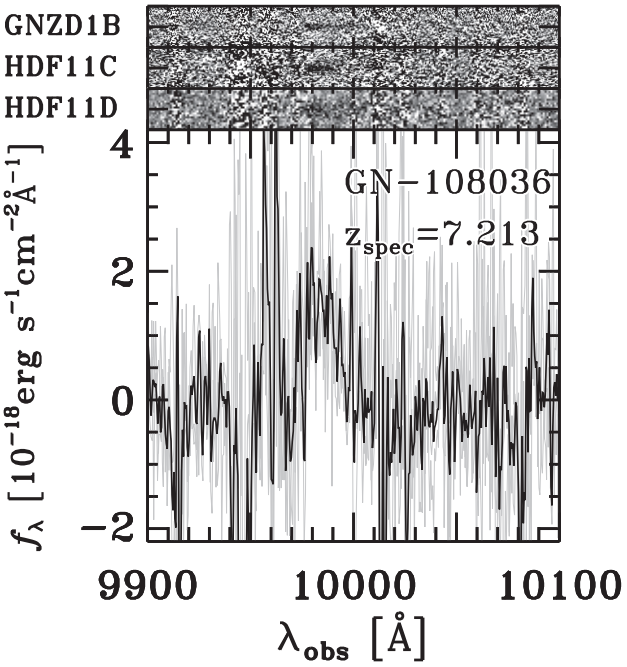

Fig. 2. Spectrum of the $z = 7.213$ z-dropout galaxy, GN-108036. The top panels show its two-dimensional spectra obtained with the GNZD1B, HDF11C, and HDF11D masks. The size along the spatial axis is $5''.0$ for each two-dimensional spectrum. The HDF11D spectrum is binned in 2×2 pixels. A line is visually identified at $\simeq 9980$Å in the spectra of GNZD1B and HDF11C, whose exposure times are 5 hours and $\simeq 4$ hours, respectively, while the line is marginally seen in the spectrum of HDF11D, whose exposure time is 2 hours. In the bottom panel, we show the one-dimensional spectra. The gray solid lines are spectra obtained with individual masks. The composite spectrum is shown as the black solid line. All the one-dimensional spectra illustrate a line detection at around 9980 Å, and the S/N ratio of the line in the composite spectrum is $\simeq 6$. This figure is reproduced by permission of the AAS.

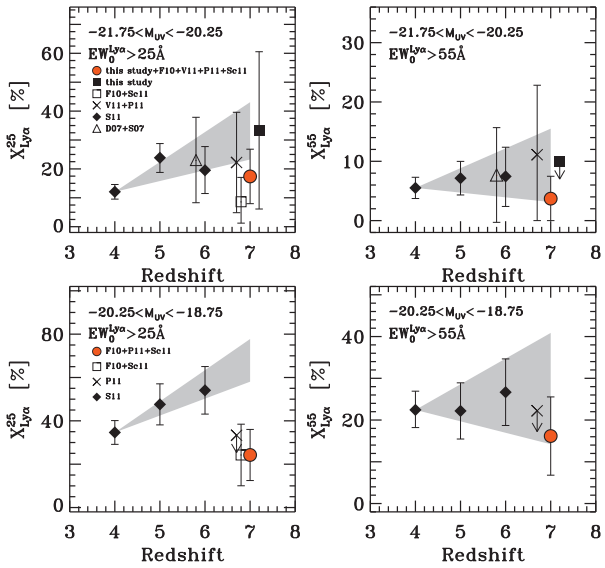

Fig. 3. Evolution in the fraction of strong LAEs in LBGs with $-21.75 < M_{\rm UV} < -20.25$ (top panels) and $-20.25 < M_{\rm UV} < -18.75$ (bottom panels) over $4 < z < 7$. The left panels show the fraction of galaxies with EW larger than 25Å, while the right panels show the fraction of those with EW larger than 55Å. The filled square is our results. The filled diamonds, open squares, triangles, and crosses are taken from the literature. The red filled circles indicate the composites of results from our study and the literature. The filled diamonds, open squares, triangles, and crosses are shifted in redshift for clarity. The shaded area is derived by extrapolating the trend seen in lower redshifts to $z \sim 7$. This figure is reproduced by permission of the AAS.

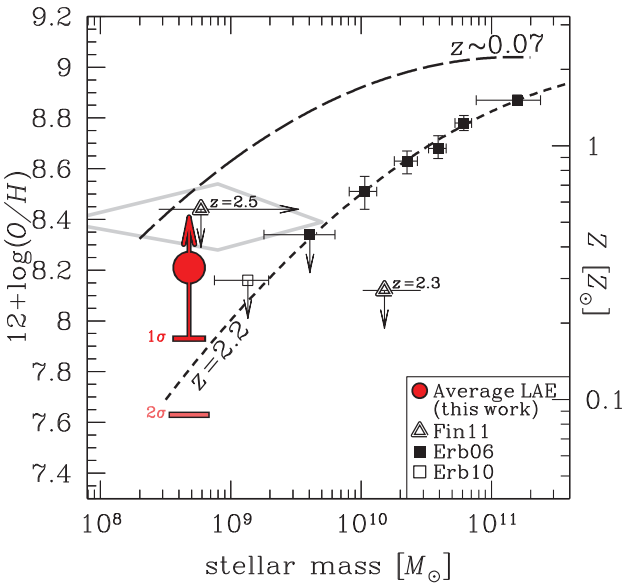

Fig. 4. Mass-Metallicity ($M-Z$) relation of UV-selected galaxies and LAEs at $z \sim 2$. The red circle with an arrow represents our stacked LAE. The red ticks show the lower limits of metallicity at 1 and 2σ levels as labeled next to the ticks. The open triangles show two LAEs at $z \sim 2.3$ and 2.5 from the literature whose upper limits denote the 2σ confidence limits. The curves indicate the $M-Z$ relation observed at $z \sim 0.07$ and $z \sim 2.2$. The filled squares are stacked data points of $z \sim 2.2$ UV-selected galaxies and the open square indicates BX418, which is considered to be the most metal-poor UV-selected galaxy. The gray diamond area shows the median stellar mass and metallicity for $z = 0.195 - 0.44$ LAEs and their 1σ ranges. This figure is reproduced by permission of the AAS.

be identified individually by narrow-band imaging or deep spectroscopy. The stacked object has an Hα luminosity of 1.7×10^{42} erg s^{-1} corresponding to a star formation rate (SFR) of $14\,M_\odot$ yr^{-1}. We place, for the first time, a firm lower limit to the average metallicity of LAEs of $Z \gtrsim 0.09\,Z_\odot$ (2σ) based on the [O II]/(Hα+[N II]) index together with photo-ionization models and empirical relations. This lower limit of metallicity rules out the hypothesis that LAEs, so far observed at $z \sim 2$, are extremely metal poor ($Z < 2 \times 10^{-2}\,Z_\odot$) galaxies at the 4σ level. This limit is higher than a simple extrapolation of the observed mass-metallicity relation of $z \sim 2$ UV-selected galaxies toward lower masses ($5 \times 10^8\,M_\odot$; Fig. 4), but roughly consistent with a recently proposed fundamental mass-metallicity relation when the LAEs' relatively low SFR is taken into account (Fig. 5). The Hα and Lyα luminosities of our NB-selected LAEs indicate that the escape fraction of Lyα photons is $\sim 12 - 30\,\%$, much higher than the values derived for other galaxy populations at $z \sim 2$.

Bibliography

[1] Nakajima, K., et al. 2012, Astrophys. J. , 745, 12

Keck Spectroscopy of Lyman-Break Galaxies and Its Implications for the UV-Continuum and Lyα Luminosity Functions at $z > 6$

In collaboration with the members of University of Arizona, National Astronomical Observatory of Japan, Durham University, The University of Tokyo, Ehime University, and Kyoto University.

We have performed Keck spectroscopic observations of $z > 6$ Lyman-break galaxy (LBG) candidates in the Subaru Deep Field (SDF). The candidates were selected as i'-dropout objects down to $z' = 27$ AB magnitudes from an ultra-deep SDF z'-band image. With the Keck spectroscopy we identified 19 LBGs with prominent Lyα emission lines at $6 \leq z \leq 6.4$. The median value of the Lyα rest-frame equivalent widths (EWs) is ~ 50 Å, with four EWs > 100 Å. This well-defined spectroscopic sample spans a UV-continuum luminosity range of $-21.8 \leq M_{\rm UV} \leq -19.5$ ($0.6 \sim 5\,L^*_{\rm UV}$) and a Lyα luminosity range of $(0.3 \sim 3) \times 10^{43}$ erg s^{-1} ($0.3 \sim 3\,L^*_{{\rm Ly}\alpha}$). We derive the UV and Lyα luminosity functions (LFs) from our sample at $\langle z \rangle \sim 6.2$ after we correct for sample incompleteness. We find that our measurement of the UV LF is consistent with the results of previous studies based on photometric LBG samples at $5 < z < 7$. Our Lyα LF is also generally in agreement with the results of Lyα-emitter surveys at $z \sim 5.7$ and 6.6. This study shows that deep spectroscopic observations of LBGs can provide unique constraints on both the UV and Lyα LFs at $z > 6$.

Bibliography

[1] Jiang, L., et al. 2011, Astrophys. J. , 743, 65

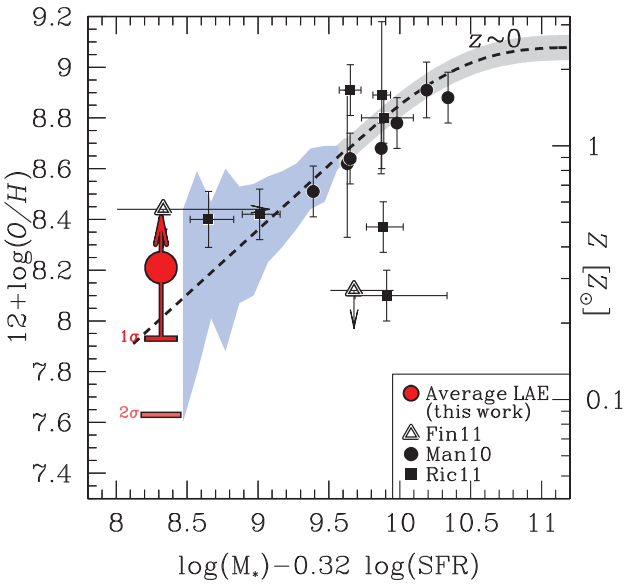

Fig. 5. Fundamental $M-Z$ relation. The dashed curve indicates the best-fit relation for $z\sim 0$ SDSS galaxies, whose typical distribution ranges are shown as the gray shaded (for those with $M_\star \gtrsim 10^{9.2} M_{\odot,\mathrm{chabrier}}$) and the blue shaded ($M_\star \lesssim 10^{9.2} M_{\odot,\mathrm{chabrier}}$) regions. The black circles are $z\sim 2.2$ UV-selected galaxies, the black squares are $1.5<z<2.5$ lensed galaxies, and the open triangles show two LAEs at $z\sim 2.3$ and 2.5. The red circle with an arrow is our result; it is located near a smooth extrapolation of the fundamental $M-Z$ relation toward lower stellar masses. This figure is reproduced by permission of the AAS.

Completing the Census of Lyα Emitters at the Reionization Epoch

In collaboration with the members of National Astronomical Observatory of Japan, Graduate University for Advanced Studies, The University of Tokyo, Durham University, University of Arizona, Ehime University, University of California Los Angeles, and Space Telescope Science Institute.

We have carried out extended spectroscopic confirmations of Lyα emitters (LAEs) at $z=6.5$ and 5.7 in the Subaru Deep Field. Now, the total number of spectroscopically confirmed LAEs is 45 and 54 at $z=6.5$ and 5.7, respectively, and at least 81% (70%) of our photometric candidates at $z=6.5$ (5.7) have been spectroscopically identified as real LAEs. We made careful measurements of the Lyα luminosity, both photometrically and spectroscopically, to accurately determine the Lyα and rest-UV luminosity functions (LFs). The substantially improved evaluation of the Lyα LF at $z=6.5$ shows an apparent deficit from $z=5.7$ at least at the bright end, and a possible decline even at the faint end, though small uncertainties remain. The rest-UV LFs at $z=6.5$ and 5.7 are in good agreement, at least at the bright end, in clear contrast to the differences seen in the Lyα LF. These results imply an increase in the neutral fraction of the intergalactic medium from $z=5.7$ to 6.5. The rest-frame equivalent width (EW_0) distribution at $z=6.5$ seems to be systematically smaller than $z=5.7$, and it shows an extended tail toward larger EW_0. The bright end of the rest-UV LF can be reproduced from the observed Lyα LF and a reasonable EW_0-UV luminosity relation. Integrating this rest-UV LF provides the first measurement of the contribution of LAEs to the photon budget required for reionization. The derived UV LF suggests that the fractional contribution of LAEs to the photon budget among Lyman break galaxies significantly increases toward faint magnitudes. Low-luminosity LAEs could dominate the ionizing photon budget, though this inference depends strongly on the uncertain faint-end slope of the Lyα LF.

Bibliography

[1] Kashikawa, N., et al. 2011, Astrophys. J. , 734, 119

Primary Cosmic Ray Group

[Spokesperson : Hiroko Miyahara]
ICRR, Univ. of Tokyo, Kashiwa, Chiba 277-8582

Measurement of carbon-14 in tree rings

In collaboration with the members of Univ. of Tokyo, Yamagata Univ. Hirosaki Univ. and Australian National Univ.

We have been conducting measurements of carbon-14 content with the precision of 0.3The reconstruction of solar cycle lengths in the past can be also useful for constraining the history of absolute solar activity level. Low resolution records of carbon-14 are often contaminated with the information on the changes in geomagnetic field and carbon cycle. The detection of lengthening/shortening of solar cycles can be an independent proxy for the history of solar activities. We have also started high precision measurements of carbon-14 in annual tree rings to determine the absolute ages of annual-scale cosmic ray events occurred around the Maunder Minimum. The existence of the events has been suggested by beryllium-10 record obtained using ice cores. In order to utilize the AMS facility installed at the Yamagata University in 2009, our group has been trying to achieve 0.1

Bibliography

[1] F. Steinhilber et al., 9,400 years of cosmic radiation and solar activity from ice cores and tree rings, PNAS **109** (2012), doi:10.1073/pnas.1118965109.

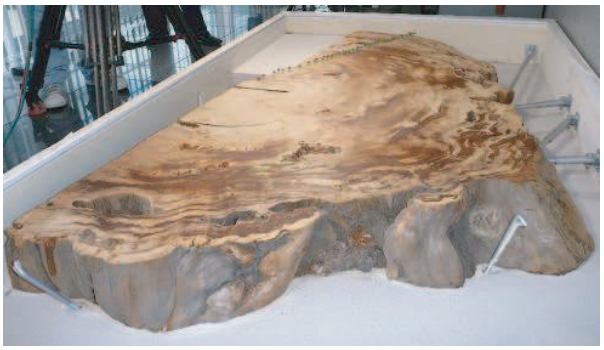

Fig. 1. Japanese cedar tree used in this study. The tree has been obtained from the Yaku Island.

Reconstruction of paleo-climate

In collaboration with the members of Univ. of Tokyo, Nagoya Univ. Hirosaki Univ. and Tokyo Inst. Tech.

We have found that the characteristic variations of cosmic ray 22-year variations are reflected in northern hemispheric climate variations. For example, lengthening and shortening of 22-year cycles as well as the phase transition of 22-year cycles are found in climate proxy records. The phase transition of 22-year cycle is related to the drift effect of cosmic rays in the heliosphere. Generally, the flux of incident cosmic rays tends to be higher at the phases positive solar magnetic polarity, however, the intensity becomes much higher at negative magnetic polarity only around the grand solar minima. The manifestation of 22-year cycles and their phase transitions in climate records strongly suggested that cosmic rays are one of the important external forcing of climate change. The galactic cosmic rays have been considered to promote cloud formation, however the detailed physical mechanism is not fully understood. Although the physical mechanism should be clarified through both laboratory experiment such as the CLOUD experiment at CERN and the direct observation in the actual atmosphere, the anomalous spikes in cosmic rays found at the Maunder Minimum can be also utilized to trace the response of climate system to cosmic rays. The cosmic ray spikes are 1-year duration respectively and four events are identified in total. We are now measuring stable isotopes in tree rings obtained from Japan and Asian countries to trace the response of Asian monsoon to 1-year cosmic ray enhancements. So far we have found the decrease in winter northern temperature in northern hemisphere, enhancement of relative humidity in Japan around the rainy season, and the decrease of winter temperature in Japan. Mapping of the temperature and precipitation over the globe around the cosmic ray spikes can shed light on the response of monsoonal activities as well as the response of overall climate system.

Tracing the impact of solar rotations on cloud activities In collaboration with the members of Univ. of Tokyo, Hokkaido Univ., Yamagata Univ. Osaka City Univ., TIFR, and JKUAT.

We have been conducting the analyses of cloud amount records obtained by satellite based observations. It is known that lightening activity often show 27-day variation, which is close to the time scale of solar rotations. It is also known that the lightening activity tends to be frequent at solar activity maxima. In order to examine the impact of 27-day solar rotational period in meteorological phenomena, we are analyzing the record of Outgoing Long-wave Radiation (OLR), which is available since AD1974. Continuous record is available only since AD1979, but this records covers at least three solar cycles. In 2010, we found that the monthly variations in cloud height around the tropical regions are under the influence of solar rotations. 27-day signals were found in cloud activity around the Indian Ocean and the western Pacific Ocean, only around the maximal period of solar cycles. The appearance of sunspots and faculae around solar cycle maxima cause the changes in total solar irradiance and ultra violet radiation. Large solar flares caused by sunspot activities also cause the changes in incident cosmic rays at the Earth. Although the actual parameter to mediate the connection between solar rotations and cloud activities is yet unclear, it is suggested that solar impact is also significant at this monthly time scales. Further investigations on this phenomenon would improve the predictability of weather and climate. We are now planning to conduct cloud and aerosol measurements at the places where we have found that the setting is sensitive to external forcing. The problem of satellite based observation is that the data are available only on a daily basis and thus cannot be used to examine the impact of cosmic rays on the cloud micro physics. Also, most of the records obtained by the missions so far do not have altitude distribution, which would be essential to trace the cosmic ray impact. We are now discussing the possibility to conduct measurement with 1 km height distribution. There are two steps in cosmic ray impacts. One is the production of Cloud Condensation Nuclei by ionizing the atmospheric molecules. The other is the promotion of coagulation between the pre-existing cloud droplet and aerosols. For the latter part, it is suggested that the impact of cosmic rays could be different at different height. LIDAR observation, ground-based observation at high altitude mountain, aircraft measurements and aerosol sonde are the candidates for the methodology. As a pilot observation, we have started monitoring cloud by deploying all sky cloud monitors in Kenya and at Mt. Ooty in India.

Fig. 2. All sky image obtained by the camera deployed at Mt. Ooty.

Theory Group

We have studied particle physics (mainly particle physics phenomenology) and astroparticle physics (mainly particle cosmology).

The supersymmetric (SUSY) extension of the standard model (SM) in the particle physics is considered to be one of the most promising models beyond the standard model. It solves the naturalness problem for the Higgs boson mass term in the standard model, and it is also compatible with the grand unified theories (GUTs). Our group has been studying phenomenological and cosmological aspects of the SUSY models.

Recent cosmological observations determine precisely the mean densities of matter and baryon in the Universe, and existence of non-baryonic dark matter is established. Weakly interacting massive particles (WIMPs) are considered to be good candidates of the dark matter. They act as the cold dark matter in the structure formation of the universe. Our

group has been studying model building for dark matter and detectability in direct and indirect search experiments.

For understanding of the early universe, a role of the elementary particle physics is crucial. Recent progress in the particle physics such as grand unification theories and supersymmetry leads us to a more deeper insight into the fundamental aspects of the early universe. In the inflationary universe, the quantum fluctuations of the scalar field which drives the inflation become the density fluctuations and lead to formation of the structure observed in the present universe. On the other hand cosmology and astrophysics are used to test new theories in particle physics. Such particle cosmology is one of main subjects of our group.

Big Bang Nucleosynthesis (BBN) is one of the most important subjects in modern cosmology. Predicted abundances of the light elements are very sensitive to the cosmological scenario. On the other hand, physics beyond the standard model predicts the new particles which would have existed at the BBN epoch. Such particles may spoil the success of BBN, which leads to constraints on the new particles and the particle physics models.

The grand unified theories (GUT) predict that our universe undergoes several vacuum phase transitions. In the course of phase transitions topological defects (monopoles, cosmic strings and domain walls) are generally produced depending on symmetries of the vacua. Our group has studied evolution of various topological defects.

Particle Phenomenology

[Spokesperson : M. Ibe]

Pure Gravity Mediation with $m_{3/2} = 10 - 100$TeV

In collaboration with the members of IPMU.

Recently, the ATLAS and CMS collaborations reported exciting hints of a Standard Model-like Higgs boson with a mass around 125 GeV. Such a Higgs boson mass can be easily obtained in the minimal supersymmetric Standard Model based on the "pure gravity mediation model" where the sfermion masses and the Higgs mass parameters are in tens to hundreds TeV range while the gauginos are in the hundreds GeV to TeV range. In this paper, we discuss details of the gaugino mass spectrum in the pure gravity mediation model. We also discuss the signals of the model at the current and future experiments such as cosmic ray observations and the LHC experiments. In particular, we show that the parameter space which is consistent with the thermal leptogenesis can be fully surveyed experimentally in the foreseeable future.

Bibliography

[1] M. Ibe, S. Matsumoto and T. T. Yanagida, Phys. Rev. D **85**, 095011 (2012) [arXiv:1202.2253 [hep-ph]].

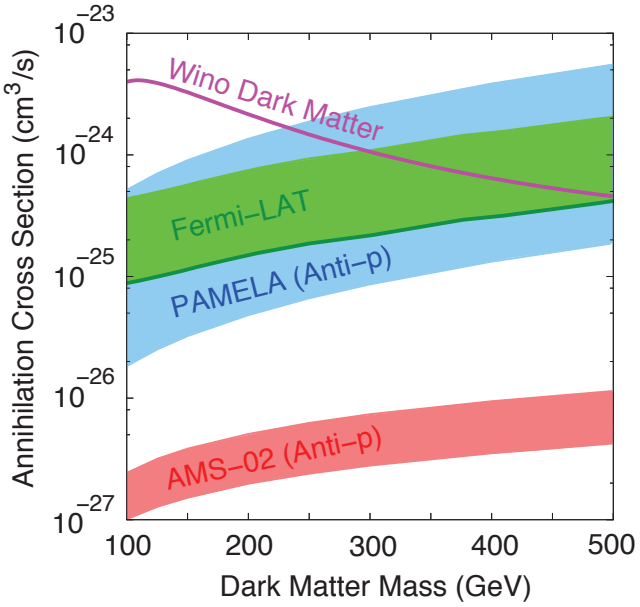

Fig. 1. Constraints and future prospects of indirect detection experiments of dark matter. Theoretical prediction of the neutral wino dark matter is also shown. The wino annihilation cross section is bounded from above by Fermi-LAT and PAMELA experiments (the bands show the uncertainties). The expected reach of AMS-02 experiment is shown as a red band.

A 125GeV Higgs Boson and Muon g-2 in More Generic Gauge Mediation

In collaboration with the members of IPMU, Univ. of California, Lawrence Berkelry National Laboratory.

Recently, the ATLAS and CMS collaborations reported exciting hints of a Stan- dard Model-like Higgs boson with a mass around 125 GeV. A Higgs boson this heavy is diffcult to realize in conventional models of gauge mediation. Here we revisit the lightest Higgs boson mass in "more generic gauge mediation," where the Higgs dou- blets mix with the messenger doublets. We show that a Higgs boson mass around 125 GeV can be realized in more generic gauge mediation models, even for a relatively light gluino mass, $m_{\rm gluino} \sim 1$TeV. We also show that the muon anomalous magnetic moment can be within 1σ of the experimental value for these models, even when the Higgs boson is relatively heavy. We also discuss the LHC constraints and the prospects of discovery.

Bibliography

[1] J. L. Evans, M. Ibe, S. Shirai and T. T. Yanagida, Phys. Rev. D **85**, 095004 (2012) [arXiv:1201.2611 [hep-ph]].

The Lightest Higgs Boson Mass in Pure Gravity Mediation Model

In collaboration with the members of IPMU.

We discuss the lightest Higgs boson mass in the minimal supersymmetric Stan- dard Model with "pure gravity mediation". By requiring that the model provides the observed dark

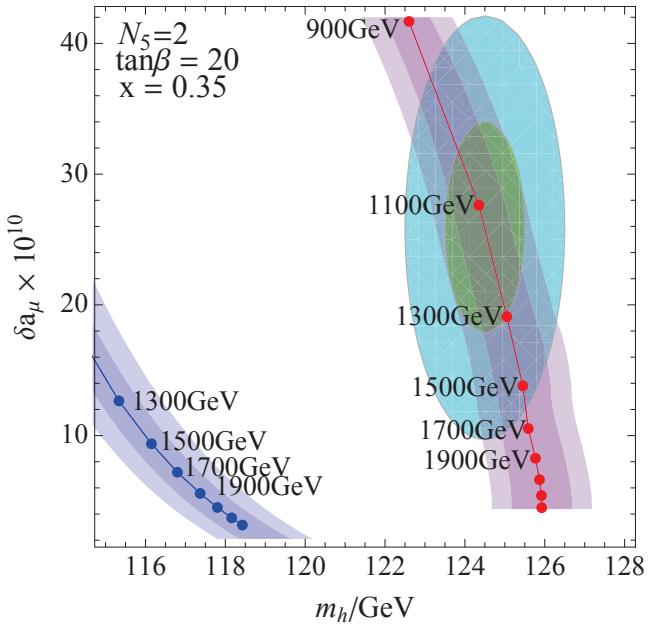

Fig. 2. The correlation between the lightest Higgs boson mass and the muon g—2 for the present work (red) and the conventional gauge mediation models (blue). Each band corresponds to uncertainties in the Higgs mass estimation. The green and the light blue shaded oval regions roughly show the parameter regions where the muon g-2 is within 1 and 2 σ of the experimental results. The gluino masses for a each point are also shown.

matter density, we find that the lightest Higgs boson is predicted to be below 132 GeV. We also find that the upper limit on the lightest Higgs boson mass becomes 128 GeV, if we further assume thermal leptogenesis mechanism as the origin of baryon asymmetry of universe. The interrelations between the Higgs boson mass and the gaugino masses are also discussed.

Bibliography

[1] M. Ibe and T. T. Yanagida, Phys. Lett. B **709**, 374 (2012) [arXiv:1112.2462 [hep-ph]].

The GeV-scale dark matter with B-L asymmetry

In collaboration with the members of IPMU.

One of important properties of dark matter is its stability. The $U(1)_{B-L}$ gauge symmetry is the most attractive symmetry to guarantee the stability. Though the symmetry is expected to be broken at very high energy scale to account for tiny neutrino masses through the seesaw mechanism, the residual discrete symmetry of $U(1)_{B-L}$ can stabilize the dark matter naturally. We prove that, when there is new physics connecting B-L charges of dark matter and standard model particles at the scale between the electroweak and the $U(1)_{B-L}$ breaking, the mass of dark matter is de?nitely predicted to be $(5-7)/Q_{DM}$ GeV (Q_{DM} is the B-L charge of dark matter) independent not only of details of the new physics but also of its energy scale. We also show two attractive examples. First one is the scalar dark matter with the B-L charge of one, which turns out to be very consistent with current CoGeNT results. Another one is the fermionic dark matter having the B?L charge of one third, which is also attractive from the viewpoint of model building.

Bibliography

[1] M. Ibe, S. Matsumoto and T. T. Yanagida, Phys. Lett. B **708**, 112 (2012) [arXiv:1110.5452 [hep-ph]].

Relatively Heavy Higgs Boson in More Generic Gauge Mediation

In collaboration with the members of IPMU.

We discuss gauge mediation models where the doublet messengers and Higgs doublets are allowed to mix through a "charged" coupling. The charged coupling replaces messenger parity as a means of suppressing flavor changing neutral currents without introducing any unwanted *CP* violation. As a result of this mixing between the Higgs doublets and the messengers, relatively large A-terms are generated at the messenger scale. These large A-terms produce a distinct weak scale mass spectrum. Particularly, we show that the lightest Higgs boson mass is enhanced and can be as heavy as 125 GeV for a gluino mass as light as 2 TeV. We also show that the stops are heavier than that predicted by conventional gauge mediation models. It is also shown that these models have a peculiar slepton mass spectrum.

Bibliography

[1] J. L. Evans, M. Ibe and T. T. Yanagida, Phys. Lett. B **705**, 342 (2011) [arXiv:1107.3006 [hep-ph]].

R-symmetry Matching In SUSY Breaking Models

In collaboration with the members of Univ. of California.

Low energy descriptions of metastable supersymmetry breaking models often possess an accidental R-symmetry. Viable phenomenological applications of this class of models require R-symmetry to be broken in the ground state. This can be achieved in O'Raifeartaigh-like models where some of the chiral superfield carry negative R-charges. In this paper we con- sider UV completions of this class of models and formulate necessary conditions that they must satisfy. We show that the R-symmetry of the IR description can be traced to an anomalous or anomaly-free R-symmetry of the UV theory and discuss several representative examples.

Bibliography

[1] J. Goodman, M. Ibe, Y. Shirman and F. Yu, Phys. Rev. D **84**, 045015 (2011) [arXiv:1106.1168 [hep-th]].

Constraints on Direct Gauge Mediation Models with Complex Representations

In collaboration with the members of Univ. of Michigan, IPMU, Univ. of California.

We discuss constraints from cosmology on the models with direct gauge mediation based on the ISS supersymmetry breaking models. It is a generic feature that the ISS models possess a $U(1)$ symmetry which is eventually spontaneously broken, when the models are based on the gauge symmetries with complex representations. We show that the resultant pseudo Nambu-Goldstone boson causes problems in cosmology, which leads to severe constraints on the models. We also show that most parameter space of the models can be probed by observing gravitational waves emitted from the cosmic string network when the $U(1)$ symmetry is a gauge symmetry.

Bibliography

[1] K. Hanaki, M. Ibe, Y. Ookouchi and C. S. Park, JHEP **1108**, 044 (2011) [arXiv:1106.0551 [hep-ph]].

Simplified R-Symmetry Breaking and Low-Scale Gauge Mediation

In collaboration with the members of IPMU.

We argue that some of the difficulties in constructing realistic models of low-scale gauge mediation are artifacts of the narrow set of models that have been studied. In particular, much attention has been payed to the scenario in which the Goldstino superfield in an OfRaifeartaigh model is responsible for both supersymmetry breaking and R-symmetry breaking. In such models, the competing problems of generating sufficiently massive gauginos while preserving an acceptably light gravitino can be quite challenging. We show that by sharing the burdens of breaking supersymmetry and R-symmetry with a second field, these problems are easily solved even within the OfRaifeartaigh framework. We present explicit models realizing minimal gauge mediation with a gravitino mass in the eV range that are both calculable and falsifiable.

Bibliography

[1] J. L. Evans, M. Ibe, M. Sudano and T. T. Yanagida, JHEP **1203**, 004 (2012) [arXiv:1103.4549 [hep-ph]].

Astrophysics and Cosmology

[Spokesperson : M. Kawasaki]

Improved estimation of radiated axions from cosmological axionic strings

In collaboration with the members of YITP, IPMU, Nagoya Univ., RESCEU.

Cosmological evolution of axionic string network is analyzed in terms of field-theoretic simulations in a box of 512^3 grids, which are the largest ever, using a new and more e?cient identi?cation scheme of global strings. The scaling parameter is found to be $\xi = 0.87 \pm 0.14$ in agreement with previous results. The energy spectrum is calculated precisely using a pseudo power spectrum estimator which significantly reduces the error in the mean reciprocal comoving momentum. The resultant constraint on the axion decay constant leads to $f_a \leq 3 \times 10^{11}$ GeV. We also discuss implications for the early Universe.

Bibliography

[1] T. Hiramatsu, M. Kawasaki, T. Sekiguchi, M. Yamaguchi and J. 'i. Yokoyama, Phys. Rev. D **83**, 123531 (2011) [arXiv:1012.5502 [hep-ph]].

Cosmological constraints on dark matter models with velocity-dependent annihilation cross section

In collaboration with the members of Nagoya Univ., KEK, Tohoku Univ., Univ. of Tokyo.

We derive cosmological constraints on the annihilation cross section of dark matter with velocity-dependent structure, motivated by annihilating dark matter models through Sommerfeld or Breit-Wigner enhancement mechanisms. In models with annihilation cross section increasing with decreasing dark matter velocity, big-bang nucleosynthesis and cosmic microwave background give stringent constraints.

Bibliography

[1] J. Hisano, M. Kawasaki, K. Kohri, T. Moroi, K. Nakayama and T. Sekiguchi, Phys. Rev. D **83**, 123511 (2011) [arXiv:1102.4658 [hep-ph]].

Differentiating CDM and Baryon Isocurvature Models with 21 cm Fluctuations

In collaboration with the members of Nagoya Univ., Saga Univ.

We discuss how one can discriminate models with cold dark matter (CDM) and baryon isocurvature fluctuations. Although current observations such as cosmic microwave background (CMB) can severely constrain the fraction of such isocurvature modes in the total density fluctuations, CMB cannot differentiate CDM and baryon ones by the shapes of their power spectra. However, the evolution of CDM and baryon density fluctuations are different for each model, thus it would be possible to discriminate those isocurvature modes by extracting information on the fluctuations of CDM/baryon itself. We discuss that observations of 21 cm fluctuations can in principle differentiate these modes and demonstrate to what extent we can distinguish them with future 21 cm surveys. We show that, when the isocurvature mode has a large blue-tilted initial spectrum, 21 cm surveys can clearly probe the difference.

Bibliography

[1] M. Kawasaki, T. Sekiguchi and T. Takahashi, JCAP **1110**, 028 (2011) [arXiv:1104.5591 [astro-ph.CO]].

Gravitino dark matter and baryon asymmetry from Q-ball decay in gauge mediation

In collaboration with the members of Nagoya Univ., Saga Univ.

We investigate the Q-ball decay in the gauge-mediated SUSY breaking. Q balls decay mainly into nucleons, and partially into gravitinos, while they are kinematically forbidden to decay into sparticles which would be cosmologically harmful. This is achieved by the Q-ball charge small enough to be unstable for the decay, and large enough to be protected kinematically from unwanted decay channel. We can then have right amounts of the baryon asymmetry and the dark matter of the universe, evading any astrophysical and cosmological observational constraints such as the big bang nucleosynthesis, which has not been treated properly in the literatures.

Bibliography

[1] S. Kasuya and M. Kawasaki, Phys. Rev. D **84**, 123528 (2011) [arXiv:1107.0403 [hep-ph]].

Non-Gaussianity from Curvatons Revisited

In collaboration with the members of IPMU, RESCEU, Tohoku Univ.

We investigate density perturbations sourced by a curvaton with a generic energy potential. The key feature of a curvaton potential which deviates from a quadratic is that the curvaton experiences a non-uniform onset of its oscillation. This sources additional contributions to the resulting density perturbations, and we especially find that the non-Gaussianity parameter $f_{\rm NL}$ can become large with either sign no matter whether the curvaton dominates or subdominates the universe when it decays. Such non-quadratic curvaton potentials are required in order to produce a red-tilted density perturbation spectrum (without invoking large-field inflation), and are also motivated by explicit curvaton models based on microscopic physics. We further apply our generic results to the case where the curvaton is a pseudo-Nambu-Goldstone (NG) boson of a broken $U(1)$ symmetry, and show that the resulting density perturbations are strongly enhanced towards the hilltop region of the energy potential, accompanied by a mild increase of the non-Gaussianity. Such hilltop NG curvatons can produce observationally suggested density perturbations under wide ranges of inflation/reheating scales, and further predict the non-Gaussianity of the density perturbations to lie within the range $10 \lesssim f_{\rm NL} \lesssim 30$.

Bibliography

[1] M. Kawasaki, T. Kobayashi and F. Takahashi, Phys. Rev. D **84**, 123506 (2011) [arXiv:1107.6011 [astro-ph.CO]].

Primordial seeds of supermassive black holes

In collaboration with the members of IPMU, Univ. of California.

Supermassive black holes exist in the centers of galaxies, including Milky Way, but there is no compelling theory of their formation. Furthermore, observations of quasars imply that supermassive black holes have already existed at some very high redshifts, suggesting the possibility of their primordial origin. In a class of well-motivated models, inflationary epoch could include two or more periods of inflation dominated by different scalar fields. The transition between such periods of inflation could enhance the spectrum of density perturbations on some specific scale, which could lead to formation of primordial black holes with a very narrow range of masses of the order of 10^5 solar masses. These primordial black holes could have provided the requisite seeds for the observed population of supermassive black holes.

Bibliography

[1] M. Kawasaki, A. Kusenko and T. T. Yanagida, Phys. Lett. B **711**, 1 (2012) [arXiv:1202.3848 [astro-ph.CO]].

Time-dependent quark masses and big bang nucleosynthesis revisited

In collaboration with the members of Soongsil Univ., NAOJ, Univ. Tokyo, Graduate Univ. for Advanced Studies, ICRR and Univ. Notre Dame.

We reinvestigate the constraints from primordial nucleosynthesis on a possible time-dependent quark mass. The limits on such quark-mass variations are particularly sensitive to the adopted observational abundance constraints. Hence, in the present study we have considered updated light-element abundances and uncertainties deduced from observations. We also consider new nuclear reaction rates and an independent analysis of the influence of such quark-mass variations on the resonance properties of the important He3(d,p)He4 reaction. We find that the updated abundance and resonance constraints imply a narrower range on the possible quark-mass variations in the early universe. We also find that, contrary to previous investigations, the optimum concordance region reduces to a (95% C.L.) value of $-0.005 \lesssim \delta m_q/m_q \lesssim 0.007$ consistent with no variation in the averaged quark mass.

Bibliography

[1] M. -K. Cheoun, T. Kajino, M. Kusakabe and G. J. Mathews, Phys. Rev. D **84**, 043001 (2011) [arXiv:1104.5547 [astro-ph.CO]].

Signals of the cosmological reionization in the radio sky through C and O fine structure lines

In collaboration with the members of ICRR and IPMU.

We study the excitation of the fine structure levels of C_I, C_{II} and O_I by ultraviolet (UV) photons around strong UV sources which are also ionizing sources of the cosmological reionization at a redshift of ~ 10. The evolutions of ionized regions around a point source are calculated by solving rate equations for non-equilibrium chemistry. Signals of UV photons through the fine structure lines are considered to be

stronger at locations of more abundant chemical species of C_I, C_{II} and O_I. Such environments would be realized at locations where strong fluxes of non-ionizing UV line photons available for the pumping up of fine structure levels exist, and simultaneously ionizing UV photons are effectively shielded by dense H_I regions. Signals from H_I regions of moderately large densities induced by redshifted UV photons emitted at the point sources are found to be dominantly large over those of others. We discuss the detectability of the signals, and show that signals from idealized environments will be possibly detected by radio observations with next-generation arrays to come after the Atacama Large Millimeter/submillimeter Array (ALMA).

Bibliography

[1] M. Kusakabe and M. Kawasaki, MNRAS **419**, 873 (2012) [arXiv:1004.1087 [astro-ph.CO]].

Production of dark matter axions from collapse of string-wall systems

In collaboration with the members of ICRR, YITP and Nagoya Univ.

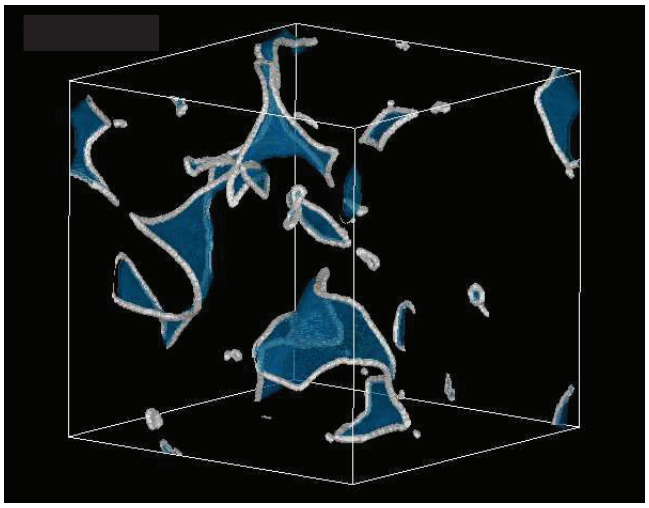

Fig. 3. Visualization of the simulation for the domain wall. The white lines corresponds to the position of strings, while the blue surfaces correspond to the position of the center of domain walls.

We analyze the spectrum of axions radiated from collapse of domain walls, which have received less attention in the literature. The evolution of topological defects related to the axion models is investigated by performing field-theoretic lattice simulations. We simulate the whole process of evolution of the defects, including the formation of global strings, the formation of domain walls and the annihilation of the defects due to the tension of walls. The spectrum of radiated axions has a peak at the low frequency, which implies that axions produced by the collapse of domain walls are not highly relativistic. We revisit the relic abundance of cold dark matter axions and find that the contribution from the decay of defects can be comparable with the contribution from strings. This result leads to a severer upper bound on the axion decay constant.

Bibliography

[1] T. Hiramatsu, M. Kawasaki, K. Saikawa and K. Sekiguchi, Phys. Rev. D **85** (2012) 105020 [arXiv:1202.5851 [hep-ph]].

Higher order corrections to the primordial gravitational wave spectrum and its impact on parameter estimates for inflation

In collaboration with the members of Saga Univ.

We study the impact of the use of the power series expression for the primordial tensor spectrum on parameter estimation from future direct detection gravitational wave experiments. The spectrum approximated by the power series expansion may give large deviation from the true (fiducial) value when it is normalized at CMB scale because of the large separation between CMB and direct detection scales. We derive the coefficients of the higher order terms of the expansion up to the sixth order within the framework of the slowroll approximation and investigate how well the inclusion of higher order terms improves the analytic prediction of the spectrum amplitude by comparing with numerical results. Using the power series expression, we consider future constraints on inflationary parameters expected from direct detection experiments of the inflationary gravitational wave background and show that the truncation of the higher order terms can lead to incorrect evaluation of the parameters. We present two example models; a quadratic chaotic inflation model and mixed inflaton and curvaton model with a quartic inflaton potential.

Bibliography

[1] S. Kuroyanagi and T. Takahashi, JCAP **1110**, 006 (2011) [arXiv:1106.3437 [astro-ph.CO]].

Prospects for determination of thermal history after inflation with future gravitational wave detectors

In collaboration with the members of Univ. of Tokyo and Univ. of California at Berkeley

Thermal history of the Universe between inflation and big-bang nucleosynthesis has not yet been revealed observationally. It will be probed by the detection of primordial gravitational waves generated during inflation, which contain information on the reheating temperature as well as the equation of state of the Universe after inflation. Based on the Fisher information formalism, we examine how accurately the tensor-to-scalar ratio and reheating temperature after inflation can be simultaneously determined with space-based gravitational wave detectors such as the DECI-hertz Interferometer Gravitational-wave Observatory and the Big-Bang Observer. We show that the reheating temperature is best determined if it is around 107 GeV for tensor-to-scalar ratio of around 0.1, and explore the detectable parameter space. We also find

that equation of state of the early Universe can be also determined accurately enough to distinguish different equation-of-state parameters if the inflationary gravitational waves are successfully detected. Thus, future gravitational wave detectors provide a unique and promising opportunity to reveal the thermal history of the Universe around 10^7 GeV.

Bibliography

[1] S. Kuroyanagi, K. Nakayama and S. Saito, Phys. Rev. D **84**, 123513 (2011) [arXiv:1110.4169 [astro-ph.CO]].

Cosmological effects of decaying cosmic string loops with TeV scale width

In collaboration with the members of ICRR and Univ. of Tokyo.

In supersymmetric theories, cosmic strings produced in the early Universe often have a width of TeV scale, while the tension is much larger. In a scaling regime, an infinite cosmic string releases significant fraction of its energy in the form of string loops. These thick string loops lose their energies efficiently by particle emissions, and hence it may have effects on cosmological observations. We study cosmological implications of string loops with TeV scale width in detail and derive constraints on the tension of the string. Implications on future gravitational wave detectors are also discussed.

Bibliography

[1] M. Kawasaki, K. Miyamoto and K. Nakayama, arXiv:1105.4383 [hep-ph].

Isocurvature perturbations in extra radiation

In collaboration with the members of ICRR, Univ. of Tokyo and Nagoya Univ.

Recent cosmological observations, including measurements of the CMB anisotropy and the primordial helium abundance, indicate the existence of an extra radiation component in the Universe beyond the standard three neutrino species. In this paper we explore the possibility that the extra radiation has isocurvatrue uctuations. A general formalism to evaluate isocurvature perturbations in the extra radiation is provided in the mixed in aton-curvaton system, where the extra radiation is produced by the decay of both scalar fields. We also derive constraints on the abundance of the extra radiation and the amount of its isocurvature perturbation. Current observational data favors the existence of an extra radiation component, but does not indicate its having isocurvature perturbation. These constraints are applied to some particle physics motivated models. If future observations detect isocurvature perturbations in the extra radiation, it will give us a hint to the origin of the extra radiation.

Bibliography

[1] M. Kawasaki, K. Miyamoto, K. Nakayama and T. Sekiguchi, JCAP **1202**, 022 (2012) [arXiv:1107.4962 [astro-ph.CO]].

Forecast constraints on cosmic string parameters from gravitational wave direct detection experiments

In collaboration with the members of ICRR, Nagoya Univ, Kumamoto Univ and Institut df Astrophysique.

Gravitational waves (GWs) are one of the key signatures of cosmic strings. If GWs from cosmic strings are detected in future experiments, not only their existence can be confirmed but also their properties might be probed. In this paper, we study the determination of cosmic string parameters through direct detection of GW signatures in future ground-based GW experiments. We consider two types of GWs, bursts and the stochastic GW background, which provide us with different information about cosmic string properties. Performing the Fisher matrix calculation on the cosmic string parameters, such as parameters governing the string tension $G\mu$ and initial loop size α and the reconnection probability p, we find that the two different types of GW can break degeneracies in some of these parameters and provide better constraints than those from each measurement.

Bibliography

[1] S. Kuroyanagi, K. Miyamoto, T. Sekiguchi, K. Takahashi and J. Silk, Phys. Rev. D **86**, 023503 (2012) [arXiv:1202.3032 [astro-ph.CO]].

Non-Gaussian isocurvature perturbations in dark radiation

In collaboration with the members of ICRR, Univ. of Tokyo and Nagoya Univ.

We study non-Gaussian properties of the isocurvature perturbations in the dark radiation, which consists of the active neutrinos and extra light species, if exist. We first derive expressions for the bispectra of primordial perturbations which are mixtures of curvature and dark radiation isocurvature perturbations. We also discuss CMB bispectra produced in our model and forecast CMB constraints on the nonlinearity parameters based on the Fisher matrix analysis. Some concrete particle physics motivated models are presented in which large isocurvature perturbations in extra light species and/or the neutrino density isocurvature perturbations as well as their non-Gaussianities may be generated. Thus detections of non-Gaussianity in the dark radiation isocurvature perturbation will give us an opportunity to identify the origin of extra light species and lepton asymmetry.

Bibliography

[1] E. Kawakami, M. Kawasaki, K. Miyamoto, K. Nakayama and T. Sekiguchi, JCAP **1207**, 037 (2012) [arXiv:1202.4890 [astro-ph.CO]].

Open inflation in the landscape

In collaboration with the members of Stanford Univ. and YITP.

The open inflation scenario is attracting a renewed interest in the context of the string landscape. Since there are a large number of metastable de Sitter vacua in the string landscape, tunneling transitions to lower metastable vacua through the bubble nucleation occur quite naturally, which leads to a natural realization of open inflation. Although the deviation of Ω_0 from unity is small by the observational bound, we argue that the effect of this small deviation on the large-angle CMB anisotropies can be significant for tensor-type perturbation in the open inflation scenario. We consider the situation in which there is a large hierarchy between the energy scale of the quantum tunneling and that of the slow-roll inflation in the nucleated bubble. If the potential just after tunneling is steep enough, a rapid-roll phase appears before the slow-roll inflation. In this case the power spectrum is basically determined by the Hubble rate during the slow-roll inflation. On the other hand, if such a rapid-roll phase is absent, the power spectrum keeps the memory of the high energy density there in the large angular components. Furthermore, the amplitude of large angular components can be enhanced due to the effects of the wall fluctuation mode if the bubble wall tension is small. Therefore, although even the dominant quadrupole component is suppressed by the factor $(1-\Omega_0)^2$, one can construct some models in which the deviation of Ω_0 from unity is large enough to produce measurable effects. We also consider a more general class of models, where the false vacuum decay may occur due to Hawking-Moss tunneling, as well as the models involving more than one scalar field. We discuss scalar perturbations in these models and point out that a large set of such models is already ruled out by observational data, unless there was a very long stage of slow-roll inflation after the tunneling. These results show that observational data allow us to test various assumptions concerning the structure of the string theory potentials and the duration of the last stage of inflation.

Bibliography

[1] D. Yamauchi, A. Linde, A. Naruko, M. Sasaki and T. Tanaka, Phys. Rev. D **84**, 043513 (2011) [arXiv:1105.2674 [hep-th]].

Weak lensing by cosmic (super-)strings

In collaboration with the members of Kumamoto Univ., Hirosaki Univ., YITP.

We clarified the observational signature of a cosmic (super-)string network on the weak lensing experiment. We showed that the string-lensed spectra decay more slowly on small scales compared with primordial scalar perturbations, and the non-vanishing signals for B-mode cosmic shear and curl-mode deflection angle naturally arise. We found that the weak lensing signals are shown to be potentially detectable from the upcoming cosmic shear and cosmic microwave background lensing observations.

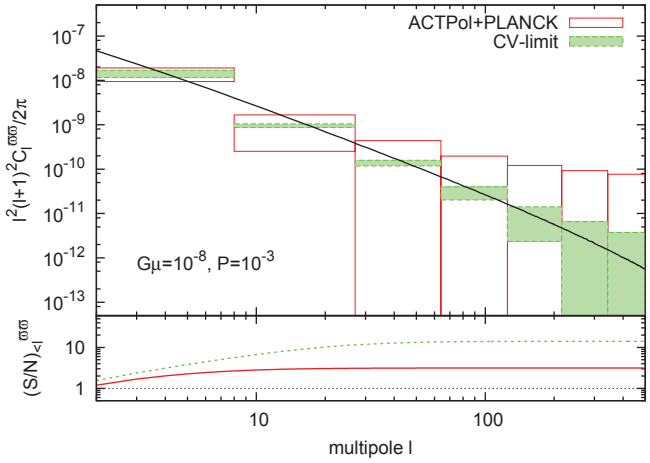

Fig. 4. The angular power spectrum of the curl-mode deflection angle from the vector perturbations generated by the cosmic string network. The error boxes represents the expected variance of angular power spectrum from ACTPol+PLANCK(empty red), CV-limit (shaded green). The bottom panel shows the signal-to-noise ratio as a function of maximum multipole for each survey.

Bibliography

[1] D. Yamauchi, K. Takahashi, Y. Sendouda and C. -M. Yoo, Phys. Rev. D **85**, 103515 (2012) [arXiv:1110.0556 [astro-ph.CO]].

[2] T. Namikawa, D. Yamauchi and A. Taruya, JCAP **1201**, 007 (2012) [arXiv:1110.1718 [astro-ph.CO]].

Multi-field open inflation model and multi-field dynamics in tunneling

In collaboration with the members of YITP.

We consider a multi-field open inflation model, in which one of the fields dominates quantum tunneling from a false vacuum while the other field governs slow-roll inflation within the bubble nucleated from false vacuum decay. We call the former the tunneling field and the latter the inflaton field. In the limit of a negligible interaction between the two fields, the false vacuum decay is described by a Coleman-De Luccia instanton. Here we take into account the coupling between the two fields and construct explicitly a multi-field instanton for a simple quartic potential model. We also solve the evolution of the scalar fields within the bubble. We find our model realizes open inflation successfully. This is the first concrete, viable model of open inflation realized with a simple potential. We then study the effect of the multi-field dynamics on the false vacuum decay, specifically on the tunneling rate. We find the tunneling rate increases in general provided that the multi-field effect can be treated perturbatively.

Bibliography

[1] K. Sugimura, D. Yamauchi and M. Sasaki, JCAP **1201**, 027 (2012) [arXiv:1110.4773 [gr-qc]].

Cosmological Aspects of Inflation in a Supersymmetric Axion Model

In collaboration with the members of Univ. of Tokyo, KEK.

We show that the hybrid inflation is naturally realized in the framework of a supersymmetric axion model, which is consistent with the WMAP observation if the Peccei-Quinn symmetry breaking scale is around 10^{15} GeV. By solving the post-inflationary scalar dynamics, it is found that the scalar partner of the axion, saxion, oscillates with large amplitude and its decay produces a huge entropy and dilutes the axion. As a result, the axion coherent oscillation can be the dominant component of the dark matter in the Universe. Cosmological gravitino and axino problems are solved.

Bibliography

[1] M. Kawasaki, N. Kitajima and K. Nakayama, Phys. Rev. D **83**, 123521 (2011) [arXiv:1104.1262 [hep-ph]].

Revisiting the cosmological coherent oscillation

In collaboration with the members of YITP.

It is often the case that scalar fields are produced in the early Universe in the form of coherent oscillation. These scalar fields may have huge abundances and affect the evolution of the Universe. In particular, if the lifetime is long enough, they may cause cosmological disasters. We revisit the issue of coherent oscillation of the scalar field when it couples with another oscillating scalar field, and find a situation that the abundance, or the amplitude of the oscillation, is significantly reduced by a variant type of the adiabatic suppression mechanism. As a concrete example, it is applied to the saxion, a at direction in the supersymmetric axion model, and we show that the cosmological saxion problem is solved in a particular setup.

Bibliography

[1] M. Kawasaki, N. Kitajima and K. Nakayama, arXiv:1112.2818 [hep-ph].

Resonant annihilation of long-lived massive colored particles through hadronic collisions

In collaboration with the members of ICRR.

Hypothetical long-lived massive colored particles (MCPs or Ys) would be confined in colorless exotic strongly interacting massive particles (SIMPs) at color confinement temperature of $T_C \sim 200$ MeV. Two long-lived MCPs form a bound state (YY) at collisions of two SIMPs. We study sensitivities of MCP annihilation to decay properties of resonances $(Y\bar{Y})$, and binding energies or energy levels of exotic SIMPs. The $(Y\bar{Y})$ formation is assumed to dominantly proceed through resonances of $(Y\bar{Y})$ in this paper. We make a toy model of the effective cross section for $Y\bar{Y}$ annihilation. Abundances of SIMPs are then calculated for different sets of parameters specifying properties of $(Y\bar{Y})$ resonances, binding energies of SIMPs, the initial abundance and the mass of MCP. Calculated relic abundances for respective SIMP species are 2×10^{-8}–3×10^{-4} times that of baryon. They can be much higher but cannot be much smaller than the previous estimate. The abundances can be consistent depending on parameters with the possible scenario that SIMPs bind to nuclei and subsequent exotic nuclear reactions reduce the primordial abundance of ^{7}Li or enhance those of ^{9}Be and/or B in the early Universe. A unique information on the quark-hadron phase transition in the early Universe may become available in future by elaborated studies on the annihilation process with light element abundances as observables.

Bibliography

[1] M. Kusakabe and T. Takesako, Phys. Rev. D **85**, 015005 (2012) [arXiv:1112.0860 [hep-ph]].

Hubble Induced Mass in Radiation Dominated Universe

In collaboration with the members of ICRR and IPMU.

We reconsider the effective mass of a scalar field which interact with visible sector via Planck-suppressed coupling in supergravity framework. We focus on the radiation-dominated (RD) era after inflation. In this era, the effective mass is given by thermal average of interaction terms. To make our analysis clear, we rely on Kadanoff-Baym equations to evaluate the thermal average. We find that, in RD era, a scalar field acquires the effective mass of the order of H.

Bibliography

[1] M. Kawasaki and T. Takesako, Phys. Lett. B **711**, 173 (2012) [arXiv:1112.5823 [hep-ph]].

OBSERVATORIES AND A RESEARCH CENTER

Location of the Institute and the Observatories in Japan

Norikura Observatory

Location:	Iwaitani, Nyukawa-cho, Takayama-shi, Gifu Prefecture 506-2254 N 36°06′, E 137°33′, 2770 m a.s.l.
Telephone (Fax):	+263-33-7456
Telephone (satellite):	090-7721-5674
Telephone (car):	090-7408-6224

Akeno Observatory

Location:	5259 Asao, Akeno-machi, Hokuto-shi, Yamanashi Prefecture 407-0201 N 35°47′, E 138°30′, 900 m a.s.l.
Telephone / Fax:	+551-25-2301 / +551-25-2303

Kamioka Observatory

Location:	456 Higashi-mozumi, Kamioka-cho, Hida-shi, Gifu Prefecture 506-1205 N 36°25′26″, E 137°19′11″, 357.5 m a.s.l.
Telephone / Fax:	+578-85-2116 / +578-85-2121

Research Center for Cosmic Neutrinos

Location:	5-1-5 Kashiwanoha, Kashiwa, Chiba Prefecture 277-8582
Telephone / Fax:	+4-7136-3138 / +4-7136-3115

NORIKURA OBSERVATORY

Introduction

Norikura Observatory (36.10°N and 137.55°E) was founded in 1953 and attached to ICRR in 1976. It is located at 2770 m above sea level, and is the highest altitude manned laboratory in Japan. Experimental facilities of the laboratory are made available to all the qualified scientists in the field of cosmic ray research and associated subjects. The AC electric power is generated by the dynamo and supplied throughout the observatory. In 1996, two dynamos of 70 KVA each were replaced with the new ones. The observatory can be accessed easily by car and public bus in summer (July-September). The 50th anniversary of Norikura Observatory was celebrated in 2003.

Fig. 1. Norikura Observatory.

The feasibility of the automatic operation of Norikura Observatory during winter period has been tested since winter 2004 in order to study the possibilities to reduce maintenance and labor costs without seriously damaging to the use of researches. A long-distance (∼40km) wireless LAN system (11M bps) was set up in 2003. Two new easy-to-handle and easy-to-maintain dynamos of 115 KVA each were installed in 2004 as well. The unmanned operation of Norikura Observatory has been mostly successful in winter, during which the battery backed-up solar panels and/or wind power generators kept supplying the electricity to the wireless LAN and on-going cosmic-ray experiments.

Present major scientific interests of the laboratory is focused on the modulation of high energy cosmic rays in the interplanetary space associated with the solar activity and the generation of energetic particles by the solar flares, both of which require long-term monitoring. This research has been carried out by the group of universities, where ICRR provides them with laboratory facility. A part of the facility has been open for the environmental study at high altitude such as aerosol-related mechanism in the atmosphere, observation of total ozone and UV solar radiation, for botanical study in the high-altitude environment, etc.

Fig. 2. A dynamo of 115KV.

Cosmic Ray Physics

A neutron monitor has been continuously operated to study the correlation of solar activities and cosmic ray flux for a long time. It is the only active one in Japan now. The neutron monitor data are open to researchers worldwide as a world observation network point (WDC).

In addition, space weather observation is actively made by a 25 m^2 muon hodoscope at Norikura Observatory[1], [2], [3], [4], [5], [6], [7], [8], [9].

The anisotropy observed with the global muon detector network (GMDN) provides us with a unique information of the spatial gradient of the GCR density which reflects the large-scale magnetic structure in the heliosphere. The solar cycle variation of the gradient gives an important information on the GCR transport in the heliosphere, while the short-term variation of the gradient enables us to deduce the large-scale geometry of the magnetic flux rope and the interplanetary coronal mass ejection (ICME). Real-time monitoring of the precursory anisotropy which has often been observed at the Earth preceding the arrival of the ICME accompanied by a strong shock may provide us with useful tools for forecasting the space weather with a long lead time. By using a self-supporting power system utilizing the solar panels and batteries, we keep a 25 m^2 muon hodoscope running at the Mt. Norikura Cosmic Ray Observatory as an important component detector of the GMDN. The total power consumption of this detector has been suppressed as low as 36 Watt by replacing all amplifier boards with those using CMOS ICs and by introducing a new recording system using the FPGA. This new system, in which the observation has been automatically car-

ried out by a PC connected with the internet, also enabled us to monitor the data on the real-time basis for the space weather study.

The Sun is the nearest site to the Earth capable of accelerating particles up to high energies. When the Sun becomes active, flares are frequently observed on its surface. The flare accelerates the proton and ion to high energy and they are detected on the Earth soon after the flare. Among the particles generated by the flare, high energy neutrons provide the most direct information about the acceleration mechanism as they come straight from the flare position to the Earth without deflected by the magnetic field.

Observation of solar neutron has been conducted at the Norikura Observatory since 1990. Neutron is used to clarify the acceleration mechanism of high energy particles in association with solar flares, because the neutron is not reflected by the interplanetary magnetic field. The $64m^2$ solar neutron telescope was constructed in 1996, which is one of 7 solar neutron telescopes deployed at different longitudes to make up a network of 24 hour observation of solar neutrons. The Norikura $64m^2$ solar neutron telescope has been operated by solar batteries and windmills since 2004.

This collaborative work has started since fiscal 2007 succeeding to the previous project titled 'Observation of solar neutrons by using a new method.' Although solar cycle 24 has started since 2008, the solar activity has continued to be inactive, and no new solar neutron event has been detected by the network since 2006. The last solar neutron event was on September 7, 2005. This event is unique because it indicates ions were accelerated or trapped at the acceleration region longer than electrons. The summary of 11 solar neutron events detected until 2005 shows that it may not be probable that a very efficient acceleration such as the shock acceleration works for ions at solar flares. This is given by deriving the energy spectrum of neutrons at the solar surface for each solar neutron event with a power law. Power law indices obtained span from 3 to 7. The energy spectrum of the original ions is softer than that of neutron. Therefore an efficient acceleration has not been detected by the observation of solar neutrons so far.This work continues in solar cycle 24 to accumulate more events to obtain definite results related with particle acceleration at the solar surface.

Another effort aiming at observation of highest-energy solar cosmic rays started at the Norikura Observatory. The Sun is an accelerator of protons and electrons in the universe. In association with large solar flares, protons and electrons are accelerated into high energies. It is known that protons are accelerated over 50 GeV in the largest solar flares[24]. These high energy particles produce the Ground Level Enhancement(GLE). In order to understand the acceleration mechanism of protons, we have prepared several solar neutron telescopes at the high altitude laboratories in the world. They are located at Gornergrat (3,135m), Mt. Aragats in Armenia (3,200m), Tibet (4,200m), Mauna-Kea in Hawaii (4,200m), Mt. Chacaltaya in Bolivia (5,250m), and at Mt. Sierra Negra in Mexico (4,900m). We have constructed a solar neutron telescopes at Mt. Norikura Cosmic Ray Observatory (2,770m) in 1990 and operated it until 2004[21]. However due to the lack of power supply during the winter time since 2005, the first solar neutron telescope ($36\ m^2$) has not been operated. From 2008 to 2009, we have decided to make a new solar neutron telescope to utilize the large amount of the plastic scintillator ($0.5m^3$), as shown in Fig. 3, left at the observatory.

Fig. 3. 0.5-m^2 plastic scintillation counter for a new neutron telescope.

The new solar neutron telescope with use of the recycled plastic scintillator consists of main target where neutrons are converted into protons and of the anti-counters surrounding the target. The signals of neutrons converted into protons are observed by using one photomultiplier from bottom side to reduce the electric power. Furthermore a lead plate with the thickness of 1cm is located over the target and the lead plate is sandwiched by two layers of the plastic scintillator to identify gamma-rays from neutrons. The new solar neutron telescope has a function to reject charged particles with an efficiency of 90%. Therefore the new solar neutron telescope has capability of 1/3 of the $64m^2$ large solar neutron telescope located at the same place. We are waiting large solar flares over our detectors.

In addition to the long-term cosmic-ray observations mentioned above, various kinds of short-dated experiments are carried out every year taking an advantage of the high altitude of the observatory.

High-energy radiations from thunderstorms have been observed by flight measurement, high-mountain observations and ground-based measurement. There are two types of those radiations associated with thunderstorms. One is short-duration radiations with duration of 1 ms or less. The other is long-duration emissions lasting for a few seconds to a few minutes, or a few tens of minutes on rare occasions. It is believed that both emissions originate from electrons accelerated in strong electric fields formed in lightning and thunderclouds. However, compared with the former, the latter has remained less understood due to lack of a large sample of observations.

To investigate production mechanism of long-duration emissions and the relevant electron acceleration, we installed at Norikura Cosmic-ray Observatory a radiation detection system and environmental sensors to measure light and electric fields during 2008−2010. The radiation system consists of a spherical NaI scintillator and a thin plastic scintillator that is placed just above the NaI counter. During the period, the system detected one long-duration bursts as well as five short-duration events.

Figure 4 (left) shows the long-duration event observed during thunderstorms on 2008 September 20[25]. The event lasted for 90 sec. Figure 1(right) represents an observed photon spectrum extending from 10 keV to 10 MeV. This indicates that electrons can be accelerated to at least 10 MeV in a quasi-stable thundercloud electric field. In addition, we compared the observed spectrum with model ones, and concluded that a gamma-ray source is located 60 m−130 m (at 90% confidence level) apart from our detector. Given these results, the observed emission was found to consist of not only gamma rays but also electrons. This was the first simultaneous observation of gamma rays and electrons in long-duration bursts

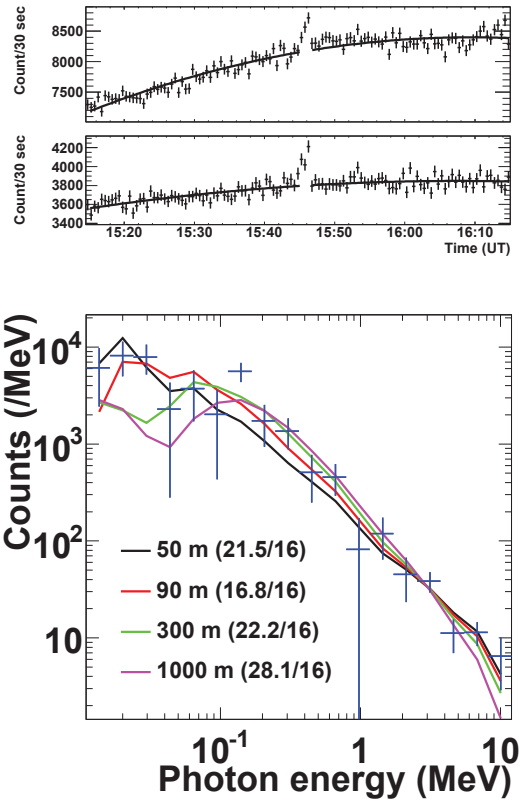

Fig. 4. (Left) Count rates per 30 sec observed by the >10 keV NaI scintillator (top) and > 100 keV plastic one (bottom). (Right) The photon spectrum observed by the NaI scintillator.

Observation of night sky background is carried out at Mt.Norikura for basic study of ultra high energy cosmic-ray physics.

The JEM-EUSO mission is going on in order to study ultra high energy cosmic rays (UHECRs), especially above 10^{20}eV. A 2.5m telescope with 60° FoV will be attached to the International Space Station in 2017 and detect fluorescence in near UV band from extensive air showers induced by UHECRs. Observation of UHECRs from a satellite orbit has not been done yet, so that the knowledge of background light intensity is important to realize the observation. We have measured it from a balloon altitude, but the opportunity is limited. We started the background measurement at Mt.Norikura.

Two 1 inch multi-anode photomultipliers (MAPMTs) developed for EUSO was used with UV filters. The center wavelengths of the filters were 337, 350, 358, 370, 380, 391, 400nm with 10nm band width. In addition BG3 filter was used to detect light in wider range from 330nm to 430nm. The MAPMTs were collimated to 7° FoV. The data was taken with the photon counting method.

We have observed several nights for three years. The intensity at zenith was almost constant at 600-800 photons/ns sr m^2 for BG3 filter. The spectral intensity was about 1.5-2 times larger than those measured at La Palma and Namibia. The estimated portion of star light and zodiacal light was ∼30% and artificial light and nightglow at upper atmosphere may be the main components at Mt.Norikura.

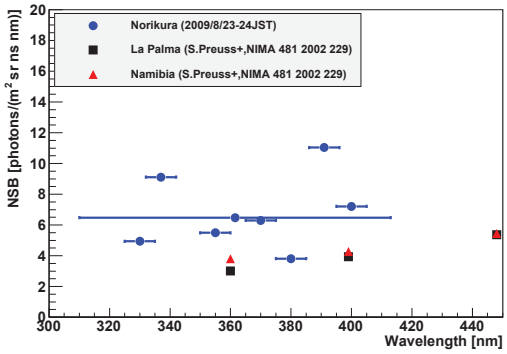

Fig. 5. Spectrum of night sky background measured at Mt.Norikura compared with those at La Palma and Namibia.

Environmental Study

One of the interesting topics is atmospheric environment especially relating with atmospheric aerosol particles and water soluble gases. The cosmic ray observatory at Mt. Norikura provides us very unique opportunity for the observations of atmosphere at free-tropospheric conditions with its high altitude, AC power supply at the site, accommodation facility,

and easy accessibility. From year 2000 to 2007, we conducted continuous monitoring (mostly mid-May to mid-October) of meteorological parameters, number-size distribution of aerosols, aerosol chemical composition, ozone and radon concentrations, and column amount of aerosols from sky radiometer and ceilometers. We also collected rain, fog, water-condensed aerosol samples. These samples combined with other observed parameters were used in publications in the following subjects[26, 27, 28]:

(1) Polluted air pumping effects over central Japanese Alps in summer
(2) Seasonal variation of aerosol chemistry in free troposphere
(3) Vertical profiles of aerosols and clouds near the top of the atmospheric boundary layer.

Ceilometer (lidar with small output energy) was installed in summer 2002, and was operated in 6 summer seasons. The aerosol and cloud profiles near the top of the atmospheric boundary layer have been observed. Some events of Asian dust were detected.

Observations of total ozone and UV solar radiation with Brewer spectrophotometer on the Norikura mountains are also made[29, 30, 31]. Aerological Observatory started "Observations of total ozone and UV solar radiation with Brewer spectrophotometer at Norikura mountains" as a joint project with Institute for Cosmic Ray Research (ICRR), University of Tokyo at the Norikura Observatory of ICRR (Brewer site: 36.11 N, 137.56 E, 2,772 m a.s.l.), locating at the Northern Japanese Alps in every summer seasons from 2009 (Ito *et al.*: 2011). Purpose of this study is based on the concept of developing Regional Brewer Calibration Centre in Asia and study of total ozone, total sulfur oxide and global/diffuse UV included solar radiation on the high mountains. Observation results by using Brewer spectrophotometers and other instruments for the observation period of three summer seasons of recent three years between 2009 to 2011 are summarized as follows;

(1) Daily means of ds O_3 (total ozone) at Norikura for the observation periods were approx. 280 to 290 m atm-cm and were running on the lower values of approx. -3 to -6% compared to the value at Tsukuba (36.06 N, 140.13 E, 39 m a.s.l.) at almost same latitude. Day-to-day variations at Norikura were also small against Tsukuba. On the other hand, daily mean of ds SO_2 (total sulfur oxide) values were not recognized at Norikura.

(2) Absolute calibration of Brewers for ds O_3 and ds SO_2 observations could be carried out within the range of air mass from 7.928 (maximum) to 1.028 (minimum) at Norikura in the clear day. O_3 and SO_2 Extra-Terrestrial Coefficients (=ETC) of Brewers could be produced as about 10 samples satisfying the condition of "R^2¿0.9997" by the calibrations. As an example of the calibration in 2011, the average of O_3 ETC of Brewers was identical within 1% to the currently used coefficient.

(3) In comparison to the data acquired at Tsukuba, the average of daily total GL_{UV} (global UV, e.g. CIE) for the observation periods indicated the intensities of approx. +23 % in 2009 to -6 % in 2011. The low intensity in 2011 was due to the bad weather on the Norikura Mountain. In the case of clear days, the GL_{UV} at Norikura indicated high intensities of approx. +35 to +52 % against the values at Tsukuba. On the other hand, the GL_{UV} increased in the short wavelength range at Norikura against the average at Tsukuba. The altitudinal increasing rate of GL_{UV} in the clear day indicated the calculated amounts of approx. +13 to +18 % per 1,000 m.

This joint project had been clarifying the low total O_3, high UV in clear day, low turbidity and etc. at Norikura against the value at Tsukuba. Those environmental conditions are useful for the intercomparison and the absolute calibrations with Brewers. The continuous observations with Brewers and other instrument are very important for the clarification of the seasonal variation and the coefficient trends.

Botanical Study

Effects of snow cover on pine shrub Pinus pumila in the alpine region of Mt. Norikura

High mountainous habit is one of the most severe habits for plant life and sometimes dwarf shrubs cannot survive. In the alpine regions of Japan, the dwarf shrub Pinus pumila (Japanese name : Haimatsu) forms communities together with small alpine plants, whereas dwarf shrubs occur only in the transition zone between the alpine region and the subalpine forest in Europe and North America. This characteristic of alpine vegetation is considered to be owing to winter heavy snow in the alpine regions of Japan. The purpose of this study is to elucidate how snow cover protects Haimatsu from winter environmental stresses in the alpine region of Mt. Norikura.

Study site

Tree height of Haimatsu and snow depth differ greatly as a result of slight difference in topography. Two site of the study area were selected. (i) site P (wind-protected) and (ii) site E (wind-exposed). At site P, mean tree height was 1.1 m. There was a lot of snow accumulation and Haimatsu was almost entirely covered with snow during the winter. Needle browning and death occurred rarely. At site E, mean tree height was 0.4 m. Snow accumulation was minimal, and Haimatsu was not entirely covered with snow. Needle browning and death was observed frequently.

Winter needle death in Haimatsu[32]

At site E, the browning and death of needles of Haimatsu occurred mainly in early spring at the point where the shoot protrudes from the snowpack. They are thought to be caused by excessive water loss due to mechanical damage to the cuticle and/or to a thinner cuticle. However, needle browning and death in Haimatsu were not related to mechanical damage of the cuticle but might be due to changes in the quality and structure of the cuticle wax and resultant increase in water loss from needle cells.

Photosynthetic capacity in Haimatsu[33]

At site E, needles of Haimatsu had lower biomass, nitrogen, Rubisco (enzyme) and cell wall per unit area, and had higher photosynthetic capacity and shorter needle life-span than Haimatsu at site P. These results suggest that Haimatsu at wind-exposed site produces needles at low cost with high productivity to compensate for a short leaf life-span which may be imposed by wind stress when needles appear above the snow surface in winter.

Bibliography

[1] K. Munakata, S. Yasue, C. Kato, J. Kota, M. Tokumaru, M. Kojima, A. A. Darwish, T. Kuwabara and J. W. Bieber, "On the cross-field diffusion of galactic cosmic rays into the magnetic flux rope of a CME", *Advances in Geosciences*, 2, 115-124, eds. W. H. Ip and M. Duldig (World Scientific Publishing Co., USA), (2006).

[2] T. Kuwabara, J. W. Bieber, J. Clem, P. Evenson, R. Pyle, K. Munakata, S. Yasue, C. Kato, S. Akahane, M. Koyama, Z. Fujii, M. L. Duldig, J. E. Humble, M. R. Silva, N. B. Trivedi, W. D. Gonzalez and N. J. Schuch, "Real-time cosmic ray monitoring system for space weather", *Space Weather*, 4, S08001-1 10, (2006).

[3] M. R. Da Silva, A. Dal Lago, E. Echer, A. de Lucas, W. D. Gonzalez, N. J. Schuch, K. Munakata, L. E. A. Vieira, and F. L. Guarnieri, "Muon and neutron observations in connection with the corotating interaction regions", *Adv. Space Res.*, 40, pp348-352, (2007).

[4] Y. Okazaki, A. Fushishita, T. Narumi, C. Kato, S. Yasue, T. Kuwabara, J. W. Bieber, P. Evenson, M. R. Da Silva, A. Dal Lago, N. J. Schuch, Z. Fujii, M. L. Duldig, J. E. Humble, I. Sabbah, J. Kta and K. Munakata, "Drift effects and the cosmic ray density gradient in a solar rotation period: First observation with the Global Muon Detector Network (GMDN)", *Astrophys. J.*, 681, 693-707, (2008).

[5] T. Kuwabara, J. W. Bieber, P. Evenson, K. Munakata, S. Yasue, C. Kato, A. Fushishita, M. Tokumaru, M. L. Duldig, J. E. Humble, M. R. Silva, A. Dal Lago, and N. J. Schuch, "Determination of ICME Geometry and Orientation from Ground Based Observations of Galactic Cosmic Rays", *J. Geophys. Res., 114*, A05109-1 10, doi:10.1029/2008JA013717, (2009).

[6] A. Fushishita, T. Kuwabara, C. Kato, S. Yasue, J. W. Bieber, P. Evenson, M. R. Da Silva, A. Dal Lago, N. J. Schuch, M. Tokumaru, M. L. Duldig, J. E. Humble, I. Sabbah, H. K. Al Jassar, M. M. Sharma, and K. Munakata, "Precursors of the Forbush Decrease on 2006 December 14 observed with the Global Muon Detector Network (GMDN)", *Astrophys. J.*, 715, 1239-1247, (2010).

[7] A. Fushishita, Y. Okazaki, T. Narumi, C. Kato, S. Yasue, T. Kuwabara, J. W. Bieber, P. Evenson, M. R. Da Silva, A. Dal Lago, N. J. Schuch, M. Tokumaru, M. L. Duldig, J. E. Humble, I. Sabbah, J. Kta, and K. Munakata, "Drift effects and the average features of cosmic ray density gradient in CIRs during successive two solar minimum periods", *Advances in Geosciences*, eds. W. H. Ip and M. Duldig (World Scientific Publishing Co., USA), 21, 199-210, (2010).

[8] M. Tokumaru, M. Kojima, K. Fujiki, K. Munakata, T. Kuwabara and K. Marubashi, "Relation between loop-shaped interplanetary disturbances and the magnetic flux rope", *Advances in Geosciences*, eds. W. H. Ip and M. Duldig (World Scientific Publishing Co., USA), 21, 21-32, (2010).

[9] M. Rockenbach, A. Dal Lago, W. D. Gonzalez, K. Munakata, C. Kato, T. Kuwabara, J. W. Bieber, N. J. Schuch, M. L. Duldig, J. E. Humble, H. K. Al Jassar, M. M. Sharma, and I. Sabbah, "Geomagnetic Storms Precursors Observed from 2001 to 2007 with the Global Muon Detector Network GMDN", *Geophys. Res. Lett.*, 38, L16108-1 4, doi:10.1029/2011GL048556, (2011).

[10] "Solar neutron events of OctoberNovember 2003", Watanabe, K. *et al.*, Astrophys. J., **636**, 1135–1144, 2006.

[11] " Solar neutron events in association with large solar flares in November 2003", Watanabe, K. *et al.*, Adv. Space Res., **38**, 425–430, 2006.

[12] "Long-lived solar neutron emission in comparison with electron-produced radiation in the 2005 September 7 solar flare", Sako, T. *et al.*, Astrophys. J., **651**, L69–L72, 2006.

[13] " Highly significant detection of solar neutrons on 2005 September 7", Watanabe, K. *et al.*, Adv. Space Res., **39**, 1462–1466, 2007.

[14] " A solar neutron telescope in Tibet and its capability examined by the 1998 November 28th event", Muraki, Y. *et al.*, Astroparticle Phys., **28**, 119–131, 2007.

[15] " Simultaneous detection of high-energy solar neutrons and protons at Chacaltaya observatory on April 15, 2001", Muraki, Y. *et al.*, in Proc. 30th Int. Cosmic Ray Conf, Merida, **1**, 25–28, 2007.

[16] " Search for solar neutrons associated with series of X-class flares during the declining period of solar cycle 23", Matsubara, Y. *et al.*, in Proc. 30th Int. Cosmic Ray Conf, Merida, **1**, 29–32, 2007.

[17] " Ion acceleration and neutral emission mechanisms for 2005 September 7 flare", Watanabe, K. *et al.*, in Proc. 30th Int. Cosmic Ray Conf, Merida, **1**, 45–48, 2007.

[18] " Emission profile of solar neutrons obtained from the ground-based observations for the 7 September 2005 event", Sako, T. *et al.*, in Proc. 30th Int. Cosmic Ray Conf, Merida, **1**, 53–56, 2007.

[19] " Energy spectrum for the solar neutron event of September 7 2005, derived from the SNT at Sierra Negra", Gonzalez, L. X. *et al.*, in Proc. 30th Int. Cosmic Ray Conf, Merida, **1**, 57–60, 2007.

[20] " Status of the world-wide network of solar neutron telescopes in solar cycle 24", Matsubara, Y. *et al.*, in Proc. 31st Int. Cosmic Ray Conf, Lodz, **1**, On Conference homepage, 2009.

[21] " Detection of high-energy solar neutrons and protons by ground level detectors on April 15, 2001", Muraki, Y. *et al.*, Astropart. Phys., **29**, 229–242, 2008.

[22] " Solar neutron events as a tool to study particle acceleration at the Sun", Valdes-Galicia, J. F. *et al.*, Adv. Space Res., **43**, 565–572, 2009.

[23] " Physics of ion acceleration in the solar flare on 2005 September 7 determines γ-ray and neutron production", Watanabe, K. *et al.*, Adv. Space Res., **44**, 789–793, 2009.

[24] " Observation of solar neutrons associated with the large flare on 1991 June 4", Muraki, Y. *et al.*, ApJ, **400**, L75-L78 , 1992.

[25] " Observation of an energetic radiation burst from mountain-top thunderclouds", H. Tsuchiya *et al.*, Phys. Rev. Lett. **102**, 255003 (2009), Citation Index:13.

[26] Nishita, C., K. Osada, K. Matsunaga, Y. Iwasaka, e, J. Geophys. Res., **113**, D06202, doi:10.1029/2007JD009302, 2008.

"Nucleation mode particles in up-slope valley winds at Mt. Norikura, Japan: implications for the vertical extent of new particle formation events in the lower tropospher", Nishita, C., K. Osada, K. Matsunaga, Y. Iwasaka, J. Geophys. Res., **113**, D06202, doi:10.1029/2007JD009302, 2008.

[27] "Temporal variation of water-soluble ions of free tropospheric aerosol particles over central Japan", Osada, K., Kido, M., Nishita, C., Matsunaga, K., Iwasaka, Y., Nagatani, M., Nakada, H., Tellus, **59B**, 742-754, 2007.

[28] "Number-size distributions of free tropospheric aerosol particles at Mt. Norikura, Japan: effects of precipitation and air-mass transportation pathways", Nishita, C., K. Osada, K. Matsunaga, Y. Iwasaka, J. Geophys. Res., 112, doi:10.1029/2006JD007969, 2007.

[29] " Observations of total ozone and UV solar radiation with Brewer spectrophotometers on the Norikura mountains in 2009.", Ito, M., M. Takano, H. Oguri, M. Takita, H. Shimodaira and H. Ishitsuka, Jour. of the Aerological Observatory, **69**, 41-54 2011.

[30] " Observations of total ozone and UV solar radiation with Brewer spectrophotometers on the Norikura mountains, Northern Japanese Alps, from 2009.", Ito, M., S. Shimizu, Y. Noto, T. Shimamura, M. Takano, M. Takita, H. Shimodaira and H. Ishitsuka, The 13th WMO Biennial Brewer Workshop, Beijing, China in 2011, 2011.

[31] " Total ozone and UV solar radiation with Brewer spectrophotometers at Norikura of Northern Japanese Alps, in recent three years.", Ito, M., S. Shimizu, Y. Noto, T. Shimamura, M. Takita, H. Shimodaira and H. Ishitsuka, Jour. of the Aerological Observatory, **70**, in contribution.

[32] "Needle browning and death in Pinus pumila in the alpine region of central Japan were not related to mechanical damage of cuticle and cuticle thickness.", Nakamoto A., Ikeda T., Maruta E., Can. J. For. Res. 42, 167-178 (2012).

[33] "Needle traits of an evergreen, coniferous shrub growing at wind-exposed and protected sites in a mountain region: does Pinus pumila produce needles with greater mass per area under wind-stress conditions?", Nagano S., Nakano T., Hikosaka K and Maruta E., Plant Biology 11(Suppl.1), 94-100, (2009).

AKENO OBSERVATORY

Introduction

The Akeno Observatory is situated in Akeno of Hokuto-city, 20 km northwest of Kofu and 130 km west of metropolitan Tokyo. The location is at the longitude of 138.5°E and the latitude of 35.8°N. The altitude is ∼900 m above sea level. It was established in 1977 as a research center for air shower studies in the very high energy region, and it has been administered by the ICRR as a facility of joint-university-use.

Akeno Air Shower Experiments

The Akeno Air Shower Experiment started in 1979 with an array covering 1 km^2 area (the 1 km^2 array, see Fig.1). The array was enlarged to 20 km^2 in 1984 and was gradually expanded to Akeno Giant Air Shower Array (AGASA) of approximately 100 km^2 area by 1990. The AGASA was built

Fig. 1. Aerial View of Akeno Observatory and 1 km^2 Array Area

to detect Ultra-High Energy Cosmic Rays (UHECRs) in the energy range of 10^{20} eV.

One of the distinctive features of Akeno experiments is that the measurements were made over five decades of energies well covering 10^{15} eV - 10^{20} eV by using both the surface detector for electromagnetic component, and the shielded detector for muon component (Fig.2). The wide energy coverage was accomplished by the arrays of scintillation detectors of various inter-detector spacings from 3 m to 1 km and with different triggering conditions. This feature of Akeno air shower measurement is well demonstrated in Fig.3, in which the spectra from Akeno 1 km^2 array for $10^{14.5}$ eV - $10^{18.8}$ eV [24] and AGASA for $10^{18.5}$ eV - $10^{20.3}$ eV [25] are plotted.

AGASA

The AGASA was composed of 111 surface detectors, each with plastic scintillator of 2.2 m^2 area and 5 cm thickness. The counters were deployed with ∼1 km spacing covering the

Fig. 2. One of the muon detector housings with concrete shielding.

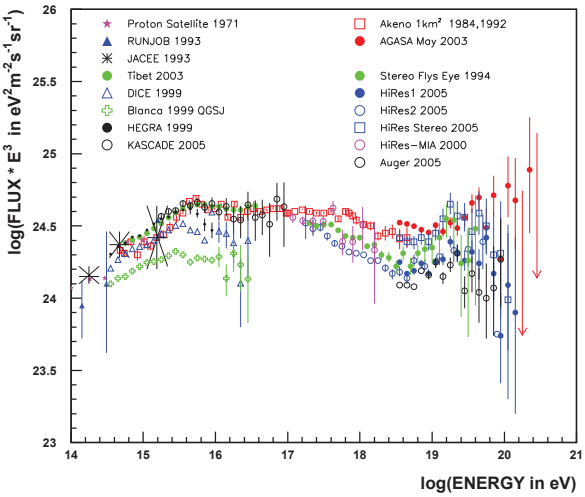

Fig. 3. Akeno energy spectrum measurements for 10^{15} eV - 10^{20} eV.

ground area of about 100 km^2 in the suburban area of Akeno, outside of the observatory campus. All counters were connected with optical fibers for the timing measurement and digital data transfer to the observatory. The AGASA served as the largest air shower array in the world since its commissioning in 1990 until it stopped data taking in January 2004, when the construction of the succeeding experiment, Telescope Array (TA), started in Utah. It was dismantled in 2007 together with other Akeno air shower arrays.

An exposure of 5.8 × 10^{16} m^2 s sr above 10^{19} eV was accumulated by AGASA in 13 years of operation. Extensive air showers with zenith angles smaller than 45° and with core locations inside the array area were used for the analysis. The AGASA reported an extension of the energy spectrum beyond the predicted Greisen-Zatsepin-Kuzmin (GZK) cutoff in 1998 [26] and a total of eleven UHECR events were observed above

*[24] M. Nagano et al., J. Phys. **G10**, 1295 (1984); M. Nagano et al., J. Phys. **G18**, 423 (1992).
*[25] M. Takeda et al., Astropart. Phys. **19**, 447 (2003).
*[26] M. Takeda et al., Phys. Rev. Lett. **81**, 1163 (1998).

10^{20} eV by 2003.

Measurement of UHECRs

Since the AGASA measurement in 1998, High Resolution Fly's Eye (HiRes) [27], Pierre Auger Observatory (PAO) [28], and Telescope Array (TA) [29] measured the energy spectra of UHECRs with higher statistics.

The HiRes observed the UHECR using the fluorescence telescope. The PAO and TA measure the spectrum using the surface array consisting of either water tanks (PAO) or plastic scintillators (TA), but the energy scale of the array is determined by the fluorescence telescope using a subset of events observed by the fluorescence telescope and surface array at the same time. The adoption of the energy scale by the fluorescence telescopes is based on its small dependence on the air shower simulation.

The energy spectra above 10^{18} eV by AGASA and other experiments are compiled and compared by the working group represented by UHECR experiments in the UHECR-2012 symposium held at CERN for Feb. 13th - 16th, 2012 [30]. The result is plotted in Fig.4 with the energy scale of each experiment adjusted to a reference energy, which is set halfway between the PAO and TA/HiRes. Following factors were applied for the energy scale; $\times 1.10$ for PAO, $\times 0.91$ for TA and HiRes, $\times 0.65$ for AGASA and $\times 0.56$ for Yakutsk.

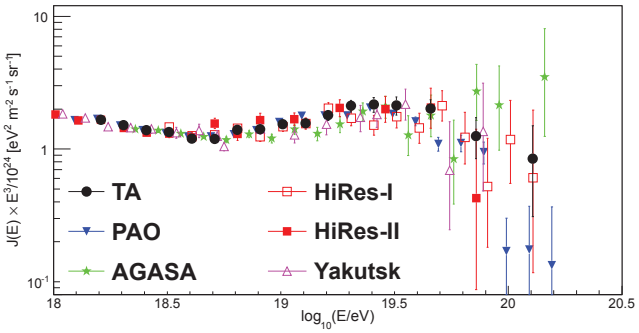

Fig. 4. Recent compilation of UHECR energy spectra. The energy scale of each experiment is adjusted as described in the text.

As seen in Fig.4, the overall agreement between experiments is good, and a "dip" structure was seen around $10^{18.7}$ eV by all experiments. The HiRes, PAO and TA confirmed a strong flux suppression above approximately $10^{19.7}$ eV. Although the AGASA spectrum does not demonstrate the cutoff structure, the number of events above 10^{20} eV became only two after the energy rescaling, making the claim of the extended spectrum statistically insignificant. The estimate of systematic uncertainty of the energy measurement is approximately 20% for all the experiments, and rescalings for the TA/HiRes and PAO are within this limit. Rescaling of the surface array energy, $\times 0.65$ for AGASA and $\times 0.56$ for Yaktsuk, indicates that there exist larger systematic uncertainties than originally estimated by running the air shower simulation. This difference of energy scale obtained by the surface array and by the fluorescence telescope remains as a basic question in the understanding of the air shower phenomena.

*27 R.U. Abbasi et al., Phys. Rev. Lett. **100**, 101101 (2008).
*28 J. Abraham et al., Phys. Lett. **B685**, 239 (2010).
*29 T. Abu-Zayyad et al., arXiv:1205.5067v1 (2012).
*30 http://indico.cern.ch/conferenceDisplay.py?confId=152124

Recent Research Activities

The study of UHECRs by AGASA in Akeno was succeeded by the Telescope Array (TA) experiment in Utah, USA since 2008. After the cessation of AGASA, the Akeno observatory has been used for small scale cosmic ray experiments, astrophysical observations and as a test and maintenance facility of TA by the ICRR and university researchers. Research activities in JFY 2011 (April 2011 - March 2012) are described in the following.

Research and development for the Telescope Array observation in Utah by the TA collaboration

All the fluorescence imaging cameras and a part of the surface detectors of TA were assembled in the Akeno observatory by the TA collaboration team. The detectors were tested in Akeno and shipped to the Utah observation site for the installation. All the unit mirrors of the TA fluorescence telescope were tested in Akeno and the atmospheric monitoring lidar of TA using YAG laser was developed in Akeno. In JFY 2011, a part of the experimental hall was prepared for the test and temporary storage of KAGRA gravitational antenna equipment.

Observation by the multi-color imager for transients, survey and monstrous explosions (MITSuME) by N. Kawai (Tokyo Institute of Technology) et al.

One of the three MITSuME robotic telescopes was installed in the Akeno observatory in 2003 on the roof of the unused concrete muon house. The telescope has an aperture of 50 cm, an FOV of 28' $\times$ 28' and is equipped with a tricolor CCD camera capable of $g'R_CI_C$-bands photometry. It is operated remotely from the Tokyo Tech using dedicated ADSL connections. Upon receiving a GRB alert from Swift or Fermi satellite, it quickly directs the telescope (9°/s maneuverability) toward the GRB direction, and makes a prompt observation of the GRB and its afterglow. Since its commissioning in 2004, the MITSuME telescope in Akeno has been making more than $\sim$10 GRB follow-up observations every year, and detected more than 10 GRB afterglows. In JFY 2011, the MITSuME was triggered by 12 GRBs and succeeded to observe afterglows of 3 GRBs, 110530A, 110921A and 111228A [31]. It has been joining the multi-wavelength campaign for observing AGNs and other transient objects as well.

Observation of galactic cosmic rays by large area muon telescope by S. Shibata (Chubu University) et al.

Four layers of proportional counter telescopes, each with 25 m^2 area, were installed in three muon houses in Akeno (Fig.2) and have been continuously measuring the cosmic ray muons since 2003. The mode energy of the primary cosmic rays is approximately 25 GeV corresponding to 2m thick concrete ceiling of the muon house and the latitude of Akeno observatory. The measurement in Akeno is combined with a simultaneous measurement in Ooty, India, and the modulation

*31 GCN Circular No.1768, 12410 and 12048.

effects of galactic cosmic rays by the solar activity such as the Forbush decrease and its precursor have been continuously monitored [32]. In JFY 2011, the observation was resumed in September after 6 months of discontinuity caused by the Great East Japan Earthquake on March 11th, 2011.

Research and development for a small atmospheric Cherenkov telescope in Akeno observatory by T. Yoshikoshi, M. Ohishi (ICRR) and K.Nishijima (Tokai University) et al.

A small alt-azimuth telescope is being setup in Akeno for prototype tests with atmospheric Cherenkov observations of gamma rays [33]. Refurbishing of the telescope control system, the unit mirror and optics was made in 2010 and 2011. A test of a prototype camera using silicon photomultiplier is planned in JFY 2012.

*[32] T. Nonaka.et al, Proc. of the 29th ICRC, **1**, 363-366 (2005).
*[33] T. Yoshikoshi et al., Proc. of the 32nd ICRC, Beijing, **9**, 226-229 (2011).

KAMIOKA OBSERVATORY

Kamioka observatory is located at 1000 m underground (2700 m water equivalent) in the Kamioka Mine, Gifu prefecture, about 200 km west of Tokyo. The observatory was established in 1995 in order to operate Super-Kamiokande. The underground laboratories are located under Mt.Ikeno-yama and accessible to the experimental site through a 1.7 km horizontal tunnel. The observatory also has surface research buildings and a dormitory located at the distance of 15 minutes drive from the entrance of the mine.

The Super-Kamiokande experiment had discovered neutrino oscillations through the observations of atmospheric and solar neutrinos (see the section for Neutrino and Astroparticle Division). The atmospheric neutrino oscillation was confirmed by the K2K accelerator neutrino experiment, which was conducted between 1999 and 2004. A new long baseline neutrino oscillation experiment (the T2K experiment) using a high intensity beam, 50 times of the K2K neutrino beam, by the J-PARC proton accelerator has started in 2009. In 2011, the experiment has discovered 6 ν_e appearance events indicating non-zero θ_{13} which was as yet determined the last neutrino oscillation parameter.

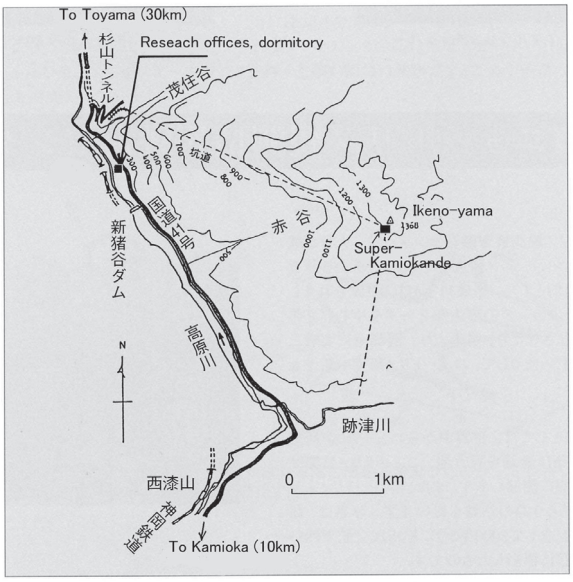

Fig. 1. Map of Kamioka observatory.

The low cosmic ray flux and low seismic noise environment in the underground site enables us to conduct various researches. There is a 100 m long laser interferometer, which is a proto-type of the planned 3 km gravitational wave antenna (see section of Astrophysics Gravity Division). Using the low radioactive background environment in the Kamioka Mine, A dark matter experiment, called XMASS is operating. The XMASS group has constructed a 800kg liquid xenon detector and start commissioning run in late 2010. The R&D study of a tracking type detector for dark matter search by the Kobe University group (the NEWAGE experiment) has also been performed in an underground laboratory. The commissioning run of the CANDLE experiment (Osaka Univ.), a double beta decay experiment is now conducted. The study to improve the neutrino detection sensitivity by adding gadolinium to Super-Kamiokande is on going. Especially in 2010, a new 200 ton test tank dedicated for the R&D study of the gadolinium project was completed. In order to support those experiments and also related R&D works, the Observatory is equipped with low background Germanium detector, ICP-MS and so on to measure extremely low radioactive backgrounds.

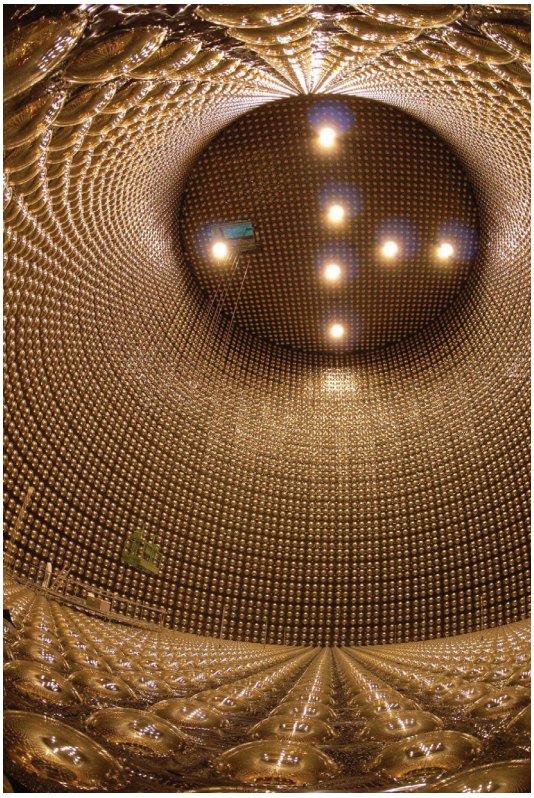

Fig. 2. Super-Kamiokande detector.

RESEARCH CENTER FOR COSMIC NEUTRINOS

The Research Center for Cosmic Neutrinos (RCCN) was established in April, 1999. The main objective of this center is to study neutrinos based on data from various observations and experiments. In order to promote studies of neutrino physics, it is important to provide the occasion to discuss theoretical ideas and experimental results on neutrino physics. Therefore, one of the most important practical jobs of this center is the organization of neutrino-related meetings. On March 29, 2012, we hosted this year's domestic neutrino workshop, whose topic was "θ_{13}". About 35 physicists participated in this meeting.

Members of this center have been involved in the Super-Kamiokande and T2K experiments, carrying out researches in neutrino physics. (Please see the Super-Kamiokande and T2K pages for the scientific results.) Atmospheric neutrino data from Super-Kamiokande give one of the most precise pieces of information on neutrino oscillations. With increased data, it is more important to have better predictions of the neutrino flux. Therefore, in addition to data analysis of the data from these experiments, we work on calculating the atmospheric neutrino flux. In 2011, we updated the calculated flux for the neutrinos with the energies below 1 GeV.

It is important that the general public knows about the achievements of the present science. For this reason, we hold public lectures every year. From FY2009, two public lectures per year have been co-sponsored by this Institute and the Institute for the Physics and Mathematics of the Universe. The spring lecture is co-organized by RCCN and the Public Relation Office of ICRR. Unfortunatelly, due to the effect of the Tohoku Earthquake, the public lecture in the spring of 2011 was canceled.

RCCN, together with the computer committee of ICRR, is in charge of operating the central computer system in ICRR. It had been highly utilized for the analyses and simulations of various cosmic-ray physics. In the summer of 2011, the system was operated with the reduced number of CPU's, due to the shortage of the electricity available in the Tokyo area. In addition, a backup system for the electricity was installed in order to keep running the computer system, even for an unexpected power shutdown. RCCN also supports the users of the computer system, including physicists working outside ICRR.

Since 2004, RCCN has been acting as a body for accepting the ICRR inter-university programs related to the low-background underground facility in the Kashiwa campus. The facility is currently equipped with 4 Ge detectors mainly for the measurements of cosmic radioactive isotopes. The scientific activities that are related to this facility is described elsewhere.

APPENDICES

A. ICRR Workshops and Ceremonies

Italy-Japan workshop

Date: Oct 4-5st, 2011
Place: ICRR, Kashiwa, Chiba, Japan

Outline: In order to conduct research on the next generation gravitational wave detector, LCGT (now KAGRA) and ET (Einstein Telescope project in EU) exchanged technical information to develop cryogenic techniques underground with appropriate anti-vibration system. This workshop was partially supported by Italian embassy and advertised by the embassy's report.

Participants: 31 from Japan, 7 from Italy, 1 from France.

B. ICRR Seminars

1. Apr 27, 2011: Kimihiro Okumura (ICRR), "Physics Results from the first year of the T2K run"
2. May 20, 2011: Ken-ichi Sakai (KEK), "Measurement of cosmic-ray antiproton spectrum at solar minimum with a long-duration balloon flight in Antarctica"
3. Jun 1, 2011: Masahiro Teshima (ICRR), "Very High Energy Gamma Ray Astronomy and Future Prospects"
4. Jun 8, 2011: Masanori Iye (NAOJ), "Subaru Telescope, Adaptive Optics, and Thirty Meter Telescope"
5. Jun 15, 2011: Masato Shiozawa (ICRR), "The latest results from the T2K long baseline neutrino oscillation experiment"
6. Jun 22, 2011: Yasuo Tanaka (Max Planck Institute), "Relativisitically Broad Iron-K Line"
7. Jun 29, 2011: Hideaki Takabe (Institute of Laser Engineering, Osaka University), "Laser Astrophysics: Topics mainly on SNR Shock and Particle Acceleration"
8. Jul 6, 2011: Marco Casolino (RIKEN - Advanced Science Institute and INFN - Rome Tor Vergata), "Energy spectrum of proton and helium measured by PAMELA and acceleration of cosmic rays in the galaxy"
9. Jul 13, 2011: Hiroyuki Nakayama (KEK), "Status of SuperKEKB/Belle-II project"
10. Jul 20, 2011: Osamu Tajima (KEK), "Quest for signal from inflationary universe - precise measurement of CMB polarization"
11. Aug 31, 2011: Shoji Torii (Faculty of Science and Engineering, Waseda University), "CALET Project: Astrophysical Mission for Japanese Experiment Module (Kibo) at the ISS"
12. Oct 12, 2011: Sergey Ostapchenko (Norwegian University for Science and Technology), "Interaction models: ultrahigh energy cosmic rays and LHC data"
13. Oct 19, 2011: Hiroko Miyahara (ICRR), "Effects of Galactic Cosmic Rays on Climate and Weather"
14. Nov 9, 2011: Susumu Inoue (ICRR), "Multi-Messenger Quest for the Origin of High Energy Cosmic Rays"
15. Nov 25, 2011: Masaki Ishitsuka (Tokyo Institute of Technology, Department of Physics), "First Results from the Double Chooz experiment"
16. Nov 30, 2011: Alexander Kusenko (UCLA/IPMU), "Cosmic connections: from cosmic rays, to gamma rays, to cosmic backgrounds"
17. Dec 5, 2011: Thierry Lasserre (CEA-Saclay), "Testing the Reactor Antineutrino Anomaly with a 10g 144Ce-144Pr source deployed inside a Large Liquid Scintillator Detector"

18. Dec 14, 2011: Sadakazu Haino (INFN Perugia), ”Status of Alpha Magnetic Spectrometer (AMS)”
19. Dec 21, 2011: Seiji Kawamura (ICRR), ”Gravitational wave astronomy by LCGT”
20. Jan 25, 2012: Saku Tsuneta (National Astronomical Observatory of Japan), ”Magnetic Universe as revealed with solar observation satellite Hinode”
21. Feb 8, 2012: Takuji Nakamura (National Institute of Polar Research), ”Atmospheric Science in Antarctic Research”
22. Mar 28, 2012: Masataka Fukugita (ICRR), ”From elementary particle research to astrophysics”

C. List of Publications

(a) Papers Published in Journals

1. ”Improvement of low energy atmospheric neutrino flux calculation using the JAM nuclear interaction model”, M. Honda, T. Kajita, K. Kasahara, S. Midorikawa Phys.Rev. D83, 123001, 2011.
2. ”Measurement of K+ production cross section by 8 GeV protons using high energy neutrino interactions in the SciBooNE detector”, SciBooNE Collaboration (G. Cheng et al.), Phys.Rev.D.84.012009, 2011.
3. ”Decay into Charged Anti-lepton plus Meson in Super-Kamiokande I and II”, Super-Kamiokande Collaboration (H. Nishino, et al.), to be published, 2012, [arXiv:1203.4030 [hep-ex]].
4. ”Search for GUT Monopoles at Super-Kamiokande”, Super-Kamiokande Collaboration (K. Ueno et al.), to be published, 2012, [arXiv:1203.0940 [hep-ex]].
5. ”First Muon-Neutrino Disappearance Study with an Off-Axis Beam”, T2K Collaboration (K. Abe (Tokyo U., ICRR) et al.). Phys.Rev. D85, 031103, 2012, [arXiv:1201.1386 [hep-ex]].
6. ”Supernova Relic Neutrino Search at Super-Kamiokande”, Super-Kamiokande Collaboration (K. Bays (UC, Irvine) et al.), Phys.Rev. D85,052007, 2012, [arXiv:1111.5031 [hep-ex]].
7. ”Measurements of the T2K neutrino beam properties using the INGRID on-axis near detector”, Super-Kamiokande Collaboration (K. Abe et al.), to be published, 2012, [arXiv:1109.4227 [hep-ex]].
8. ”The Search for n-n oscillation in Super-Kamiokande I”, Super-Kamiokande Collaboration (K. Abe et al.), to be published, 2011, [arXiv:1111.3119 [physics.ins-det]].
9. ”Study of Non-Standard Neutrino Interactions with Atmospheric Neutrino Data in Super-Kamiokande I and II”, Super-Kamiokande Collaboration (K. Abe et al.), Phys.Rev. D84, 113008, 2011, [arXiv:1109.1889 [hep-ex]].
10. ”Search for Differences in Oscillation Parameters for Atmospheric Neutrinos and Antineutrinos at Super-Kamiokande”, Super-Kamiokande Collaboration (K. Abe (Tokyo U., ICRR & Tokyo U., IPMU) et al.), Phys.Rev.Lett. 107, 241801, 2011, [arXiv:1109.1621 [hep-ex]].
11. ”An Indirect Search for WIMPs in the Sun using 3109.6 days of upward-going muons in Super-Kamiokande”, Super-Kamiokande Collaboration (T. Tanaka (Nagoya U.) et al.), Astrophys.J. 742, 78, 2011, [arXiv:1108.3384 [astro-ph.HE]].
12. ”Indication of Electron Neutrino Appearance from an Accelerator-produced Off-axis Muon Neutrino Beam”, T2K Collaboration (K. Abe (Tokyo U., ICRR) et al.), Phys.Rev.Lett. 107, 041801, 2011, [arXiv:1106.2822 [hep-ex]].
13. ”Scintillation-only Based Pulse Shape Discrimination for Nuclear and Electron Recoils in Liquid Xenon”, XMASS Collaboration (K. Ueshima (Kamioka Observ.) et al.), Nucl.Instrum.Meth. A659,161-168, 2011, [arXiv:1106.2209 [physics.ins-det]].
14. ”The T2K Experiment”, T2K Collaboration (K. Abe (Kamioka Observ.) et al.), PNucl.Instrum.Meth. A659, 106-135, 2011, [arXiv:1106.1238 [physics.ins-det]].
15. ”Observation of Diffuse Cosmic and Atmospheric Gamma Rays at Balloon Altitudes with an Electron-tracking Compton Camera”, A. Takada, H. Sekiya, A. Takeda et al., The Astrophysical Journal, 733:13, 2011.

16. ”A new imaging device based on UV scintillators and a large area gas photomulitiplier”, H. Sekiya et al, Nuclear Instruments and Methods in Physics Research A633, S36-S39, 2011.

17. ”Searches for Very High Energy Gamma Rays from Blazars with CANGAROO-III Telescope in 2005-2009”, Y. Mizumura, et al., Astropart. Phys., 35, 563-572, 2012, [arXiv:1202.2181 [astro-ph]].

18. ”CANGAROO-III Observation of TeV Gamma Rays from the Unidentified Gamma-Ray Source HESS J1614-518”, T. Mizukami, et al., Astrophys. J., 740, 78, 2011, [arXiv:1107.4007 [astro-ph]].

19. ”A Tunable Delay Line for Fast Analog Pulses as Key Element of a New Sum-Trigger for Cherenkov Telescopes”, D. Haefner, T. Schweizer, M. Shayduk, R. Mirzoyan, M. Teshima, IEEE Transactions on Nuclear Science, vol. 59, 2, 289-293, 2012.

20. ”Design concepts for the Cherenkov Telescope Array CTA: An advanced facility for ground-based high-energy gamma-ray astronomy”, CTA Consortium Collaboration (M. Actis, K. Ioka, H. Kubo, R. Orito, H. Tajima, M. Teshima, T. Totani, T. Yoshida, T. Yoshikoshi, 60 other CTA-Japan members et al.), Exper.Astron. 32, 193-316, 2011.

21. ”Development of an ASIC for Dual Mirror Telescopes of the Cherenkov Telescope Array”, Justin Vandenbroucke, Keith Bechtol, Stefan Funk, Akira Okumura, Hiro Tajima, Gary Varner, [arXiv:1110.4692 [astro-ph.HE]].

22. ”Detection of VHE γ-rays from HESS J0632+057 during the 2011 February X-ray outburst with the MAGIC Telescopes”, MAGIC Collaboration (J. Aleksic, R. Orito, K. Saito, H. Takami, M. Teshima, et al.), 2012, [arXiv:1203.2867 [astro-ph.HE]].

23. ”Discovery of VHE gamma-rays from the blazar 1ES 1215+303 with the MAGIC Telescopes and simultaneous multi-wavelength observations”, MAGIC Collaboration (J. Aleksic, R. Orito, K. Saito, H. Takami, M. Teshima, et al.)., 2012, [arXiv:1203.0490 [astro-ph.HE]].

24. ”Morphological and spectral properties of the W51 region measured with the MAGIC telescopes”, MAGIC Collaboration (J. Aleksic, R. Orito, K. Saito, H. Takami, M. Teshima, et al.), 2012, [arXiv:1201.4074 [astro-ph.HE]].

25. ”Discovery of VHE gamma-ray emission from the BL Lac object B3 2247+381 with the MAGIC telescopes”, MAGIC Collaboration (J. Aleksic, R. Orito, K. Saito, H. Takami, M. Teshima, , et al.), 2012, Astron.Astrophys. 539, A118, 2012, [arXiv:1201.2634 [astro-ph.HE]].

26. ”Detection of very high energy gamma-ray emission from NGC 1275 by the MAGIC telescopes”, MAGIC Collaboration (J. Aleksic, R. Orito, K. Saito, H. Takami, M. Teshima, et al.), 2011, [arXiv:1112.3917 [astro-ph.HE]].

27. ”Detection of the gamma-ray binary LS I +61 303 in a low flux state at Very High Energy gamma-rays with the MAGIC Telescopes in 2009”, MAGIC Collaboration (J. Aleksic, R. Orito, K. Saito, H. Takami, M. Teshima, et al.), Astrophys. J. 746, 80, 2012, [arXiv:1111.6572 [astro-ph.HE]].

28. ”The 2010 very high energy gamma-ray flare & 10 years of multi-wavelength observations of M 87”, H.E.S.S. and VERITAS Collaborations (A. Abramowski, R. Orito, K. Saito, H. Takami, M. Teshima, et al.), Astrophys. J. 746, 151, 2012, [arXiv:1111.5341 [astro-ph.HE]].

29. ”Constraining Cosmic Rays and Magnetic Fields in the Perseus Galaxy Cluster with TeV observations by the MAGIC telescopes”, MAGIC Collaboration (J. Aleksic, R. Orito, K. Saito, H. Takami, M. Teshima, et al.), Astron.Astrophys. 541, A99, 2012, [arXiv:1111.5544 [astro-ph.HE]].

30. ”MAGIC contributions to the 32nd International Cosmic Ray Conference”, MAGIC Collaboration (J. Aleksic, R. Orito, K. Saito, H. Takami, M. Teshima, et al.), [arXiv:1111.0879 [astro-ph.HE]].

31. ”Phase-resolved energy spectra of the Crab Pulsar in the range of 50-400 GeV measured with the MAGIC Telescopes”, MAGIC Collaboration (J. Aleksic, R. Orito, K. Saito, H. Takami, M. Teshima, et al.), [arXiv:1109.6124 [astro-ph.HE]].

32. ”Field test of the hybrid photodetector R9792U-40 on the MAGIC camera”, T.Y. Saito, S. Sun, R. Orito, E. Lorenz, R. Mirzoyan, M. Teshima, M. Garczarczyk, [arXiv:1109.6099 [astro-ph.HE]].

33. ”Observations of the Crab pulsar between 25 GeV and 100 GeV with the MAGIC I telescope”, MAGIC Collaboration (J. Aleksic, R. Orito, K. Saito, H. Takami, M. Teshima, et al.), Astrophys. J. 742, 43, 2011, [arXiv:1108.5391 [astro-ph.HE]].

34. ”Performance of the MAGIC stereo system obtained with Crab Nebula data”, MAGIC Collaboration (J. Aleksic, R. Orito, K. Saito, H. Takami, M. Teshima, et al.), Astropart.Phys. 35, 435-448, 2012, [arXiv:1108.1477 [astro-ph.HE]].

35. ”Fermi large area telescope observations of Markarian 421: The missing piece of its spectral energy distribution”, MAGIC Collaboration (A.A. Abdo, R. Orito, K. Saito, H. Takami, M. Teshima, et al.), Astrophys. J. 736, 131, 2011.

36. ”Mrk 421 active state in 2008: the MAGIC view, simultaneous multi-wavelength observations and SSC model constrained”, J. Aleksic, R.Orito, K. Saito, H. Takami, M. Teshima, et al., published in A&A 7 January 2012, [arXiv:1106.1589 [astro-ph.HE]].

37. ”A search for Very High Energy gamma-ray emission from Scorpius X-1 with the MAGIC telescopes”, MAGIC Collaboration (J. Aleksic, R.Orito, K. Saito, H.Takami, M. Teshima, et al.), Astrophys.J. 735, L5, 2011, [arXiv:1103.5677 [astro-ph.HE]].

38. ”Searches for Dark Matter annihilation signatures in the Segue 1 satellite galaxy with the MAGIC-I telescope”, MAGIC Collaboration (J. Aleksic, R.Orito, K. Saito, H.Takami, M. Teshima, et al.)., JCAP 1106, 035, 2011, [arXiv:1103.0477 [astro-ph.HE]].

39. ”MAGIC discovery of VHE Emission from the FSRQ PKS 1222+21”, MAGIC Collaboration (J. Aleksic, R.Orito, K. Saito, H.Takami, M. Teshima, et al.), Astrophys. J. 730, L8, 2011, [arXiv:1101.4645 [astro-ph.HE]].

40. ”PG 1553+113: five years of observations with MAGIC”, MAGIC Collaboration (J. Aleksic, R.Orito, K. Saito, H.Takami, M. Teshima, et al.), Astrophys. J. 748, 46, 2012, [arXiv:1101.2764 [astro-ph.HE]].

41. ”MAGIC observations and multiwavelength properties of the quasar 3C279 in 2007 and 2009”, MAGIC Collaboration (J. Aleksic (Barcelona, IFAE) et al.), Astron. Astrophys. 530, A4, 2011, [arXiv:1101.2522 [astro-ph.HE]].

42. ”Spectral Energy Distribution of Markarian 501: Quiescent State vs. Extreme Outburst”, VERITAS and MAGIC Collaborations (V.A. Acciari, R.Orito, K. Saito, H.Takami, M. Teshima, et al.). Astrophys. J. 729, 2, 2011, [arXiv:1012.2200 [astro-ph.HE]].

43. ”Insights Into the High-Energy Gamma-ray Emission of Markarian 501 from Extensive Multifrequency Observations in the Fermi Era”, LAT and MAGIC and VERITAS Collaborations (A.A. Abdo, R.Orito, K. Saito, H.Takami, M. Teshima, et al.), Astrophys. J. 727, 129, 2011, [arXiv:1011.5260 [astro-ph.HE]].

44. ”Observations of the Blazar 3C 66A with the MAGIC Telescopes in Stereoscopic Mode”, MAGIC Collaboration (J. Aleksic R.Orito, K. Saito, H.Takami, M. Teshima, et al.), Astrophys. J. 726, 58, 2011, [arXiv:1010.0550 [astro-ph.HE]].

45. ”Gamma-ray excess from a stacked sample of high- and intermediate-frequency peaked blazars observed with the MAGIC telescope”, MAGIC Collaboration (J. Aleksic, R.Orito, K. Saito, H.Takami, M. Teshima, et al.), Astrophys. J. 729, 115, 2011, [arXiv:1002.2951 [astro-ph.HE]].

46. ”The surface detector array of the Telescope Array experiment”, Telescope Array Collaboration (T. Abu-Zayyad et al.), to be published in Nucl. Instrum. Meth., 2012, [arXiv:1201.4964 [astro-ph.IM]].

47. ”The Energy Spectrum of Telescope Array’s Middle Drum Detector and the Direct Comparison to the High Resolution Fly’s Eye Experiment”, Telescope Array Collaboration (T. Abu-Zayyad et al.), to be published in Astropart. Phys., 2012, [arXiv:1202.5141 [astro-ph.IM]].

48. ”Calibration of photomultiplier tubes for the fluorescence detector of telescope array experiment using a Rayleigh scattered laser beam”, S.Kawana et al., Nucl. Instrum. Meth. A681, 68, 2012, [arXiv:1202.1934 [astro-ph.IM]].

49. ”New air fluorescence detectors employed in the telescope Array experiment”, H.Tokuno et al., Nucl. Instrum. Meth. A676, 54, 2012, [arXiv:1201.0002 [astro-ph.IM]].

50. ”The atmospheric transparency measured with a LIDAR system at the Telescope Array experiment”, T.Tomida et al., Nucl. Instrum. Meth. A654, 653, 2011, [arXiv:1109.1196 [astro-ph.IM]].

51. ”OBSERVATIONAL SEARCH FOR PeV–EeV TAU NEUTRINO FROM GRB081203A”, Ashra-1 Collaboration (Y. Aita et al.), ApJ, 736, L12, 2011, [arXiv:1106.2572 [astro-ph]].

52. ”Performance of a 20-inch Photoelectric Lens Image Intensifier Tube”, Yoichi Asaoka, Makoto Sasaki, Nucl. Instr. Meth., A647, 34, 2011, [arXiv:1106.2608 [astro-ph]].

53. ”Observation of the Fermi pulsar catalog at TeV energies with the Tibet air shower experiment”, M. Amenomori et al., Astrophysics and Space Sciences Transactions, 7, 211-215, 2011.

54. ”The Japanese space gravitational wave antenna: DECIGO”, Seiji Kawamura, et al., Class. Quantum Grav. 28, 094011, 2011.

55. ”Quest for Direct Detection of Gravitational Waves and Large-scale Cryogenic Gravitational wave Telescope (LCGT) Project in Japan!”, Shinji Miyoki, LCGT Collaboration, Journal of the Vacuum Society of Japan, 54, 587-596, 2011, (in Japanese).

56. ”Optical Configuration and Control of Ultra-sensitive Gravitational Wave Detectors!” Yoichi Aso, LCGT Collaboration, Journal of the Vacuum Society of Japan, 54, 597-603, 2011, (in Japanese).

57. ”Characteristics of Laser System Used in Large-Scale Cryogenic Gravitational Wave Telescope”, Noriaki Ohmae, Norikatsu Mio, Journal of the Vacuum Society of Japan, 54, 604-609, 2011, (in Japanese).

58. ”Vibration Isolation System for Mirrors”, Ryutaro Takahashi, Journal of the Vacuum Society of Japan, 54, 610-613, 2011, (in Japanese).

59. ”Development of Cryogenic Laser Interferometer Observatory (CLIO) and Local Suspension Point Interferometer (LSPI) in Kamioka”, Takanori Saito, Souichi Telada, Takashi Uchiyama, Shinji Miyoki, Osamu Miyakawa, Masatake Ohashi, Journal of the Vacuum Society of Japan, 54, 614-620, 2011, (in Japanese).

60. ”Production Process of the Interferometer Beam Tubes in LCGT Project”, Yoshio Saito, Ryutaro Takahashi, Journal of the Vacuum Society of Japan, 54, 621-626, 2011, (in Japanese).

61. ”Thermal performance in high power SHG characterized by phase-matched calorimetryh, H. H. Lim, T. Katagai, S. Kurimura, T. Shimizu, K. Noguchi, N. Ohmae, N. Mio, I. Shoji, OPTICS EXPRESS 19 (23) (2011) 22588-22593.

62. ”Reflectivity Measurements of Metals for LCGT Thermal Radiation Shields at Cryogenic Temperature and Wavelength of 10 μm”, Yusuke Sakakibara et al., J. Cryo. Super. Soc. Jpn, 46, 434-440, 2011, (in Japanese).

63. ”Large-scale Cryogenic Gravitational wave Telescope”, Kazuaki Kuroda, J. Cryo. Super. Soc. Jpn, 46, 385-391, 2011, (in Japanese).

64. ”Experimental Demonstration of Cryogenic Mirror Technique -Achievement of CLIO-”, Takashi Uchiyama, Shinji Miyoki, J. Cryo. Super. Soc. Jpn, 46, 392-399, 2011, (in Japanese).

65. ”Vacuum and Insulation Technology”, Takao Ohmori, Satoshi Takada, Yoshihiro Sato, Yoshio Saito, Ryutaro Takahashi, J. Cryo. Super. Soc. Jpn, 46, 408-414, 2011, (in Japanese).

66. ”Conduction Cooling Using Ultra-piure Fine Metal Wire I -Pure Aluminum-”, Takayuki Tomaru, Hiroaki Hoshikawa, Hiroshi Tabuchi, Takakazu Shintomi, J. Cryo. Super. Soc. Jpn, 46, 415-420, 2011, (in Japanese).

67. ”Conduction Cooling Using Ultra-piure Fine Metal Wire II -Pure Copper-”, Takakazu Shintomi, Takayuki Tomaru, Kenji Yajima, J. Cryo. Super. Soc. Jpn, 46, 421-425, 2011, (in Japanese).

68. ”Cryogenic Mirror -The State-of-the-art in Interferometric Gravitational Wave Detectors-”, Kazuhiro Yamamoto, J. Cryo. Super. Soc. Jpn, 46, 426-433, 2011, (in Japanese).

69. ”Search for gravitational waves associated with the August 2006 timing glitch of the Vela pulsar”, J. Abadie, B.P. Abbott, R. Abbott, et al., Physical Review D83, 042001, 2011.

70. ”Sensitivity studies for third-generation gravitational wave observatories”, S. Hild, M. Abernathy, F. Acernese et al., Classical and Quantum Gravity 28, 094013, 2011.

71. ”Search for gravitational waves from binary black hole inspiral, merger, and ringdown”, J. Abadie, B.P. Abbott, R. Abbott, et al., Physical Review D83, 122005, 2011.

72. ”SEARCH FOR GRAVITATIONAL WAVE BURSTS FROM SIX MAGNETARS”, J. Abadie, B.P. Abbott, R. Abbott, et al., Astrophysical Journal Letters 734, L35, 2011.

73. ”BEATING THE SPIN-DOWN LIMIT ON GRAVITATIONAL WAVE EMISSION FROM THE VELA PULSAR”, J. Abadie, B.P. Abbott, R. Abbott, et al., Astrophysical Journal 737, 93, 2011.

74. ”Thermorefractive noise of finite-sized cylindrical test masses”, D. Heinert, A. G. Gurkovsky, R. Nawrodt, S. P. Vyatchanin, and K. Yamamoto, Physical Review D84, 062001, 2011.

75. ”Laser interferometry with translucent and absorbing mechanical oscillators”, D. Friedrich, H. Kaufer, T. Westphal, K. Yamamoto, A. Sawadsky, F Ya Khalili, S L. Danilishin, S. Goβler, K. Danzmann and R. Schnabel, New Journal of Physics 13, 093017, 2011.

76. ”Directional Limits on Persistent Gravitational Waves Using LIGO S5 Science Data”, J. Abadie, B.P. Abbott, R. Abbott, et al., Physical Review Letters 107, 271102, 2011.

77. ”All-sky search for periodic gravitational waves in LIGO S5 the full data”, J. Abadie, B.P. Abbott, R. Abbott, et al., Physical Review D85, 022001, 2012.

78. ”Search for gravitational waves from low mass compact binary coalescence in LIGO’s sixth science run and Virgo’s science runs 2 and 3”, J. Abadie, B.P. Abbott, R. Abbott, et al., Physical Review D85, 082002, 2012.

79. ”The cross-correlation search for a hot spot of gravitational waves”, Sanjeev Dhurandhar, Hideyuki Tagoshi, Yuta Okada, Nobuyuki Kanda, and Hirotaka Takahashi, Phys. Rev. D 84 (2011) 083007.

80. ”Prospects for true calorimetry on Kerr black holes in core-collapse supernovae and mergers”, Maurice H.P.M. van Putten, Nobuyuki Kanda, Hideyuki Tagoshi, Daisuke Tatsumi, Fujimoto Masa-Katsu and Massimo Della Valle, Phys Rev D 83 (2011) 044046.

81. ”Post-Newtonian factorized multipolar waveforms for spinning, non-precessing black-hole binaries”, Yi Pan, Alessandra Buonanno, Ryuichi Fujita, Etienne Racine, Hideyuki Tagoshi, Phys. Rev. D 83 (2011) 064003.

82. ”First observational upper limit on gravitational wave backgrounds at 0.2 Hz with a torsion-bar antenna”, Koji Ishidoshiro, Masaki Ando, Akiteru Takamori, Hideyuki Tagoshi, Kenshi Okada, Nobuyuki Matsumoto, Wataru Kokuyama, Nobuyuki Kanda, Yoichi Aso, and Kimio Tsubono, Phys Rev Letter 106, (2011) 161101.

83. ”Beating the Spin-down Limit on Gravitational Wave Emission from the Vela Pulsar”, J. Abadie, et al. K. Hayama, et al., ApJ 737 (2011) 93.

84. ”Search for Gravitational Wave Bursts from Six Magnetars”, J. Abadie, et al. K. Hayama, et al., ApJ 734 (2011) 353.

85. ”Average Metallicity and Star Formation Rate of Lyα Emitters Probed by a Triple Narrowband Survey”, Nakajima, K., M. Ouchi, et al., Astrophys. J., 745, 12, 2012, [arXiv:1105.2824 [astro-ph]].

86. ”Spectroscopic Confirmation of Three z-dropout Galaxies at z = 6.844-7.213: Demographics of Lyα Emission in $z \sim 7$ Galaxies”, Ono, Y., M. Ouchi, et al., Astrophys. J., 744, 83, 2012, [arXiv:1107.3159 [astro-ph]].

87. ”The First Systematic Survey for Lyman Alpha Emitters at z=7.3 with Red-sensitive Subaru/Suprime-Cam”, Shibuya, T. et al., to be published in Astrophys. J., [arXiv:1112.3997 [astro-ph]].

88. ”Keck Spectroscopy of Lyman-break Galaxies and Its Implications for the UV-continuum and Lyα Luminosity Functions at $z \sim 6$”, Jiang, L. et al., Astrophys. J., 743, 65, 2011, [arXiv:1109.0023 [astro-ph]].

89. ”Completing the Census of Lyα Emitters at the Reionization Epoch”, Kashikawa, N. et al., Astrophys. J., 734, 119, 2011, [arXiv:1104.2330 [astro-ph]].

90. ”Matter Distribution around Galaxies”, Masaki, S., M. Fukugita, and N. Yoshida, Astrophys. J., 746, 38, 2012, [arXiv:1105.3005 [astro-ph]].

91. ”Milky Way Tomography IV: Dissecting Dust”, Berry, M. et al., [arXiv:1111.4985 [astro-ph]].

92. ”Supernovae in the Subaru Deep Field: the rate and delay-time distribution of Type Ia supernovae out to redshift 2”, Graur, O. et al., Monthly Notices of the Royal Astronomical Society, 417, 916, 2011, [arXiv:1102.0005 [astro-ph]].

93. ”Microwave Emission from the Edgeworth-Kuiper Belt and the Asteroid Belt Constrained from the Wilkinson Microwave Anisotropy Probe”, Ichikawa, K. and M. Fukugita, Astrophys. J., 736, 122, 2011, [arXiv:1011.4796 [astro-ph]].

94. ”Destruction of ^{7}Be in big bang nucleosynthesis via long-lived sub-strongly interacting massive particles as a solution to the Li problem”, M. Kawasaki, M. Kusakabe, Phys. Rev. D83, 055011, 2011, [arXiv:1012.0435 [hep-ph]].

95. ”Improved estimation of radiated axions from cosmological axionic strings”, T. Hiramatsu, M. Kawasaki, T. Sekiguchi, M. Yamaguchi and J. Yokoyama, Phys. Rev. D83, 123531, 2011, [arXiv:1012.5502 [hep-ph]].

96. ”Cosmological constraints on dark matter models with velocity-dependent annihilation cross section”, J. Hisano, M. Kawasaki, K. Kohri, T. Moroi, K. Nakayama, T. Sekiguchi, Phys. Rev. D83, 123511, 2011, [arXiv:1102.4658 [hep-ph]].

97. ”Differentiating CDM and Baryon Isocurvature Models with 21 cm Fluctuations”, M. Kawasaki, T. Sekiguchi, T. Takahashi, JCAP 1110, 028, 2011, [arXiv:1104.5591 [astro-ph.CO]].

98. ”Gravitino dark matter and baryon asymmetry from Q-ball decay in gauge mediation”, S. Kasuya, M. Kawasaki, Phys. Rev. D84, 123528, 2011, [arXiv:1107.0403 [hep-ph]].

99. ”Non-Gaussianity from Curvatons Revisited”, M. Kawasaki, T. Kobayashi, F. Takahashi, Phys. Rev. D84, 123506, 2011, Phys. Rev. D85, 029905, 2012, [arXiv:1107.6011 [astro-ph.CO]].

100. ”Primordial seeds of supermassive black holes”, M. Kawasaki, A. Kusenko and T. T. Yanagida, Phys. Lett. B711, 1, 2012, [arXiv:1202.3848 [astro-ph.CO]].

101. ”Pure Gravity Mediation with $m_{3/2} = 10$-100TeV”, M. Ibe, S. Matsumoto and T. T. Yanagida, Phys. Rev. D85, 095011, 2012, [arXiv:1202.2253 [hep-ph]].

102. ”A 125GeV Higgs Boson and Muon g-2 in More Generic Gauge Mediation”, J. L. Evans, M. Ibe, S. Shirai and T. T. Yanagida, Phys. Rev. D85, 095004, 2012, [arXiv:1201.2611 [hep-ph]].

103. ”The Lightest Higgs Boson Mass in Pure Gravity Mediation Model”, M. Ibe and T. T. Yanagida, Phys. Lett. B709, 374, 2012, [arXiv:1112.2462 [hep-ph]].

104. ”The GeV-scale dark matter with B-L asymmetry”, M. Ibe, S. Matsumoto and T. T. Yanagida, Phys. Lett. B708, 112, 2012, [arXiv:1110.5452 [hep-ph]].

105. ”Relatively Heavy Higgs Boson in More Generic Gauge Mediation”, J. L. Evans, M. Ibe and T. T. Yanagida, Phys. Lett. B 705, 342, 2011, [arXiv:1107.3006 [hep-ph]].

106. ”R-symmetry Matching In SUSY Breaking Models”, J. Goodman, M. Ibe, Y. Shirman and F. Yu, Phys. Rev. D84, 045015, 2011, [arXiv:1106.1168 [hep-th]].

107. ”Constraints on Direct Gauge Mediation Models with Complex Representations”, K. Hanaki, M. Ibe, Y. Ookouchi and C. S. Park, JHEP, 1108, 044, 2011, [arXiv:1106.0551 [hep-ph]].

108. ”Simplified R-Symmetry Breaking and Low-Scale Gauge Mediation”, J. L. Evans, M. Ibe, M. Sudano and T. T. Yanagida, JHEP 1203, 004, 2012, [arXiv:1103.4549 [hep-ph]].

109. ”Evolution of string-wall networks and axionic domain wall problem”, T. Hiramatsu, M. Kawasaki and K. Saikawa, JCAP 08, 030, 2011, [arXiv:1012.4558 [astro-ph.CO]].

110. ”Study of gravitational radiation from cosmic domain walls”, M. Kawasaki and K. Saikawa, JCAP 09, 008, 2011, [arXiv:1102.5628 [astro-ph.CO]].

111. ”Higher Order Corrections to the Primordial Gravitational Wave Spectrum and its Impact on Parameter Estimates for Inflation”, S. Kuroyanagi and T. Takahashi, JCAP 1110, 006, 2011, [arXiv:1106.3437 [astro-ph.CO]].

112. ”Prospects for determination of thermal history after inflation with future gravitational wave detectors”, S. Kuroyanagi, K. Nakayama and S. Saito, Phys. Rev. D84, 123513, 2011, [arXiv:1110.4169 [astro-ph.CO]].

113. ”Isocurvature perturbations in extra radiation”, M. Kawasaki, K. Miyamoto, K. Nakayama and T. Sekiguchi, JCAP 1202, 022, 2012, [arXiv:1107.4962 [astro-ph.CO]].

114. ”Multi-field open inflation model and multi-field dynamics in tunneling”, K. Sugimura, D. Yamauchi, and M. Sasaki, JCAP 1201, 027, 2011, [arXiv:1110.4773 [gr-qc]].

115. ”Full-sky lensing reconstruction of gradient and curl modes from CMB maps”, T. Namikawa, D. Yamauchi, and A. Taruya, JCAP 1201, 007, 2012, [arXiv:1110.1718 [astro-ph.CO]].

116. ”Weak lensing of CMB by cosmic (super-)strings”, D. Yamauchi, K. Takahashi, Y. Sendouda, and C.-M. Yoo, Phys. Rev. D85, 103515, 2011, [arXiv:1110.0556 [astro-ph.CO]].

117. ”Open inflation in the landscape”, D. Yamauchi, A. Linde, A. Naruko, M. Sasaki, and T. Tanaka, Phys. Rev. D84, 043513, 2011, [arXiv:1105.2674 [hep-th]].

118. ”Cosmological Aspects of Inflation in a Supersymmetric Axion Model”, M. Kawasaki, N. Kitajima and K. Nakayama, Phys. Rev. D83, 123521, 2011, [arXiv:1104.1262 [hep-ph]].

119. ”Revisiting the cosmological coherent oscillation”, M. Kawasaki, N. Kitajima and K. Nakayama, [arXiv:1112.2818 [hep-ph]].

120. ”Resonant annihilation of long-lived massive colored particles through hadronic collisions”, M. Kusakabe and T. Takesako, Phys. Rev. D85, 015005, 2012, [arXiv:1112.0860 [hep-ph]].

121. ”Hubble Induced Mass in Radiation Dominated Universe”, M. Kawasaki and T. Takesako, Phys. Lett. B711, 173, 2012, [arXiv:1112.5823 [hep-ph]].

122. ”Time-dependent quark masses and big bang nucleosynthesis revisited”, M.-K. Cheoun, T. Kajino, M. Kusakabe, G. J. Mathews, Phys. Rev. D84, 043001, 2011, [arXiv:1104.5547 [astro-ph.CO]].

123. ”Signals of the cosmological reionization in the radio sky through C and O fine structure lines”, M. Kusakabe and M. Kawasaki, MNRAS 419, 873, 2012, [arXiv:1004.1087 [astro-ph.CO]].

124. ”Anomalous deformation of the Earth’s bow shock in the lunar wake: Joint measurement by Chang’E-1 and SELENE”, Nishino, M. N., X. D. Wang, M. Fujimoto, H. Tsunakawa, Y. Saito, S. Yokota, W. Bian, C. L. Li, M. Matsushima, H. Shibuya, H. Shimizu, F. Takahashi, and T. Terasawa, Planet. Space Sci., 59, 378-386, Apr. 2011.

125. ”Detection of transient ELF emission caused by the extremely intense cosmic gamma-ray flare of 27 December 2004”, Tanaka, Y. T., M, Hayakawa, Y. Hobara, A. P. Nickolaenko, K. Yamashita, M. Sato, Y. Takahashi, T. Terasawa, and T. Takahashi, Geophys. Res. Lett., 38, L08805.1-4, Apr. 2011.

126. ”Collisionless shocks and particle acceleration: Lessons from studies of heliospheric shocks”, Terasawa, T., IAU Symposium, Volume 274, p. 214-219, June 2011.

127. ”First results from the 2009.2010 MU radar head echo observation programme for sporadic and shower meteors: the Orionids 2009”, Kero, J., C. Szasz, T. Nakamura, D. D. Meisel, M. Ueda, Y. Fujiwara, T. Terasawa, H. Miyamoto, and K. Nishimura, Mon. Not. R. Astron. Soc., 416, 2550-2559, Oct. 2011.

128. ”The Role of Stochastic Acceleration in the Prompt Emission of Gamma-Ray Bursts: Application to Hadronic Injection”, Murase, K., K. Asano, T. Terasawa, and P. Meszaros, Astrophys. J., 746, 164-175, Feb. 2012.

129. ”Implications for the low latitude cloud formations from solar activity and the Quasi-Biennial Oscillation”, P.K. Hong et al., Journal of Atmospheric and Solar-Terrestrial Physics, 73, 587, 2011, [doi:10.1016/j.jastp.2010.11.026].

130. ”A decade of the Moderate Resolution Imaging Spectroradiometer: is a solar - cloud link detectable?”, B. Laken et al., Journal of Climate, 2012, [doi:http://dx.doi.org/10.1175/JCLI-D-11-00306.1.].

131. ”Discrimination of new physics models with the International Linear Collider”, Masaki Asano, et al., Phys. Rev. D84, 115003, 2011, [arXiv:1106.1932 [hep-ph]].

(b) Conference Papers

1. ”T2K: New physics results”, S. Nakayama (on behalf of the T2K collaboration), Proceedings of the 12th International Conference on Topics in Astroparticle and Underground Physics (TAUP 2011), 2011.

2. ”Direct Detection of Dark Matter”, S. Moriyama, Proceedings of the 3rd Subaru International Conference, 2011.

3. ”Messengers of new physics”, W.Rodejohann and M.Shiozawa, Nucl.Phys.Proc.Suppl. 217, 383-387, 2011.

4. ”Letter of Intent: The Hyper-Kamiokande Experiment — Detector Design and Physics Potential —.”, K. Abe et al., [arXiv:1109.3262 [hep-ex]].

5. ”T2K Neutrino Oscillation Results”, K. Okumura for T2K collaboration, Proceedings of 19th Particles and Nuclei International Conference (PANIC), 2011.

6. ”Analysis of nuclear de-excitation gamma-rays using T2K data”, K. Ueno, Proceedings of the 32nd International Cosmic Ray Conference, 2011.

7. ”Status of XMASS”, A. Takeda, Proceedings of the 2nd International Workshop towards the Giant Liquid Argon Charge Imaging Experiment, 2011.

8. ”Data acquisition system for nearby supernova bursts at Super-Kamiokande”, T.Yokozawa, Proceedings of the 32nd International Cosmic Ray Conference, 2011.

9. ”Development of data acquisition system for nearby supernova bursts at Super-Kamiokande”, T.Yokozawa, Proceedings of 2011 IEEE Nuclear Science Symposium, 2011.

10. ”Development of a UV/X-ray imaging device based on large area gas photo-multiplier”, H. Sekiya, Proceedings of the Technology and Instrumentation in Particle Physics (TIPP 2011), 2011.

11. ”R & D Studies for Very High Energy Gamma-Ray Astrophysics at Energies Greater than 10 TeV”, T. Yoshikoshi, et al., Proc. of 32nd Internat. Cosmic Ray Conf. (Beijing), 9, 226-229, 2011.

12. ”AGN Population Studies for CTA”, Y. Inoue, Proc. of AGN Physics in the CTA era, 2011, [arXiv:1112.5813 [astro-ph.HE]].

13. ”Design Study of a CTA Large Size Telescope”, M. Teshima et al., Proc. of ICRC2012 at Beijing China, [arXiv:1111.2183 [astro-ph.HE]].

14. ”Development of PMT Clusters for CTA-LST Camera”, R.Orito et al., Proc. of ICRC2012 at Beijing China, [arXiv:1111.2183 [astro-ph.HE]].

15. ”Experimental summary and future prospects”, M.Fukushima, Proceedings of the International Symposium on Future Directions in UHECR Physics (UHECR2012), CERN, Switzerland, 2012.

16. ”HiRes and TA Composition Measurements”, Y.Tameda, Proceedings of the International Symposium on Future Directions in UHECR Physics (UHECR2012), CERN, Switzerland, 2012.

17. ”Ultra-high energy cosmic-ray spectra measured by the Telescope Array experiment from hybrid observations”, D.Ikeda, Proceedings of the 32nd International Cosmic Ray Conference (ICRC2011), Beijing, China, 2011.

18. ”Measurement of UHECR Mass Composition by TA FD Stereo”, Y.Tameda, Proceedings of the 32nd International Cosmic Ray Conference (ICRC2011), 2011, Beijing, China.

19. ”Absolute energy calibration of the Telescope Array fluorescence detector with an Electron Linear Accelerator”, T.Shibata, Proceedings of the 32nd International Cosmic Ray Conference (ICRC2011), Beijing, China, 2011.

20. ”Recent Results from Telescope Array”, D.Ikeda, Proceedings of the 12th International Conference on Topics in Astroparticle and Underground Physics (TAUP 2011), Munich, Germany, 2011.

21. ”Results from the Telescope Array Experiment”, H.Sagawa, Proceedings of the TeV Particle Astrophysics (TeVPA), Stockholm, Sweden, 2011.

22. ”The TIBET AS+MD Project; progress report 2011”, M. Amenomori et al. (The Tibet ASγ Collaboration), Proceedings of the 32nd International Cosmic Ray Conference, Beijing, China, 11-18 August 2011, OG.1.5 (ID: 351), 2011.

23. ”Correlation between Solar Activity and the Sunfs Shadow Observed by the Tibet Air Shower Array”, M. Amenomori et al. (The Tibet ASγ Collaboration), Proceedings of the 32nd International Cosmic Ray Conference, Beijing, China, 11-18 August 2011, SH.3.5 (ID: 352), 2011.

24. ”Air-shower core detector array to study the mass composition of cosmic rays beyond 100 TeV by Tibet hybrid experiment”, M. Amenomori et al. (The Tibet ASγ Collaboration), Proceedings of the 32nd International Cosmic Ray Conference, Beijing, China, 11-18 August 2011, OG.1.2 (ID: 356), 2011.

25. ”Modeling of the galactic cosmic-ray anisotropy at TeV energies”, M. Amenomori et al. (The Tibet ASγ Collaboration), Proceedings of the 32nd International Cosmic Ray Conference, Beijing, China, 11-18 August 2011, SH.3.3 (ID: 361), 2011.

26. ”Time Dependence of Loss Cone Amplitude measured with the Tibet Air-shower Array”, M. Amenomori et al. (The Tibet ASγ Collaboration), Proceedings of the 32nd International Cosmic Ray Conference, Beijing, China, 11-18 August 2011, HE.1.1 (ID: 379), 2011.

27. ”Observation of atmospheric charged particles associated with thunderstorms at Tibet”, M. Amenomori et al. (The Tibet ASγ Collaboration), Proceedings of the 32nd International Cosmic Ray Conference, Beijing, China, 11-18 August 2011, SH.4.2 (ID: 497), 2011.

28. ”Observation of Sub-PeV Gamma Rays from the Galactic Plane Using the Tibet Air Shower Array with the Proto Type Muon Detector”, M. Amenomori et al. (The Tibet ASγ Collaboration), Proceedings of the 32nd International Cosmic Ray Conference, Beijing, China, 11-18 August 2011, OG.2.1 (ID: 748), 2011.

29. ”Variability of TeV Gamma-ray Flux from the Crab Nebula with the Tibet Air Shower Array”, M. Amenomori et al. (The Tibet ASγ Collaboration), Proceedings of the 32nd International Cosmic Ray Conference, Beijing, China, 11-18 August 2011, OG.2.1 (ID: 786), 2011.

30. ”TibetAS+MD detector simulation using GEANT4”, M. Amenomori et al. (The Tibet ASγ Collaboration), Proceedings of the 32nd International Cosmic Ray Conference, Beijing, China, 11-18 August 2011, OG.2.5 (ID: 1058), 2011.

31. ”On temporal variations of the multi-TeV cosmic ray anisotropy using the Tibet III Air Shower Array”, M. Amenomori et al. (The Tibet ASγ Collaboration), Proceedings of the 32nd International Cosmic Ray Conference, Beijing, China, 11-18 August 2011, HE.1.1 (ID: 1167), 2011.

32. ”Study of the large Tyvek bag technique for the water Cherenkov detector in TIBET AS+MD”, M. Amenomori et al. (The Tibet ASγ Collaboration), Proceedings of the 32nd International Cosmic Ray Conference, Beijing, China, 11-18 August 2011, OG.1.5 (ID:1168), 2011.

33. ”Calibration of the Yangbajing air-shower core detector (YAC) using the beam of BEPC”, M. Amenomori et al. (The Tibet ASγ Collaboration), Proceedings of the 32nd International Cosmic Ray Conference, Beijing, China, 11-18 August 2011, HE.1.4 (ID:1217), 2011.

34. ”Test of the hadronic interaction models at around *10 TeV with Tibet EAS core data”, M. Amenomori et al. (The Tibet ASγ Collaboration), Proceedings of the 32nd International Cosmic Ray Conference, Beijing, China, 11-18 August 2011, HE.1.1 (ID:1238), 2011.

35. ”A Monte Carlo study to measure the energy spectra of the primary proton and helium components at the knee using a new Tibet AS core detector array”, M. Amenomori et al. (The Tibet ASγ Collaboration), Proceedings of the 32nd International Cosmic Ray Conference, Beijing, China, 11-18 August 2011, HE.1.1 (ID:1239), 2011.

36. ”Measurement of some properties of EAS-cores using new air-shower core detectors array developed for the Tibet hybrid experiment”, M. Amenomori et al. (The Tibet ASγ Collaboration), Proceedings of the 32nd International Cosmic Ray Conference, Beijing, China, 11-18 August 2011, HE.1.4 (ID:1241), 2011.

37. ”The forward particle production in the energy range of 1015eV as seen with the Tibet hybrid experiment”, M. Amenomori et al. (The Tibet ASγ Collaboration), Proceedings of the 32nd International Cosmic Ray Conference, Beijing, China, 11-18 August 2011, HE.1.1 (ID:1251), 2011.

38. ”TeV Gamma Ray Survey on the Direction of Fermi-LAT Pulsars with the Tibet Air Shower Array”, M. Amenomori et al. (The Tibet ASγ Collaboration), Proceedings of the First Session of the Sant Cugat Forum on Astrophysics, Sant Cugat, Spain, edited by Nanda Rea and Diego F. Torres, p491-495 2011.

39. ”Present Design of LCGT Cryogenics Payload - Status of cryogenics design -”, N. KIMURA, Y. SAKAKIBARA, S. KOIKE,T. SUZUKI, H. YAMAOKA, andLCGT Collaboration, GWADW 2011 22-28 May, 2011 La Biodola, Isola d’Elba, Italy http://agenda.infn.it/conferenceDisplay.py?confId=3351.

40. ”Refrigerator and Cryostat Design for LCGT”, N. KIMURA, T. SUZUKI, S. KOIKE,T. KUME, T. OHMORI, K. SASAKI,Y. SAITO, Y. SATO, H. YAMAOKA and LCGT Collaboration, ibid.

41. ”Current status of LCGT project”, S.Miyoki and LCGT collaboration, TAUP2011 in Minich (Germany, Munchen) 5-9 Sept. 2011.

42. ”Gravitational Waves: Current and future experiments”, K. Kuroda, TAUP2011 in Minich (Germany, Munchen) 5-9 Sept. 2011.

43. ”The Present Status of LCGT Project”, S.Miyoki and LCGT collaboration, ICGAC10 in Qui Nhon (Vietnam, Qui Nyon), 20 Dec., 2011.

44. ”Cryogenic system of LCGT”, S.Miyoki and KAGRA Cryogenic group, Korea-Japan Workshop on KAGRA (Korea, Seoul), 13 Jan., 2012.

45. ”Cryogenic System design of LCGT”, N. Kimura, S. Koike, T. Kume, T. Ohmori, Y. Saito, Y. Sakakibara, K. Sasaki, Y. Sato, T. Suzuki, T. Uchiyama, K. Yamamoto, H. Yamaoka and LCGT Collaboration, Italy-Japan workshop, Kashiwa, 5 Oct., 2011.

46. ”Effect of exotic long-lived sub-strongly interacting massive particles in big bang nucleosynthesis and a new solution to the Li problem”, M. Kawasaki and M. Kusakabe, Hadron Nuclear Physics 2011 (HNP2011) ”Quarks in Hadrons, Nuclei, and Hadronic Matter”, (21 - 24 February 2011, Pohang, Korea), EPJ Web of Conferences **20**, 04001, 2012.

47. ”Signatures of long-lived exotic strongly interacting massive particles on light element abundances through reactions triggered by the particles”, M. Kusakabe and M. Kawasaki, 7th International Workshop on the Dark Side of the Universe, (26 - 30 September 2011, Beijing, China), to be published in the IOP Journal of Physics: Conference Series, 2011.

48. ”Destructions of 7Be and 7Li in big bang nucleosynthesis through reactions with exotic long-lived sub-strongly interacting massive particles”, M. Kusakabe and M. Kawasaki, International Symposium on Origin of Matter and Evolution of Galaxies, (14 - 17 November 2011, Wako, Japan), to be published in the AIP Conference Series, 2011.

49. ”Air Shower Detection by Bistatic Radar, International Symposium on the recent progress of ultra-high energy cosmic ray observation”, Othman, M. A., C. Allen, J. Belz, D. Besson, B. Farhang-Boroujeny, D. keda, S. Kunwar, J. P. Lundquist, I. Kravchenko, I. Myers, T. Nakamura, H. Sagawa, P. Sokolsky, H. Takai, T. Terasawa, and G. B. Thomson, AIP Conference Proceedings, 1367, 143-146, Sept. 2011.

(c) ICRR Reports

1. ICRR-Report-584-2011-1
”Cosmological Aspects of Inflation in a Supersymmetric Axion Model”
Masahiro Kawasaki, Naoya Kitajima, and Kazunori Nakayama.

2. ICRR-Report-585-2011-2
”Open inflation in the landscape”
Daisuke Yamauchi, Andrei Linde, Atsushi Naruko, Misao Sasaki, and Takahiro Tanaka.

3. ICRR-Report-586-2011-3
”R-symmetry Matching In SUSY Breaking Models”
Jessica Goodman, Masahiro Ibe, Yuri Shirman, and Felix Yu.

4. ICRR-Report-587-2011-4
”Cosmological effects of decaying cosmic string loops with TeV scale width”
Masahiro Kawasaki, Koichi Miyamoto, Kazunori Nakayama.

5. ICRR-Report-588-2011-5
”Constraints on Direct Gauge Mediation Models with Complex Representations”
Kentaro Hanaki, Masahiro Ibe, Yutaka Ookouchi, and Chang-Soon Park.

6. ICRR-Report-589-2011-6
”Higher Order Corrections to the Primordial Gravitational Wave Spectrum and its Impact on Parameter Estimates for Inflation”
Sachiko Kuroyanagi, and Tomo Takahashi.

7. ICRR-Report-590-2011-7
”Relatively Heavy Higgs Boson in More Generic Gauge Mediation”
Jason L. Evans, Masahiro Ibe, and Tsutomu T. Yanagida.

8. ICRR-Report-591-2011-8
”Gravitino dark matter and baryon asymmetry from Q-ball decay in gauge mediation”
Shinta Kasuya, and Masahiro Kawasaki.

9. ICRR-Report-592-2011-9
”Non-Gaussianity from Curvatons Revisited”
Masahiro Kawasaki, Takeshi Kobayashi, and Fuminobu Takahashi.

10. ICRR-Report-593-2011-10
”Isocurvature perturbations in extra radiation”
Masahiro Kawasaki, Koichi Miyamoto, and Kazunori Nakayama.

11. ICRR-Report-594-2011-11
”Weak lensing of CMB by cosmic (super-)strings”
Daisuke Yamauchi, Keitaro Takahashi, Yuuiti Sendouda, and Chul-Moon Yoo.

12. ICRR-Report-595-2011-12
”Full-sky lensing reconstruction of gradient and curl modes from CMB maps”
Toshiya Namikawa, Daisuke Yamauchi, and Atsushi Taruya.

13. ICRR-Report-596-2011-13
”Multi-field open inflation model and multi-field dynamics in tunneling”
Kazuyuki Sugimura, Daisuke Yamauchi, and Misao Sasaki.

14. ICRR-Report-597-2011-14
”Prospects for determination of thermal history after inflation with future gravitational wave detectors”
Sachiko Kuroyanagi, Kazunori Nakayama, and Shun Saito.

15. ICRR-Report-598-2011-15
”The GeV-scale dark matter with B-L asymmetry”
Masahiro Ibe, Shigeki Matsumoto, and Tsutomu T. Yanagida.

16. ICRR-Report-599-2011-16
”Non-Anomalous Discrete R-symmetry Decrees Three Generations”
Jason L. Evans, Masahiro Ibe, John Kehayias, and Tsutomu T. Yanagida.

17. ICRR-Report-600-2011-17
”Resonant annihilation of long-lived masive colored particles through hadronic collisions”
Motohiko Kusakabe, and Tomohiro Takesako.

18. ICRR-Report-601-2011-18
”The Lightest Higgs Boson Mass Pure Gravity Mediation Model”
Masahiro Ibe, and Tsutomu T. Yanagida.

19. ICRR-Report-602-2011-19
”Hubble Induced Mass in Radiation Dominated Universe”
Masahiro Kawasaki, and Tomohiro Takesako.

20. ICRR-Report-603-2011-20
”Revisiting the cosmological coherent oscillation”
Masahiro Kawasaki, Naoya Kitajima, and Kazunori Nakayama.

21. ICRR-Report-604-2011-21
”A 125 GeV Higgs Boson and Muon g-2 in More Generic Gauge Mediation”
Jason L. Evans, Masahiro Ibe, Satoshi Shirai, and Tsutomu T. Yanagida.

22. ICRR-Report-605-2011-22
”Pure Gravity Mediation with $m_{3/2}$ = 10-100TeV”
Masahiro Ibe, Shigeki Matsumoto, and Tsutomu T. Tanagida.

23. ICRR-Report-606-2011-23
”Forecast constraints on cosmic string parameters from gravitational wave direct detection experiments”
Sachiko Kuroyanagi, Koichi Miyamoto, Toyokazu Sekiguchi, Keitaro Takahashi, and Joseph Silk.

24. ICRR-Report-607-2011-24
”Primordial seeds of supermassive black holes”
Masahiro Kawasaki, Alexander Kusenko, and Tsutomu T. Yanagida.

25. ICRR-Report-608-2011-25
”Production of dark matter axions from collapse of string-wall systems”
Takashi Hiramatsu, Masahiro Kawasaki, Ken’ichi Saikawa, and Toyokazu Sekiguchi.

26. ICRR-Report-609-2011-26
”Non-Gaussian isocurvature perturbations in dark radiation”
Etsuko Kawakami, Masahiro Kawasaki, Koichi Miyamoto, Kazunori Nakayama, and Toyokazu Sekiguchi.

27. ICRR-Report-610-2011-27
”Weak lensing generated by vector perturbations and detectability of cosmic strings”
Daisuke Yamauchi, Toshiya Namikawa, and Atsushi Taruya.

28. ICRR-Report-611-2011-28
”Axino dark matter and baryon number asymmetry from Q-ball decay in gauge mediation”
Shinta Kasuya, Etsuko Kawakami, and Masahiro Kawasaki.

D. Doctoral Theses

1. ”Search for the diffuse supernova neutrino background at Super-kamiokande Kirk Ryan Bays”, IRVINE Tristan James, Ph.D Thesis, Feb. 2012.
2. ”Study of neutral-current de-excitation gamma-rays with the T2K neutrino beam”, K. Ueno, Ph.D Thesis, Mar. 2012.
3. ”Large Scale Anisotropy of Ultra-High Energy Cosmic Rays measured by Telescope Array experiment”, E. Kido, Ph.D Thesis, Mar. 2012.

E. Public Relations

(a) ICRR News

ICRR News is a newspaper published quarterly in Japanese to inform the Institute’s activities. This year’s editor is Hideo Itoh. It includes :

1. reports on investigations by the staff of the Institute or made at the facilities of the Institute,
2. reports of international conferences on topics relevant to the Institute’s research activities,
3. topics discussed at the Institute Committees,
4. list of publications published by the Institute [ICRR-Report, ICRR-Houkoku (in Japanese)],
5. list of seminars held at the Institute,
6. announcements,
7. and other items of relevance.

The main topics in the issues in 2010 fiscal year were:

No.77 (Aug 31, 2011)

- About JFY2011, Takaaki Kajita.
- XMASS experiment aiming direct dark matter detection, Yasuhiro Kishimoto.
- Establishment of Gravitatonal Wave Project Office, Kazuaki Kuroda.
- Staff reassignment.
- ICRR-Seminar.
- ICRR-Report.

No.78 (Dec 15, 2011)

- Supersymmetric Standard Models in the LHC era, Masahiro Ibe.
- Recent results from Telescope Array experiment, Hiroyuki Sagawa.
- Staff reassignment.
- ICRR-Seminar.
- ICRR-Report.

No.79 (Feb 29, 2012)

- Observed extremely active galaxy on dawn of the universe, Masami Ouchi.
- Status report -EGADS project-, Masayuki Nakahata.
- Physics of the early universe by gravitational wave, Sachiko Kuroyanagi.
- Staff reassignment.
- ICRR-Seminar.
- ICRR-Report.

No.80 (Mar 31, 2012)

- Report on the Meeting for Presenting the Results of Inter-University Research in JFY2011, Takanori Yoshikoshi.
- Report of public lecture, Groundbreaking and publiced nickname ceremony of the KAGRA, Hideo Itoh.
- ICRR-Report.

(b) Public Lectures

- ”Neutrino and Dark Matter”, Mar. 28, 2012, Middle school of Kamioka, Hida-city, Gifu, Hiroyuki Sekiya (ICRR, University of Tokyo).
- ”Solar neutrino”, Feb. 4, 2012, Gifu, Yusuke Koshio (ICRR, University of Tokyo).
- ”Detection of cosmic rays”, Nov. 23, 2011, ICRR, Kashiwa-city, Chiba, Hideo Itoh (ICRR, University of Tokyo).
- ”Detecting Dark Matter”, Nov. 3, 2011, Hamamatsu-City, Shizuoka, Yoichiro Suzuki (ICRR, University of Tokyo).
- ”Detecting Dark Matter”, Oct. 27, 2011, University of Toyama, Toyama, Yoichiro Suzuki (ICRR, University of Tokyo).
- ”SSH Nanao High School”, Oct. 7, 2011, Kamioka-cho, Hida-city, Gifu, Yoshihita obayashi (ICRR, University of Tokyo).
- ”Visualization ideas of invisible matter”, Sep. 25, 2011, ICRR, Kashiwa-city, Chiba, Hideo Itoh (ICRR, University of Tokyo)
- ”Visualization ideas of invisible matter”, Sep. 24, 2011, ICRR, Kashiwa-city, Chiba, Hideo Itoh (ICRR, University of Tokyo).
- ”New results of T2K”, Sep. 13, 2011, University of Okayama, Okayama, Shoei Nakayama (ICRR, University of Tokyo).
- ”SSH Toyounaka High School”, Sep. 6, 2011, Kamioka-cho, Hida-city, Gifu, Makoto Miura (ICRR, University of Tokyo).
- ”SSH Senior High School Attached to Kyoto University of Education”, Aug. 23, 2011, Kamioka-cho, Hida-city, Gifu, jun Kameda (ICRR, University of Tokyo).
- ”SSH Ikuno High School”, Aug. 17, 2011, Kamioka-cho, Hida-city, Gifu, Hiroyuki Sekiya (ICRR, University of Tokyo).
- ”Dark Matter and Gravitational Wave”, Aug. 10, 2011, ICRR, Kashiwa-city, Chiba, Hideo Itoh (ICRR, University of Tokyo)
- ”SSH Sanda Shounkan High School”, Aug. 10, 2011, Kamioka-cho, Hida-city, Gifu, Kon Abe (ICRR, University of Tokyo).
- ”SSH Okazaki High School”, Aug. 9, 2011, Kamioka-cho, Hida-city, Gifu, Yoshihita Obayashi (ICRR, University of Tokyo).
- ”SSH Niigata Minami High School”, Aug. 4, 2011, Kamioka-cho, Hida-city, Gifu, Jun Kameda (ICRR, University of Tokyo).
- ”SSH Kashiwazaki High School”, Aug. 2, 2011, Kamioka-cho, Hida-city, Gifu, Atsushi Takeda (ICRR, University of Tokyo).

- ”Visualization ideas of invisible matter”, Aug. 1, 2011, ICRR, Kashiwa-city, Chiba, Hideo Itoh (ICRR, University of Tokyo).
- ”New results of T2K”, Jul. 27, 2011, University of Osaka, Osaka, Shoei Nakayama (ICRR, University of Tokyo).
- ”Detecting Dark Matter”, Jul. 21, 2011, Tokyo, Yoichiro Suzuki (ICRR, University of Tokyo).
- ”Early Universe and Particle Physics”, Jul. 14, 2011, Tokyo city university junior and senior high school, Hideo Itoh (ICRR, University of Tokyo).
- ”New results of T2K”, Jul. 14, 2011, University of Shinshu, Nagano, Shoei Nakayama (ICRR, University of Tokyo).
- ”Yoshiki High School”, Jul. 14, 2011, Kamioka-cho, Hida-city, Gifu, Koh Abe (ICRR, University of Tokyo).
- ”Nutrino and Dark Matter”, Jun. 11, 2011, Gifu, Yoichiro Suzuki (ICRR, University of Tokyo).
- ”SSH Shizuoka-kita High School”, Apr. 21, 2011, Kamioka-cho, Hida-city, Gifu, Yoshihita Obayashi (ICRR, University of Tokyo).

(c) Visitors

KASHIWA Campus (Total: 5 groups, 216 peoples)

- Chiba Advanced Technology Experience Program
- Induction course of the University of Tokyo
- Niigata Prefectural Kokusai Joho High School
- Others: 2 groups

KAMIOKA Observatory (Total: 169 groups, 3154 peoples)

- Yumeno Tamago Jyuku (Hida Academy for High School Students)
- MEXT Super Science High School (SSH) project: total 10 schools
- Schools and Universities: total 37 groups
- Researchers: total 13 groups
- Others: 108 groups

F. Inter-University Researches

Numbers of Researchers

	Number of Applications	Number of Adoptions	Number of Researchers
Facility Usage			
Kamioka Observatory	40	40	868
Norikura Observatory	6	6	66
Akeno Observatory	6	6	82
Emulsion and Air Shower Facilities in Kashiwa	1	1	6
Low-level Radio-isotope Measurement Facilities in Kashiwa	6	6	33
Gravitational Wave Facilities in Kashiwa	2	2	20
Computer Facilities in Kashiwa	12	12	236
Over Sea Facilities	8	8	213
Others	23	23	561
Collaborative Researches			
Cosmic Neutrino Researches	31	31	768
High Energy Cosmic Ray Researches	45	45	932
Theoretical Researches or Rudimental Researches	26	26	376
Research Center for Cosmic neutrinos	2	2	9
Others			
Conferences	3	3	89

Research Titles

1. Study of simulation for atmospheric neutrino
2. Study of nucleon decay $p \rightarrow \nu K$
3. Energy calibration for Super-Kamiokande
4. Sidereal daily variation of $\sim$10TeV galactic cosmic ray intensity observed by the Super-Kamiokande
5. Study of Supernova Relic Neutrinos
6. Tokai to Kamioka Long Baseline Experiment T2K
7. Study of solar neutrino energy spectrum
8. 3-flavor oscillation study in atmospheric neutrinos
9. Neutrino interaction study using accelerator data
10. Precise measurement of Day/Night effect for B8 solar neutrinos
11. Study of Solar Neutrino Flux
12. Search for proton decay via $e^+\pi^0$ mode
13. Study of atmospheric neutrino flux and neutrino oscillations
14. R&D of Mton water Cherenkov Hyper-Kamiokande
15. Study of flavor identification of atmospheric and beam neutrinos
16. Study of ambient gamma-ray and neutron flux at Kamioka Observatory

17. Development of low concentration radon detection system
18. Study for the electron neutrino appearance search in the T2K experiment
19. Study for Supernova monitor
20. Study in upward-going muons and high energy neutrinos
21. Neutrino workshop
22. Study for lowering backgrounds of radioisotopes in large volume detectors
23. Direction-sensitive dark matter search experiment
24. Study for double beta decay of 48Ca
25. Development of InP solid state detector for measurement of solar pp/7Beν
26. A search for Dark Matter using Liquid Xenon Detector
27. Analysis of Spatial Distribution of Radon Family Underground and Its Dosimetry
28. Integration of crustal activity observation around the Atotsugawa fault
29. Study for upgrade of XMASS detector
30. Strain, tilt, seismic measurement in Kamioka-mine
31. Development of radon detector for purified gases
32. A study on decay time of liquid xenon scintillation
33. Study for the impurity in the XMASS detector for the dark matter search
34. R&D for a Small Atmospheric Cherenkov Telescope in Akeno Observatory
35. Observation of Galactic Cosmic ray by Large Area Muon Telescope
36. Construction of optical system of a small Cherenkov telescope at Akeno Observatory
37. Multi-Color Imager for Transients, Survey and Monstrous Explosions
38. Observation of solar neutrons in solar cycle 24
39. Space weather observation using muon hodoscope at Mt. Norikura
40. Observations of total ozone and UV solar radiation with Brewer spectrophotometer on the Norikura mountains
41. Evaluation of altitude dependent doses of secondary cosmic neutrons
42. Ecophysiological studies of alpine plants
43. Observation of nightglow and its reflected and scattered light on a mountain
44. Study of the composition of cosmic-rays at the Knee
45. Observation of high-energy cosmic-ray electrons with emulsion chambers
46. Sidereal daily variation of $\sim$10TeV galactic cosmic ray intensity observed by the Tibet air shower array
47. Experimental Study of High-energy Cosmic Rays in the Tibet AS γ Experiment
48. Bolivian Air Shower Joint Experiment
49. Study on High Energy Cosmic Ray Sources by Observations in Space
50. Study of Galactic Diffuse Gamma Rays
51. Development of the Optical Elements for CTA Large Size Telescope
52. Calibration for TA FD with RC helicopter

53. Development of advanced photon counter for the future IACT
54. Study of absolute energy calibration of air shower by a compact electron linac
55. Observation of TeV gamma-ray spectra from galactic objects
56. Comparative study of astrophysical particle acceleration processes
57. Observational study of particle acceleration process in Crab nebula/pulsar
58. A R&D for a new atmospheric monitoring system
59. Study of radio detection of highest energy cosmic rays
60. CTA R&D (Development of segment mirrors and System integration)
61. Development of calibration system for CTA telescopes
62. Study on cosmic ray mass composition in the low energy region
63. Observations of Very-High-Energy Gamma Rays in Australia
64. Development of the readout system for CTA LST
65. Study of cosmic-ray influence on the growth of atmospheric aerosol particles
66. A study on variation of interplanetary magnetic field with the cosmic-ray shadow by the sun
67. All-sky Survey High Resolution Air-shower detector (Ashra) Project: Management for Safety and Health and Collaboration meetings
68. Development of the sensor for Detection of Cosmic ray in Ashra
69. Workshop on High Energy Gamma-Ray Astrophysics and Fundamental Physics
70. Cosmic ray interactions in the knee and the highest energy regions
71. CTA-Japan Physics - Monte Carlo Simulation Joint Research
72. Integration of the optical fiber trigger system for Ashra
73. Observation with the Ashra detector
74. Study of Extremely-high Energy Cosmic Rays by Telescope Array
75. Observation of airshower fluorescence light at the TA FD site by using an Imaging UV telescope
76. Development of the Photodetector for CTA Large Size Telescope
77. Detection of Molecular Bremsstrahlung Radiations using ELS
78. Preparatory Study for Cerenkov Telescope Array Project
79. Development of new surface detector for observation of ultra high energy cosmic ray at Telescope Array site
80. Study of quantum noise and quantum non-demolition scheme for LCGT
81. Research of Cryogenic Silicon mirror for 3rd generation GWDs
82. Development of an optical cavity to stabilize ultranarrow lasers
83. Data analysis using CLIO data
84. Gravitational Wave Detector in Kamioka (X)
85. Development of Sapphire Mirror Suspension for LCGT (VII)
86. Research on ultra-low frequency anti-vibration system for LCGT
87. Study for LCGT data analysis and Research for its System

88. Research of the Earths free oscillations based on simultaneous observations with a laser strainmeter and a superconducting gravimeter
89. Development of Very Low Vibration Cryo-Cooler System
90. Research of Large-scale Gravitational wave Telescope
91. Development of an valuation system of a high-quality sapphire for LCGT
92. Development of precision profiler for mirrors of LCGT interferometer
93. Hierarchical Structure Formation Probed with Large Optical Near-Infrared Telescopes
94. Evolution of the universe and particle physics
95. Frontier of the planetary material science
96. Detection of time variations for cosmogenic Be-7
97. Detection of low level radioisotopes in tree rings
98. Continuous Measurement of Underground Laboratory Environment
99. Study of solar activity, cosmic rays and climate change based on the analyses of cosmogenic nuclides and stable isotopes
100. Chemical study for Antarctic micrometeorites
101. Determination of ^{26}Al in Antarctic meteorite samples
102. Precise calculation of the atmospheric neutrino flux
103. Simulation Study for the IceCube Neutrino Observatory
104. Evaluation of the erupted radioactivities into the environment

G. List of Committee Members

(a) Board of Councillors

KAJITA, Takaaki	ICRR, University of Tokyo
TERASAWA, Toshio	ICRR, University of Tokyo
KURODA, Kazuaki	ICRR, University of Tokyo
NAKAHATA, Masayuki	ICRR, University of Tokyo
YAMAGATA, Toshio	University of Tokyo
MATSUMOTO, Yoichiro	University of Tokyo
NISHIKAWA, Koichiro	KEK
KUGO, Taichi	YITP, Kyoto university
MIYAMA, Shoken	National Astronomical Observatory
TORII, Shoji	Waseda University
MASAIKE, Akira	University of Tokyo
MURAKI, Yasushi	Nagoya University
MAKINO, Fumiyoshi	Institute of Space and Astronautical Science
SATO, Katsuhiko	National Institutes of Natural Sciences
KOMAMIYA, Yukio	ICEPP, University of Tokyo

(b) Advisory Committee

KAJITA, Takaaki	ICRR, University of Tokyo
NOJIRI, Mihoko	KEK
SAITO, Naohito	KEK
YAMAMOTO, Hitoshi	Tohoku University
AIHARA, Hiroaki	University of Tokyo
ITOW, Yoshitaka	STEL, Nagoya University
MORI, Masaki	Ritsumeikan University
KAJINO, Fumiyoshi	Konan University
MUNAKATA, Kazuki	Shinshu University
TOTANI, Tomonori	Kyoto University
FUKUSHIMA, Masaki	ICRR, University of Tokyo
SUZUKI, Yoichiro	ICRR, University of Tokyo
KURODA, Kazuaki	ICRR, University of Tokyo
TERASAWA, Toshio	ICRR, University of Tokyo
NAKAHATA, Masayuki	ICRR, University of Tokyo
KAWASAKI, Masahiro	ICRR, University of Tokyo

(c) Inter-University Research Advisory Committee

NISHIJIMA, Kyoshi	Tokai University
OHASHI, Hideo	Tokyo University of Marine Science and Technology
KANDA, Nobuyuki	Osaka City University
MUNAKATA, Kazuoki	Shinshu University
TASAKA, Shigeki	Gifu University
TAMURA, Tadahisa	Kanagawa University
YAMAMOTO, Tokonatsu	Konan University
OGIO, Shoichi	Osaka City University
FUKUSHIMA, Masaki	ICRR, University of Tokyo
OHASHI, Masatake	ICRR, University of Tokyo
TAKITA, Masato	ICRR, University of Tokyo
YOSHIKOSHI, Takanori	ICRR, University of Tokyo
SHIOZAWA, Masato	ICRR, University of Tokyo

H. List of Personnel

Director KAJITA, Takaaki,

Vice-Director FUKUSHIMA, Masaki,

Kamioka Observatory (Neutrino and Astroparticle Division)

Scientific Staff	ABE, Ko,	HAYATO, Yoshinari,	HIRAIDE, Katsuki,
	KAMEDA, Jun,	KISHIMOTO, Yasuhiro,	KOBAYASHI, Kazuyoshi,
	KOSHIO, Yusuke,	MIURA, Makoto,	MORIYAMA, Shigetaka,
	NAKAHATA, Masayuki,	NAKAYAMA, Shoei,	OBAYASHI, Yoshihisa,
	OGAWA, Hiroshi,	SEKIYA, Hiroyuki,	SHIOZAWA, Masato,
	SUZUKI, Yoichiro,	TAKEDA, Atsushi,	TOMURA, Tmonobu,
	YAMASHITA, Masaki,		
Administrative Staff	TAKAKURA, Koji,		
Technical Staff	KANBE, Tomio,	NOZAWA, Noriyuki,	ONOUE, Tatsuya,
	TAMORI, Yukio,		
Research Fellow	BAI, Lili,	MARTIMAGRO, Lluis,	NISHIMURA, Yasuhiro
	TAKENAGA, Yumiko,	YANG, Byeongsu,	
Secretary	MAEDA, Yukari,	OKURA, Yoko,	TAKAMATSU, Midori,
	TANIMURA, Naoko,		

Research Center for Cosmic Neutrinos (Neutrino and Astroparticle Division)

Scientific Staff	KAJITA, Takaaki,	OKUMURA, Kimihiro,
Administrative Staff	MASUDA, Kimiaki,	
Technical Staff	SHINOHARA, Masanobu,	
Research Fellow	KAJI, Hiroshi,	LAING, Andrew Brian,
Secretary	KITSUGI, Atsuko,	WATANABE, Keiko,

High Energy Cosmic Ray Division

Scientific Staff	ASAOKA, Yoichi,	ENOMOTO, Ryoji,	FUKUSHIMA, Masaki,
	NONAKA, Toshiyuki,	TAKEDA, Masahiro,	TAKITA, Masato,
	TERASAWA, Toshio,	TESHIMA, Masahiro,	ONISHI, Munehiro,
	OISHI, Michiko,	SASAKI, Makoto,	SHIBATA, Tatsunobu,
	YOSHIKOSHI, Takanori,		
Technical Staff	AOKI, Toshifumi,	IKEBA, Kiriko,	KOBAYASHI, Takahide,
	KOIZUMI, Chikako,	MASUDA, Masataka,	MORIMOTO, Yusuke,
	OKI, Kaoru,		
Research Fellow	AITA, Yuichi,	CHEN, Ding,	IKEDA, Daisuke,
	INOUE, Susumu,	KAWATA, Kazumasa,	TAMEDA, Yuichiro,
Secretary	FUKUI, Misa,	KOKUBUN, Yayoi,	OKAMURA, Takako,
	SUGAHARA, Midori,		

Akeno Observatory (High Energy Cosmic Ray Division)

Scientific Staff	SAGAWA, Hiroyuki,	
Technical Staff	OHOKA, Hideyuki,	SHIMIZU, Kanetoshi,

Norikura Observatory (High Energy Cosmic Ray Division)

Technical Staff	AGEMATSU, Yoshiaki,	ISHITSUKA, Hideki,	SHIMODAIRA, Hideaki,
	TOKOKU, Chihiro,	USHIMARU, Tsukasa,	YAMAMOTO, Kuniyuki,

Astrophysics and Gravity Division

Scientific Staff	FUKUGITA, Masataka,	IBE, Masahiro,	KAWAMURA, Seiji,
	KAWASAKI, Masahiro,	KIMURA, Nobuhiro,	KURODA, Kazuaki,
	MIYAHARA, Hiroko,	MIYAKAWA, Osamu,	MIYOKI, Shinji,
	NAKATANI, Ichiro,	OHASHI, Masatake,	OISHI, Naoko,
	OUCHI, Masami,	SAITO, Yoshio,	SUZUKI, Toshikazu,
	TAKAHASHI, Ryutaro,	TANAKA, Yasuo,	UCHIYAMA, Takashi,
	YAMAMOTO, Kazuhiro,		
Technical Staff	IWASAKI, Utako,	KAMIIZUMI, Masahiro,	SAKAI, Akiko,
Research Fellow	FRIEDRICH, Daniel Dieter,	HIROSE, Eiichi,	KUROYANAGI, Sachiko,
	KUSAKABE, Motohiko,	SHIOMI, Sachie,	SUGIYAMA, Shohei,
	YAMAUCHI, Daisuke,		
Secretary	KIKUCHI, Rie,	MASHIMA, Chieko,	SATO, Ritsuko,

Graduate Students

Doctor	IRVINE, Tristan James,	KIDO, Eiji,	KAWAKAMI, Etsuko,
	KITAJIMA, Naoya,	LEE, Ka-pik,	McLACHLAN, Thomas Fukuei,
	MIYAMOTO, Hideaki,	MIYAMOTO, Koichi,	OBI, Yoshio,
	SAIKAWA, Kenichi,	SAITOH, Takanori,	SHINOZAKI, Akihiro,
	TAKESAKO, Tomohiro,	TOYAMA, Takeshi,	UENO, Ko,
	YOKOZAWA, Takaaki,		
Master	HIEDA, Keisuke,	HIRANO, Shigetoshi,	MIKAMI, Ryo,
	NAKANO, Yuki,	NAKAO, Yuta,	SAKAKIBARA, Yusuke,
	SEKIGUCHI, Takanori,	TAKACHIO, Osamu,	TAKEDA, Naoyuki,
	TAKEISHI, Ryuji,	UMEMOTO, Daigo,	YAMADA, Masaki,
	YOSHIGOE, Koichi,	YOSHINO, Kazuyoshi,	

Administration Division

Scientific Staff	ITOH, Hideo,		
Administrative Staff	AKIYAMA, Makiko,	FUJIE, Tamiko,	IRIMAJIRI, Aki,
	KANEKO, Saho,	MARUMORI, Yasuko,	MATSUZAWA, Noboru,
	OGURA, Satoshi,	SAITO, Akiko,	SETO, Mikako,
	TAKANO, Eri,	WATANABE, Wataru,	YAMAGUCHI, Akiko,